



**HAL**  
open science

# Caractérisation des circuits intégrés micro-onde à base d'Arséniure de Gallium par sondage électro-optique utilisant un faisceau laser continu

Stefan Lauffenburger

► **To cite this version:**

Stefan Lauffenburger. Caractérisation des circuits intégrés micro-onde à base d'Arséniure de Gallium par sondage électro-optique utilisant un faisceau laser continu. domain\_other. Télécom ParisTech, 2003. English. NNT : . pastel-00000621

**HAL Id: pastel-00000621**

**<https://pastel.hal.science/pastel-00000621>**

Submitted on 16 Apr 2004

**HAL** is a multi-disciplinary open access archive for the deposit and dissemination of scientific research documents, whether they are published or not. The documents may come from teaching and research institutions in France or abroad, or from public or private research centers.

L'archive ouverte pluridisciplinaire **HAL**, est destinée au dépôt et à la diffusion de documents scientifiques de niveau recherche, publiés ou non, émanant des établissements d'enseignement et de recherche français ou étrangers, des laboratoires publics ou privés.



# Thèse

présentée pour obtenir le grade de docteur de l'École Nationale Supérieure des Télécommunications

Spécialité: Électronique et Communications

## Stefan Lauffenburger

Caractérisation des circuits intégrés micro-onde à base d'Arséniure de Gallium par sondage électro-optique utilisant un faisceau laser continu

( *Characterization of microwave Gallium Arsenide integrated circuits with electro-optic probing using a continuous laser beam* )

Soutenu le 21 Février 2003 devant le jury composé de

Georges Alquié

Président

Lionel Duvillaret  
Smaïl Tedjini

Rapporteurs

Georg Guekos

Examineur

Didier Erasme  
Bernard Huyart

Directeurs de thèse



*“In great attempts it is glorious even to fail.”*

Cassius Longinus,  
Greek rhetorician and philosopher.



# Remerciements

Je tiens à exprimer en quelques mots ma reconnaissance aux personnes qui m'ont aidé avec leurs soutiens scientifiques, techniques et moraux. Sans eux, cette thèse n'aurait jamais vu le jour.

J'adresse tout d'abord mes remerciements à Georges Alquié (*Professeur à l'Université Pierre & Marie Curie*) pour avoir présidé le jury. Toute ma gratitude va aux rapporteurs Lionel Duvillaret (*Maître de Conférence à l'Université de Haute Savoie*) et Smaïl Tedjini (*Professeur à l'École Supérieure d'Ingénieurs en Systèmes Industriels Avancés Rhône-Alpes*) pour avoir relu attentivement le rapport et pour leurs remarques constructives. Je tiens également à exprimer ma profonde gratitude envers Georg Guekos (*Professeur à l'École Polytechnique Fédérale de Zurich*) pour m'avoir donné l'opportunité de faire une thèse à Paris, pour ses commentaires enrichissants et pour avoir accepté d'être examinateur dans le jury.

Je veux aussi remercier les responsables de l'ENST pour m'avoir donné la possibilité de réaliser ce travail. En particulier, il y a Didier Erasme et Bernard Huyart qui ont surveillé mes activités, Guy Debarge qui m'a aidé avec les calculs mathématiques, Claude Chabran, Renaut Gabet, et Yves Jaouën qui m'ont soutenu pendant la réalisation de l'expérience, Xavier Begaud qui a mis à disposition des logiciels de simulations micro-onde et Alain Croullebois qui a fabriqué les montages mécaniques.

J'aimerais aussi exprimer ma reconnaissance pour l'aide financière du *Conseil de bourse de ABB* et de la *Conférence des Recteurs des Universités Suisses*.

Je ne peux pas m'abstenir de mentionner les aides précieux des "supports techniques" de "National Instruments", "Agilent" et "Keithley" qui ont répondu à beaucoup de questions très particulières.

J'aimerais aussi salué tous les autres thésards et stagiaires qui étaient à l'origine de la bonne ambiance indispensable à la réalisation d'un travail scientifique. Je commence par ordre chronologique: Amal pour m'avoir initié aux problèmes d'une "thésarde abandonnée", Olivier pour avoir éclairé avec ses "halos" notre bureau sombre, Céline et Sandrine pour leurs gâteaux, Catherine et François-Xavier pour leur introduction à "l'art de vivre" à la française, Christophe Brutel pour ses renseignements informatiques et Loïc pour sa bonne humeur. Je suis reconnaissant pour le soutien informatique et moral de Cédric accompagné de sa cannette "Coca Light" posant des questions métaphysiques. Le calme de nos deux mexicains (Carlos et Gabriel) m'a beaucoup inspiré dans les situations difficiles. La réalisation de la manipe était facilitée par le fait que Helena, Lydia & Virginie ne m'ont que rarement enlevé de l'équipement mais m'ont rendu d'autres services. Il m'a été d'une grande aide de toujours pouvoir récupérer mes affaires à proximité des trous noirs du labo gérés par Christophe Gosset en collaboration avec Joseph Désiré. La rédaction du rapport était devenue seulement supportable par mes deux superbes collègues de bureau (Sabine et Ghaya) qui m'ont rendu beaucoup de services. J'aurais presque oublié "l'inoubliable" stagiaire allemande (Petra) qui m'a donné beaucoup de confiance. Je devrais ajouter encore beaucoup de lignes pour d'autres personnes (Ali Reza, Anne-Claire, Béatrice, Bruno, David, Fabien, Hedi, Ines, Jérémie, Georgia alias Yolada, Laurent, Mariam, Mohamad, Sébastien, Souheil et al.), mais j'ai bien peur qu'il ne manque encore une fois du papier dans l'imprimante....

Paris, en Mars 2003.



# *Abstracts*

## *Abstract*

The number of microwave integrated circuits (IC) has increased in recent years following the trend towards higher carrier frequencies. This kind of IC is commonly used in telecommunications where they can be found in cellular phone equipment or in devices for satellite communications. The possession of simulation software and probing tools is vital for further development of such ICs. These tools can localize the critical points in the IC and so the design can be improved. Considering that an IC has a limited number of input and output ports, it is rather difficult to characterize the electrical signal inside an IC. Several different probing techniques based on different approaches were proposed and developed recently.

In this thesis we focus on the probing of Microwave Monolithic Integrated Circuits (MMIC) made of Gallium Arsenide (GaAs). The basic idea is to exploit the electro-optic properties of the semiconductor. We focus a laser beam onto the Device Under Test (DUT). Considering that GaAs is “transparent” for the chosen wavelength, a part of the laser beam will enter the substrate and will be reflected from the back face of the device. The reflected laser beam will be modulated in

## *Résumé*

Pendant les dernières années le nombre de Circuits Intégrés (CIs) micro-ondes a fortement augmenté suite à l'utilisation de fréquences porteuses de plus en plus élevées. Ces types de CI sont très fréquemment utilisés dans les télécommunications, dans l'équipement pour des téléphones portables ou pour la communication satellite. Pour le développement et l'amélioration des CIs, il est important d'avoir à disposition des outils de mesure et de simulation. Avec ces outils, on peut localiser les points critiques et la conception peut être améliorée. Considérant que le nombre d'entrées et de sorties d'un CI est limité, la mesure des signaux électriques dans un CI est une tâche délicate. Plusieurs techniques de mesure ont donc été proposées ces derniers temps ou sont en cours de développement.

Cette thèse est centrée sur le sondage des circuits Microwave Monolithic Integrated Circuits (MMIC) à base d'Arséniure de Gallium (AsGa). L'idée principale est d'exploiter les propriétés électro-optiques du semiconducteur. Un faisceau laser est focalisé sur le circuit testé. Considérant que le AsGa est “transparent” pour la longueur d'onde choisie, le faisceau entre dans le composant et il se réfléchit sur la face arrière. Le faisceau réfléchi est modulé en fonction du signal micro-onde recherché car les pro-

## *Zusammenfassung*

Als Folge der immer höheren Trägerfrequenzen hat die Anzahl von Integrierten Schaltungen (IS) bei Mikrowellenanwendungen in letzter Zeit stark zugenommen. Häufig werden solche IS in der Telekommunikation eingesetzt, zum Beispiel in Mobilfunktelefone oder für Satellitenkommunikation. Für die Weiterentwicklung solcher Schaltkreise ist es wichtig über geeignete Simulations- und Meßinstrumente zu verfügen. So können die Schwachstellen der Schaltungen lokalisiert und behoben werden. Da IS nur über eine beschränkte Anzahl von Ein- und Ausgänge verfügen, ist es eine schwierige Aufgabe, die elektrischen Signale in den IS zu messen. Mehrere verschieden Meßmethoden für das charakterisieren von IS basierend auf unterschiedlichen Ansätzen existieren oder sind in Entwicklung.

In dieser Doktorarbeit konzentrieren wir uns auf das Ausmessen von “Microwave Monolithic Integrated Circuits” (MMIC) auf der Basis von Galliumarsenid (GaAs). Die Grundidee ist, die elektro-optische Eigenschaft des Halbleitermaterials GaAs auszunutzen. Dazu wird ein Laserstrahl auf die auszumessende Schaltung fokussiert. Da GaAs für diese Wellenlänge “durchsichtig” ist, wird ein Teil des Laserstrahls erst an der Rückseite des Halbleiters reflektiert. Der reflektierte Laserstrahl wird in Funktion des gesuchten Mikrowellensignals moduliert, da die optischen Eigen-

function of the microwave signal sought after as the optical properties of the GaAs substrate depend on this parameter. We can measure this modulation and hence we can determine the microwave electric field inside the device.

The goal of this thesis is the construction of a prototype of a probing tool based on previous work in our laboratory. The aim is a simple set-up with low material costs. As a consequence we use only standard equipment. The essential improvement of the presented work is the use of new and more powerful equipment. Explicitly we use polarization maintaining fibers, we avoid all free space setups and we review the acquisition software. Furthermore we have a look at some theoretical problems neglected in the previous thesis e.g. we calculate the influence of the electric field direction on the probing results.

In this thesis, we describe the development of the probing tool as well as the obtained results. We demonstrate the agreement between the experimental measurements and the theoretical description. We show that we can probe the microwave signal with a sensitivity of about  $2[\text{mV}/\sqrt{\text{Hz}}]$  and that the operational frequency of the probing tool is only limited by the characteristics of the photodiode and the corresponding amplifier. On the other hand, we analyze the major technical problems. Therefore we mention the variation in power and polarization of the laser source used for probing and we analyze the problems of adequately focusing the laser beam onto the IC.

priétés optiques de l'AsGa dépendent de ce paramètre. Nous pouvons mesurer cette modulation et nous pouvons en déduire le champ électrique dans le CI.

L'objectif de cette thèse est la construction d'un prototype basé sur des travaux précédents réalisés dans notre laboratoire. Le but principal est une conception simple avec des coûts de matériel faibles. Par conséquent on n'utilise que des composants standards. Le progrès de la thèse présentée est l'utilisation d'équipements nouveaux nettement plus performants. En particulier on utilise des fibres à maintien de polarisation, on évite toutes les manipulations du faisceau laser en espace libre et on renouvelle les logiciels d'acquisition. De plus on traite quelques problèmes théoriques négligés dans les travaux précédents: par exemple, on vérifie la validité de nos résultats de sondage si la direction du champ électrique n'est pas connue exactement.

Dans cette thèse nous décrivons le développement de l'outil et les résultats correspondants. Nous démontrons que les résultats mesurés correspondent avec la description théorique. Nous illustrons que nous pouvons mesurer un signal micro-onde avec une sensibilité d'environ  $2[\text{mV}/\sqrt{\text{Hz}}]$  et que la fréquence opérationnelle de l'outil de sondage est seulement limitée par les caractéristiques de la photodiode. Un autre objectif de ce travail fut de trouver les limites techniques et leurs origines. Dans ce contexte nous avons dû constater la dépendance de la polarisation et de la puissance de la source laser en fonction de la longueur d'onde. Nous analysons le problème de la focalisation adéquate du faisceau laser sur le CI.

schaften von GaAs von diesem Parameter abhängen. Diese Modulation kann ausgemessen werden und so kann das elektrische Signal bestimmt werden.

Das Ziel dieser Doktorarbeit ist die Realisierung eines Prototypen eines Meßgerätes basierend auf vorhergehenden Arbeiten. Da das Meßgerät möglichst einfacher sein soll, und die Materialkosten niedrig gehalten werden müssen, werden nur Standardkomponenten eingesetzt. Die Neuerungen bei dieser Arbeit sind der Einsatz von aktueller, leistungsfähigerer Ausrüstung: Es werden polarisationserhaltende Glasfasern eingesetzt, die Laserstrahlmanipulationen im freien Raum werden vermieden und die Computerprogrammierung der Instrumente wird verbessert. Zusätzlich schließen wir noch einige Lücken in der Theorie: Wir berechnen den Einfluß auf die Meßresultate, wenn die Richtung des zu messenden elektrischen Feldes nicht genau bekannt ist.

In der vorliegenden Arbeit beschreiben wir die Entwicklung des Meßgerätes und die erzielten Ergebnisse. Wir zeigen, daß die experimentellen Resultate weitgehend mit der theoretischen Beschreibung übereinstimmen. Wir demonstrieren, daß wir ein Signal mit einer Sensitivität von  $2[\text{mV}/\sqrt{\text{Hz}}]$  ausmessen können und daß die maximale Arbeitsfrequenz nur durch die Eigenschaften der Photodiode und dem dazugehörigen Verstärker begrenzt werden. Wir erörtern die wesentlichen technischen Probleme und ihr Ursprünge: Dazu zählen die Charakteristik der Laser-Quelle (Variation der Leistung als auch der Polarisation). Eine weitere Schwierigkeit war das adäquate Fokussieren des Laserstrahls auf die Schaltung.

# Contents

<i>Remerciements</i> .....	<i>v</i>
<i>Abstracts</i> .....	<i>vii</i>
<i>Contents</i> .....	<i>ix</i>
<i>Introduction</i> .....	<i>1</i>
1.    Requirements for Probing	1
1.1. Requested Information	1
1.2. General qualities for probing	2
2.    Several methods for chip characterizations	4
2.1. Probing with a mechanical tip	4
2.2. Probing with an antenna	5
2.3. Optical probing of Silicon CMOS integrated circuits	5
2.3.1. Hot luminescence technique	5
2.3.2. Laser Voltage Probing	7
2.4. Electron Beam Probing	8
2.5. Sampling Force Probing	9
2.6. External Electro-Optic sampling	10
2.7. Internal Electro-Optic Sampling	12
2.7.1. GaAs based devices and MMIC (Microwave Monolithic Integrated Circuits)	12
2.7.2. Internal probing	13
2.8. Project for the thesis	14
<i>Theory</i> .....	<i>15</i>
3.    Electro-Optic Effect	15
3.1. General description of the problem	15
3.1.1. Isotropic and Anisotropic Material	15
3.1.2. Electro-Optic properties of Materials	16
3.1.3. Principle of the Ellipsoid	18
3.1.4. Representation as an ellipsoid	20
3.1.5. Classification of different Anisotropic Materials	21
3.2. Refractive index for different direction of the electric field in GaAs	22
3.2.1. Ex	22
3.2.2. Ey	23
3.2.3. Ez	24
3.2.4. Ex + Ez	25
3.3. Comment	26
4.    Electro-optic crystals in a Fabry Perot Cavity	27

4.1.	Response of a Fabry Perot Cavity	27
4.2.	Minima and Maxima of the Cavity Response	29
4.3.	Comment	30
5.	Amplitude Modulation	31
5.1.	Modulation caused by the electro-optic crystal	31
5.2.	Modulation for a laser polarization not parallel to optical axis	33
5.3.	Modulation for an electric field $E_x+E_z$	34
5.4.	Comment	36
6.	Polarization modulation	37
6.1.	Setup	37
6.2.	Modulation	37
6.2.1.	Polarization modulation with a wave plate	39
6.3.	Comment	40
7.	Phase modulation	41
7.1.	Setup	41
7.2.	Comment	42
8.	Other considerations & Problems	43
8.1.	Gaussian beam	43
8.2.	Spot Size and spatial resolution	46
8.2.1.	Spot size without cavity	47
8.2.2.	Spot Size on the device	48
8.2.3.	Modified Calculation for the Fabry Perot Cavity	50
8.3.	Magnitude of the electric fields	52
8.4.	Choice of the wavelength of the laser beam	53
8.5.	Comment	54
9.	Conclusion of the Theory	55

*Measurements* .....57

10.	Characterization of the Components	57
10.1.	Characteristics of the laser	58
10.1.1.	Measurement setup	58
10.1.2.	Results	59
10.2.	Characteristics of the circulator	60
10.2.1.	Measurement setup	60
10.2.2.	Results	61
10.3.	Characteristics of the focuser	62
10.3.1.	Measurement setup	62
10.3.2.	Results	62
10.4.	Comment	63
11.	Measurement of the Fabry Perot Cavity Response	64
11.1.	Measurement for different magnification factors	64
11.1.1.	Measurement setup	64
11.1.2.	Results	64
11.2.	Measurement of the different reflections with a optical reflecto-meter	66
11.2.1.	Measurement Setup	66
11.2.2.	Results	66
11.3.	Comment	68
12.	The electro-optic signal	69
12.1.	The Electro-Optic Signal	69

12.1.1.	Measurement Setup	69
12.1.2.	Results	69
12.2.	The electro-optic signal for different directions of the polarization	71
12.2.1.	Measurement Setup	71
12.2.2.	Results	72
12.3.	Linearity and the Signal to Noise Ratio	73
12.3.1.	Measurement Setup	73
12.3.2.	Results	74
12.4.	Comment	77
13.	Mapping of the electric field in a MMIC	78
13.1.	Measurement of the electric field beside a microwave guide	78
13.1.1.	Measurement Setup	78
13.1.2.	Results	78
13.1.3.	Simulation	79
13.2.	Mapping of the electric field on a chip	80
13.2.1.	Measurement Setup	80
13.2.2.	Results	80
13.3.	Comment	81
14.	Measurement of the S-parameters	82
14.1.	Measurement Setup	82
14.2.	Results	83
14.3.	Comment	84
15.	Signal processing with Stimulated Brillouin Scattering	85
15.1.	Principles of Stimulated Brillouin Scattering	86
15.1.1.	Spontaneous Brillouin Scattering	86
15.1.2.	Stimulated Brillouin Scattering	86
15.2.	Verification of the threshold and spectrum of the lightwave	88
15.2.1.	Measurement Setup	88
15.2.2.	Results	90
15.3.	Modulation depth enhancement and the Signal to Noise Ratio	91
15.3.1.	Measurement Setup	91
15.3.2.	Results	92
15.4.	Application of the Brillouin scattering in the probing setup	94
15.4.1.	Measurement Setup	94
15.4.2.	Results	94
15.5.	Comments	96
16.	Conclusions of the Measurements	97
<i>Conclusion</i> .....		99
<i>References</i> .....		101
17.	Books and Thesis	101
18.	Publications, Journals and Proceedings	101
18.1.	Optical probing of Silicon CMOS chips	101
18.2.	Electron Beam Probing	102
18.3.	Scanning Force Probing	102
18.4.	Electro-Optic Probing	102
18.5.	External Electro-Optic Probing	103
18.6.	Internal Electro-Optic Probing	103
18.7.	MMIC and GaAs	104

18.8.	Other References	104
19.	Internet/Electronic Data	104

*Appendix* ..... **105**

A.	Constants	105
A.1.	General Constants in Vacuum	105
A.2.	Material Constants	105
B.	Acronyms	109
C.	Symbols	110
D.	Units	111
D.1.	Optical Units	111
D.2.	Electrical Units	111
D.3.	Relation of Electrical and Optical Units	113
E.	Calculations	115
E.1.	Calculation of the eigenvalues	115
E.2.	Calculation of the eigenvectors	116
E.3.	Calculation of reflection and transmission coefficients	119
E.4.	Calculation of the Cavity response	121
E.5.	Calculation of the partial derivative	122
E.6.	Calculation of the Minimum and Maximum of the Fabry-Perot Cavity response	123
E.7.	Calculation of the relation between the reflection and R and r	124
E.8.	Calculation of the modulation for a polarization between the optical axis	126
E.9.	Calculation of the modulation for $E=E_x+E_z$	127
E.10.	Calculation of the Polarization Modulation	130
E.11.	Calculation of the Polarization Modulation with two $1/8$ wave plate	132
E.12.	Calculation of the phase shift modulation	134
E.13.	Calculation of the Gaussian beam in free space	135
E.14.	Spot Size of our probing device	138
E.15.	Recalculation of the cavity response	140

# *Introduction*

In the last few years, the use of electronic equipment increased constantly following the rapid development of computer technology, mobile phones and satellite communication. The steady trend towards faster and more powerful equipment as well as the limitation of frequency forced a development toward higher and higher frequencies. Hence numerous new electronic applications appeared and the part of microwave devices grew quickly.

For the development, design and production of new integrated electronic devices, it is important to have powerful design and probing tools to characterize your new device. There are several possibilities to determine the characteristics of an Integrated Circuit (IC). First you can connect your Device Under Test (DUT) to electronic measurement equipment like a network analyzer or similar. Unfortunately modern integrated devices consist of a large number of integrated elements and provide a rather small number of output and input pins for external connections. So there are a lot of functions you cannot verify this way. Another method to analyze the characteristics of a DUT is to use a computer to simulate the operation of the device. Apart the fact that your device might be too complicated or not suitable for a simulation, you have to consider that the software will fail to find a problem if the simulator does not take into account the corresponding (known or unknown) physical effect. The third approach of characterizing an IC's is to measure the electric signal inside the semiconductor. This sounds simpler than it is in reality because integrated devices are so complex that you have to have sophisticated probing techniques to find and acquire your signal.

Parallel with the development of new semiconductor devices, new probing techniques appeared. These new techniques can probe the electric signal inside the IC. Hence they allow improving the actual design. They can also provide the data to improve the electrical models of the simulation software.

By probing a semiconductor device, you are looking for some specific information or signal data. In this chapter we will first have a look at the different kind of information, you can acquire by probing. We will indicate the general condition for the data acquisition. Afterwards we will investigate several "state of the art" probing techniques.

## **1 Requirements for Probing**

### **1.1 Requested Information**

Before we discuss the different measurement techniques, we should think what kind of information we want to acquire with our measurements. Depending on our goal we might have different interests in different information.

One goal might be to probe the electric or magnetic field distribution inside integrated devices. In the case of a “perfect” probing, it would be possible to measure all field components (x, y or z) of the electric ( $E(r)$ ) or magnetic field ( $H(r)$ ) including their phase shift ( $\phi$  and  $\zeta$  respectively) for any possible position  $r$  (Equation (1)).

$$\vec{E}(r) = \begin{bmatrix} E_x(r)e^{-i\phi_x(r)} \\ E_y(r)e^{-i\phi_y(r)} \\ E_z(r)e^{-i\phi_z(r)} \end{bmatrix} \text{ or } \vec{H}(r) = \begin{bmatrix} H_x(r)e^{-i\zeta_x(r)} \\ H_y(r)e^{-i\zeta_y(r)} \\ H_z(r)e^{-i\zeta_z(r)} \end{bmatrix} \quad (1)$$

If you have the distribution of your electric field inside your device, you can determine almost all other parameters. For example you can use the field distribution to detect cross talking between parallel wave guides, you can use it to approve an electrical model of a transistor or you can determine the characteristics of antennas.

If you are debugging or designing an IC for Radio Frequency (RF) applications your basic interest is not the electric field distribution all over your device. You are much more interested in the behavior of parts of your device. This can be described by the two-port matrix (Figure 1) under the condition that the output and input impedance are well known. So you can analyze what each IC-part is doing and so you are able to locate possible malfunctions. With some probing techniques, you cannot measure all  $s_{xx}$ -parameter but only the forward transfer function ( $s_{21}$ ).

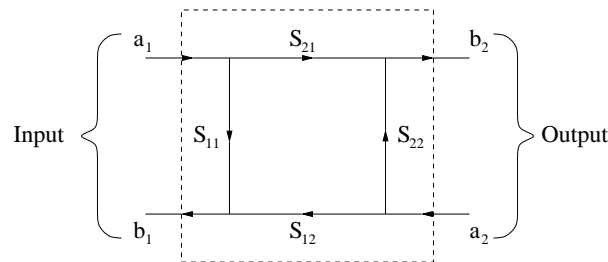


**Figure 1** S-parameters of two ports are used to describe micro-wave devices.

For some digital application, it is interesting to observe the propagation of the signal e.g. the clock signal through an IC. So you want to know when a signal impulse is reaching the transistor at the far end of your device.

In some cases it might be interesting to measure several defined parameters of your ICs just after the production of your wafer as quality control before a possible bonding and packaging of your device. In this case you are not interested in the electric field or the transfer function. You just want the reproducibility of the measurements.

## 1.2 General qualities for probing

We list below the qualities for a ‘good’ probing technique:

- i) The measurement technique should be ‘non destructive’ and not require to modify the DUT. It would be a disadvantage if you have to remove passivation layers or if you

would have to establish supplementary connections to probe your signal.

- ii) Your measurement techniques should not have any or only very small influence on the signals in the ICs. In some cases the probe itself introduces a supplementary resistor, capacitor or inductance in the setup and so it influences the signal on the chip and the measurements will be systematically wrong.
- iii) The frequency bandwidth of the measurement techniques should be so that you can operate your device at any requested frequency. This implies that your system has to operate at 40 [GHz] or even at higher frequencies.
- iv) The cost for the probing tool should be 'reasonable'.
- v) If you are interested in mapping the electric field in an IC, you will have to acquire a big number of data points. So you have to make sure that one acquisition does not take a prohibitive long time.
- vi) The required signal to noise ratio of the measurement system, which defines the smallest detectable signal, should be as high as possible.

## 2 Several methods for chip characterizations

There are several measurement techniques for integrated devices based on different physical effects and metrological setups. Each approach operates in a slightly different way and leads to different results. There are also very specific advantages and disadvantages for each type of measurement technique. For the understanding of the advantages of a specific method, it is interesting to understand the weak points of other setups. So we will have a look at some “state of the art” probing techniques.

### 2.1 Probing with a mechanical tip

The probing with a mechanical tip consists in placing a metal tip in contact with the metal layer (Figure 2). A travel translation stage is used to place the mechanical tip on the surface of the semiconductor and an optical microscope monitors the actual tip position. The other end of the metal tip is connected to an instrument for the signal analysis of the microwave signal. The metal probing technique is common and several commercial solutions are available.

The mechanical probing with a tip is one of the simplest methods for debugging ICs. There are no semiconductor material or layout properties required. You can even use the mechanical probe to force an electrical signal into any point of the IC by connecting the probe to a signal generator.

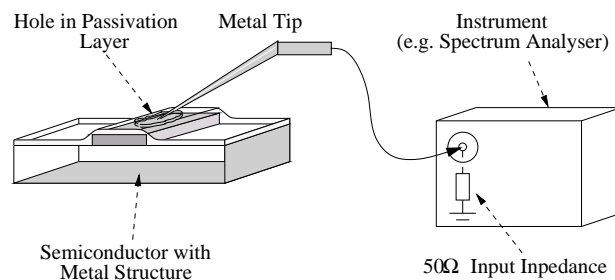


**Figure 2** Probing with a mechanical tip.

On the other hand there are several weak points for the probing with a metal tip apart the fact that it is potentially destructive. First there has to be no passivation layer to provide direct access to the metal layer. Also your probing point should not be hidden by another metal structure or other vital part of the IC. If you want to probe an already protected chip you need some facilities for removing its passivation layers. But the passivation is not the only problem. Some other problems arise if you try to probe highly ICs at microwave frequencies.

Putting a mechanical probe connected to an instrument onto a metal layer induces another capacitance into your IC. Depending on the length of your tip and the signal frequency, you even risk having an emitting antenna just in front of your DUT. Another inconvenience is the fact that most microwave instruments have an input impedance of 50 [Ω] to avoid introducing reflections. So by analyzing the signal you risk to add a supplementary impedance to your device.

Another drawback with this probing technique is the decreasing size of the metal structure of IC to a size below the wavelength of visible light (about 0.3 [μm]). So it is not possible anymore to use standard optical microscopes. Hence you have to look for other possibilities to adjust the position of

your metal tip on your IC.

The drawbacks of the mechanical probing caused the research for other more sophisticated probing techniques.

## 2.2 Probing with an antenna

Another technique of probing a device is to use small antennas to measure the electric field just above the surface of the circuits as proposed in [ 47 ]. By using a unipolar antenna made of a coaxial cable, it is possible to probe the electric field normal to the surface as shown in Figure 3. With a bipolar antenna it is possible to sense the electric field parallel to the surface. By calibrating the antennas with a known electric field, it is possible to investigate the x, y and z component of the electric field above the circuit.

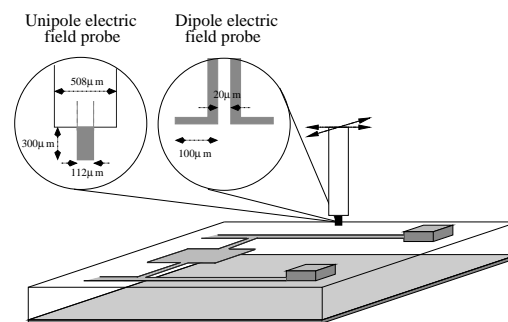


**Figure 3** Probing of the electric field above the surface of a circuit [ 47 ].

The problem of this technique is its coarse spatial resolution. Hence it is generally used for the characterization of “large” devices like patch antennas.

## 2.3 Optical probing of Silicon CMOS integrated circuits

Considering that Complementary Metal-Oxide Semiconductors (CMOS) made of silicon substrate is the most widely used type of IC, we present a short overview of two non-destructive CMOS based probing techniques.

### 2.3.1 Hot luminescence technique

With hot luminescence technique ([ 13 ], [ 14 ] and [ 15 ]), we can probe field effect transistors (FET) which are standard elements of a CMOS device. When a FET is conducting an electric current, there are free electric charges (electrons for a n-type FET and holes for a p-type FET) moving in the transistor channel. The free carriers are accelerated by the strong electric field inside the transistor until they scatter with lattice vibrations, impurities or other carriers. Then the cycle of acceleration and scattering restarts. During this acceleration, the energy of the mobile carrier is increased. So some carriers can acquire a kinetic energy of up to 1 [eV] due to the electric field of up to  $10^3$  [V/cm]. These interactions heat up the mobile carrier as well as the lattice and so the energy distribution of the mobile carrier is changing. The energy distribution can be described by

the Boltzmann distribution (Equation (2)),

$$P \sim e^{\left(\frac{-U}{k \cdot T_E}\right)} \quad (2)$$

where  $P$  is the probability that a carrier has a given kinetic energy,  $k$  is the Boltzmann constant,  $U$  the kinetic energy level and  $T_E$  represents the effective temperature. Typical values for  $T_E$  for electrons in FET transistors are as high as 2000-3000 [K]. So these electrons are called ‘hot carriers’.

In a conducting transistor, energy states in the conduction band can become occupied which would rest unoccupied in the absence of an electric field. These include also states directly (same wavevector) above the lowest conduction band. These new occupied states introduce the slight possibility of a light emitting transition down to the lowest level of the conduction band and hence the generation of photon.

In a silicon n-type FET there are only a few photons generated per second and the generation is even weaker in the case of p-type transistor. But the emission is strong enough to be detected by sophisticated photo multiplier systems or to be converted into an electric signal by sensitive avalanche photodiode. Considering that the emission is proportional to the current or the electric field in the transistor, we can determine if a device is switching or not (Figure 4).

One possible application of the hot luminescence technique is the observation of the propagation of the clock signal in an IC (Figure 5). When the clock arrives to a logical gate, it causes a switching or no switching of the logical gate. If the gate is switching, there will be a current in the transistor and this current causes the generation of some “hot luminescence” photons which can be detected. By monitoring the entire chip with a sensitive camera, triggering the acquisition with a delay to the clock signal and by averaging the data acquisition over several hours you can monitor the propagation of the signal.

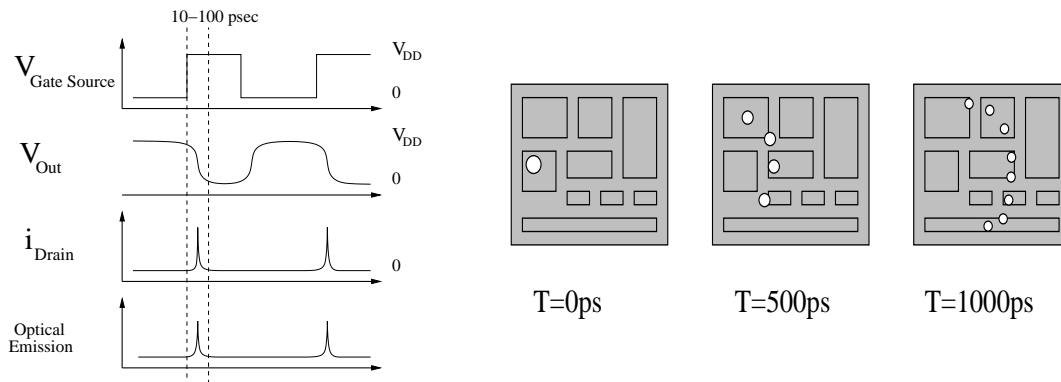


**Figure 4** Basic idea of hot luminescence technique: The switching current in logic gates (e.g. inverter) causes the generation of some photons [ 13 ].

**Figure 5** One possible application of hot luminescence technique: The “hot spots” indicate the location of the switching transistors. So we can observe the propagation of the clock inside an IC.

The advantage of the hot luminescence technique is that it can be used for almost all modern CMOS devices assembled in flip-chip packages. The disadvantages are the fact that you need very sensitive equipment to monitor the luminescence and so you can only approximate the voltage or current inside a transistor. Also the transistor under test has to be visible and should not be hidden by another element of the IC.

### 2.3.2 Laser Voltage Probing

For the Laser Voltage Probing (LVP) ([ 13 ], [ 15 ] and [ 16 ]) a laser beam of a well specified wavelength  $\lambda$  is focused on a p-n junction in the silicon CMOS DUT. The principle is that the reflection of the laser beam will change in function of the strong electric field inside the p-n junctions (Figure 6) due to the variations of optical absorption in the semiconductor.

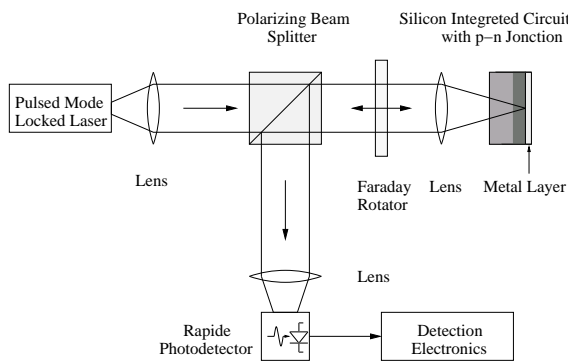


**Figure 6** Basic idea of LVP: A laser beam is focus on a p-n junction and its reflections change in function of the electric field in the junction [ 16 ].

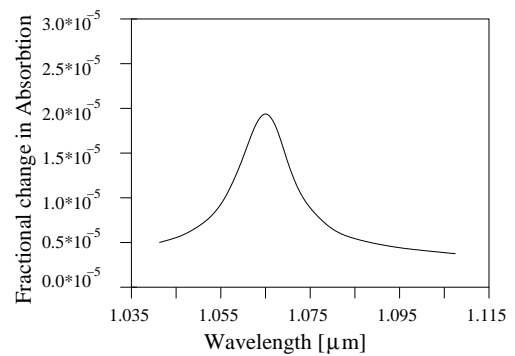


**Figure 7** Measured electro-absorption in heavily doped p+ silicon substrate as a function of the laser wavelength [ 16 ].

The absorption coefficient of undoped silicon changes in function of the wavelength of the incident laser beam. If the energy of the photons is larger than the band gap of silicon (typically higher than  $1.12 \text{ [eV]} = 1.80 \cdot 10^{-19} \text{ [J]}$  or shorter than  $1.06 \text{ [}\mu\text{m]}$  for the wavelength of the laser beam) the photons will be absorbed and causes the generation of a hole/electron pair. If the energy of the incident photon is smaller (wavelength longer than  $1.06 \text{ [}\mu\text{m}]$ ) it will not interact with the semiconductor lattice. Hence the silicon is transparent. In a p-n junction the silicon is heavily doped and there might be also a strong electric field ( $\sim 10^5 \text{ [V/cm]}$ ). The band gap and so the optical properties or the absorption of silicon will change with these two parameters.

There are several physical effects having an influence on the optical properties of a p-n junction. The most important in the case of LVP is the electro-absorption or photon-assisted tunneling. The presence of a strong electric field in a p-n junction causes the generation of tunneling states in the forbidden energy gap near the edges of the conduction and the valance bands. These tunneling states induced by the electric field reduce the size of the band gap of the substrate. This phenomenon is called the Franz-Keldysh effect. It changes the absorption coefficient if the energy of the incident photons are about the same value as the band gap of silicon (Figure 7) as the energy gap of the semiconductor is changing slightly in function of the applied electric field.

The measurement setup in (Figure 6) shows a pulsed mode locked laser with a wavelength of  $1.064 \text{ [}\mu\text{m}]$  which is focused from the backside of a flip-chip mounted IC onto a p-n junction. The reflection is recollected by the same lens and is transported to a photo detector where the laser beam is converted into an electric signal. Considering that the absorption variation is rather weak, a stroboscopic detection technique is used to recover the waveform of the signal (Figure 8).

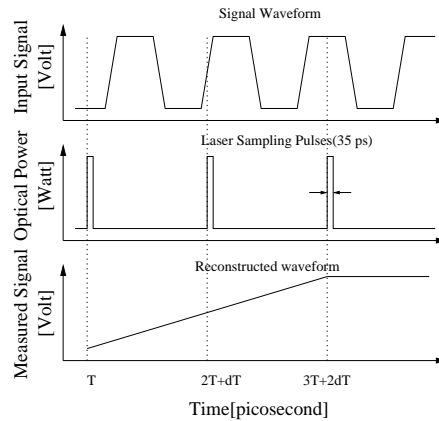


**Figure 8** Schematic diagram showing the principles of stroboscopic sampling. In such setup the bandwidth is normally limited to about  $0.36/\delta t$ , where  $\delta t$  is the pulse width of the laser pulse. In the case of a laser pulse width of 35 [ps] you can sample signals up to 10 [GHz] [ 16 ].

The advantages of the LVP technique are its high bandwidth and the fact that it can test flip-chip devices in its packages except for devices with an absorbing substrate. There you would have to remove a little bit of the substrate to decrease the absorption. The disadvantages is that the spatial resolution is limited by the spot size of the laser beam and the fact that you can only probe in doped regions (e.g. transistors) of your integrated device.

## 2.4 Electron Beam Probing

For Electron Beam Probing ([ 17 ], [ 18 ], [ 19 ] and [ 20 ]) the DUT is placed in vacuum and a pulsed electron beam is focused on the DUT. The impact of the electron beam on the surface of the device causes the generation of so-called ‘secondary electrons’. The number of ‘secondary electrons’ depends on electric potential of the surface around the impact spot. The collection of this ‘secondary electrons’ allows the detection of the local electric field.

The setup of an electron beam probing system consists of several parts (Figure 9). An electron source and an accelerating anode are providing an electron beam with a typical energy of 500-2500 [eV] for the electrons. The electron beam passes then a blaster system that can generate short pulse of a pulse width of down to 5 [ps] [ 19 ]. In the next stage, the electron beam is focused on the chip by a system of electric lenses to a spot size of about 50 [pm]. On the IC the primary electrons of the incident electron beam interact with the atoms of the surface. The interaction causes the generation of secondary electrons with energy ranging from 0 [eV] up to 20 [eV] [ 20 ]. The number and energy of secondary electrons depend on the electric potential of the surface around the impact of the electron beam. The secondary electrons are collected by an electric or a magnetic extractor system and they are guided to a detector system and converted into an ‘electric’ signal.

For the probing of microwave signal, a stroboscopic setup up is used (Figure 8). So with a pulse width of down to 5 [ps], you can probe signals with a frequency up to about 80 [GHz]. If we are interested in a microwave signal, you do not even have to remove the passivation layer of the DUT. The alternating electric potential is passing the passivation like a capacitance. By having some losses you can even probe electrical signal which are buried by several non-conducting layers. Only if you

are interested in the continuous electric potential (DC offset), you have to have direct access to the metal structure. Hence you have to ‘drill’ holes into the passivation layer.

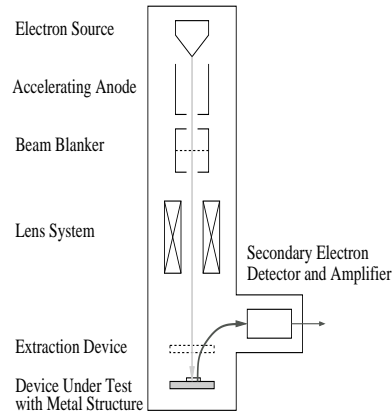


**Figure 9** Electron Beam Probing in a vacuum tube [ 20 ].

The advantages of the electron beam probing are its excellent spatial resolution (about 50 [pm]) and the fact that it is a rather experienced method and that commercial tools are available. On the other side there are problems with measurement at high frequencies. In this case you have to have a careful design for your blanker and extraction system to avoid influence to the electric signal in the circuit under test.

## 2.5 Sampling Force Probing

A recent and commercially available method of probing the microwave signal inside an IC is the Sampling Force Probing techniques ([ 21 ], [ 22 ] and [ 23 ]). It is based on the fact that the small metal tip of a micro-machined cantilever probe and the metal structure form a capacitance (Figure 10). If the voltage applied to the capacitance is changing there is an electrostatic  $F_z$  force induced to the probe.

$$F_z = \frac{1}{2} \cdot \frac{\partial}{\partial z} C_p(x, y, z) (v_{\text{Probe}} - v_{\text{ic}}(x, y))^2 \quad (3)$$

In Equation (3)  $v_{\text{Probe}}$  is the voltage of the probe,  $v_{\text{ic}}$  is the seeked signal and  $C_p(x,y,z)$  is the value of the capacitance at the given position  $x$ ,  $y$  and  $z$ . By sensing the deflection of the probe and by knowing its spring constant, it is possible to calculate the electrostatic force and so to measure the voltage between the tip and the chip.

The problem of this approach is that above a certain frequency, typically about 100 [kHz], the response of the probe becomes very small and it is not possible to execute a data acquisition anymore. But there is a simple way to overcome this limitation. According to Equation (3) the response of the probe is proportional to the square of the applied voltage. So we can use this non-linearity to down convert the signal frequency to a range where the probe is able to response to it.

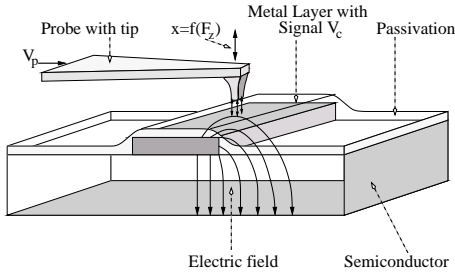


**Figure 10** Basic idea of Sampling Force Probing: A metal tip and the structure form a capacitance.

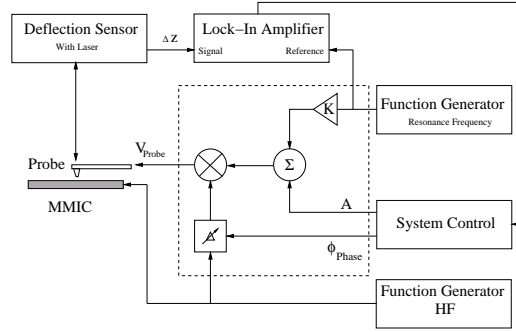


**Figure 11** Schematics for a heterodyne setup [ 22 ].

There are several possible setups for the down-converting of the signal frequency. We will have a look at a common configuration displayed in Figure 11 [ 22 ]. The basic idea is to apply a modulated voltage  $v_{Probe} = (A + K \cos(\omega_r t)) \cdot \cos(\omega_{RF} t + \phi_p)$  to the probe.  $A$ ,  $K$  and  $\phi_p$  are free parameters,  $\omega_{RF}$  is the signal frequency of your IC and  $\omega_r$  is the resonance frequency of the micro-machined cantilever probe.

$$|\Delta z| = QF_z/k \quad (4)$$

In Equation (4) we model the spring force  $F_z$ , where  $\Delta z$  is the displacement of the probe,  $k$  is its spring constant and  $Q$  the quality factor. Hence we can deduce the displacement of the probe (Equation (5)).

$$\Delta z \sim \frac{1}{2} \cdot \frac{\partial}{\partial Z} C_p \frac{Q}{k} ((A - V_c \cos(\phi_{Probe} - \phi_c)) K \cos(\omega_r t)) \quad (5)$$

If we control the three free parameters  $A$ ,  $K$  and  $\phi_p$  in a way that the displacement becomes zero we can calculate the signal amplitude  $v_{ic}$  and its phase  $\phi_{ic}$ . Hence we do not even have to know the parameters  $C_p$ ,  $Q$  and  $k$  to determine the voltage between the probe and the metal layer.

The other advantages of the sampling force probe technique are its high spatial resolution (the size of the tip is about 50 [nm]), the high dynamic range of about 20 [dB] [ 21 ] and the fact that the measurement technique is independent of the semiconductor material. Compared to other measurement techniques, it is also an advantage that you measure the voltage between one point of the metal structure on your IC and ground and not like in other techniques the electric field outside your integrated chip under test.

On the other side you need special equipment to suppress interfering vibrations and it requires a complicated setup to down convert the frequency to the resonance frequency of the probe. Also it is not possible to measure beside the metal structure to map the entire electric field distribution.

## 2.6 External Electro-Optic sampling

A crystal consists of nucleus and electrons with positive and negative electric charges ([ 27 ], [ 28 ], [ 29 ], [ 30 ], [ 31 ], [ 32 ] and [ 33 ]). An applied electric field changes the equilibrium position of the charges. Depending on the material, this process is nonlinear. Under this condition the applied

electric field causes very small variation of the refractive indices. Equation (6) is a typical description of the relation between the electric field  $E$  and the refractive index  $n(E)$  for an electro-optic crystal.

$$n(E) \approx n_o - \frac{1}{2} n^3 r_{xx} E \quad (6)$$

$n_o$  is the refractive index in the absence of an electric field and  $r_{xx}$  is the electro-optic coefficient that depends on the material and its orientation. For certain crystals e.g. Gallium Arsenide this effect is quasi instantaneous and so very interesting for the probing of fast microwave devices. The basic idea of sensing the electric field in an IC is to place an electro-optic crystal just above the surface of the DUT. A laser beam is focused into the electro-optic crystal as displayed in Figure 12. The refractive indices change in function of the electric field just above the IC and so modulates the amplitude, the polarization or the phase of the laser beam. This kind of probing technique is called “external electro-optic sampling” as you use an external electro-optic crystal to probe the electric field.

Different ways are possible to exploit the electro-optic effect. The resulting modulation depends on the polarization of the laser beam, the lattice of the crystal and the vector of the electric field. In a common setup, the electro-optic crystal changes the orientation of the laser beam polarization. Afterwards the laser beam passes through an analyzer and the intensity of the laser beam becomes proportional to the amplitude of the electric field. This effect is hardly limited in frequency but it has the inconvenience that it is very weak. The electro-optic coefficients  $r_{xx}$  have typically a magnitude between  $1 \cdot 10^{-12} [\text{m/V}]$  and  $20 \cdot 10^{-12} [\text{m/V}]$  depending on the material. So sophisticated measurement techniques are required to probe the electric field.

Figure 13 shows a common setup for external electro-optic probing [ 32 ]. It uses a phase-stabilized Ti:Sapphire laser, which provides pulses of 100 [fs] at an 80 [MHz] repetition rate as a probing beam. The laser beam passes a  $\lambda/4$  wave plate and is then focused into the electro-optic crystal. The reflected beam is analyzed in an analyzer to determine the changes of its polarization state. Harmonic mixing of the sought microwave signal frequency and an integer harmonic of the 80 [MHz] repetition rate are used to down convert the frequency. So the output signal can be analyzed with a RF-Lockin amplifier to obtain the amplitude and the phase of the microwave signal.

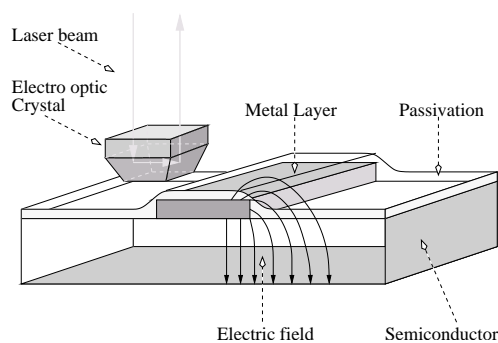


**Figure 12** Common setup for external probing: An electro-optic crystal is put close to the surface and a laser beam is sensing the changes of the refractive index.

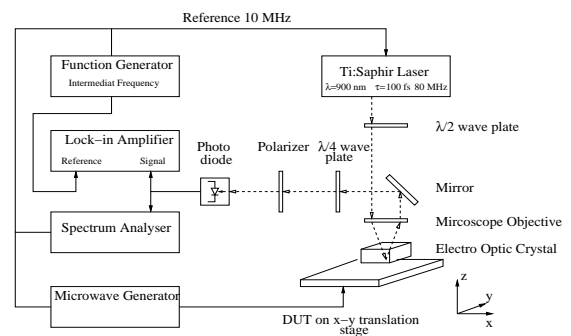


**Figure 13** Possible approach for the measurement setup using a pulsed laser [ 32 ].

The advantages of the external electro-optic probing are its independence of the substrate material. You can probe all different kind of IC with it without having any trouble with the substrate or its

passivation. It is also possible to measure all three components of the electric field including its phase shift by using different electro-optic crystals and by changing their orientation [ 28 ]. One of the most recent developments are commercial probes that can be connected to a standard oscilloscopes [ 30 ].

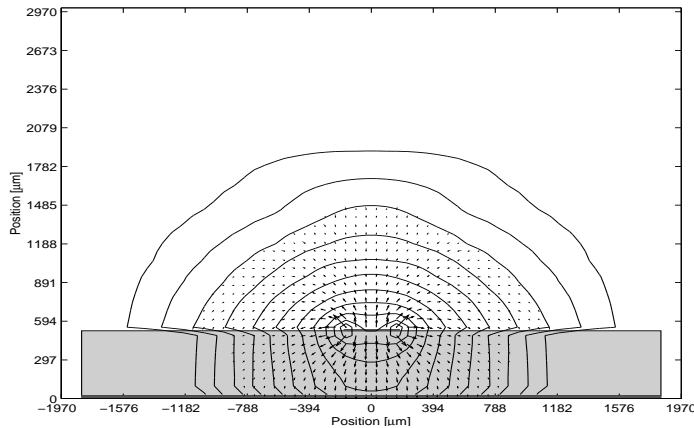


**Figure 14** Simulation of the electric field around a microwave guide on a GaAs substrate at 1 [GHz] executed with a commercial simulation tool (CST Microwave Studio). The arrows indicate the direction of the field: its length is proportional to the amplitude of electric field. The isometric lines (-3 [dB] per line) illustrate the exponential decrease of the magnitude.

The disadvantages of the external electro-optic probing is the fact, that you are not measuring the field in the chip but the electric field above your integrated device. Considering that the electric field decreases exponentially (Figure 14) with the distance above the substrate, the result depends on the position of the external probe. So it is not possible to measure the electric field inside a device but you can characterize the emission of an integrated antenna [ 31 ]. The size of the external electro-optic crystal (typically 50 [μm] x 50 [μm]) and the diameter of the probing beam inside the crystal (around 10 [μm]) limit the spatial resolution. Hence the resulting spatial resolution is rather coarse. Another inconvenience is the capacitive effect of the probe.

## 2.7 Internal Electro-Optic Sampling

The approach of internal electro-optic sampling is very similar to the external electro-optic sampling ([ 34 ], [ 35 ], [ 36 ] and [ 37 ]). A focused laser beam is modulated by the electro-optic effect and the modulated laser beam is analyzed afterwards. The difference is the absence of an external electro-optic crystal. The laser beam is modulated by the electro-optic properties of the substrate itself. The inconvenience of internal electro-optic sampling is that it is only possible for devices with electro-optic substrates like Gallium Arsenide (GaAs) or other III-V semiconductors.

### 2.7.1 GaAs based devices and MMIC (Microwave Monolithic Integrated Circuits)

There are several applications for GaAs based IC. Most are linked to the recent boom of cellular phones and the fiber optical communications networks. So GaAs chips became a common used semiconductor. Hence the sales of GaAs chips reached a marked of about \$3'750 millions in 2000 [ 40 ].

The main application of GaAs circuits is the amplification and filtering of the microwave signal. There is one reason to choose the III-V semiconductor GaAs as a material for this kind of circuit even if it is much more difficult to handle and more expensive to produce than the ‘standard’ semiconductor silicon (Si): The electron mobility of GaAs ( $0.85 \text{ [m}^2/\text{Vs}]$ ) is higher than the electron mobility of Si ( $0.135 \text{ [m}^2/\text{Vs}]$ ). There are several alternative semiconductors for microwave ICs like Silicon Germanium (SiGe) or Indium Phosphide (InP) but GaAs is still a good choice in terms of linearity and efficiency at power above about  $0.5 \text{ [W]}$  [ 40 ]. There are also recent attempts to combine GaAs and Si monolithically to explore the advantages of both materials.

One type of GaAs based IC are Microwave Monolithic Integrated Circuits (MMIC). They are used for new communications applications with frequencies in the microwave range. The difficult and expensive GaAs technology and the high frequency bandwidth cause the common GaAs MMIC technology to be rather simple. The circuit consists of a single layer of the GaAs substrate. The backside of the substrate is covered with a layer of gold and serves as ground for the entire circuit. On the front side is the layout of the circuits with transistors, resistors, inductances, capacitances and microwave guides (Figure 15 and Figure 16). The size of these guides is rather wide (wave guides for analogical applications are typical  $10 \text{ [}\mu\text{m}]$  wide) compared to recent digital silicon IC with structures as small as  $170 \text{ [nm]}$ .

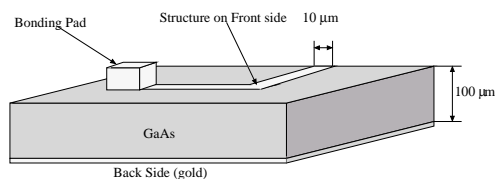


**Figure 15** Setup of a GaAs MMIC.

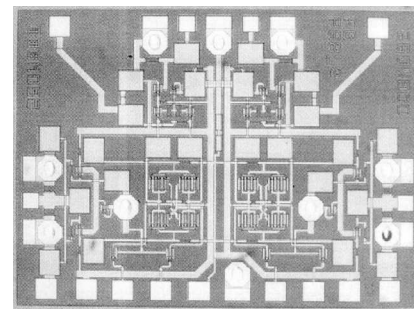


**Figure 16** Example of a standard MMIC.

### 2.7.2 Internal probing

In the internal electro-optic probing of a GaAs chip the laser beam is focused onto the chip as displayed in Figure 17. Considering that GaAs is transparent for infrared light, the infrared laser beam enters the chip, is modulated in the substrate and is reflected backwards.

The laser beam has to have certain properties in terms of wavelength, power and beam waist to make sure that the internal electro-optic sampling works well without systematic errors. A common setup for internal electro-optic probing is described in Figure 18. A continuous laser beam of a pigtailed Distributed FeedBack (DFB) laser is used as a laser source. First it passes a pigtailed optical circulator and it is focused on the chip with a system of lenses. An addition infrared camera displays the location and size of the laser beam spot on the chip. The reflected beam is recollectd by the lens, reinjected into the optical fiber and passes again the optical circulator. After leaving the circulator by the port 3, the signal is optically amplified by an Erbium Doped Fiber Amplifier (EDFA) and filtered optically. Afterwards a fast photo detector converts the laser beam into an electric signal and a network analyzer is analyzing it.

There are several advantages of internal electro-optic probing. One is the fact, that an external electro-optic crystal is not needed. So you do not have to place it just above the surface of your die and

also there is no feedback from this crystal to your MMIC. Also the spatial resolution is better than with an external approach considering that the spot size of the laser beam is typically between 15 [μm] and 30 [μm]. The internal electro-optic probing is also the only approach where you can measure the electric field inside the substrate. Another advantage is that the passivation of the chip does not have to be removed as the 0.15 [μm] thick Si<sub>3</sub>N<sub>4</sub> passivation layer [ 39 ] is transparent for the laser beam.

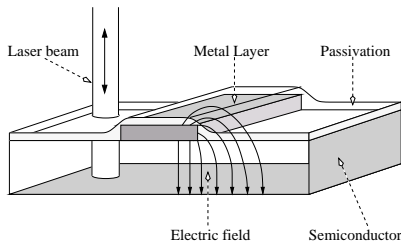


**Figure 17** Basic idea of internal electro-optic sampling.

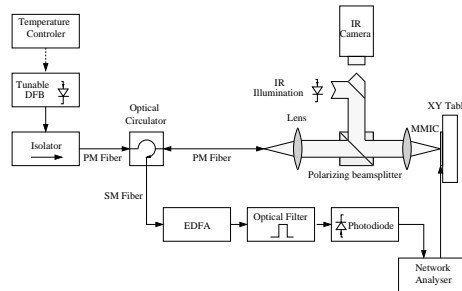


**Figure 18** Setup proposed by [ 8 ] for internal electro-optic probing.

On the other hand there are several disadvantages. You can only sample integrated devices based on a GaAs substrate. As the electro-optic effect of GaAs is rather weak the resulting signal is very small and as the laser beam has to enter the substrate, you cannot probe places hidden by wave guides.

## 2.8 Project for the thesis

The project of this Ph. D. thesis is to realize an internal probing tool for GaAs MMIC as well as to determine its theoretical and technical limits. The probing tool should be based on standard fiber equipment and standard microwave equipment. Hence the setup should be simple and “inexpensive” and should avoid the use of expensive and specially designed tools.

This thesis will continue previous work done in our laboratory. It is based on the results of the thesis of Quang-Dai Le [ 7 ] and Philipp Olivier Müller [ 8 ]. We will exploit the “basic ideas” of probing a Fabry Perot cavity with a continuous laser beam proposed in [ 7 ]. This approach has the advantage that we do not need a pulsed laser and we can avoid the difficulties with the synchronization between the microwave signal and the pulses of the probing beam. We will also use the proposition made in [ 8 ] regarding the use of standard fiber equipment and the calibration method for the probing of the absolute value of the electric field.

The original results of the presented work are the following parts: The previous works did always the assumption that the direction of the probed electric field is known e.g. parallel to the z-axis. As this assumption is not always true, we analyze the general case. We calculate the optical axis and refractive indices in function of the applied electric field and we determine the resulting modulation. The work presents the first electro-optic probing tool for MMIC using a pigtailed focuser. So we calculated the laser beam diameter and the divergence using the formalism of the Gaussian beam. Another important part is the use of new equipment. As fiber optics did a lot a progress in the last time, this had a major impact on our probing tool. We start using Polarization Maintaining (PM) fibers, a pigtailed focuser and a powerful, tunable DFB laser.

# Theory

This chapter will explain the theory of electro-optic sampling using a Fabry Perot cavity. First we will have a look at the electro-optic effect in a crystal like Gallium Arsenide (GaAs). We will continue with the calculation about the behavior of light in a Fabry Perot cavity. Afterwards we will combine both effects for the calculation of the modulation. At the end of the chapter, we will do some auxiliary considerations and comparisons.

Most of the following theory is based on the standard description of the electro-optic effect and the Fabry Perot cavity. The important part of the presented work is the description of our special configuration and its complete deduction. So we can find the origins of problems and explain them. Considering that some of the mathematical calculations are rather long and complicated, the detailed deductions are placed in the appendix. So the reader can find the missing parts of the calculations.

## 3 Electro-Optic Effect

In vacuum or other isotropic materials, the propagation of an electro-magnetic wave does not depend on the direction of propagation or on its polarization. In such isotropic materials, the electro-magnetic wave will always behave the same way. In crystals with periodic structures, the electro-magnetic wave propagation will depend on the direction of the propagation as well as on the polarization of the wave. The properties of certain crystals can be changed by applying an external electric field. As these changes affect also a laser beam propagating inside the crystal, this type of crystal is called “electro-optic”.

### 3.1 General description of the problem

#### 3.1.1 Isotropic and Anisotropic Material

In isotropic material the electric polarization  $\vec{P}$  of the material is always parallel to the applied electric field  $\vec{E}$ . So the dielectric susceptibility  $\chi_e$  is a scalar (Equation (7)).

$$\begin{bmatrix} P_x \\ P_y \\ P_z \end{bmatrix} = \epsilon_0 \cdot \chi_e \cdot \begin{bmatrix} E_x \\ E_y \\ E_z \end{bmatrix} \quad (7)$$

By using  $\vec{D} = \epsilon_0 \vec{E} + \vec{P}$  and the relative dielectric constant  $\epsilon_r = (1 + \chi_e)$  we can show that the electric displacement  $\vec{D}$  is also parallel to the applied electric field (Equation (8)).

$$\begin{bmatrix} D_x \\ D_y \\ D_z \end{bmatrix} = \epsilon_0 \cdot \epsilon_r \cdot \begin{bmatrix} E_x \\ E_y \\ E_z \end{bmatrix} \quad (8)$$

Under the condition that the crystal is not magnetic ( $\mu_r=1$ ) and that it is not absorbing ( $\epsilon_r$  real), it is easy to calculate the refractive index (Equation (9)) and hence the corresponding propagation velocity of electro-magnetic waves.

$$n = \sqrt{\epsilon_r} \quad (9)$$

For anisotropic material Equation (7) and (8) are not valid anymore because the material properties of crystals depend on the crystal axis. So we have to replace  $\chi_e$  by a [3x3] matrix called the electric susceptibility tensor  $\underline{\chi}$  (Equation (10)).

$$\begin{bmatrix} P_x \\ P_y \\ P_z \end{bmatrix} = \epsilon_0 \cdot \begin{bmatrix} \chi_{11} & \chi_{12} & \chi_{13} \\ \chi_{21} & \chi_{22} & \chi_{23} \\ \chi_{31} & \chi_{32} & \chi_{33} \end{bmatrix} \cdot \begin{bmatrix} E_x \\ E_y \\ E_z \end{bmatrix} \quad (10)$$

By applying  $\underline{\epsilon} = \epsilon_0(1 + \underline{\chi})$  we get the corresponding dielectric tensor  $\underline{\epsilon}$  (Equation (11)).

$$\begin{bmatrix} D_x \\ D_y \\ D_z \end{bmatrix} = \begin{bmatrix} \epsilon_{11} & \epsilon_{12} & \epsilon_{13} \\ \epsilon_{21} & \epsilon_{22} & \epsilon_{23} \\ \epsilon_{31} & \epsilon_{32} & \epsilon_{33} \end{bmatrix} \cdot \begin{bmatrix} E_x \\ E_y \\ E_z \end{bmatrix} \quad (11)$$

For the further calculations we assume that our crystal is homogenous (material properties are identical for all points in the crystal), nonabsorbent (there is no energy loss in the crystal and so  $\epsilon_{xx}$  are real numbers) and that the material is not magnetic ( $\mu_r=1$ ). By using the Maxwell equation [ 11 ] we can show that the dielectric tensor is symmetrical (Equation (12)) for these conditions.

$$\epsilon_{j,i} = \epsilon_{i,j} \quad (12)$$

For the following calculations, it is useful to define the impermeability tensor  $\underline{\eta}$  (Equation (13)).

$$\underline{\eta} = \epsilon_0 \cdot \underline{\epsilon}^{-1} \text{ or } \epsilon_0 \cdot \vec{E} = \underline{\eta} \cdot \vec{D} \quad (13)$$

Since  $\underline{\epsilon}$  is symmetrical its inverse matrix  $\underline{\eta}$  is also.

### 3.1.2 Electro-Optic properties of Materials

In certain types of crystals, the application of an electric field causes a displacement of parts of the lattice and its charges. According to the quantum theory, the impermeability tensor depends on the distribution of the charges in the crystal. Mathematically we can describe this modification of the impermeability tensor  $\underline{\eta}$  by a Taylor series in function of the applied electric field (Equation (14))

$$\underline{\eta}(\vec{E}) = \underline{\eta}(0) + r_{i,j,k} \cdot \vec{E} + s_{i,j,k,l}(\vec{E} \cdot \vec{E}) + \dots \quad (14)$$

where  $\underline{\eta}(0)$  is the impermeability tensor in the absence of an electric field,  $r_{i,j,k}$  (a [3x3x3] matrix) are the linear or Pockels<sup>1</sup> electro-optic coefficient.  $s_{i,j,k,l}$  ([3x3x3x3] matrix) are the quadratic or

---

1. Effect discovered by the German physicist Friedrich Pockels around 1890.

Kerr<sup>1</sup> electro-optic coefficients. The magnitude of the electro-optic coefficient depends on the material as well as on its lattice. The higher order terms of Equation (14) are rather small so they can be neglected.

In our case we are interested in the electro-optic properties of GaAs. So we will examine its impermeability tensor and the according material constant for this specific material. For GaAs  $\underline{\eta}(0)$  is represented by Equation (15). We can see that Equation (15) satisfies the condition of Equation (12). Hence in the absence of an applied electric field, GaAs is isotropic because the electric field vector and the electric displacement vector are always parallel.

$$\underline{\eta}(0) = \begin{bmatrix} 1/n_0^2 & 0 & 0 \\ 0 & 1/n_0^2 & 0 \\ 0 & 0 & 1/n_0^2 \end{bmatrix} \quad (15)$$

In Equation (16) we have the linear electro-optic coefficient of GaAs written as a [3x3x3] matrix as well as the applied electric field given in Cartesian coordinates.

$$\underline{r}_{i,j,k} = \left[ \begin{bmatrix} 0 & 0 & 0 \\ 0 & 0 & r_{41} \\ 0 & r_{41} & 0 \end{bmatrix}, \begin{bmatrix} 0 & 0 & r_{41} \\ 0 & 0 & 0 \\ r_{41} & 0 & 0 \end{bmatrix}, \begin{bmatrix} 0 & r_{41} & 0 \\ r_{41} & 0 & 0 \\ 0 & 0 & 0 \end{bmatrix} \right] \text{ and } \vec{E} = \begin{bmatrix} E_x \\ E_y \\ E_z \end{bmatrix} \quad (16)$$

The symmetry in Equation (16) imposed by the condition of Equation (12), limits the number of independent coefficients in the impermeability tensor ([3x3] matrix) to six. Very often this fact is used to reduce Equation (16) into a [6x3] matrix like Equation (17), easier to represent on a two-dimensional sheet of paper. So each of the six independent coefficient depends on  $E_x$ ,  $E_y$  as well as  $E_z$ .

$$\underline{r}_{I,k} = \begin{bmatrix} 0 & 0 & 0 \\ 0 & 0 & 0 \\ 0 & 0 & 0 \\ r_{41} & 0 & 0 \\ 0 & r_{41} & 0 \\ 0 & 0 & r_{41} \end{bmatrix} \quad (17)$$

By using Table 1, you can convert the [3x3x3] matrix of Equation (16) into the [6x3] matrix of Equation (17).

	i = 1	i = 2	i = 3
j = 1	1	6	5
j = 2	6	2	4
j = 3	5	4	3

**Table 1** Lockup table for the index I that represents the pair of indices (i,j) [ 1 ].  
So for the element  $r_{(i=3,j=2,k=1)}$  you will have to take element  $r_{I,k}(4,1)=r_{41}$ .

1. Effect discovered by the english physicist John Kerr around 1875.

In GaAs the Kerr effect is very weak or with other words, we can neglect the quadratic electro-optic coefficients. So we can describe the impermeability tensor of GaAs for an applied electric field  $\vec{E}$  by Equation (18).

$$\underline{\eta}(\vec{E}) = \begin{bmatrix} 1/n_0^2 & r_{41}E_z & r_{41}E_y \\ r_{41}E_z & 1/n_0^2 & r_{41}E_x \\ r_{41}E_y & r_{41}E_x & 1/n_0^2 \end{bmatrix} \quad (18)$$

It is important to notice that this tensor defines the propagation of an electro-magnetic wave in the crystal. So this mechanism affects the laser beam as well as a microwave signal traveling across the crystal.

In the further deductions, we are interested in the propagation of laser beam with a frequency of  $\nu_{\text{Laser}} \approx 193[\text{THz}]$ <sup>1</sup>. So for the refractive index  $n_0$ , we have to take  $n_0(\nu_{\text{Laser}}) = 3.374$  according to [ 3 ].

For the electro-optic coefficient  $r_{41}$  the choice becomes more delicate as the coefficient depends on  $\nu_{\text{Laser}}$  as well as on the frequency  $\nu_{\text{Microwave}}$  of the applied electric field  $\vec{E}$ . In our case the frequency  $\nu_{\text{Microwave}}$  is in the range of 0.1 to 20 [GHz]. Hence we can use the electro-optic coefficient  $r_{41}(\nu_{\text{Microwave}}) = 1.4 \cdot 10^{-12}[\text{m/V}]$  as proposed in [ 8 ].

We have to point out that for much higher frequencies than  $\nu_{\text{Microwave}}$ , the electro-optic coefficient  $r_{41}(\nu)$  becomes negligible. The basic physical concepts of this behavior are understood [ 12 ], but there are no reliable publications on the cut-off frequency of the electro-optic coefficient for GaAs. This ‘‘phenomenon’’ forbids the influence of the electric field of the laser beam on  $\underline{\eta}(\vec{E})$  and so the laser beam is modulated by the microwave signal and not vice versa.

### 3.1.3 Principle of the Ellipsoid

In the previous paragraph we discussed the electro-optic effect and the modification of the impermeability tensor by an applied microwave signal. For the ‘every day calculations’ the use of the impermeability tensor or the dielectric tensor is too complicated.

The method to simplify the application of the impermeability tensor is to use the eigenvectors and the eigenvalues of the tensor in Equation (18). The resulting vector of the multiplication of the matrix with its eigenvector is parallel to the original eigenvector as explained in Equation (19). The absolute value of the eigenvector has to be multiplied with its eigenvalue to get the absolute value of resulting vector.

$$\begin{bmatrix} M_{11} & M_{12} & M_{13} \\ M_{21} & M_{22} & M_{23} \\ M_{31} & M_{32} & M_{33} \end{bmatrix} \cdot \begin{bmatrix} \text{Eigenvector}_x \\ \text{Eigenvector}_y \\ \text{Eigenvector}_z \end{bmatrix} = \text{Eigenvalue} \cdot \begin{bmatrix} \text{Eigenvector}_x \\ \text{Eigenvector}_y \\ \text{Eigenvector}_z \end{bmatrix} \quad (19)$$

A symmetrical [3x3] matrix has three eigenvalues and three according eigenvectors. With linear algebra, we can prove that the three eigenvectors for a symmetrical matrix are three orthogonal vectors. Also we can demonstrate that the eigenvectors of a matrix and the eigenvectors of its inverse matrix are identical.

So the eigenvectors of the impermeability tensor are identical with the eigenvectors of the dielectric

---

1. Corresponds to a wavelength of 1550 [nm] or a photon energy of 0.80 [eV].

tensor. Hence for the direction of the eigenvectors, the electric field is parallel to the electric displacement and the corresponding electric polarization. So for this direction of the electric field, the electro-magnetic wave is propagating like in isotropic material with a dielectric constant corresponding to the eigenvalues of the dielectric tensor. For optical applications the direction of the eigenvectors are called the ‘optical axes’ of the material.

The Maxwell’s equations are linear so long as the wave power is not strong enough to significantly perturb the material. So the propagation for the other orientation of the electric field can be described by projecting the electric field vector on the three eigenvectors and by calculating the propagation for each component separately (Figure 19).

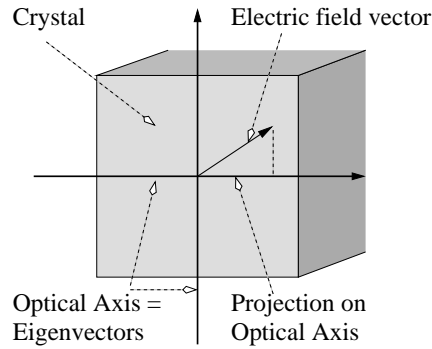


**Figure 19** Projection of the electric field vector on the eigenvectors of the material.

By using the results of Appendix E.1. on page 115, we find the eigenvalues  $\xi_{1,2,3}$  given in Equation (20) to (22) for the impermeability tensor of Equation (18).

$$\xi_1 = \frac{1}{n_o^2} + \frac{2}{\sqrt{3}}|E| \cdot \cos\left(\frac{\arccos\left(-3\sqrt{3}\frac{E_x E_y E_z}{|E|^3}\right)}{3}\right) \cdot r_{41} \quad (20)$$

$$\xi_2 = \frac{1}{n_o^2} - \frac{2}{\sqrt{3}}|E| \cdot \cos\left(\frac{\pi}{3} - \frac{\arccos\left(-3\sqrt{3}\frac{E_x E_y E_z}{|E|^3}\right)}{3}\right) \cdot r_{41} \quad (21)$$

$$\xi_3 = \frac{1}{n_o^2} - \frac{2}{\sqrt{3}}|E| \cdot \cos\left(\frac{\pi}{3} + \frac{\arccos\left(-3\sqrt{3}\frac{E_x E_y E_z}{|E|^3}\right)}{3}\right) \cdot r_{41} \quad (22)$$

In these equations  $E_x$ ,  $E_y$  and  $E_z$  are the x, y and z component of the applied electric field,  $|E| = \sqrt{E_x^2 + E_y^2 + E_z^2}$  is the magnitude of the electric field,  $r_{41}$  is the electro-optic coefficient of GaAs and  $n_o$  is the refractive index in the absence of an (microwave) electric field.

By using the results of Appendix E.2. on page 116 the corresponding non-normalized eigenvectors are given by Equation (23) to (25). So we can see that the eigenvalues of the impermeability tensor depend on the electro-optic coefficient  $r_{41}$  as well as on the amplitude of the applied electric field and its direction. As the refractive index of the material is a function of the eigenvalues, it will also depend on these parameters. On the other hand the eigenvectors (which are parallel with the optical axis of the material) depend only on the directions of the electric field.

$$\text{Eigenvector}_1 = \left[ \begin{array}{c} \frac{-E_x E_z \frac{2|E|}{\sqrt{3}} \cos(\dots) - E_y E_z^2 - E_y \left( \left( \frac{2|E|}{\sqrt{3}} \cos(\dots) \right)^2 - E_z^2 \right)}{\left( \left( \frac{2|E|}{\sqrt{3}} \cos(\dots) \right)^2 - E_z^2 \right) \cdot \left( -\frac{2|E|}{\sqrt{3}} \cos(\dots) \right)} \\ \frac{E_y E_z + E_x \frac{2|E|}{\sqrt{3}} \cos(\dots)}{\left( \frac{2|E|}{\sqrt{3}} \cos(\dots) \right)^2 - E_z^2} \\ 1 \end{array} \right] \quad \text{with}$$

$$\cos(\dots) = \cos \left( \frac{\arccos \left( -3\sqrt{3} \frac{E_x E_y E_z}{|E|^3} \right)}{3} \right) \quad (23)$$

$$\text{Eigenvector}_2 = \left[ \begin{array}{c} \frac{E_x E_z \frac{2|E|}{\sqrt{3}} \cos(\dots) - E_y E_z^2 - E_y \left( \left( \frac{2|E|}{\sqrt{3}} \cos(\dots) \right)^2 - E_z^2 \right)}{\left( \left( \frac{2|E|}{\sqrt{3}} \cos(\dots) \right)^2 - E_z^2 \right) \cdot \left( \frac{2|E|}{\sqrt{3}} \cos(\dots) \right)} \\ \frac{E_y E_z - E_x \frac{2|E|}{\sqrt{3}} \cos(\dots)}{\left( \frac{2|E|}{\sqrt{3}} \cos(\dots) \right)^2 - E_z^2} \\ 1 \end{array} \right] \quad \text{with}$$

$$\cos(\dots) = \cos \left( \frac{\pi}{3} - \frac{\arccos \left( -3\sqrt{3} \frac{E_x E_y E_z}{|E|^3} \right)}{3} \right) \quad (24)$$

$$\text{Eigenvector}_3 = \left[ \begin{array}{c} \frac{E_x E_z \frac{2|E|}{\sqrt{3}} \cos(\dots) - E_y E_z^2 - E_y \left( \left( \frac{2|E|}{\sqrt{3}} \cos(\dots) \right)^2 - E_z^2 \right)}{\left( \left( \frac{2|E|}{\sqrt{3}} \cos(\dots) \right)^2 - E_z^2 \right) \cdot \left( \frac{2|E|}{\sqrt{3}} \cos(\dots) \right)} \\ \frac{E_y E_z - E_x \frac{2|E|}{\sqrt{3}} \cos(\dots)}{\left( \frac{2|E|}{\sqrt{3}} \cos(\dots) \right)^2 - E_z^2} \\ 1 \end{array} \right] \quad \text{with}$$

$$\cos(\dots) = \cos \left( \frac{\pi}{3} + \frac{\arccos \left( -3\sqrt{3} \frac{E_x E_y E_z}{|E|^3} \right)}{3} \right) \quad (25)$$

### 3.1.4 Representation as an ellipsoid

For the visualization and for the application of the results, we use an ellipsoid. The three eigenvectors define the direction of three axis of the ellipsoid and the eigenvalues indicate the magnitudes of the axes (Figure 20).

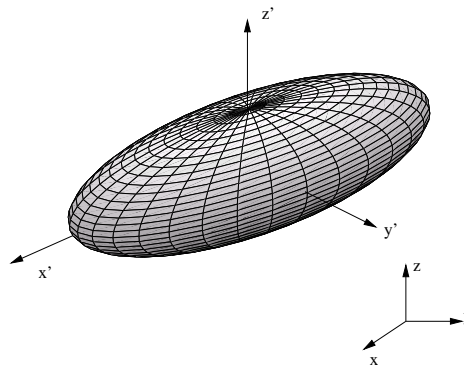


**Figure 20** An ellipsoid with its axis.

For the following deductions, we are interested in the propagation of a laser beam in a given direction with different states of polarization. This kind of propagation can also be referred to the propagation of a plane wave. For this analysis, we are only interested in the electric field direction normal to the propagation direction of the laser beam. Thus we have a look at the intersection of the ellipsoid and the plane normal to the direction of propagation passing through the origin. We will find an ellipse like in Figure 21. This ellipse allows us to analyze and calculate the light propagation in this given direction. So if the polarization is parallel to the axis 1 we have to take into account the refractive index  $n_{\text{Axis1}}$  and the according propagation velocity. If the polarization is parallel to axis 2 we have to take  $n_{\text{Axis2}}$ . For all other polarization, we have to separate our vector into the axis 1 and axis 2 component.

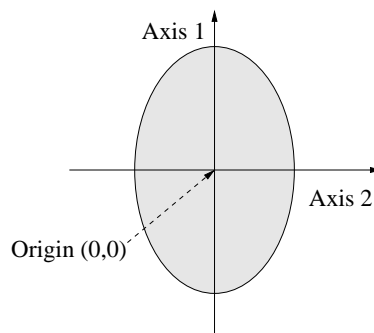


**Figure 21** Intersection of the plan through the origin and the ellipsoid.

### 3.1.5 Classification of different Anisotropic Materials

Material can be classified in function of the resulting ellipsoid. If the ellipsoid is a sphere or with other words if all three axes have the same absolute value, the material is called an isotropic material (Figure 22). Most materials and vacuum are isotropic. If only one axis of the three is different, the material is called a uniaxial material (Figure 24). If all three absolute values are different, the material is called a biaxial material (Figure 23).

If there is no electric field applied to a piece of bulk GaAs, it will show an isotropic behavior. In the next section we will see that under an applied electric field the absolute values of two axis will change. So with an applied electric field, GaAs becomes biaxial.

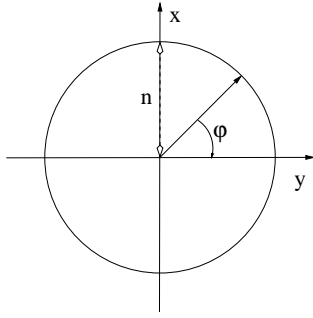


**Figure 22** Refractive index in function of the angle of light polarization for isotropic material.

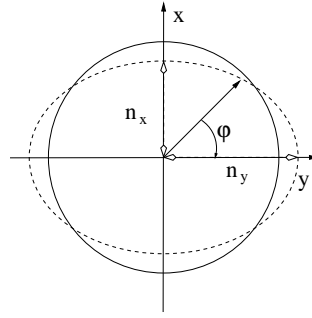


**Figure 23** Refractive index in function of the angle of light polarization for biaxial material.

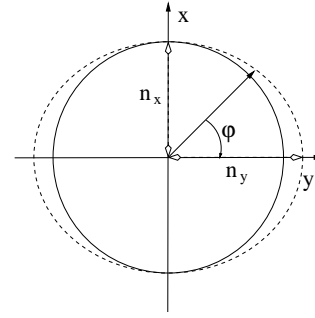


**Figure 24** Refractive index in function of the angle of light polarization for uniaxial material.

### 3.2 Refractive index for different direction of the electric field in GaAs

In the general case, the calculations are still too complicated for further analysis. Equation (20) to (25) are easier to handle if one or two elements of the electric field vanish.

#### 3.2.1 $E_x$

Under the condition that we have an electric field parallel to the x-direction,  $E_y$  and  $E_z$  vanish and Equation (18) can be rewritten as Equation (26).

$$\underline{\eta}(\vec{E}) = \begin{bmatrix} 1/n_o^2 & 0 & 0 \\ 0 & 1/n_o^2 & r_{41}E_x \\ 0 & r_{41}E_x & 1/n_o^2 \end{bmatrix} \quad (26)$$

The eigenvalues become Equation (27), (28) and (29).

$$\text{Eigenvalue}_1 = \frac{1}{n_o^2} \quad (27)$$

$$\text{Eigenvalue}_2 = \frac{1 - E_x n_o^2 r_{41}}{n_o^2} \quad (28)$$

$$\text{Eigenvalue}_3 = \frac{1 + E_x n_o^2 r_{41}}{n_o^2} \quad (29)$$

The eigenvalues of the impermeability tensor do not correspond to the refractive indices of the material but by using Equation (9) and Equation (13), we can extract the requested information. So we will get the refractive indices for the different optical axes (Equation (30), (31) and (32)).

$$n_1 = n_o \quad (30)$$

$$n_2 = \frac{n_o}{\sqrt{1 - E_x n_o^2 r_{41}}} \quad (31)$$

$$n_3 = \frac{n_o}{\sqrt{1 + E_x n_o^2 r_{41}}} \quad (32)$$

We can use  $1/\sqrt{1 + \Delta} \approx 1 - 1/2\Delta$  for  $\Delta \ll 1$  as well as the fact that the parameter  $E_x n_o^2 r_{41} \ll 1$  for a further simplification of Equation (31) and (32). So finally we get the commonly used values for the different refractive indices (Equation (33), (34) and (35)).

$$n_1 = n_o \quad (33)$$

$$n_2 \approx n_o + \frac{1}{2} n_o^3 r_{41} E_x \quad (34)$$

$$n_3 \approx n_o - \frac{1}{2} n_o^3 r_{41} E_x \quad (35)$$

For the eigenvectors, we get the following directions (Equation (36), (37) and (38)) expressed in the x, y and z-coordinate system defined in Figure 25.

$$\text{Eigenvector}_1 = \begin{bmatrix} 1 \\ 0 \\ 0 \end{bmatrix} \quad (36)$$

$$\text{Eigenvector}_2 = \begin{bmatrix} 0 \\ -1 \\ 1 \end{bmatrix} \quad (37)$$

$$\text{Eigenvector}_3 = \begin{bmatrix} 0 \\ 1 \\ 1 \end{bmatrix} \quad (38)$$

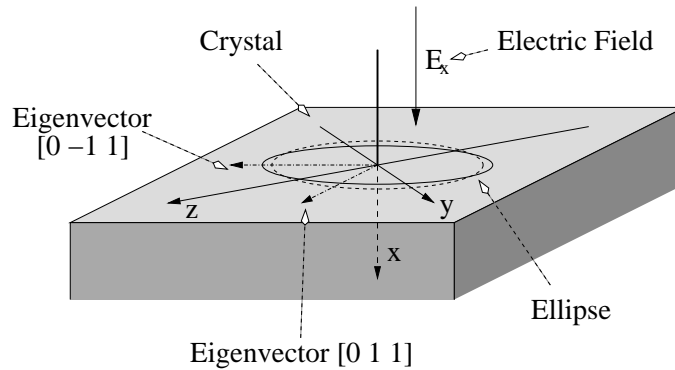


**Figure 25** Configuration of the optical axis for an applied electric field parallel to the x-axis.

### 3.2.2 $E_y$

In the case of an applied electric field parallel to the y-axis, we find for similar reasons the following refractive indices (Equation (39), (40) and (41)).

$$n_1 = n_o \quad (39)$$

$$n_2 \approx n_o + \frac{1}{2}n_o^3 r_{41} E_y \quad (40)$$

$$n_3 \approx n_o - \frac{1}{2}n_o^3 r_{41} E_y \quad (41)$$

In this case the directions of the eigenvectors are given by Equation (42), (43) and (44).

$$\text{Eigenvector}_1 = \begin{bmatrix} 0 \\ 1 \\ 0 \end{bmatrix} \quad (42)$$

$$\text{Eigenvector}_2 = \begin{bmatrix} -1 \\ 0 \\ 1 \end{bmatrix} \quad (43)$$

$$\text{Eigenvector}_3 = \begin{bmatrix} 1 \\ 0 \\ 1 \end{bmatrix} \quad (44)$$

### 3.2.3 $E_z$

We execute the same deductions for the case of an applied electric field parallel to the z-axis and so we get Equation (45), (46) and (47).

$$n_1 = n_o \quad (45)$$

$$n_2 \approx n_o + \frac{1}{2}n_o^3 r_{41} E_z \quad (46)$$

$$n_3 \approx n_o - \frac{1}{2}n_o^3 r_{41} E_z \quad (47)$$

In this case the directions of the eigenvectors are given by Equation (48), (49) and (50).

$$\text{Eigenvector}_1 = \begin{bmatrix} 0 \\ 0 \\ 1 \end{bmatrix} \quad (48)$$

$$\text{Eigenvector}_2 = \begin{bmatrix} -1 \\ 1 \\ 0 \end{bmatrix} \quad (49)$$

$$\text{Eigenvector}_3 = \begin{bmatrix} 1 \\ 1 \\ 0 \end{bmatrix} \quad (50)$$

The ‘similar’ results for all three axis are caused by the fact that the GaAs crystal cut normal to the [1 0 0] Miller plane is symmetric in the x, y and z-axis (Figure 26).

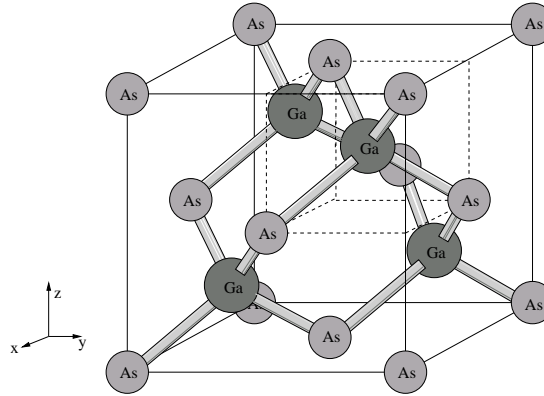


**Figure 26** GaAs lattice with a face-centered cubic lattice. In this lattice the Arsenide represents the positive ion and Gallium is the negative one.

### 3.2.4 $E_x + E_z$

In the next chapter, we will determine the modulation caused by the electro-optic property of GaAs. In most parts of these deductions, we assume that the applied electric field is parallel to z-axis. Unfortunately this assumption ( $E_x = E_y = 0$ ) will not be valid in the “real world”. In this paragraph we calculate the ellipsoid for an applied electric field vector given by  $\vec{E} = [E_x, 0, E_z]$  with  $E_x \neq 0$  and  $E_z \neq 0$ . In paragraph 5.3 we will use the following results to estimate the error caused by this assumption.

For the refractive indices, we get Equation (51), (52) and (53).

$$n_1 = n_o \quad (51)$$

$$n_2 = \frac{n_o}{\sqrt{1 - n_o^2 r_{41} \sqrt{E_x^2 + E_z^2}}} \quad (52)$$

$$n_3 = \frac{n_o}{\sqrt{1 + n_o^2 r_{41} \sqrt{E_x^2 + E_z^2}}} \quad (53)$$

By defining  $E_{\text{Amplitude}} = \sqrt{E_x^2 + E_z^2}$  and by using again  $1/\sqrt{1 + \Delta} \approx 1 - 1/2\Delta$  for  $\Delta \ll 1$ , we find Equation (54), (55) and (56).

$$n_1 = n_o \quad (54)$$

$$n_2 \approx n_o + \frac{1}{2} n_o^3 r_{41} E_{\text{Amplitude}} \quad (55)$$

$$n_3 \approx n_o - \frac{1}{2} n_o^3 r_{41} E_{\text{Amplitude}} \quad (56)$$

The eigenvectors are directed according to Equation (57), (58) and (59). Again we can remark that the direction of the eigenvectors depend on the direction of the applied electric field.

$$\text{Eigenvector}_1 = \begin{bmatrix} \frac{E_x}{E_z} \\ 0 \\ 1 \end{bmatrix} \quad (57)$$

$$\text{Eigenvector}_2 = \begin{bmatrix} \frac{E_z}{E_x} \\ -\sqrt{\frac{E_x^2 + E_z^2}{E_x}} \\ 1 \end{bmatrix} \quad (58)$$

$$\text{Eigenvector}_3 = \begin{bmatrix} \frac{E_z}{E_x} \\ \sqrt{\frac{E_x^2 + E_z^2}{E_x}} \\ 1 \end{bmatrix} \quad (59)$$

If  $E_z \gg E_x$  the ratio  $E_z / E_x$  increases infinitely but this does not cause any problems because the eigenvectors are not normalized. By using the relations of Equation (60) we can show that this results are consistent with Equation (48) to Equation (50).

$$\begin{bmatrix} \infty \\ -\infty \\ 1 \end{bmatrix} \parallel \begin{bmatrix} 1 \\ -1 \\ 0 \end{bmatrix} \text{ and } \begin{bmatrix} \infty \\ \infty \\ 1 \end{bmatrix} \parallel \begin{bmatrix} 1 \\ 1 \\ 0 \end{bmatrix} \quad (60)$$

For the other cases with  $\vec{E} = [E_x, E_y, 0]$  or  $\vec{E} = [0, E_y, E_z]$  we can find similar results.

### 3.3 Comment

In the previous paragraph, we explained the standard representation of the electro-optic effect in the GaAs crystal. We performed the calculation in general and for several special cases. We showed that the ellipsoid and hence the refractive index of the material changes in function of the applied electric field. We proved that the direction of the optical axes depend on the direction of the electric field which is unfavorable for our application. The variation of the refractive index depends on the magnitude of the applied electric field as well as on its direction. As the modifications of the refractive index are extremely weak, the resulting modulation will be small as well.

## 4 Electro-optic crystals in a Fabry Perot Cavity

In our measurement setup, we will focus the laser beam onto an IC and we will analyze its reflections. The air / GaAs interface and the golden back face of the substrate frame a Fabry Perot cavity. So will have a look at the mathematical response of the cavity by taking into account that there is electro-optic material inside the cavity.

For the initial calculations we do several assumption to simplify the deductions. We assume that the incident laser beam is perfectly parallel or with other words that the wave front is a plane wave. The incident laser beam should also have a well-defined linear polarization. Also we assume that the spectral linewidth of the laser is narrow enough so that the corresponding coherence length is much longer than the cavity length.

### 4.1 Response of a Fabry Perot Cavity

Before we start the calculation of the Fabry Perot response, we should recall one principle. For the calculation of the reflections, we use the electric field of the laser beam. So at the end of all our deduction we have to convert the amplitude of the electric field into the laser beam intensity by using Equation (61)<sup>1</sup>. So we find a value proportional to the power sensed by the photo detectors.

$$I_{\text{Laserbeam}} = \frac{1}{2Z_{\text{Material}}} |E_{\text{Laserbeam}} \times E_{\text{Laserbeam}}^*| \quad (61)$$

In Equation (61)  $I_{\text{Laserbeam}}$  is the intensity or the power of the laser beam,  $E_{\text{Laserbeam}}$  is the corresponding electric field and  $Z_{\text{Material}}$  is the wave impedance of the material in this case the wave impedance of the surrounding air.

For the deduction of the Fabry Perot response, we know that at the first air / GaAs interface one part of the laser beam is reflected and the other part passes through (Figure 27). We can describe this mathematically by Equation (62),

$$E_{\text{Reflected}} = r_{\text{Interface}} \cdot E_{\text{Incident}} \quad \text{and} \quad E_{\text{Transmitted}} = t_{\text{Interface}} \cdot E_{\text{Incident}} \quad (62)$$

where  $E_{\text{Incident}}$ ,  $E_{\text{Reflected}}$  and  $E_{\text{Transmitted}}$  are the electric field amplitudes of the incident, reflected and transmitted laser beam and  $r_{\text{Interface}}$  and  $t_{\text{Interface}}$  are the reflection and transmission coefficients respectively.

We assume that there is no loss or gain of energy in the air / GaAs interface. By using the energy conservation law and the boundary conditions, we can calculate the transmission and reflection coefficient for a plane wave with normal incidence (Appendix E.3. on page 119) in function of the material properties. In our case these coefficients are given by Equation (63) and Equation (64), where  $n_{\text{GaAs}}$  and  $n_{\text{Air}}$  are the refractive indices of GaAs and of the surrounding air.<sup>2</sup>

$$r_{\text{Air-GaAs}} = \frac{n_{\text{GaAs}} - n_{\text{Air}}}{n_{\text{GaAs}} + n_{\text{Air}}} \quad \text{and} \quad t_{\text{Air-GaAs}} = \frac{2 \cdot n_{\text{Air}}}{n_{\text{Air}} + n_{\text{GaAs}}} \quad (63)$$

- 
1. The intensity represents a power per surface or [Watt/Meter<sup>2</sup>]. In our case the "surface" of the laser beam will always remain constant. Hence the intensity is directly proportional to the power of the laser beam.
  2. With  $n_{\text{GaAs}}=3.374$  and  $n_{\text{Air}}=1$  we find  $r_{\text{Air-GaAs}}=-r_{\text{GaAs-Air}}=0.54$  and  $t_{\text{Air-GaAs}}=t_{\text{GaAs-Air}}=0.83$ .

$$r_{\text{GaAs-Air}} = \frac{n_{\text{Air}} - n_{\text{GaAs}}}{n_{\text{GaAs}} + n_{\text{Air}}} \text{ and } t_{\text{GaAs-Air}} = \frac{2 \cdot n_{\text{GaAs}}}{n_{\text{Air}} + n_{\text{GaAs}}} \quad (64)$$

Afterwards the laser beam passes through the semiconductor substrate and is reflected at the golden backside. This propagation in the semiconductor causes a phase shift  $\phi$  described by Equation (65),

$$\phi = 2\pi \frac{2d}{\lambda_0} n_o = 2\pi \frac{2d\nu}{c_0} n_o \quad (65)$$

where  $d$  is the thickness of the GaAs layer,  $\lambda_0$  is the wavelength of the laser beam in vacuum,  $\nu$  is the corresponding frequency and  $n_o$  is the refractive index of GaAs in the absence of an applied electric field. For the purpose of our work the undoped GaAs substrate can be considered as transparent. However there will be a slight absorption of the laser beam as given by Equation (66).

$$\text{Absorbtion} = e^{-\alpha 2d} \quad (66)$$

$2d$  represents the distance and  $\alpha$  is the absorption coefficient of the material. For infrared laser light around 1550 nm  $\alpha$  is about 0.006 [cm<sup>-1</sup>] [1]. There are still some losses caused by the reflection at the golden back face which can be represented by  $R'$ <sup>1</sup>. So we can “add” the attenuations during a round trip in the cavity (Equation (67)).

$$R = R' \cdot e^{-\alpha 2d} \quad (67)$$

By taking into account the phase shift of  $\pi$  at the golden back face of the cavity due to the boundary conditions at the interface between a dielectric and a metal material, we can execute the summation of the different reflection according to Figure 27.

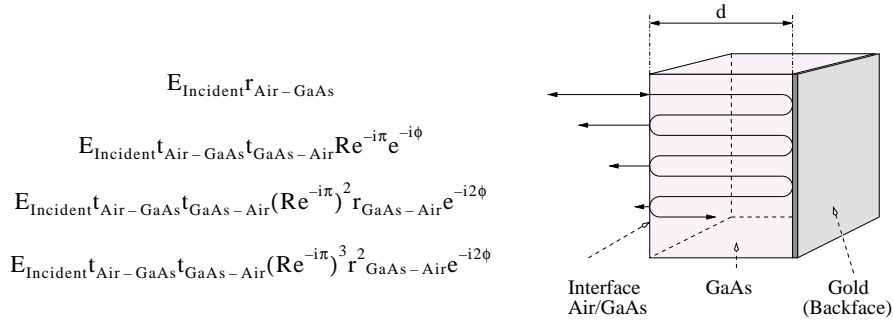


**Figure 27** Summation of  $E_{\text{Reflected}}$ .

By defining  $t^2 = t_{\text{Air-GaAs}} t_{\text{GaAs-Air}}$  as well as  $r = r_{\text{GaAs-Air}} = -r_{\text{Air-GaAs}}$  we can calculate the sum in Equation (68).

$$E_{\text{Reflected}} = E_{\text{Incident}} (-r - t^2 R e^{-i\phi} (1 - R r e^{-i\phi} + (R r e^{-i\phi})^2 - (R r e^{-i\phi})^3 + \dots)) \quad (68)$$

Per definition  $|R r e^{-i\phi}| < 1$  and so we can use the results of Appendix E.4. on page 121 to simplify the summation of  $E_{\text{Reflected}}$  as given in Equation (69).

1. According to [4] the reflectance coefficient of opaque gold film is 0.986 for a laser beam with a wavelength of 1000 [nm] and 0.994 at 5000 [nm]. So theoretically  $R'$  should be close to unity but in reality we have to calculate with loss of at least 2 [dB]. The supplementary losses are probably due to an uneven surface.

$$E_{\text{Reflected}} = -E_{\text{Incident}} \left( \frac{r + R e^{-i\phi}}{1 + R r e^{-i\phi}} \right) \quad (69)$$

As mentioned above, our principle interest is the reflected intensity and not the magnitude of the reflected electric field. So by using Equation (61) we can calculate the intensity of the reflected laser beam as given Equation (70).

$$I_{\text{Reflected}} = I_{\text{Incident}} \frac{r^2 + R^2 + 2Rr \cos(\phi)}{1 + R^2 r^2 + 2Rr \cos(\phi)} \quad (70)$$

Figure 28 shows the response of a cavity for common values of  $r$ ,  $R$  with a typical range for the wavelength  $\lambda_0$ .

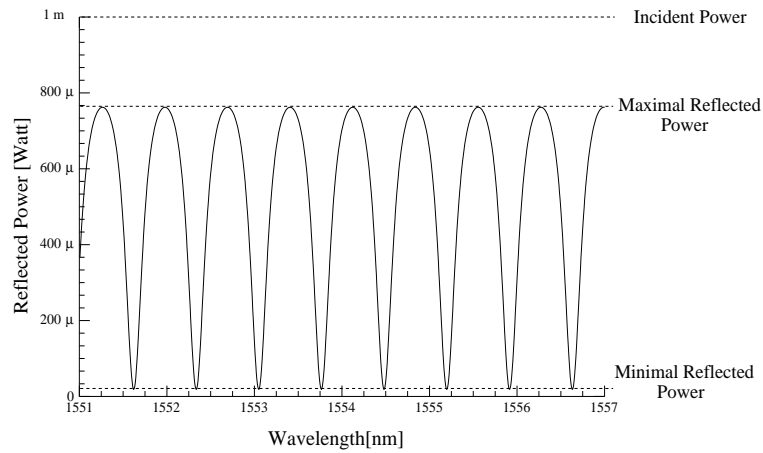


**Figure 28** The response (reflected power) of the cavity with  $r=0.54$ ,  $R=0.63$  ( $-2$  [dB]),  $d=500$  [ $\mu\text{m}$ ] and  $P_{\text{Incident}}=1$  [mW].

## 4.2 Minima and Maxima of the Cavity Response

It might be of some interest to know the position of the maximal and minimal values of the cavity response. By using the results of Appendix E.6. on page 123 we find that the maximum and the minimum are at  $\phi=0$  respective at  $\phi=\pi$  (Equation (71) and (72)).

$$I_{\text{Maximum}}(\phi = 0) = I_{\text{Incident}} \frac{(r + R)^2}{(1 + rR)^2} \quad (71)$$

$$I_{\text{Minimum}}(\phi = \pi) = I_{\text{Incident}} \frac{(r - R)^2}{(1 - rR)^2} \quad (72)$$

By using these results we can show that reflected intensity is equal to incident intensity, if  $r=1$  or  $R=1$  or if both reflection coefficients represent a perfect mirror ( $R=r=1$ ). For all other values, the maximum reflected power is smaller than the incident power. Equation (72) indicates that the minima become zero only in the case when the term  $(r-R)$  vanishes. In this case both reflection coefficient have to be equal.

Though we do not need the reflection coefficient  $r$  and  $R$  for the further calculations, it is interesting

to calculate their values. Considering that it is very simple to determine  $I_{\text{Maximum}}$ ,  $I_{\text{Minimum}}$  and  $I_{\text{Incident}}$ , we try to express  $r$  and  $R$  in function of these parameters.

$$A = \sqrt{I_{\text{Maximum}}/I_{\text{Incident}}} \text{ and } B = \sqrt{I_{\text{Minimum}}/I_{\text{Incident}}} \quad (73)$$

By using the definitions for  $A$  and  $B$  given in Equation (73), we can resolve the system of equations given by Equation (71) and (72). According to Appendix E.7. on page 124, we find for the reflection coefficient  $R$  and  $r$  Equation (74) and (75) respectively.

$$R = \frac{1-AB - \sqrt{(1-A^2)(1-B^2)}}{A-B} \quad (74)$$

$$r = \frac{1 - \sqrt{(1-B^2)/(1-A^2)}}{B - A\sqrt{(1-B^2)/(1-A^2)}} \quad (75)$$

### 4.3 Comment

In the previous paragraph, we reformulated the derivation of the Fabry Perot response. This “standard” description is simple and easy to use. The only inconvenience is the impreciseness of the reflection coefficient  $R$  as we cannot determine it properly.

We could determine the maximal and minimal reflected intensities in function of the incident intensity and the reflection coefficients  $r$  and  $R$  respectively. As we managed to inverse these relations, we could express the reflection coefficients  $r$  and  $R$  in function of the incident, maximal reflected and minimal reflected intensity. This is interesting as the three parameters are measurable with our experimental setup. Hence we can measure the reflection coefficients  $r$  and  $R$ .

## 5 Amplitude Modulation

### 5.1 Modulation caused by the electro-optic crystal

In this paragraph we will investigate the modulation caused by the electric field parallel to the z-axis as displayed in Figure 29 and Figure 30. For this calculations we assume that  $E_x \ll E_z$  and  $E_y \ll E_z$  and hence we put  $E_x=0$  and  $E_y=0$ .

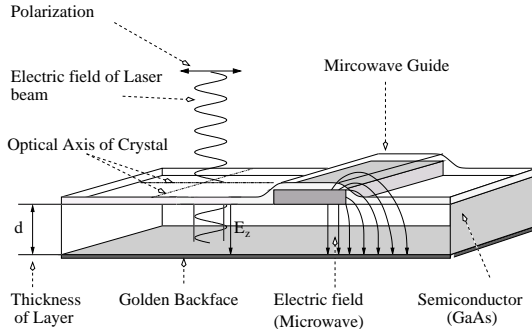


**Figure 29** Configuration to measure the electric field  $E_z$  inside the MMIC.

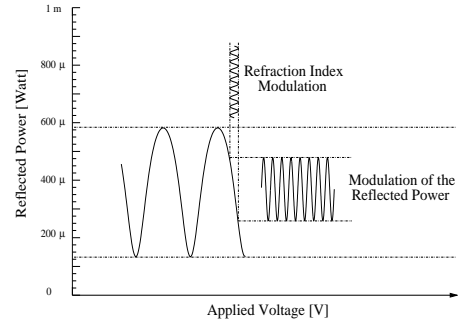


**Figure 30** Principal idea of the amplitude modulation in a Fabry Perot cavity.

In this case the refractive indices of the GaAs crystal are given by Equation (45), (46) and (47). For a polarization parallel to the optical axis of the crystal, the phase shift  $\phi$  due to the propagation in the semiconductor is given by Equation (76).

$$\phi \approx \frac{4\pi d}{\lambda_o} \left( n_o + \frac{1}{2} n_o^3 r_{41} E_z \right) \quad (76)$$

$E_z$  is the applied electric field parallel to the z-direction. So the response of the cavity Fabry Perot becomes Equation (77).

$$I_{\text{Reflected}}(\lambda_o, E_z) = I_{\text{Incident}} \frac{r^2 + R^2 + 2Rr \cos\left(\frac{4\pi d}{\lambda_o} \left( n_o + \frac{1}{2} n_o^3 r_{41} E_z \right)\right)}{1 + R^2 r^2 + 2Rr \cos\left(\frac{4\pi d}{\lambda_o} \left( n_o + \frac{1}{2} n_o^3 r_{41} E_z \right)\right)} \quad (77)$$

In GaAs the electro-optic coefficients are very weak. Hence the electro-optic effect is rather weak and so the modulation will be small. The weak modulation allows us to linearize  $I_{\text{Reflected}}$  in function of  $\Delta\phi$  or more practical in function of  $E_z$  (Equation (78)).

$$I_{\text{Reflected}}(\lambda_o, E_z) \approx I_{\text{Reflected}}|_{E_z=0} + \left. \frac{\partial I_{\text{Reflected}}}{\partial E_z} \right|_{E_z=0} \cdot E_z \quad (78)$$

By changing the partial derivative according to Appendix E.5. on page 122, we get Equation (79). So we can replace the unknown function  $\partial I_{\text{Reflected}} / \partial E_z$  by the determinable function  $\partial I_{\text{Reflected}} / \partial \lambda_o$ . If we know or if we can measure the response of the cavity  $I_{\text{Reflected}}(\lambda_o)$ , we can determine the parameter  $\partial I_{\text{Reflected}} / \partial \lambda_o$ .

$$\left. \frac{\partial I_{\text{Reflected}}}{\partial E_z} \right|_{E_z=0} \approx \frac{\partial I_{\text{Reflected}}}{\partial \lambda_o} \cdot \frac{-n_o^2 r_{41} \lambda_o}{2} \quad (79)$$

The amplitude of the intensity modulation can be described in this case by Equation (80). This signal is called the electro-optic signal.

$$I_{\text{ElectroOptic}} \approx -\frac{\lambda_o n_o^2 r_{41}}{2} \cdot \frac{\delta I_{\text{Reflected}}}{\delta \lambda_o} \cdot E_z \quad (80)$$

By knowing the wavelength of the laser beam  $\lambda_o$ , the refractive index  $n_o$  as well as the electro-optic coefficient  $r_{41}$  and by measuring the electro-optic signal  $I_{\text{ElectroOptic}}$  and the response of the cavity  $I_{\text{Reflected}}(\lambda_o)$ , we can calculate the electric field applied  $E_z$  across the cavity. So we have the ability to determine the voltage applied between the microwave structure and the back face of the substrate.

Last but not least we must have a look at the signs of Equation (80). The refractive index  $n_o$ , the wavelength  $\lambda_o$  and the electro-optic coefficient  $r_{41}$  are ‘per definition’ positive and so we do not have to care about their signs. The electric field  $E_z$  can be positive or negative in function of its direction. The derivative  $\partial I_{\text{Reflected}}/\partial \lambda_o$  can be either positive or negative depending on the wavelength  $\lambda_o$ . On the other side optical intensities are always positive. In Equation (78) the intensity of a laser beam is always positive but in Equation (80) we are looking at the variation of the reflected intensity to a given reference level ( $I_{\text{Reflected}}|_{E_z=0}$ ) and so  $I_{\text{ElectroOptic}}$  might have a negative sign.

In Equation (81)  $E_z$  is the electric field of a microwave signal, where  $E_{\text{Microwave}}$  is the ‘per definition’ positive amplitude and  $f$  is the corresponding frequency.  $E_{\text{Offset}}$  is the continuous part of our microwave signal. In some cases an offset is used to set a working point of a microwave device. Unfortunately a high offset can also polarize the electro-optic modulator. For all further calculations and examples we assume that  $E_{\text{Offset}}$  does not affect the electro-optic modulation and therefore we neglect  $E_{\text{Offset}}$ .

$$E_z = E_{\text{Microwave}} \cos(2\pi ft) + E_{\text{Offset}} \quad (81)$$

So in Equation (82)  $I_{\text{ElectroOptic}}$  is the amplitude of the optical intensity modulation. This amplitude is defined as the difference between the maximal and average intensity of the laser beam and so ‘per definition’ positive. So according to this all parts in Equation (82) are positive except the derivative  $\partial I_{\text{Reflected}}/\partial \lambda_o$  which might become negative.

$$I_{\text{ElectroOptic}} \cdot \cos(\omega t) \approx -\frac{\lambda_o n_o^2 r_{41}}{2} \cdot \frac{\delta I_{\text{Ref}}}{\delta \lambda_o} \cdot E_z \cdot \cos(\omega t) \quad (82)$$

Considering that  $I_{\text{ElectroOptic}}$  has to be positive we can introduce a phase shift of  $\pi$  in the left part of Equation (82) to match or if you prefer patch the signs. We have to take into account a last ‘optical specialty’: Up to now we treated the intensity of the modulation as it would be an amplitude. Unfortunately optical modulations are often expressed in ‘peak to peak’ values. So we have to multiply  $I_{\text{ElectroOptic}}$  with two. So we display the ‘peak to peak’ modulation of Equation (83) in Figure 31.

$$I_{\text{Modulation}} \approx \lambda_o n_o^2 r_{41} \cdot \left| \frac{\delta I_{\text{Ref}}}{\delta \lambda_o} \right| \cdot E_{\text{Microwave}} \quad (83)$$

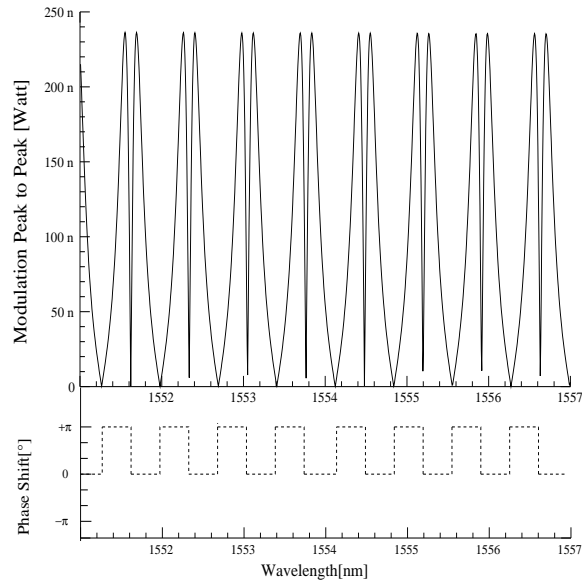


**Figure 31** Amplitude and phase shift of the electro-optic signal. For this figure we used the following parameters:  $n_o=3.374$ ,  $r_{41}=1.42 \cdot 10^{-12}$  [m/V],  $r=0.54$ ,  $R=0.63$  (-2 [dB]),  $d=500$  [ $\mu\text{m}$ ],  $E_{\text{Microwave}}=1$  [V]/d [m] and  $P_{\text{Incident}}=1$  [mW].

## 5.2 Modulation for a laser polarization not parallel to optical axis

For technical reasons, it is difficult to align the polarization of the incident laser beam perfectly with the optical axis of the GaAs crystal. So in this paragraph we will calculate the influence of the polarization deviations.

We still assume that the incident laser beam has got a linear polarization and it is propagating as a plane wave in direction of the z-axis. But the polarization of the incident laser beam is off the optical axis of the crystal by the angle  $\varphi$  as defined in Figure 32.

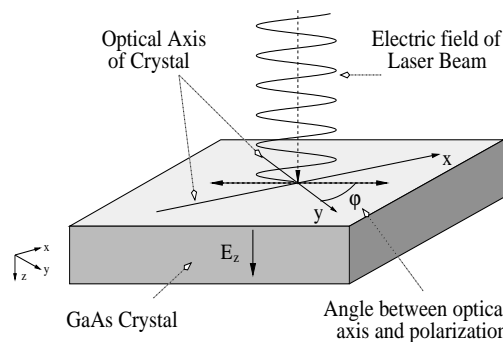


**Figure 32** Situation if the polarization of the laser beam is not aligned with the optical axis.

So in this case we will have to calculate the cavity response twice. We project the electric field of the laser onto the two optical axes of the crystal and we calculate the Fabry Perot response for both of them as given in Equation (84).

$$I_{\text{Laser(Reflected)}} = I_{\text{Incident}} \cdot \left( \cos(\varphi)^2 \cdot \frac{r^2 + R^2 + 2Rr \cos(\phi_X)}{1 + R^2 r^2 + 2Rr \cos(\phi_X)} + \sin(\varphi)^2 \cdot \frac{r^2 + R^2 + 2Rr \cos(\phi_Y)}{1 + R^2 r^2 + 2Rr \cos(\phi_Y)} \right) \quad (84)$$

$$\text{with } \phi_X = \frac{4\pi d}{\lambda_o} \cdot \left( n_o + \frac{1}{2} n_o^3 r_{41} E_Z \right) \text{ and } \phi_Y = \frac{4\pi d}{\lambda_o} \cdot \left( n_o - \frac{1}{2} n_o^3 r_{41} E_Z \right)$$

Following the deduction in Appendix E.8. on page 126, we can linearize both terms of Equation (84) in function of the applied electric field  $E_Z$ . By reasoning the same way as in the previous paragraph, we can describe the modulation in function of the angle  $\varphi$  (Equation (85)).

$$I_{\text{Modulation}}(\varphi) \approx \lambda_o n_o^2 r_{41} \cdot |\cos(2\varphi)| \cdot \left| \frac{\delta I_{\text{Ref}}}{\delta \lambda} \right| \cdot E_{\text{Microwave}} \quad (85)$$

So the magnitude of the modulation decreases with  $\cos(2\varphi)$  and vanishes when  $\varphi$  reaches  $\pi/4$  respectively  $45^\circ$ . So for this setup, we should not find any modulation at all if we align the polarization along the bisector of the two optical axes. So an accidental deviation of the polarization of  $\Delta\varphi$  off the optical axis will decrease the modulation with a factor proportional to  $1/(1 - 2\Delta\varphi^2)$ .

### 5.3 Modulation for an electric field $E_x + E_z$

In the previous paragraph we analyzed the case with well-defined optical axis ( $[-1/\sqrt{2}, 1/\sqrt{2}, 0]$  and  $[1/\sqrt{2}, 1/\sqrt{2}, 0]$ ) imposed by the direction of the applied electric field parallel to the z-axis ( $[0, 0, 1]$ ). We assumed that the polarization of the incident laser was not perfectly aligned with the optical axis.

In this paragraph we will analyze the inverse case. We assume that the polarization of the laser beam is adjusted parallel to  $[1/\sqrt{2}, 1/\sqrt{2}, 0]$  which allows the probing of an applied electric fields parallel to the z-axis. It might be that the electric field is changing its direction after the adjustment of the polarization or that the laser beam will be displaced to another location on the DUT with a different electric field vector. With the direction of the electric field, the optical axes of the crystal will change. The polarization of the incident laser beam is not aligned anymore with the optical axis and hence the modulation will change. Under real conditions it is very likely that the electric field has a component normal to the z-axis. So we will analyze the configuration displayed in Figure 33.

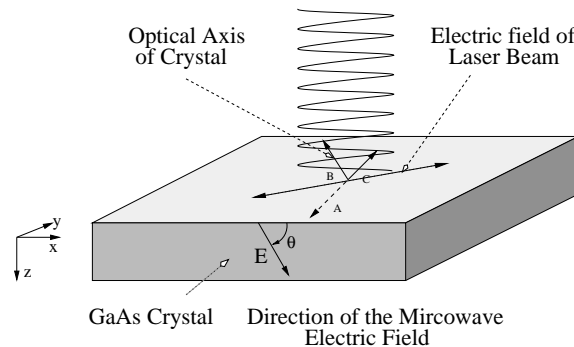


**Figure 33** The laser beam is focused on the GaAs crystal with a polarization parallel to the vector  $[1/\sqrt{2}, 1/\sqrt{2}, 0]$ . The direction of the applied electric field is given by  $[\cos(\theta), 0, \sin(\theta)]$ .

In Figure 33 the applied electric field has the direction given in Equation (86), where  $E_{\text{Amplitude}}$  indicates the magnitude of the microwave electric field and  $\theta$  is the angle between the x-axes and the electric field vector.

$$\vec{E} = E_{\text{Amplitude}} \cdot \begin{bmatrix} \cos(\theta) \\ 0 \\ \sin(\theta) \end{bmatrix} \quad (86)$$

By using Equation (57) to (59) we can determine the orientations of the three optical axis in function of the angle  $\theta$ . These vectors are normalized to simplify the further calculations. So we have got  $\text{Vector}_1$ ,  $\text{Vector}_2$  and  $\text{Vector}_3$  for the three directions of the optical axes.

$$\text{Vector}_1 = \begin{bmatrix} -\cos(\theta) \\ 0 \\ \sin(\theta) \end{bmatrix}, \text{Vector}_2 = \begin{bmatrix} \frac{\sin(\theta)}{\sqrt{2}} \\ -\frac{1}{\sqrt{2}} \\ \frac{\cos(\theta)}{\sqrt{2}} \end{bmatrix}, \text{Vector}_3 = \begin{bmatrix} \frac{\sin(\theta)}{\sqrt{2}} \\ \frac{1}{\sqrt{2}} \\ \frac{\cos(\theta)}{\sqrt{2}} \end{bmatrix} \quad (87)$$

For the further calculations we project the electric field vector defined in Equation (86) on the optical axes defined in Equation (87). For each of the three optical axes, we calculate the response of the Fabry Perot cavity. For following calculation, we assume that the reflection coefficients  $R$  as well as  $r$  are identical for all three optical axis. By inserting the result of Appendix E.9. on page 127, we get for the reflected intensity a sum of the three terms corresponding each with an optical axis (Equation (88)).

$$I_{\text{Laser(Reflected)}} = \quad (88)$$

$$\frac{\cos(\theta)^2}{2} \cdot \frac{r^2 + R^2 + 2Rr \cos(\phi_1)}{1 + R^2 r^2 + 2Rr \cos(\phi_1)} + \frac{(1 + \sin(\theta))^2}{4} \cdot \frac{r^2 + R^2 + 2Rr \cos(\phi_2)}{1 + R^2 r^2 + 2Rr \cos(\phi_2)} + \frac{(1 - \sin(\theta))^2}{4} \cdot \frac{r^2 + R^2 + 2Rr \cos(\phi_3)}{1 + R^2 r^2 + 2Rr \cos(\phi_3)}$$

with  $\phi_1 = \frac{4\pi d n_o}{\lambda_o}$ ,  $\phi_2 = \frac{4\pi d}{\lambda_o} \cdot \left( n_o + \frac{1}{2} n_o^3 r_{41} E_{\text{Amplitude}} \right)$  and  $\phi_3 = \frac{4\pi d}{\lambda_o} \cdot \left( n_o - \frac{1}{2} n_o^3 r_{41} E_{\text{Amplitude}} \right)$

We linearize the three independent terms of Equation (88) in function of the applied electric field  $E_{\text{Amplitude}}$ . By reasoning the same way as in the previous paragraphs, we can describe the modulation in function of the angle  $\theta$  by Equation (89).

$$I_{\text{Modulation}} = \left( \frac{1 + \sin(\theta)^2}{2} \right) \left| \frac{\partial I_{\text{Reflected}}}{\partial \lambda_o} \right| \cdot n_o^2 r_{41} \lambda_o E_{\text{Microwave}} \quad (89)$$

We have to make some comments about this result. If the applied electric field is parallel to z-axis,  $\theta$  becomes  $\pi/2$  and thus we find again the result of Equation (83). On the other hand if the electric field vector is parallel to the x-axis, the modulation decrease to a half but it will not vanish. Hence the modulation is not proportional to projection of the electric field vector on the z-axis or proportional to  $\sin(\theta)^2$ . So our probing setup is also sensible to the electric field normal to the z-axis as mentioned in [ 24 ] and [ 25 ].

## **5.4 Comment**

The mathematical description of the amplitude modulation is straight forward compared to the other modulation techniques described in the following paragraphs. It is valuable to have a simple relation between the applied electric field and the probed intensity. Hence we can calculate the searched electric field. The only theoretical inconvenience is the fact that the results are wrong if the applied field is not parallel to the z-axis.

## 6 Polarization modulation

In most publications about electro-optic sampling systems, a slightly different configuration is used. The polarization is aligned between the two optical axes. So the state of polarization is modulated in function of the applied electric field. As proposed in [ 24 ] and [ 25 ], we analyze this configuration for the same conditions as the amplitude modulation.

### 6.1 Setup

The continuous wave (CW) laser beam is focused beside a microwave guide as shown in Figure 34. The alignment of the polarization is between the two optical axes of the crystal. The polarization state of the reflected laser beam is modulated in function of the applied field  $E_z$  of the microwave signal. A beam splitter is used as an analyzer. This analyzer is aligned rectangular to the incident polarization and so converts the polarization modulation into an amplitude modulation which can be detected by a photodiode.

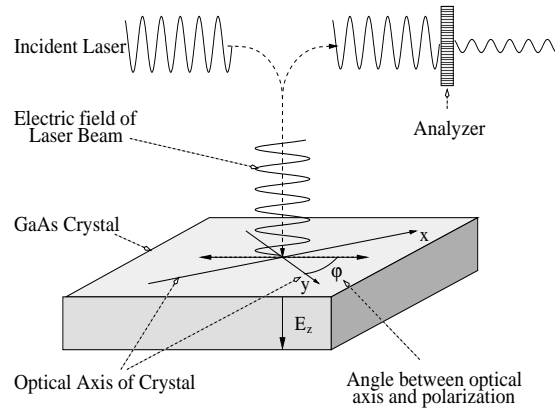


**Figure 34** Configuration using the polarization shift to measure the microwave signal.

### 6.2 Modulation

By using the result of Appendix E.10. on page 130, we can estimate the intensity at the output of the analyzer. Thus the polarization state modulation is given by Equation (90). We assume that the reflection coefficient  $r$  and  $R$ , the refractive index  $n_o$  and electro-optic coefficient  $r_{41}$  of GaAs as well as the substrate thickness  $d$  are constant parameters. For the examination of the modulation the amplitude of the electric field  $E_{\text{Microwave}}$  is also fixed. The wavelength  $\lambda_o$  is changing in a given range as well as the angle between the angle  $\varphi$  does.

$$I_{\text{Polarizer}}(E_z, \lambda_o, \varphi) \approx I_{\text{Incident}} \cdot \sin(2\varphi)^2 \cdot \frac{\sin\left(\frac{2\pi d n_o^3 r_{41} E_z}{\lambda_o}\right)^2 \cdot R^2 (1 - r^2)^2}{\left(1 + r^2 R^2 + 2rR \cos\left(\frac{4\pi d}{\lambda_o} n_o\right)\right)^2} \quad (90)$$

Before we will print out the modulation caused by Equation (90), we discuss the influence of the different variables. First we have a look at the microwave signal  $E_z$ . If  $E_z$  is zero, there will be no birefringence and hence no light will pass the analyzer. If  $E_z$  is not zero, the output intensity is proportional to  $\sin(E_z)^2$  and hence the frequency of the modulated laser beam is twice the frequency of the microwave signal. This effect is due to the fact that the laser beam intensity cannot become negative.

The term  $\sin(2\varphi)^2$  becomes maximal if  $\varphi$  is equal to  $\pi/4$ . Hence we have a maximal modulation if we align the laser beam polarization along the bisector of the optical axes of the crystal. The polarization before the analyzer and hence the intensity at the output wont change at all if the polarization of the incident laser beam is parallel to one of the optical axis of the GaAs substrate as  $\sin(\varphi = 0) = 0$ .

As we can see in Equation (90), the resulting modulation is also a function of the wavelength  $\lambda_0$ . For an ‘efficient’ modulation we chose the wavelength  $\lambda_0$  in a way that  $\cos(4\pi dn_0/\lambda_0) = -1$ . Hence the denominator becomes minimal. The wavelength  $\lambda_0$  also appears in the numerator but there the modulation increases with the decreasing wavelength. So we should chose the shortest technical possible wavelength so that denominator is minimal.

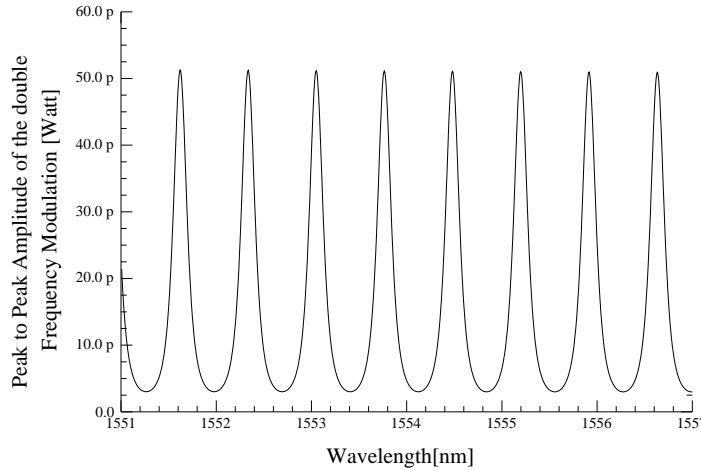


**Figure 35** Amplitude at the output of the analyzer. For this figure we used the following parameters:  $n_o=3.374$ ,  $r_{41}=1.42 \cdot 10^{-12}$  [m/V],  $r=0.54$ ,  $R=0.63$  (-2 [dB]),  $d=500$  [ $\mu\text{m}$ ],  $E_{\text{Microwave}}=1$  [V]/d [m] and  $P_{\text{Incident}}=1$  [mW].

The polarization state of the reflected laser beam is changing in function of the microwave signal that causes the modulation. For further analysis, it is of some interest to estimate the maximal variation as this effect can also appear accidentally.

We want to investigate if there are major changes (e.g. turning of 45 degrees or circular polarization) or if it remains unchanged. As a general analysis would be too complicated, we just try to estimate it numerically. We do this by comparing the components parallel and normal to analyzer. As we can see in Figure 35, the maximal component parallel to the analyzer is about  $I_{\text{Parallel}}=50$  [pW]. By using the Fabry Perot response of Figure 28, the minimal component normal to the direction of the analyzer is about  $I_{\text{Normal}}=20$  [ $\mu\text{W}$ ]. In the worst case we have normal component of 20 [ $\mu\text{W}$ ] and a parallel one of 50 [pW]. By assuming that the reflected laser beam is polarized linearly, we can calculate the angle  $\Delta\varphi$  between the polarization of the incident beam and the reflected one. So with this configuration, the polarization state is slightly modified by the microwave signal as we can see in Equation (91).

$$\Delta\varphi \sim \text{ArcTan}\left(\frac{I_{\text{Parallel}}}{I_{\text{Normal}}}\right) = \text{ArcTan}\left(\frac{50 \cdot 10^{-12} [\text{W}]}{20 \cdot 10^{-6} [\text{W}]}\right) \sim 0.0001 [^\circ] \quad (91)$$

### 6.2.1 Polarization modulation with a wave plate

In most applications using the polarization modulation, the configuration is slightly different. In Equation (90), the magnitude of the modulation is proportional to  $\sin(\rho = 2\pi d n_0^3 r_{41} E_z / \lambda_0)^2$ , which is unfavorable for the modulation because of the vanishing derivative of  $\sin(\rho)^2$  and as  $\rho$  remains very small. The  $\sin(\rho)^2$  proportionality causes also the doubling of the modulated signal frequency. In most application a  $\lambda/4$  wave plate is introduced to overcome this problem. In our probing tool, we would have to introduce a  $\lambda/8$  wave plate which would be passed twice. The optical axis of the wave plate would have the same directions as the optical axis of the GaAs crystal. The intensity at the output of the analyzer is given by Equation (92) according to Appendix E.11. on page 132.

$$I_{\text{Output}}(E_z, \lambda_0, \varphi) = I_{\text{Incident}} \frac{\sin(2\varphi)^2}{4} \quad (92)$$

$$\frac{(r^2 + R^2 + 2rR \cos(\phi_1))(1 + r^2 R^2 + 2rR \cos(\phi_2)) + \Pi + (r^2 + R^2 + 2rR \cos(\phi_2))(1 + r^2 R^2 + 2rR \cos(\phi_1))}{(1 + r^2 R^2 + 2rR \cos(\phi_1)) \cdot (1 + r^2 R^2 + 2rR \cos(\phi_2))}$$

$$\text{with } \Pi = -4 \cdot (r \cdot (1 - r^2) \cdot R \cdot (R(1 + r^2) \cos\left(\frac{\phi_1 - \phi_2}{2}\right) + r(1 + R^2) \cos\left(\frac{\phi_1 + \phi_2}{2}\right))) \cdot \sin\left(\frac{\phi_1 - \phi_2}{2}\right),$$

$$\phi_1 \approx \frac{4\pi d}{\lambda_0} n_0 + \frac{1}{2} n_0^3 r_{41} E_z \quad \text{and} \quad \phi_2 \approx \frac{4\pi d}{\lambda_0} \left(n_0 - \frac{1}{2} n_0^3 r_{41} E_z\right)$$

The introduced  $\pi/2$  phase shift changes the working point and hence the modulations. As the intensity at the output does not vanish in the absence of  $E_z$ , we have to use Equation (93) to compute the peak to peak modulation as plotted in Figure 36. An analytical solution would be too complicated.

$$I_{\text{Modulation}}(E_{\text{Microwave}}, \lambda_0, \varphi) = |I_{\text{Output}}(E_z = E_{\text{Microwave}}, \lambda_0, \varphi) - I_{\text{Output}}(E_z = -E_{\text{Microwave}}, \lambda_0, \varphi)| \quad (93)$$

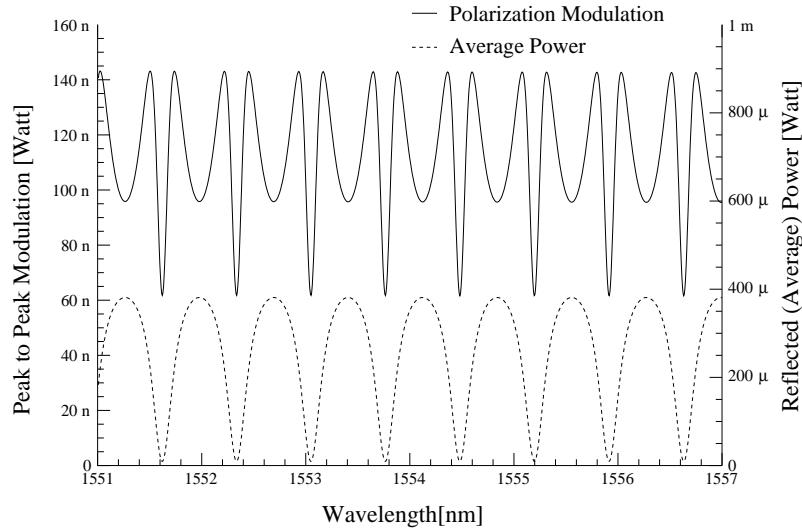


**Figure 36** “Peak to peak” modulation and the reflected intensity at the output of the analyzer. The delay of  $\lambda/4$  is caused by the two pass of the  $\lambda/8$  wave plat. For this example we used the same parameters as in the previous example:  $n_0=3.374$ ,  $r_{41}=1.42 \cdot 10^{-12}$  [m/V],  $r=0.54$ ,  $R=0.63$  (-2 [dB]),  $d=500$  [ $\mu\text{m}$ ],  $E_{\text{Microwave}}=1$  [V] /  $d$  [m] and  $P_{\text{Incident}}=1$  [mW].

Different measurement techniques use other possibilities to boost the polarization modulation. One possibility is to increase the path length through the electro-optic crystal. So the polarization has “more time” to “turn more”. Also crystals with higher electro-optic coefficients than the GaAs one can be used to probe the electric signal. Another option is the use of a pulsed laser with very high output power. So by adjusting all this parameter, it should not be a problem to obtain a decent signal level.

### **6.3 Comment**

There are several reasons, why we do not use a probing technique based on polarization modulation. Without introducing a wave plate, the magnitude of the calculated signal is much weaker than the results obtained in chapter 5 and the modulation frequency is twice the frequency of the microwave signal. Hence we would have to use a  $\lambda/8$  wave plate (difficult to obtain). The  $\lambda/8$  wave plate complicates the mathematical description. We cannot find an exploitable relation between the electric field  $E_{\text{Microwave}}$  and the intensity of the modulation  $I_{\text{Modulation}}$  comparable to Equation (83).

The technical disadvantage of the polarization modulation is the difficulty to handle the state of polarization in standard optical fibers or in polarization maintaining fiber used in our setup. Very often the polarization is turning very slowly in standard optical fibers and polarization maintaining fibers insert another unknown birefringence.

## 7 Phase modulation

The phase modulation is another possible configuration for the probing of the electric field. Though this technique is used very often in pigtailed fiber optical modulators, it is rarely used in electro-optic probing. We just have a look at it to complete the comparison.

### 7.1 Setup

For the phase modulation, we split the incident laser beam into two CW beams of equal power as shown in Figure 37. The first one is injected into the DUT with the polarization parallel with the optical axis of the crystal. The second part is delayed and it is used as reference beam. Afterwards both parts are recombined and the interferences caused by the phase shift are used to obtain an amplitude modulation.

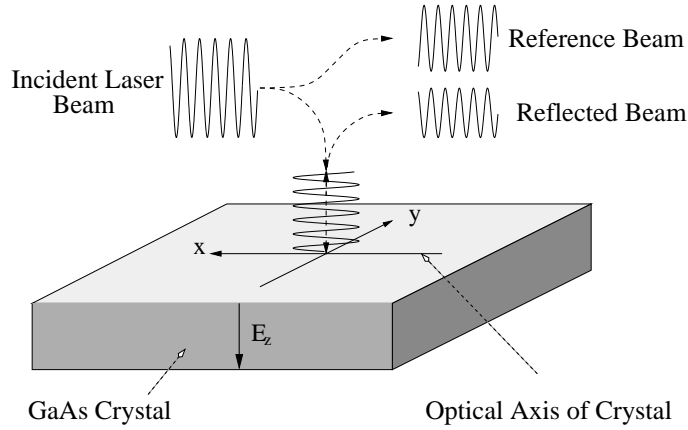


**Figure 37** Configuration using the phase shift between the reflected and a reference beam to measure the signal.

The principle of phase modulation can be described by Equation (94), where  $E_{\text{Laser,Output}}$  is the resulting electric field of the recombined beam in function of the electric field  $E_z$  of the microwave signal and the wavelength of the laser  $\lambda_0$ .

$$E_{\text{Laser,Output}}(E_z, \lambda_0) = E_{\text{Laser,Input}} \left( \frac{1}{2} \cdot A_{\text{Probe}}(E_z, \lambda_0) \cdot e^{-i\vartheta_{\text{Probe}}(E_z, \lambda_0)} + \frac{1}{2} \cdot A_{\text{Reference}} \cdot e^{-i\vartheta_{\text{Reference}}(\lambda_0)} \right) \quad (94)$$

The further parameters are the field of the incident laser beam  $E_{\text{Laser,Input}}$ , the attenuation and phase shift of the reference beam given by  $A_{\text{Reference}}$  and  $\vartheta_{\text{Reference}}$  and the same parameters for the beam passing through the DUT defined by  $A_{\text{Probe}}$  and  $\vartheta_{\text{Probe}}$ .

For an optimal phase modulation, the difference between the phase shift  $\vartheta_{\text{Probe}}$  and  $\vartheta_{\text{Reference}}$  should be  $\pi/2$ . So we obtain a linear response in function of electric field. In our setup, the situation is more complicated as  $\vartheta_{\text{Probe}}$  depends also on the wavelength  $\lambda_0$  and not only on the electric field  $E_z$ . So for the further mathematical analysis of the phase modulation, we define the reference phase shift as  $\vartheta_{\text{Reference}} = \vartheta_{\text{Probe}}(E_z = 0, \lambda_0) + \pi/2$ . For  $A_{\text{Reference}}$  we have a similar problem. For an efficient phase modulation,  $A_{\text{Probe}}$  and  $A_{\text{Reference}}$  should be equal to obtain a good contrast. Unfortunately  $A_{\text{Probe}}$  is changing in function of  $\lambda_0$ . In this case we set  $A_{\text{Reference}}$  to one. So with Appendix E.12.

on page 134 we can express the intensity of the modulated beam  $I_{\text{Response}}$  by Equation (95).

$$I_{\text{Response}}(E_z, \lambda_o) = \frac{I_{\text{Incident}}}{4} \cdot (1 + A_{\text{Probe}}^2 + 2A_{\text{Probe}} \cdot \cos(\vartheta_{\text{Probe}} - \vartheta_{\text{Reference}})) \quad (95)$$

$$\text{with } A_{\text{Probe}} = \sqrt{\frac{r^2 + R^2 + 2Rr\cos(\phi)}{1 + R^2r^2 + 2Rr\cos(\phi)}}, \quad \vartheta_{\text{Probe}} = \text{ArcTan}\left(\frac{R(r^2 - 1)\sin(\phi)}{r(1 + R^2) + \cos(\phi)R(1 + r^2)}\right), \text{ and}$$

$$\phi \approx \frac{4\pi d}{\lambda_o} \left( n_o + \frac{1}{2}n_o^3r_{41}E_z \right)$$

For illustration, we compute the response for the same parameters as in the previous paragraphs. For the calculations of the modulation we use an approach similar to Equation (93). In Figure 38 we can see that the results of the phase modulation is similar to the magnitudes of the other modulations.

In Equation (95) the modulation is not only caused by the phase shift between the reference and the probe beam. The term  $A_{\text{Probe}}$  is also changing in function due to the amplitude modulation. So the obtained modulation is caused by the amplitude modulation as well as by the phase modulation.

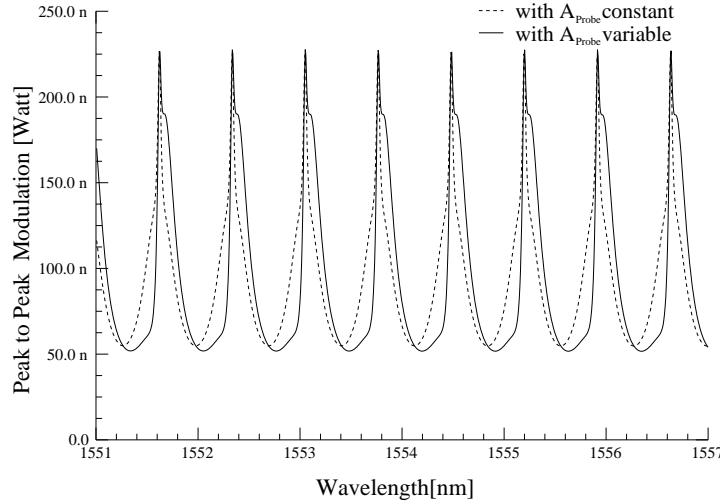


**Figure 38** Amplitude of the output of the phase modulations. For this figure we used the following parameters:  $n_o=3.374$ ,  $r_{41}=1.42 \cdot 10^{-12}$  [m/V],  $r=0.54$ ,  $R=0.63$  (-2 [dB]),  $d=500$  [ $\mu\text{m}$ ],  $E_{\text{Microwave}}=1$  [V] /  $d$  [m] and with  $P_{\text{Incident}}=1$  [mW]. You have to notice that  $A_{\text{Probe}}$  is changing in function of the applied electric field  $E_z$ . So we computed a graph where  $A_{\text{Probe}}$  is constant and another one where  $A_{\text{Probe}}$  is changing.

## 7.2 Comment

There are several reasons why we do not use a probing technique base on the phase modulation. As for the polarization modulation, the mathematical description is complicated. Again we cannot provide an exploitable relation between the electric field  $E_z$  and the intensity of the modulation  $I_{\text{Modulation}}$  comparable to Equation (83).

There are also some technical inconveniences with the phase modulation. For an optimal modulation, we have to adjust the wavelength  $\lambda_o$  of the incident laser beam according to Figure 38. In function of this wavelength we would have to introduce a delay of  $\lambda/4$  into the reference branch to cause the  $\pi/2$  phase shift.

## 8 Other considerations & Problems

In this chapter we will do some further theoretical analysis. We will take into account that a “real” laser beam is not a plane wave and so it diverges during propagation. This will cause further loss and it will limit the spatial resolution. At the end we will do some auxiliary considerations.

### 8.1 Gaussian beam

At the beginning of chapter 4, we did several assumptions to simplify the calculations. One of the assumption was that the incident laser beam is perfectly parallel. With other words the wave front should be a plane wave of a given width as displayed in Figure 39 and Figure 40. Unfortunately this simplification is rather coarse as the plane wave of Figure 39 does not even satisfy the Maxwell equations for electro-magnetic waves. As we assumed that the laser beam is a TEM (Transverse Electro Magnetic) wave, it cannot take into account the focus onto a small spot. One possibility to describe mathematically a laser beam is the formalism of a Gaussian beam.

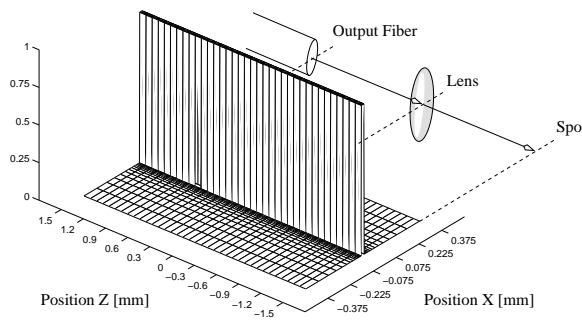


**Figure 39** In this figure we plot the magnitude of the electric field as a function of the Z-axis (direction of propagation) and the X-axis (distance from the center of the beam). In this case we have at the output of the fiber a 10 [μm] wide plane wave.

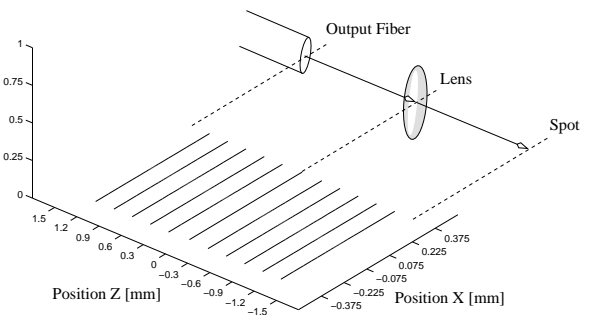


**Figure 40** The isometric lines of the wavevector  $k$  for the beam of Figure 39.

We can solve the Maxwell equation under the condition that the laser beam is propagating in a given direction ([ 5 ],[ 12 ]). One possible solution is the Gaussian beam. The solution is called the Gaussian beam because the spatial distribution of the beam intensity is proportional to the Gaussian or normal distribution. In Equation (96)  $r^2=x^2+y^2$  indicates the distance from the center of the laser beam as defined in Figure 41.  $W(z)$  is called the beam waist given in function of the position  $z$ ,  $W_0$  is  $W(z=0)$  and  $I_0$  represents the intensity of the Gaussian beam.

$$I(r, z) = I_0 \cdot \frac{W_0^2}{W(z)^2} \cdot e^{-\frac{2 \cdot r^2}{W(z)^2}} \quad \text{with} \quad \int_0^{\infty} I(r, z) \cdot 2\pi r \cdot dr = \frac{I_0 \cdot \pi \cdot W_0^2}{2} \quad (96)$$

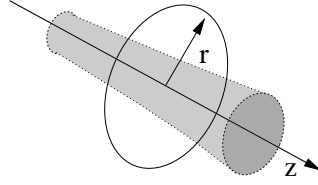


**Figure 41** The direction of propagation  $z$  and the distance from the center of the laser beam normal to  $z$ .

As indicated in the second part of Equation (96), the integral of the Gaussian distribution is always constant and does not depend on the parameter  $W(z)$ . So the energy in the laser beam is preserved but the distribution is changing with the position.

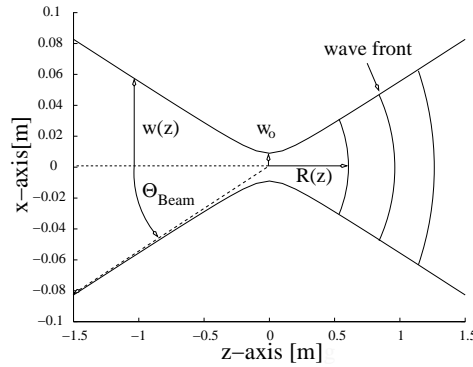


**Figure 42** Definition of the parameters of a Gaussian beam.

For the following deduction, we use the distribution of the electric field instead of the distribution of the intensity. So we can compute the electric field distribution for a given position with Equation (97).

$$E(r, z) \sim \frac{1}{q(z)} \cdot e^{-i \frac{kr^2}{2q(z)}} \quad (97)$$

It is important to notice that the parameter  $q(z)$  defines the entire electric field distribution of a laser beam. For the further deductions we will call  $q(z)$  the complex beam parameter. By using [ 5 ] we can define this parameter by Equation (98). The parameter  $\lambda_0$  is the wavelength of the laser beam in vacuum and  $R(z)$  is the wave front curvature. The beam waist  $W(z)$  indicates the distance where the beam intensity drops to  $1/e^2$  or to 0.135 of the maximal value in the center of the beam. Further  $W_0$  is defined as the minimal radius (usually at  $z=0$ ),  $z_0$  is an auxiliary variable called the Rayleigh length and  $n_{\text{Material}}$  is the refractive index of material as defined in Figure 42.

$$\frac{1}{q(z)} = \frac{1}{R(z)} - i \cdot \frac{\lambda}{\pi W(z)^2} \quad \text{with} \quad (98)$$

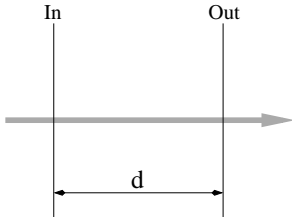
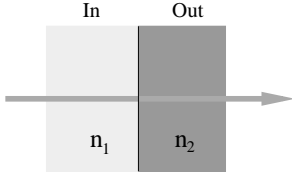
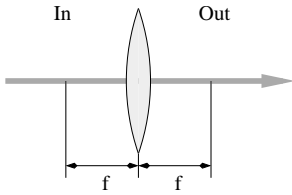
$$R(z) = z \cdot \left( 1 + \left( \frac{z_0}{z} \right)^2 \right), \quad W(z) = W_0 \cdot \sqrt{1 + \left( \frac{z}{z_0} \right)^2} \quad \text{and} \quad z_0 = \frac{\pi W_0^2 n_{\text{Material}}}{\lambda_0}$$

By passing through a lens or a dielectric or by propagating through free space the Gaussian beam will change and so the complex beam parameter  $q(z)$  will be modified. For some simple cases, the

modifications of  $q(z)$  can be expressed by Equation (99),

$$q_{\text{Out}}(z) = \frac{A \cdot q_{\text{In}}(z) + B}{C \cdot q_{\text{In}}(z) + D} \quad (99)$$

where A, B, C and D are elements of the ray transformation matrix. Table 2 gives several transformation matrices for common laser beam manipulations.

Straight propagation passing a distance d.		$\begin{bmatrix} A & B \\ C & D \end{bmatrix} = \begin{bmatrix} 1 & d \\ 0 & 1 \end{bmatrix}$
Interface between two dielectric materials with refractive indices $n_1$ respective $n_2$ .		$\begin{bmatrix} 1 & 0 \\ 0 & \frac{n_1}{n_2} \end{bmatrix}$
Lens with a focal distance f.		$\begin{bmatrix} 1 & 0 \\ -\frac{1}{f} & 1 \end{bmatrix}$

**Table 2** Transformation matrices for some standard operations [ 12 ].

So by knowing the complex beam parameter  $q(z)$  at a given position we can compute the spatial distribution of the electric field by using Equation (100) [ 5 ], where  $k=2\pi n_{\text{Material}}/\lambda_o$  is the wavevector of the beam.

$$E(x, y, z) \sim \frac{W_o}{W(z)} \cdot e^{-\left(\frac{r^2}{W(z)^2}\right)} \cdot e^{-i \cdot \left(kz + \frac{k \cdot r^2}{2R(z)} - \text{ArcTan}\left(\frac{z}{z_o}\right)\right)} \quad (100)$$

With the Gaussian formalism, we can also estimate the beam divergence. The angular divergence  $\theta_{\text{Beam}}$  of the beam is therefore defined by Equation (101).

$$\theta_{\text{Beam}} = \text{ArcTan}\left(\frac{\lambda_o}{\pi W_o n_{\text{Material}}}\right) \approx \frac{\lambda_o}{\pi W_o n_{\text{Material}}} \quad (101)$$

For our probing technique, we will use a pigtailed injector. So our probing beam will leave an optical fiber, will spread out and a lens will focus it onto a spot. For illustration we computed the electric field distribution of such a laser beam in Figure 43 and Figure 44.

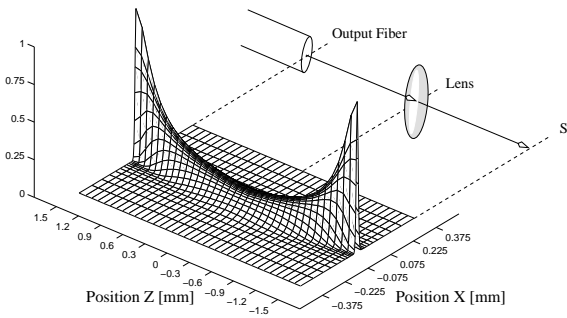


**Figure 43** In this figure we plot the magnitude of the electric field in function of the Z-axis (direction of propagation) and the X-axis (distance from the center of the beam) for a Gaussian beam. As well as in Figure 39 we have a  $w_0=10$  [ $\mu\text{m}$ ] wide beam at the output of a fiber.

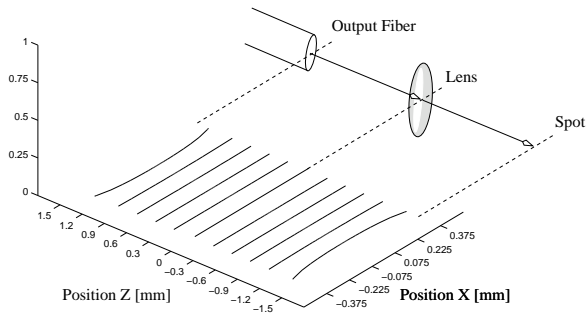


**Figure 44** The isometric lines of the wavevector  $k$  for the beam of Figure 43.

The disadvantage of the Gaussian beam formalism is that analytic calculations are only possible for very simple configuration e.g. the passing of a laser beam through a lens or the reflection on a mirror. There is hardly any possibility to analyze the reflection or transmission of a Gaussian beam at the interface between two dielectric materials. The reason is the angle of incidence which is not the same for the entire beam. So we could not use this formalism to improve the calculation of the cavity but we could apply it to estimate the spot size of the incident laser beam and the losses due to an improper reinjection into the optical fiber.

## 8.2 Spot Size and spatial resolution

The spatial resolution is a measure for the size of the probe. If the spatial resolution is coarse, the size of the probe is big and hence a big region will influence the probing result. A small probe size and hence a good spatial resolution is required for the probing of integrated devices.

The spatial resolution of our probing tool is given by the beam waist of the laser beam. A small beam waist will improve the spatial resolution. But by decreasing the beam waist, we will increase the divergence or Numerical Aperture (NA) of the laser beam. By using the formalism of the Gaussian beam, we will adapt the calculation made by [ 7 ] to our configuration and try to find the best trade off.

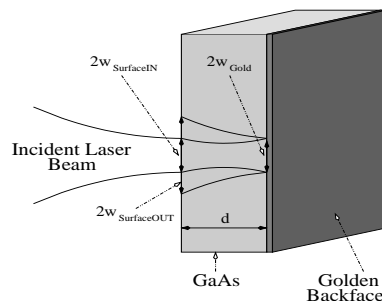


**Figure 45** Calculation of the minimal spot size [ 7 ].

We have a look at the value of  $2w_{\text{SurfaceIN}}$  and  $2w_{\text{SurfaceOUT}}$  given in Figure 45. For symmetry rea-

sons, we get the smallest spatial resolution when  $w_{\text{SurfaceIN}}=w_{\text{SurfaceOUT}}$ . Hence the Gaussian beam has its smallest diameter on the golden back face of the cavity or with other words the focus of the laser beam is on this point. In our further deduction we will see that this choice minimize also the losses of power in the cavity. Hence the spatial resolution is defined by the beam waist  $w_{\text{Surface}}$  at the air / GaAs interface.

### 8.2.1 Spot size without cavity

As introduction to the Gaussian formalisms, we calculate the characteristics of our laser beam in free space without the cavity. For the analysis of the setup given in Figure 46, we use the formalism explained in paragraph 8.1. The laser beam is leaving the end of the optical fiber as a plane wave and so its wave front curvature  $R$  is infinite respectively the real part of complex beam parameter  $q_{\text{Fiber}}$  is zero. Its beam waist is  $w_{\text{Fiber}}$  or half the Mode Field Diameter (MFD). Afterwards the beam is propagating a distance  $A$ , is focused by a lens with a focal distance  $f$  and propagates again another distance  $B$ . In the focal point the wave front curvature has to be infinite again.

In this setup, the given parameters are the wavelength  $\lambda_o$  of the laser, the beam waist at the output of the optical fiber  $w_{\text{Fiber}}$  as well as the refractive index of the surrounding air  $n_{\text{Air}}$ . Also known are the focal distance of the lens  $f$  and the distance  $A$  between the lens and fiber output. The wanted parameters are the distance  $B$  and the beam waist  $w_{\text{spot}}$  in the spot.

With the given information there is no problem to calculate the complex beam parameter for the laser beam at the output of the fiber. By defining  $z_o = \pi w_{\text{Fiber}}^2 n_{\text{Air}} / \lambda_o$  we can rewrite  $q_{\text{Fiber}}$  as Equation (102).

$$q_{\text{Fiber}} = \frac{i \cdot \pi w_{\text{Fiber}}^2 n_{\text{Air}}}{\lambda_o} = i \cdot z_o \quad (102)$$

By using Table 2 on page 45, it is easy to find the transformation matrix of the setup. It is the product of the two propagation transformation matrices and the transformation matrix of the lens. With the transformation matrix we can get the complex beam parameter  $q_{\text{Spot}}$  in function of the unknown variable  $B$ . In the focal point the wave front curvature has to be infinite or with other words the real part of the complex parameter  $q_{\text{Spot}}$  has to be zero. By exploiting this condition we can find a solution for  $B$ . By using the results of Appendix E.13. on page 135 we can express the distance  $B$  as Equation (103).

$$B = \frac{f(A(A-f) + z_o^2)}{(A-f)^2 + z_o^2} \quad \text{with } z_o = \frac{\pi w_{\text{Air}}^2 n_{\text{Air}}}{\lambda_o} \quad (103)$$

At the first sight the result is unexpected because it is not identical with the known result from ray optics. If we assume that the beam waist at the fiber output becomes very small ( $w_{\text{Fiber}} \rightarrow 0$ ) the parameter  $z_o$  also vanishes ( $z_o \rightarrow 0$ ). In this case we get the expected result given in Equation (104).

$$B = \lim_{z_o \rightarrow 0} \frac{f(A(A-f) + z_o^2)}{(A-f)^2 + z_o^2} = \frac{fA}{A-f} \quad (104)$$

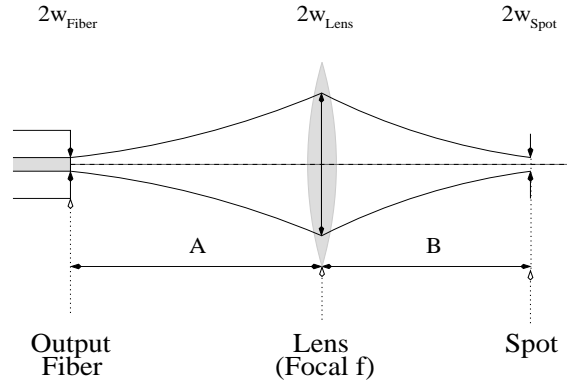


**Figure 46** Calculation of the spot size and the focal distance with a lens at the fiber output.

Considering that  $B$  is not unknown anymore, we can determine the complex beam parameter  $q_{\text{Spot}}$ . According to Appendix E.13. on page 135 it is given by Equation (105).

$$q_{\text{Spot}} = \frac{f^2}{(f - A)^2 + z_0^2} \cdot q_{\text{Fiber}} \quad (105)$$

By using the definition of complex beam parameter we can resolve the previous equation in function of the beam waist. So we get Equation (106).

$$w_{\text{Spot}} = w_{\text{Fiber}} \cdot \sqrt{\frac{f^2}{(f - A)^2 + z_0^2}} \quad (106)$$

There are several points to discuss about this result. First we will consider the case where the distance  $A$  is equal to  $B$ . In this case the magnification factor is one. The magnification factor is defined as the factor  $B / A$ . With some additional calculations you can prove that in this situation  $A$  becomes  $f + \sqrt{f^2 - z_0^2}$ . If we put this into Equation (106) we will see that both beam waists are equal.

It is also interesting to compare the theoretical values with the specification of some real pigtailed focuser with a magnification factor of one. By using the data of Table A.2.3 on page 106 we can determine the mode field diameter of a monomode fiber. Hence the theoretical spot size of a pig-tailed focuser using standard monomode fiber is given by Equation (107).

$$2w_{\text{Spot}} = 10.8 \text{ } [\mu\text{m}] \quad (107)$$

This value agrees with the specifications of commercial injectors used in our laboratory (Table A.2.5 on page 108) especially for the focuser with the shortest working distance. The differences for the focuser with longer working distances can be explained by the increasing influence of the spherical aberration. This is caused by the fact that the beam waist on the lens will increase with the working distance and so the aberrations as well.

### 8.2.2 Spot Size on the device

In this paragraph we will have a look at the different beam parameters if we focus the laser beam onto the back face of a GaAs substrate. Considering that we have to take into account an interface between air and a dielectric materials, the calculations become a little bit more complicated.

So we start with the description of the given parameters, as defined in Figure 47. Again we assume that the Gaussian beam is leaving the optical fiber as a plane wave with the beam waist  $w_{\text{Fiber}}$  equal to the half of the mode field diameter. We know the focal distance of the lens  $f$  and the distance  $A$  between the fiber output and the lens. Further we have the refractive indices of the surrounding air  $n_{\text{Air}}$  and of the GaAs substrate  $n_{\text{GaAs}}$  as well as the thickness of the substrate  $d$ .

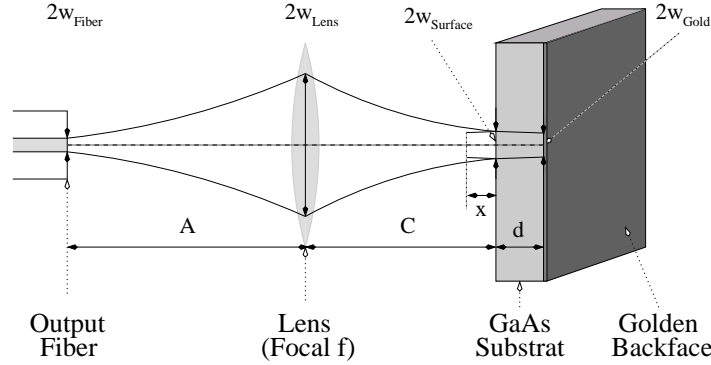


**Figure 47** Calculation of the beam parameters if the laser is focused into a GaAs substrate.

On the other hand we are interested in the beam waist in the focal point at the back face of the substrate  $w_{\text{Gold}}$  as well as in the beam waist on the front side of the GaAs  $w_{\text{Surface}}$ . Also we want to know the distance between the lens and the substrate surface  $C$  as well as the distance  $x$ . The parameter  $x$  indicates the distance between the surface of the substrate and the focal point of the reflections on the air / GaAs interface.

Apart that the calculations are more complicated than the one of the previous paragraph, there is no difference. We determine the complex beam parameter at the output of the fiber  $q_{\text{Fiber}}$ , then we calculate the transfer matrix of the setup and so the complex beam parameter in the focal point  $q_{\text{Gold}}$ . At the end we put the condition that the real part of  $q_{\text{Gold}}$  vanishes and so we determine the parameter  $C$ .

By using the conclusion of Appendix E.14. on page 138 we get for the distance  $C$  Equation (108).

$$C = \frac{f(A(A-f) + z_0^2)}{(f-A)^2 + z_0^2} - \frac{n_{\text{Air}}}{n_{\text{GaAs}}} d \quad (108)$$

For the beam waists we get Equation (109) and (110).

$$w_{\text{Gold}} = w_{\text{Air}} \cdot \sqrt{\frac{f^2}{(f-A)^2 + z_0^2}} \quad (109)$$

$$w_{\text{Surface}} = w_{\text{Gold}} \cdot \sqrt{1 + \left(\frac{d\lambda_0}{\pi w_{\text{Gold}}^2 n_{\text{GaAs}}}\right)^2} \quad (110)$$

At the end we can calculate  $x$  by subtracting  $B$  from  $C$ .

$$x = B - C = \frac{n_{\text{Air}}}{n_{\text{GaAs}}} d \quad (111)$$

As we defined  $2w_{\text{Surface}}$  as the spatial resolution, we can evaluate this parameter for several common

setups. Considering that all focusers used during the thesis had a magnification factor 1 (Appendix A.2.5. on page 108), we calculate the according beam waists given in Table 3. The real values will be larger due to spherical aberration and due to production flaws.

$w_{\text{Fiber}}^a$	A	$d_{\text{Substrate}}$	Focal Distance f	$w_{\text{Gold}}$	$w_{\text{Surface}}$	Spatial Resolution
5.4 [ $\mu\text{m}$ ]	$f + \sqrt{f^2 - z_0^2} \approx 10[\text{mm}]$	500 [ $\mu\text{m}$ ]	5 [mm]	5.4 [ $\mu\text{m}$ ]	16.4 [ $\mu\text{m}$ ]	32.8 [ $\mu\text{m}$ ]
5.4 [ $\mu\text{m}$ ]	$f + \sqrt{f^2 - z_0^2} \approx 10[\text{mm}]$	100 [ $\mu\text{m}$ ]	5 [mm]	5.4 [ $\mu\text{m}$ ]	6.3 [ $\mu\text{m}$ ]	12.6 [ $\mu\text{m}$ ]

**Table 3** Theoretical spatial resolutions.

- a. The value of  $w_{\text{Fiber}}$  is half of the Mode Field Diameter (MFD).

### 8.2.3 Modified Calculation for the Fabry Perot Cavity

In the previous calculations of the Fabry Perot response in paragraph 4.1, we assumed that the entire reflected beam is reinjected into the optical fiber. So we could express the reflection coefficients at the air / GaAs interface by the value defined by the Maxwell equations. For the reflection coefficient at the back face of the substrate we specified a loss of -2 [dB] to model the absorption losses and to avoid a reflection without loss.

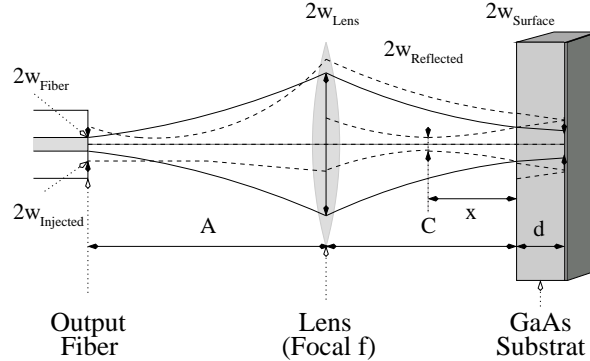


**Figure 48** Supplementary losses caused by the improper reinjection into the fiber.

If we reconsider the calculation by using the Gaussian formalism, we have to introduce supplementary losses coefficients due the beam divergence. In Figure 48 we can see that all reflections (except the first one from the gold back face) are not properly reinjected into the optical fiber. The problem is that the reinjection is different for each reflection and so we have to calculate different loss coefficients.

For the estimation of the supplementary attenuation coefficients, we calculate the complex beam parameter at the fiber output for the different reflections caused by the Fabry Perot Cavity. So we could deduce the beam waist of the beam ( $w_{\text{Injected}}$ ) reinjected into the fiber. As this diameter is greater than the mode field diameter of the fiber we calculate the attenuation coefficient in function of this parameter. For the calculation of this attenuation coefficient  $R_{\text{Attenuation}}$ , we assume that both Gaussian beam are approximately plane waves. In this case we can use the equation which describes the

losses due to mode field diameter mismatch between two single mode fibers as given in Equation (112).

$$\text{Loss}_{\text{MisMatch}} = \frac{4 \cdot \text{MFD}_1^2 \cdot \text{MFD}_2^2}{(\text{MFD}_1^2 + \text{MFD}_2^2)^2} \quad (112)$$

For the calculations of the Fabry Perot cavity, we use the electric field and not the intensity of the beam. Hence we use the root of  $\text{Loss}_{\text{MisMatch}}$  as proposed in Equation (113).

$$R_{\text{Attenuation}} = \frac{2 \cdot W_{\text{Injected}} \cdot W_{\text{Fiber}}}{W_{\text{Injected}}^2 + W_{\text{Fiber}}^2} \quad (113)$$

In Appendix E.15.2. we calculated the beam waist of the reinjected beam in function of the magnification factor and for the different reflections. The Figure 49 shows the additional attenuation coefficient for the reflection on the air / GaAs interface for several substrates with different thicknesses. The losses are negligible for the case  $A / \text{Focal Length} \sim 1$  as the laser beam is parallel and does not diverge. The losses decay also with the thickness of the substrate. In Figure 50 we plot the additional attenuation coefficient for the reflection on the back face. We calculated the attenuation for a substrate with a given thickness (500 [ $\mu\text{m}$ ]). We start with the first reflection on the golden back face in function of  $A / \text{Focal Length}$  (1 as this reflection is well reinjected into the fiber). Afterwards we calculate the attenuation coefficient for the higher order reflections. As we can see the loss increase with the order.

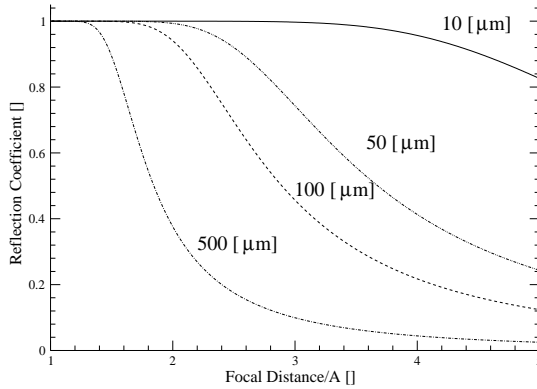


**Figure 49** Additional attenuation coefficient for the reflection from the air / GaAs interface due to the divergence of the laser beam.

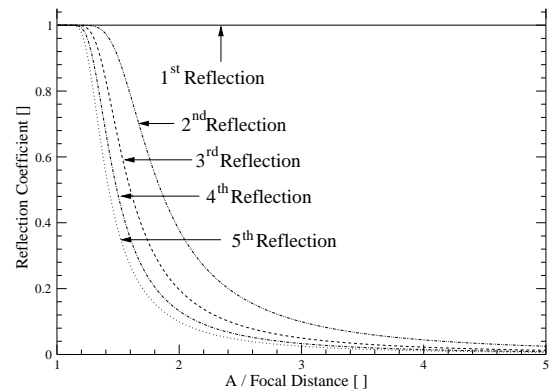


**Figure 50** Additional attenuation coefficient for the reflections from the golden back face due to the divergence of the laser beam.

As we will see during the measurements, the imprecise reinjection into the fiber causes an unpredictable problem. The divergence of the Gaussian beam induces an additional phase shift into system, similar to the problem exposed in [ 46 ]. It is difficult to say which reflection is shifted and so we choose to introduce the phase shift in the first reflection. So we can redefine the parameters of Equation (68).  $r^+$  (Equation (114)) is the new reflection coefficient of the air / GaAs interface where  $R_{\text{Front}}$  is the addition attenuation due to the beam divergence and  $e^{-i\Lambda}$  represents the additional phase shift.  $R^+$  (Equation (115)) is the modified reflection coefficient for the golden back face where  $R_{\text{Back}}$  specifies the additional loss. For simplification we assumed that  $R_{\text{Back}}$  is similar for all reflection from the back face.

$$r^+ = r \cdot R_{\text{Front}} \cdot e^{-i\Lambda} \quad (114)$$

$$R^+ = R \cdot R_{\text{Back}} \quad (115)$$

So we can recalculate the response of the Fabry Perot cavity as defined in Equation (116). In Figure 48 we plotted the corresponding response and the according derivative.

$$I_{\text{Reflected}}(\phi, \Lambda) = I_{\text{Incident}} \frac{(r \cdot R_{\text{Front}})^2 + (R \cdot R_{\text{Back}})^2 + 2(r \cdot R_{\text{Front}} \cdot R \cdot R_{\text{Back}}) \cos(\phi - \Lambda)}{1 + (r \cdot R_{\text{Front}} \cdot R \cdot R_{\text{Back}})^2 + 2(r \cdot R_{\text{Front}} \cdot R \cdot R_{\text{Back}}) \cos(\phi + \Lambda)} \quad (116)$$

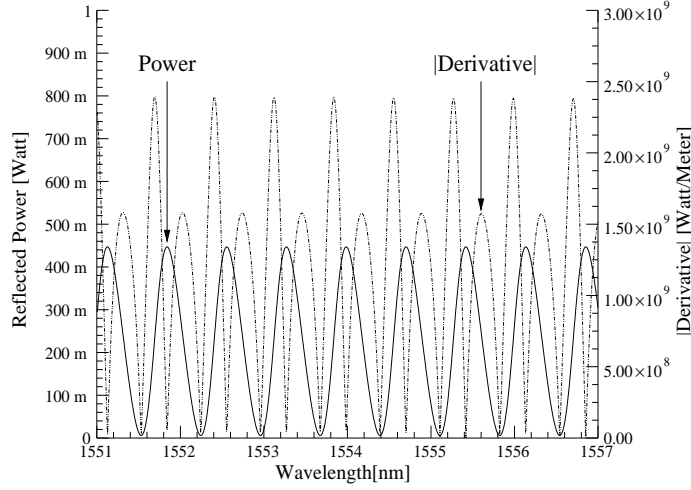


**Figure 51** Fabry Perot response with addition loss. The used parameters are  $r^+=0.37$ ,  $R^+=0.29$ ,  $d=500$  [ $\mu\text{m}$ ],  $P_{\text{Incident}}=1$  [mW],  $n_{\text{GaAs}}=3.374$ , a phase shift of  $\Lambda=\pi/4$  and  $P_{\text{Incident}}=1$  [mW].

The deduction of Equation (116) is doubtful, as we had to do several assumptions. Especially we have no justification for the phase shift. In the following chapters we will measure the Fabry Perot response and we will process the acquired data. We will try to fit the cavity response into the data and thereby we will see that we obtain much better results with Equation (116) than with Equation (70).

### 8.3 Magnitude of the electric fields

For information we have a look at typical values for the magnitude of the involved electro-magnetic fields. We will estimate the amplitude of the electric field of the microwave signal as well as the electric field of the photons.

For a microwave signal, a common amplitude is  $V_{\text{Microwave}}=1$  [V] and the crystal has thickness of  $d=100$  [ $\mu\text{m}$ ]. So according to Equation (117), the electric field  $E_{\text{Microwave}}$  has a magnitude of 10 [kV/m].

$$E_{\text{Microwave}} = \frac{V_{\text{Microwave}}}{d} = \frac{1[\text{V}]}{100 \cdot 10^{-6}[\text{m}]} = 10'000 \cdot \left[ \frac{\text{V}}{\text{m}} \right] \quad (117)$$

For the laser beam we suppose that we have a infrared laser beam with a power  $P_{\text{Laserbeam}}=1$  [mW] and that its diameter  $d = 2r \approx 20$  [ $\mu\text{m}$ ] matches the spot size of the focuser described in A.2.5. We assume that the power distribution in the spot is uniform. So we can deduce the power density as

calculated in Equation (118). By using the Pointing vector, we can determine the magnitude of the electric field (Equation (119)).

$$I_{\text{PowerDensity}} = \frac{P_{\text{Laserbeam}}}{\text{Surface}} = \frac{0.001 [W]}{\pi r^2 [m^2]} = 3.183 \cdot 10^6 \left[ \frac{W}{m^2} \right] \quad (118)$$

$$E_{\text{Laser}} = \sqrt{2 \cdot Z_{\text{GaAs}} \cdot I_{\text{PowerDensity}}} = \sqrt{2 \cdot 112 \cdot [\Omega] \cdot 3.183 \cdot 10^6 \left[ \frac{VA}{m^2} \right]} = 26'477 \cdot \left[ \frac{V}{m} \right] \quad (119)$$

$$\text{with } Z_{\text{GaAs}} = \sqrt{\frac{\mu_0}{\epsilon_0 \epsilon_r}} = 112 \cdot [\Omega]$$

We can see that the electric field of the laser beam is at least three times stronger than the electric field of the microwave signal.

## 8.4 Choice of the wavelength of the laser beam

The wavelength of the incident laser beam has to be chosen carefully for several reasons. GaAs should be “transparent” at the chosen wavelength, the material should not absorb the photons of the beam and the photons should not cause the generation of new electron-hole pairs in the semiconductor.

None of these problems will occur or they are negligible if the photon energy is smaller than the energy band gap of the GaAs. So we can calculate the shortest possible wavelength by using  $E_{\text{Photon}} < E_{\text{EnergyGap(GaAs)}}$ . So the vacuum wavelength of the laser beam has to be longer than 0.86  $[\mu\text{m}]$ . In Equation (120)  $E_{\text{Photon}}$  is the energy of the photons,  $E_{\text{EnergyGap(GaAs)}}$  is the energy gap of GaAs,  $e$  is the charge of an electron,  $h$  is the Planck constant,  $c_0$  is the speed of light in vacuum and  $\lambda_0$  is the seeked minimum vacuum wavelength of the laser.

$$E_{\text{Photon}} < E_{\text{EnergyGap(GaAs)}} \quad (120)$$

$$\frac{hc_0}{\lambda_0} < E_{\text{EnergyGap(GaAs)}}$$

$$\lambda_0 > \frac{hc_0}{E_{\text{EnergyGap(GaAs)}}$$

$$\lambda_0 > \frac{6.6260 \cdot 10^{-34} [Js] \cdot 2.9979 \cdot 10^8 \left[ \frac{m}{s} \right]}{1.43 [eV] \cdot 1.6021 \cdot 10^{-19} [As]}$$

$$\lambda_0 > 8.6702 \cdot 10^{-7} [m] = 0.86702 [\mu\text{m}]$$

On the other hand a longer wavelength is harmful because of the increasing spot size and so it would be not possible to focus on the 10  $[\mu\text{m}]$  wide microwave guide. A wavelength of 1550  $[\text{nm}]$  is slightly too long but it has the advantage that we can use a standard communication laser as the optical source.

## **8.5 Comment**

In this chapter we used the Gaussian beam formalism to improve the mathematical description of the Fabry Perot cavity. We could calculate the exact spatial resolution of the beam and hence the spatial resolution of the probing tool. The spatial resolution is proportional to the mode field diameter of the fiber and it depends on the lens configuration of the focuser as well. As the mode field diameter is typically about 10 [ $\mu\text{m}$ ] for standard monomode fibers at 1550 [nm], it is difficult to get spatial resolution better than this value. We also tried to introduce addition attenuation coefficient into the mathematical description of the cavity. Unfortunately the results were rather complex and it does explain all the phenomenons observed during the probing of the devices.

## 9 Conclusion of the Theory

In this chapter we analyzed several probing configurations for a laser beam being modulated inside a Fabry Perot cavity. We compared setups based on an “amplitude”, “polarization” and “phase modulation” and calculated theoretically the resulting modulation.

For our probing technique we choose the “amplitude modulation” describe in chapter 5. This configuration has two main advantages: Technically it is easy to realize as we do not have to add wave plates (as for the polarization modulation) and we do not have to deal with a reference branch (as for the phase modulation). The second advantage is its mathematical description. The mathematical description of the “amplitude modulation” is not only much simpler than the other ones but it allows us to calculate directly the electric field. As we know the magnitude of the modulation  $I_{\text{Modulation}}$ , the derivative  $\partial I_{\text{Reflected}}/\partial \lambda_o$  of the Fabry Perot response as well as the refractive index  $n_o$  and the electro-optic coefficient  $r_{41}$  we can use Equation (83) to calculate the electric field. For this calculation, we will divide magnitude of the modulation by the derivative of the Fabry Perot response. Hence all attenuations in the optical path are irrelevant as they are fall out of the equation.

The drawback of this approach is that it works only properly under the condition that the electric field is parallel with the z-axis. For other orientation of the electric field, the probed values will be systematically wrong.

Another drawback is that, the configuration using an “amplitude modulation” does not always provide the strongest modulation compared with the other configurations. The magnitudes of the modulation for all configurations depend strongly on the reflection coefficients and the thickness of the substrate. Hence it is difficult to provide an accurate comparison for this point.

In the last part of this chapter, we did some calculations about the shape of the laser beam at the output of the optical fiber. As the diameter of the beam defines the spatial resolution and its divergence limits the sensibility, we could observe a trade off between these two parameters. We also had to notice that the resulting spatial resolution is rather coarse.

In the next part of the thesis, we will realize this setup with standard fiber equipment and we will compare the obtained results with the theoretical description.



# Measurements

In this chapter we will expose the results of our experimental measurements. We will start with some basic characterizations of our equipment. Afterwards we will continue with the verification of the Fabry Perot response and at the end of the chapter, we will have a closer look at different kinds of electro-optic signals.

## 10 Characterization of the Components

Apart the DUT we use four optical components for the probing setup. A Distributed FeedBack (DFB) laser serves as a laser source, an optical circulator makes the optical connections and a pigtailed focuser injects the laser beam into the DUT. Afterwards a fast photo detector converts the optical modulation into an electrical signal. In this chapter we will have a closer look at the characteristics of the laser, the circulator and the focuser and we will try to estimate their influences on the probing results. Further we will use this chapter to point out some common problems with the probing setup described in Figure 52. In this chapter we will only look at the problematical parts of the setup. We assume that all other components satisfies "perfectly" the manufacture specifications and do not cause any inconveniences.

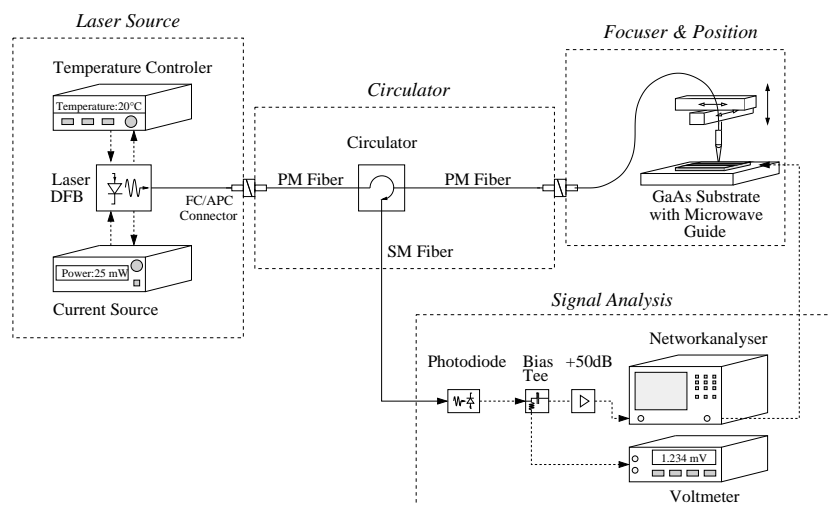


**Figure 52** General measurement setup used during the development of the probing tool.

## 10.1 Characteristics of the laser

### 10.1.1 Measurement setup

As a laser source we use a pigtailed Alcatel 1905 LMP laser. This laser is mounted into a butterfly package with an internal thermo-electric cooler element and an internal photodiode for monitoring the laser beam (Figure 53). The “fiber output” of the laser is a Polarization Maintaining (PM) fiber with a Fiber Channel Angled Physical Contact (FC/APC) connector. The polarization is aligned parallel to the slow axis of the fiber. The main feature of Alcatel 1905 LMP is that it can provide an output power up to 40 [mW].

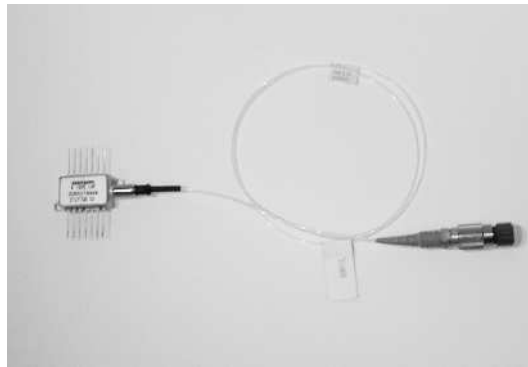


**Figure 53** Picture of the Alcatel 1905 LMP.

We noticed in the previous chapter, that it is necessary to adjust the wavelength of the laser as the modulation changes in function of the wavelength. Considering that the periodicity of the DFB structure changes with the ambient temperature, we can use the internal thermo-electric cooler element to tune the wavelength. So we connect the laser with a temperature controller to adjust the laser temperature and hence its wavelength. The drawback of this solution is the fact that the tuning of the temperature changes also the energy levels in the semiconductor of the laser. Therefore the output power of the laser is varying in function of the temperature. Considering that a constant output power is required for the probing, we connect the internal photodiode to the current source of the laser. As displayed in Figure 55 the current source controls the laser current in a way that the current in the monitor photodiode is always constant. Hence the output power is supposed to be constant as well.

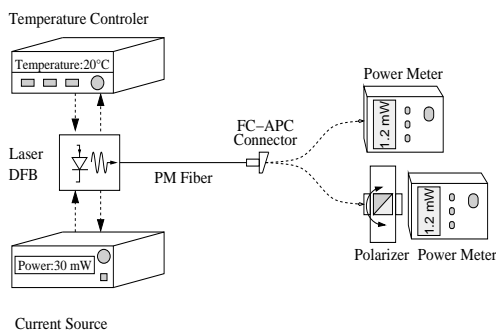


**Figure 54** Characterization of the output power and the polarization of the DFB laser.

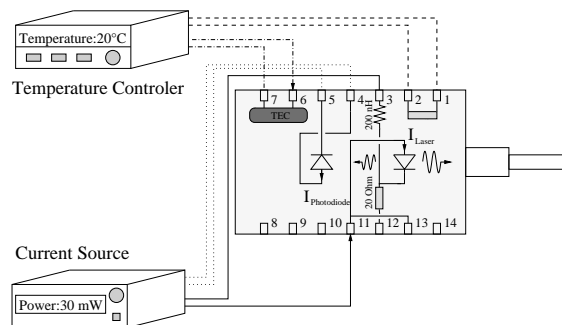


**Figure 55** Connection of the current source and the temperature controller.

For the verification of the laser characteristics we measure the output power in function of the adjusted temperature. We connect the laser to a power meter (Figure 54) and we trace the output power. With a simple analyzer (polarizer), we determine the optical power in the fast and the slow axis of the PM fiber. Afterwards we measure the wavelength of laser with an optical spectrum analyzer and we plot it in function of the temperature.

### 10.1.2 Results

In Figure 56 we plot the output power of the laser for the case of a constant current as well as with a controlled laser current. For the case with the constant current we can see that the output power decreases with the laser temperature. In the other case the output power is more stable but there is still a variation probably due to an unintentional internal cavity between the laser output and the end of the fiber or the internal optical isolator.

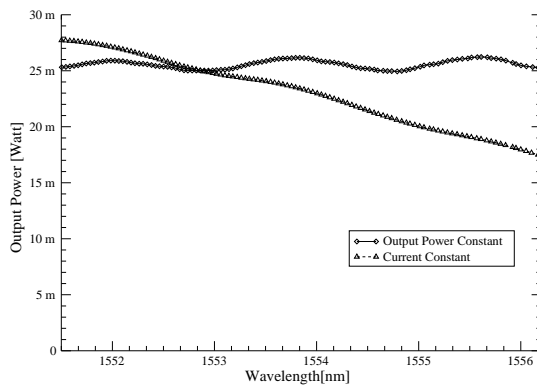


**Figure 56** Output power of the DFB laser with a controlled laser current and a constant laser current.

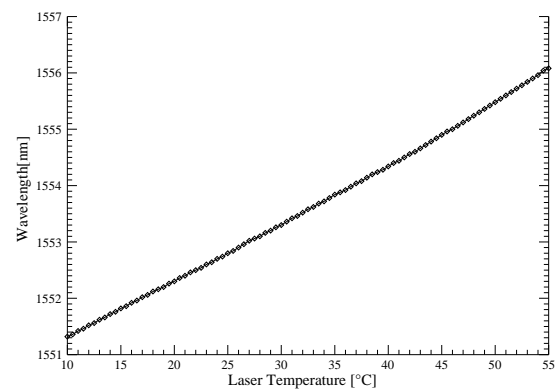


**Figure 57** Relation between the laser temperature and the according laser wavelength.

In Figure 57 we display the wavelength of the laser in function of the temperature. By computing a data fit, we could express the relation between these two parameters by Equation (121),

$$\lambda_o [nm] \approx 1550.274 [nm] + T \cdot 0.107 \left[ \frac{nm}{^\circ C} \right] - T^2 \cdot 4.297 \cdot 10^{-4} \left[ \frac{nm}{^\circ C^2} \right] + T^3 \cdot 7.23 \cdot 10^{-4} \left[ \frac{nm}{^\circ C^3} \right] \quad (121)$$

where  $\lambda_o$  indicates the wavelength and T is the temperature in degree Celsius. So the wavelength is changing of about 0.1 [nm] per degree Celsius. As we can tune the temperature between 10 [°C] and 55 [°C], we have a wavelength range of about 4.5 [nm].

In Figure 58 we plot the power in the slow as well as the power in the fast axis of the Polarization maintaining AND Absorption reducing (PANDA) fiber. As we could expect almost all the power is confined in the slow axis but there remains still some optical power in the fast axis. Considering that this part is changing in function of the wavelength, we have to assume that the orientation of polarization at the laser output is changing. Thus the axes of the polarization ellipse are slightly turning. As we used only a simple analyzer, we could not determine the polarization properties properly. To get a better impression of the situation we define the angle  $\Phi$ . The angle  $\Phi$  is defined in Equation (122) and it represents the turning of the polarization under the condition that the beam is always polarized linearly.

$$\Phi = \left| \text{ArcTan}\left(\frac{\text{Min}(I_{\text{Fast}})}{\text{Max}(I_{\text{Slow}})}\right) - \text{ArcTan}\left(\frac{\text{Max}(I_{\text{Fast}})}{\text{Min}(I_{\text{Slow}})}\right) \right| = \quad (122)$$

$$\left| \text{ArcTan}\left(\frac{9.6 \cdot 10^{-6} [\text{Watt}]}{22.1 \cdot 10^{-3} [\text{Watt}]} \right) - \text{ArcTan}\left(\frac{210 \cdot 10^{-6} [\text{Watt}]}{21.2 \cdot 10^{-3} [\text{Watt}]} \right) \right| \approx$$

$$|0.025 - 0.57| = 0.55 [\text{Degree}]$$

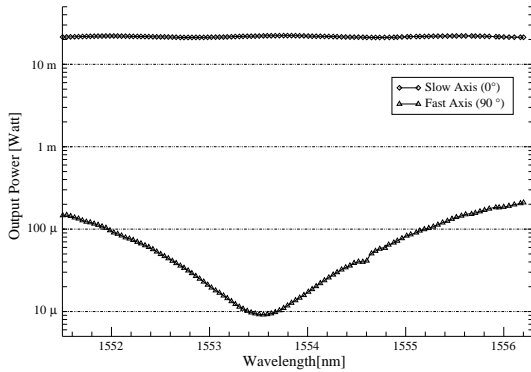


**Figure 58** Output power of the fast and the slow axis of the PM fiber. It seems that the polarization isolation (difference between  $I_{\text{Slow}}$  and  $I_{\text{Fast}}$ ) is maximal for the recommended or typical operation point with a laser current of 250 [mA] and an ambient temperature around 25 [°C].

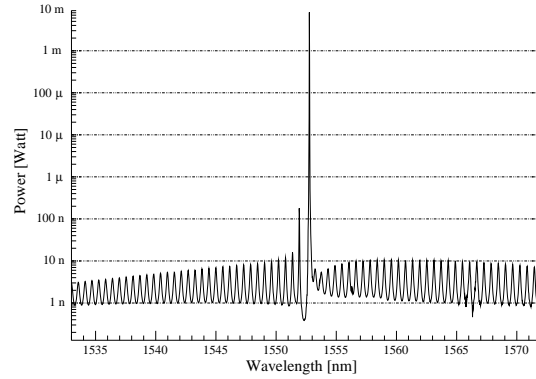


**Figure 59** Spectrum of the DFB laser: The laser is operated at 25 [°C] and the laser current is 173 [mA]. The optical spectrum analyzer was set to a resolution of 10 [pm].

Figure 59 shows the spectrum of the DFB laser taken with an optical spectrum analyzer. We can notice the high signal to noise ratio of over 40 [dB].

## 10.2 Characteristics of the circulator

### 10.2.1 Measurement setup

The circulator (Figure 60) is used to connect the laser, the focuser and the photo detector as shown in Figure 52. The fibers connected to port 1 and port 2 are PM fibers with a FC-APC connector at each end. With the angled connector we can avoid most harmful reflections caused by the interface between fibers. The polarization should be well defined at the output of the focuser. The fiber at the port 3 is a standard mono mode fiber with a Fiber Channel Physical Contact (FC-PC) connector.

For the determination of the circulator properties, we inject the laser beam into port 1 to port 3 parallel to the slow and the fast axis of the PM fiber and we have a look at the output of the other ports. So we can deduce the different attenuations caused by the circulator.

In a second time we have a look at the polarization isolation at the output of the circulator. For this measurement we connect the DFB laser with port 1 and we tune its wavelength over the entire range. Afterwards we check the power at port 2 for the slow and the fast axis with an analyzer (Figure 61).

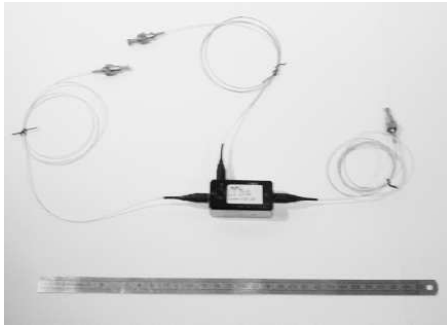


**Figure 60** Picture of a pigtailed circulator used in the measurement setup.

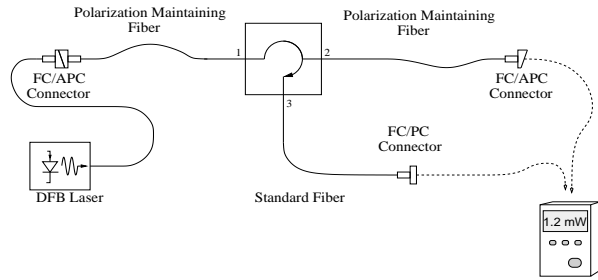


**Figure 61** Circulator and connectors used in our setup. The laser is connected to the port 1, the focuser to port 2 and the photo detector is linked to port 3.

### 10.2.2 Results

Input	Output	Attenuation
port 1(slow)	port 2	2.5 [dB]
	port 3	> 60 [dB]
port 1(fast)	port 2	1.25 [dB]
	port 3	> 60 [dB]
port 2(slow)	port 3	6.8 [dB]
	port 1	32 [dB]
port 2(fast)	port 3	2.5 [dB]
	port 1	33 [dB]
port 3	port 1	> 60 [dB]
	port 2	33 [dB]

**Table 4** Characteristics of the circulator used for the setup for  $\lambda_0=1550$  [nm]. The indicated values may change slightly after redoing the connections or by bending the fibers.

In Table 4 we can see the attenuations between the different input and output ports. If we inject the laser beam into the slow axis of the PM fiber the attenuation between port 1 and port 2 is 2.5 [dB] and it includes the losses due to both FC/APC connectors (typically 0.2-0.4 [dB] for each one). If we align the incident polarization parallel to the fast axis of the PM fiber, the output power is attenuated by 1.25 [dB]. The path between port 2 (slow) and port 3 introduces a much higher loss (6.8 [dB]) probably caused by a displacement of the fiber inside the circulator. All attenuations are higher than indicated by the specification of the producer.

In Figure 62 we show the attenuation between port 1 (slow) and port 2 in function of the wavelength. We can see that the attenuation is coarsely constant but we have to notice that the slow axis is injected into the fast axis and vice versa. We can also observe that the polarization isolation changes with the wavelength.

With a similar setup we check the attenuation between port 2 and port 3 which is displayed in Figure 63. In this case we can observe the harmful influence of an internal cavity. This cavity is probably caused by the reflections from the FC/PC connector at the end the fiber.

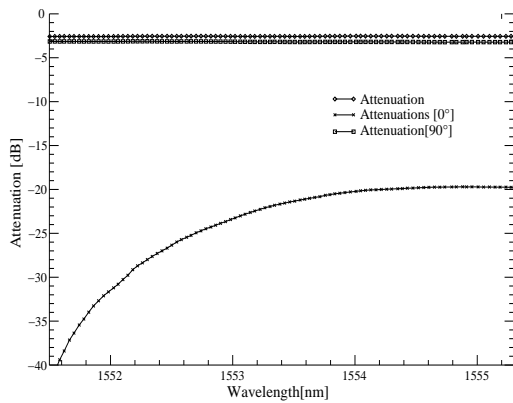


**Figure 62** Attenuation between port 1 (slow) and port 2 (slow respectively fast). We can observe that all the power went into the fast axis. At the output of port 2 the turning of the polarization in function of the wavelength increased.

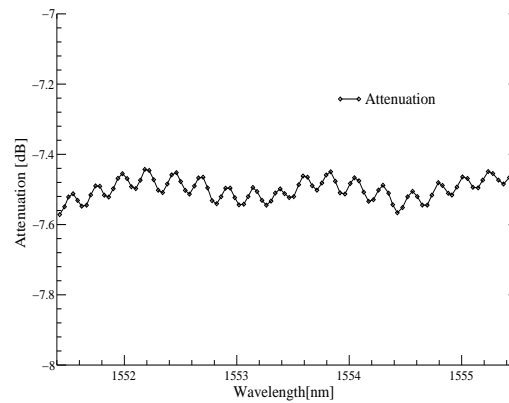


**Figure 63** Attenuation between port 2 (slow) and port 3. The value of the attenuation is a little bit higher than expected and we can see the effect of a harmful cavity probably due to the flat FC/PC connector.

### 10.3 Characteristics of the focuser

#### 10.3.1 Measurement setup

There are several unknown characteristics of the focuser. First we want to know the attenuation introduced by the focuser and its fiber connector. In the previous paragraphs, we saw that the polarization of the laser beam changes slightly in function of the wavelength. Considering that the output of the focuser is the incident laser beam on the electro-optic crystal, we are also interested in its state of polarization in function of the wavelength.

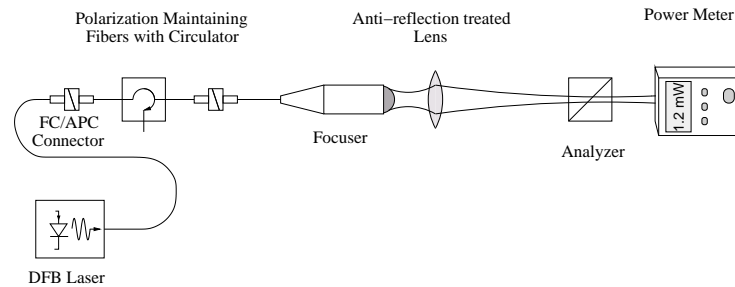


**Figure 64** Measurement setup for the characterization of the focuser.

The determination of the polarization is a little bit more complicated as the second output of the focuser is a lens for the focusing of the beam. Hence we cannot analyze the polarization with the pigtailed analyzer used in the previous setups. Considering that the focal distance is about 10 [mm], we have to insert another lens to obtain a parallel laser beam. This beam passes a polarization beam splitter and is picked up by a power meter as described in Figure 64.

#### 10.3.2 Results

As we can see in Figure 65, the attenuation of the focuser including the FC-APC connector is about

0.15 [dB] or with other words there is almost no loss.

We also display the intensity at the output for two different directions. The first direction was chosen in a way that the output was maximal and the second one was orthogonal to the first one. As we can see in Figure 65 the power in both axis are still changing in function of the wavelength. We can use the data to estimate the turning of the polarization as we already did it in Equation (122).<sup>1</sup>

$$\Phi = \left| \text{ArcTan}\left(\frac{\text{Min}(I_{\text{Second}})}{\text{Max}(I_{\text{First}})}\right) - \text{ArcTan}\left(\frac{\text{Max}(I_{\text{Second}})}{\text{Min}(I_{\text{First}})}\right) \right| = \left| \text{ArcTan}\left(\frac{0.004}{0.920}\right) - \text{ArcTan}\left(\frac{0.075}{0.834}\right) \right| \approx |0.24 - 5.13| = 5.1 [\text{Degree}] \quad (123)$$

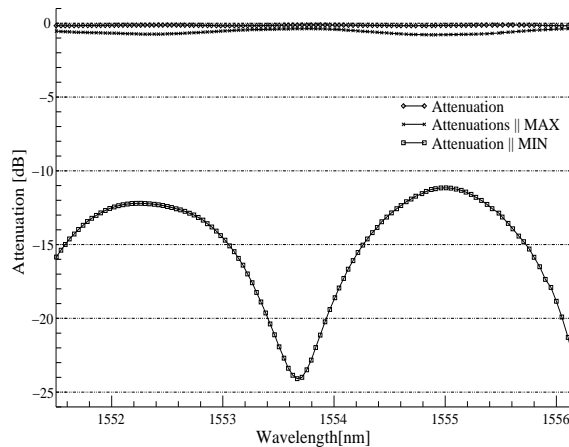


**Figure 65** We adjust the analyzer for two orthogonal axis and we trace the output power for the whole wavelength range.

## 10.4 Comment

The conclusion of the different verifications is that the polarization as well as the power at the output of the focuser are less stable than we expected. The polarization properties degrade during the propagation through the signal path. The degradation is probably due to the birefringence of the PM fiber in combination with a not perfectly aligned polarization at the output of the laser source. Also the two connections might introduce a further degradation of the polarization properties. The variation of the output power is caused by the laser. Both problems will affect the quality of the probing.

We have to add that we did not have spare equipment for the entire setup. So we could not compare if flaws of the equipment cause the mentioned problems or if we deal with a general technical or theoretical problem. Probably the difficulties are caused by both origins.

---

1. Normalized Intensity.

# 11 Measurement of the Fabry Perot Cavity Response

In this paragraph we will measure the response of the Fabry Perot cavity. We will compare the results with theory and we will analyze the factors influencing the probing results.

## 11.1 Measurement for different magnification factors

### 11.1.1 Measurement setup

For the verification of the description of the cavity, we trace the Fabry Perot cavity response with the measurement setup of Figure 66 for the sample displayed in Figure 67. The wavelength of the laser is tuned in the range between 1551 [nm] and 1556 [nm]. The laser beam passes the circulator and is focused on the GaAs substrate through a lens. As the magnification factors of the pigtailed focusers cannot be changed (it is fixed to the factor 1), we do a series of data acquisitions with a single anti-reflection treated lens with a focal distance of 1.25 [cm]. The lens is placed in front of the FC-APC connector. Its position and hence the magnification factor can be manipulated by a micro controller. At the output of the circulator, a power meter picks up the power of the reflected laser beam.

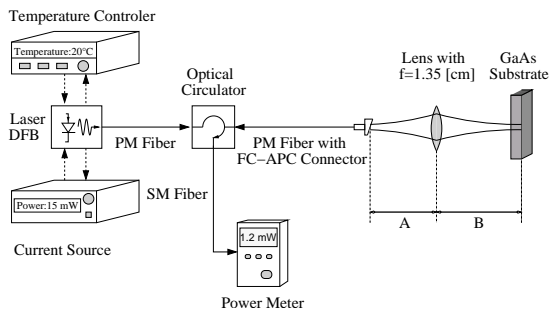


**Figure 66** Setup for the measurement of the cavity response. The DFB laser provides the laser beam and the circulator guides the beam to the lens. The same lens picks up the reflection and the circulator guides them to an optical power meter.

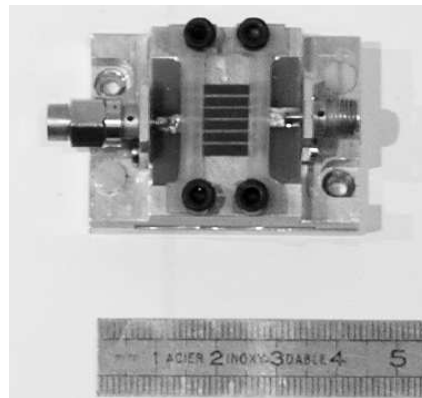


**Figure 67** Picture of the microwave guide used for the probing. The GaAs substrate (in the middle) is 500 [μm] thick and has 5 golden 330 [μm] wide microwave guides on it. This device is bigger than standard MMIC (typically 100 [μm] thick and 10 [μm] wide guides). It is easier to handle and the focus is much easier to adjust. On the left side is a 50 [Ω] impedance and on the right side is a SMA-connector for the input of the microwave signal.

### 11.1.2 Results

The results of Figure 68 correspond with the description of Figure 28 respectively of Equation (70). In Figure 69 we have several measurements for different values of A and B respectively for different magnification factors. We can see that the reflected power decreases with the magnification factor as plotted in Figure 69. So we have a trade off between the spot size (proportional to the magnification factor) and the reflected power. The spot size determines the spatial resolution and the reflected power governs the sensitivity of the probing tools.

For configurations with small magnification factors we can observe another effect (Figure 68). The response of the Fabry Perot cavity becomes asymmetric. Here we define the asymmetry as difference between the intensity for a wavelength  $\lambda_{\text{Max}} + \Delta\lambda$  and the intensity for  $\lambda_{\text{Max}} - \Delta\lambda$  as given in Equation (124). The parameter  $\lambda_{\text{Max}}$  indicates the wavelength where the reflected intensity becomes maximal and the  $\Delta\lambda$  represents a small difference in the wavelength.

$$I_{\text{Laser}}(\lambda_{\text{Max}} + \Delta\lambda) \neq I_{\text{Laser}}(\lambda_{\text{Max}} - \Delta\lambda) \quad (124)$$

This effect may be caused by a supplementary phase shift introduced by the focused Gaussian beam as explained in 8.2.3 on page 50.

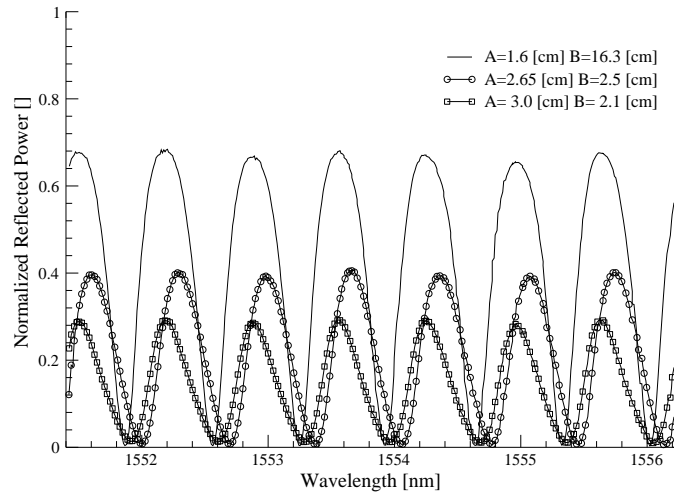


**Figure 68** Normalized (The unity is equal to 100% reflection) cavity response for different values of A and B for the substrate displayed in Figure 67. We can observe that the loss increases with the magnification factor  $M=B/A$ . By using Equation (74) and Equation (75) we can calculate the reflection coefficient  $r$  and  $R$ . For the case with  $A=1.6$  [cm] and  $B=16.3$  [cm] we get  $r=0.57$  (theoretical 0.54) and  $R=0.49$  (assumed 0.63 or -2 [dB]).

The periodicity of the Fabry Perot response depends on the refractive index and the thickness of the substrate. So by taking the wavelength  $\lambda_{\text{Max}}$  of a maximum as well as the wavelength of the next minimum  $\lambda_{\text{Min}}$  and by using Equation (125) we can recalculate the size  $d$  of the cavity.

$$d = \frac{1}{4n_o} \cdot \frac{\lambda_{\text{Max}} \cdot \lambda_{\text{Min}}}{|\lambda_{\text{Max}} - \lambda_{\text{Min}}|} = \frac{1}{4 \cdot 3.374} \cdot \frac{1555.203[\text{nm}]1555.563[\text{nm}]}{|1555.202[\text{nm}] - 1555.563[\text{nm}]|} = 496[\mu\text{m}] \quad (125)$$

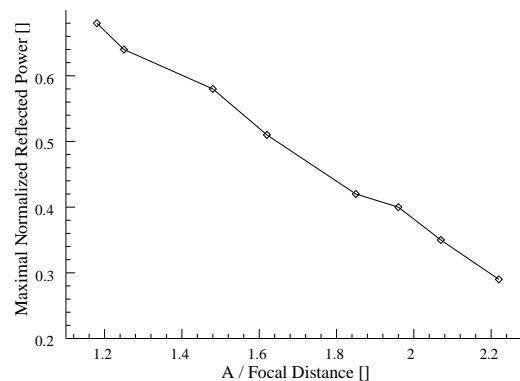


**Figure 69** The maximal reflected intensity in function of the factor  $A/\text{Focal Distance} = 1 + 1/M$  where Focal Distance describes the characteristics of the lens. The magnitudes are normalized as in Figure 68.

## 11.2 Measurement of the different reflections with a optical reflectometer

### 11.2.1 Measurement Setup

As we have an Optical Low Coherence Reflecto-meter (OLCR) in the laboratory, we are able to analyze the different reflections of the Fabry Perot cavity with this probing tool. With the setup of Figure 70 we have the possibility to look at the different reflections separately and so we can illustrate the summation of Equation (68) on page 28. The basic idea behind the reflecto-meter is to split the laser beam of a white source in two parts ([ 42 ], [ 43 ]). The first is injected into the DUT and its reflections are recollected. The second part is injected into a reference branch with a variable length. At the output the reflections from the DUT and the output of the reference branch are re-combined. As the spectrum of the white laser source is broad, the coherence length of the laser beam is very short. In this setup it is about 3.5 [ $\mu\text{m}$ ] [ 43 ]. Thus only the reflection from a very specific location (depending on the length of the reference branch) will cause constructive interferences and hence will be picked up. All other reflection will vanish due to destructive interferences.

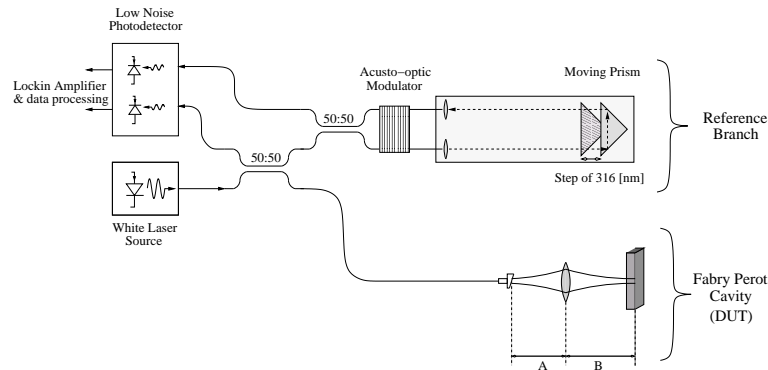


**Figure 70** Setup for the measurements with the reflecto-meter. At the bottom you can see the Fabry Perot cavity as DUT. The other parts belong to the reflectometer.

### 11.2.2 Results

In Figure 71 we can see the results of an optical low coherence reflecto-meter measurement. On the x-axis we have the delay induced by the reference branch expressed in a distance in air and hence the position of the reflection in the DUT. On the y-axis we have a value proportional to the intensity of the reflections. So the first peak represents the reflection on the air / GaAs interface. The second peak is delayed by a distance  $D_{\text{Retard}} = d \cdot n_o = 1.687[\text{mm}]$ . Here  $d$  is the thickness of the substrate (500 [ $\mu\text{m}$ ]) and  $n_o$  is the refractive index of GaAs (3.374). This peak is due to the first reflection on the golden back face of GaAs substrate. The other peaks are caused by the further reflections on the golden back face. Hence we can observe the attenuation of the signal in the cavity. We have to notice that the higher order reflections decay more than expected.

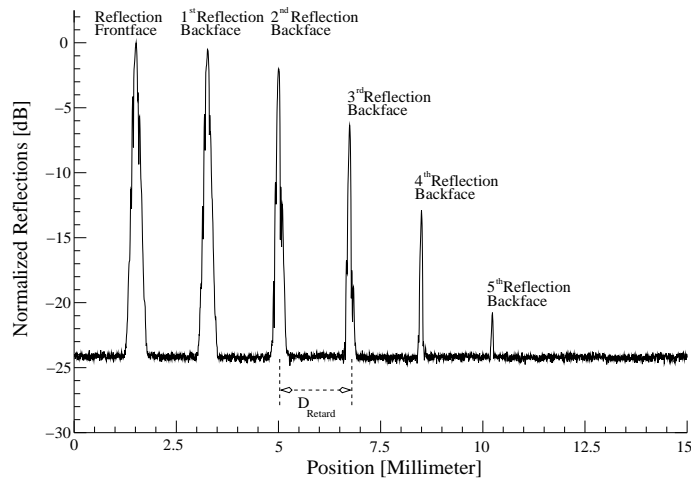


**Figure 71** Results of the measurements with the optical low coherence reflecto-meter. Here we have the reflection for a setup with a high magnification factor  $M=B/A$  as  $A=1.6$  [cm] and  $B=16$  [cm]. The distance between the reflections is  $D_{Retard}=1.7$  [mm]. By looking at the width of the reflections, we have to assume that the surface causing the reflections is uneven.

For a second series of measurement we displace the lens position. Thus we change the parameters  $A$  and  $B$  and hence we can analyze the reflections for different magnification factors as displayed in Figure 72. We can see that the higher order reflections are weaker for a setup with a lower magnification factor. In this case the laser beam diverge more and therefore the losses are higher.

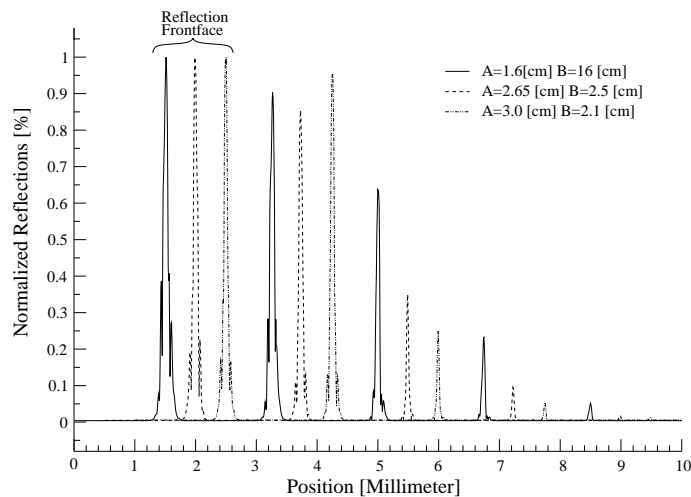


**Figure 72** We measure the reflections for different magnification factors  $M=B/A$ . We observe that the magnitude of the different reflections depend on the factor  $M$ . Hence the reflection coefficient  $r$  and  $R$  change in function of  $M$ .

### **11.3 Comment**

The response of the Fabry Perot cavity corresponds well to the mathematical description especially its periodicity. The magnitude of the reflected intensity differs slightly from the theoretical values, as we had to guess the reflection coefficient of the golden back face. It seems that the golden back face is more uneven than expected. The other drawback is the asymmetry of the response.

## 12 The electro-optic signal

In the previous paragraph, we focused the laser beam onto the GaAs substrate and we traced the intensities of the different reflections in function of the wavelength. In this chapter we will apply a microwave signal to the substrate of Figure 67 and we will analyze the resulting modulation for different conditions.

### 12.1 The Electro-Optic Signal

#### 12.1.1 Measurement Setup

For the following measurements we will apply a microwave signal with amplitude of  $-11.2[\text{dBm}_{\text{Electric}}]$  and a frequency of  $1.5[\text{GHz}]$  to the microwave guide. This signal is generated by the output of a network analyzer. At the other end of the microwave guide, we connect a resistor of  $50[\Omega]$  to avoid disturbing reflections. Hence the magnitude of the voltage applied across the  $50[\Omega]$  resistor will be about  $58[\text{mV}_{\text{rms}}]$  or  $82[\text{mV}_{\text{Amplitude}}]$ . We assume that the electric field just beside the microwave guide caused by this voltage satisfies the condition of Equation (126). We will probe this field with our probing setup.

$$E_z \gg E_x \text{ and } E_z \gg E_y \quad (126)$$

The probing setup of Figure 73 is very similar to the setup used for the acquisition of the cavity response in the previous paragraph. The only modification is the exchange of the detection unit and the use of the pigtailed focuser instead of the single lens. The power meter is replaced by a fast photodiode and a bias tee separates the DC and the RF-part of the photodiode signal. The DC-part of the signal is measured with a computer controlled voltmeter and is used to determine the power of the laser beam and hence the response of the cavity. The RF-part of the signal is amplified and connected to the input of the network analyzer. In this way the network analyzer can measure the amplitude and phase shift of the modulation.

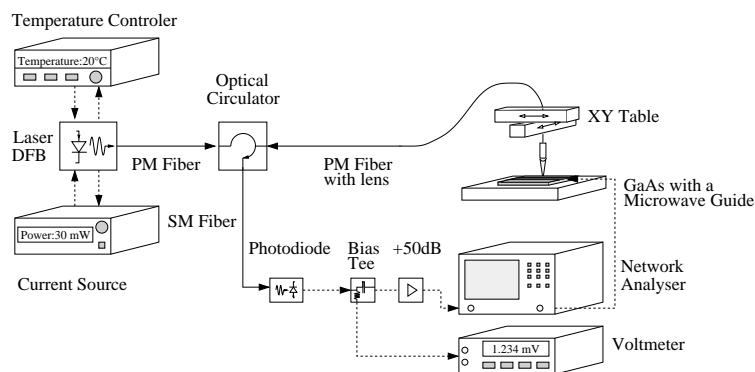


**Figure 73** Setup for the acquisition of the electro-optic signal.

#### 12.1.2 Results

In Figure 74 we plot the response of the Fabry Perot cavity. For further data analysis we will have to compute the derivative  $\partial I_{\text{Reflected}} / \partial \lambda_0$  of the response. As it is difficult to use the discrete data

points for this calculation, we put a data fit into the graph and we used the data of the fitted curve for calculation of the derivative. For all of the following data fits, we use Equation (116) as we achieve better results than with the “standard” description of the Fabry Perot cavity.

During the same measurement we also acquired the magnitude and phase shift of the modulation. The magnitude of the modulation is displayed in Figure 75 as well as the derivative of the data fit. As we can see the modulation is proportional to the derivative  $\partial I_{\text{Reflected}} / \partial \lambda_o$  as indicated by Equation (83) on page 32.

By knowing the wavelength  $\lambda_o$  and the refractive index  $n_o$  as well as the electro-optic coefficient  $r_{41}$ , we have all parameters of Equation (83). Thus we can calculate the electric field caused by the microwave signal in function of the derivative and the electro-optic signal as displayed in Equation (127). For the calculation we use the point where the electro-optic signal becomes maximal as displayed in Figure 75.

$$E_{\text{Microwave}} = \frac{I_{\text{Modulator}}}{\lambda_o n_o^2 r_{41} \cdot \left| \frac{\delta I_{\text{Ref}}}{\delta \lambda_o} \right|} = \frac{16.5 \cdot 10^{-9} [\text{W}]}{1552.21 \cdot 10^{-9} [\text{m}] \cdot 3.374^2 \cdot 1.42 \cdot 10^{-12} \left[ \frac{\text{m}}{\text{V}} \right] \cdot 65 \cdot 10^6 \left[ \frac{\text{W}}{\text{m}} \right]} = 10.13 \left[ \frac{\text{V}}{\text{m}} \right] \quad (127)$$

**Figure 74** Response of the cavity. As we have to calculate the derivative of the response, we display a data fit calculated on the basis of Equation (116) through the plot and we use the fit to compute the derivative.

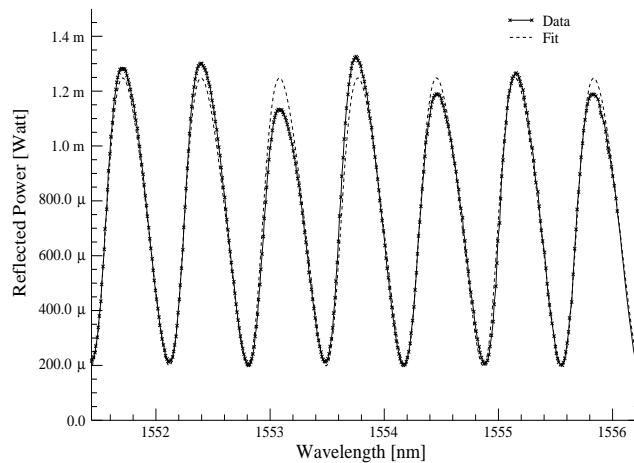
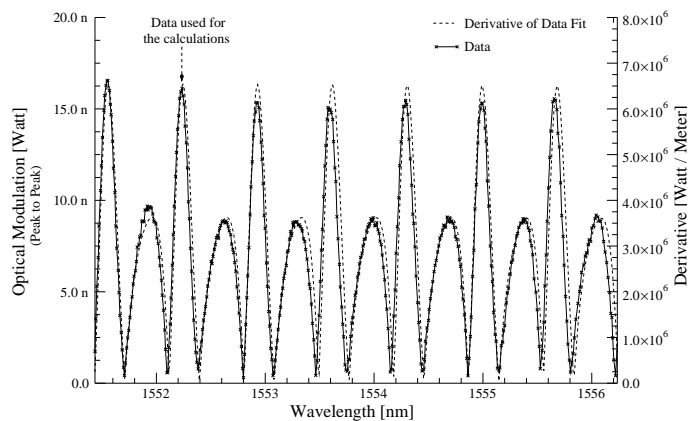


**Figure 75** Modulation picked up by the network analyzer in function of the wavelength. The derivative of the data fit of Figure 74 is proportional to the modulation magnitude.



By knowing or by measuring the thickness of the substrate we can calculate the voltage of the microwave signal. The magnitude of the probed voltage calculated in Equation (128) represents the amplitude of the microwave signal. The probed value should be around 82 [mV<sub>Amplitude</sub>] but we

find only 51 [mV<sub>Amplitude</sub>]. One possible explanation for the difference between the applied voltage and the sensed value is the position of the probing beam. This location is about 30 [μm] beside the microwave guide. We will have a closer look at this problem in chapter 13.1. Another possible explanation is the inaccuracy of the electro-optic coefficient  $r_{41}$ .

$$V_{\text{Microwave}} = E_{\text{Microwave}} \left[ \frac{V}{m} \right] \cdot d[m] = 10.13 \left[ \frac{V}{m} \right] \cdot 500 \cdot 10^{-6}[m] = 0.051[V] \quad (128)$$

The network analyzer also displays the phase shift. The absolute value of the phase shift is of no interest as it depends on the length of the cables and fibers and the phase shift induced by the photodiode and amplifier. But by tracing the phase shift for all data points we can analyze the variation of the phase shift. According to Equation (83) respectively Figure 31 on page 33 there should be a phase shift of 180° between these regions with a positive derivative  $\partial I_{\text{Reflected}}/\partial \lambda_o$  and those with a negative one. In Figure 76 we plot the phase shift acquired by the spectrum analyzer. We can observe that the measurements match well the theoretical description.

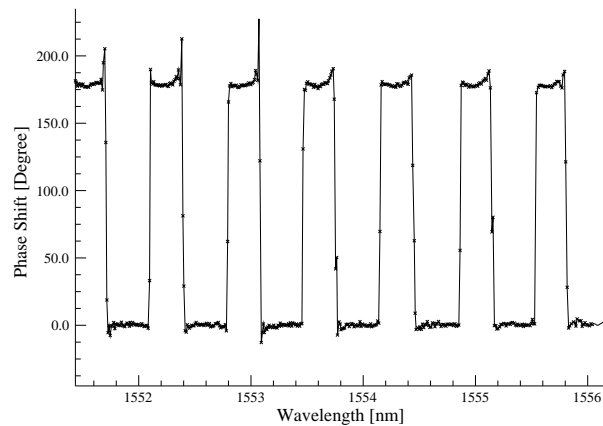


**Figure 76** The phase shift measured by the network analyzer. The “lowest” phase shift was set to 0°.

## 12.2 The electro-optic signal for different directions of the polarization

### 12.2.1 Measurement Setup

For the measurements in the previous paragraph, we aligned the polarization of incident laser beam with the optical axis caused by an electric field parallel to the z-axis. In this setup we will turn the polarization around the z-axis to illustrate the theoretical results of chapter 5.2 and to estimate the influence of a misalignment.

For this data acquisition we use the same probing setup as for the previous measurements. We just turn the focuser as displayed in Figure 77. As the polarization is known at the output of the focuser, we also change the alignment of the polarization and hence the angle between the optical axes of the crystal and the polarization of the laser beam which is defined as  $\varphi$ . Unfortunately we change also the position of the laser beam as the output of the fiber is not perfectly in the middle of the turning axis. So we had to readjust the position each time and hence the results are slightly different for each angle.

So we execute several data acquisition for different values between  $\varphi=0^\circ$  and  $\varphi=90^\circ$ . We plot the

resulting modulation and the according phase shift.

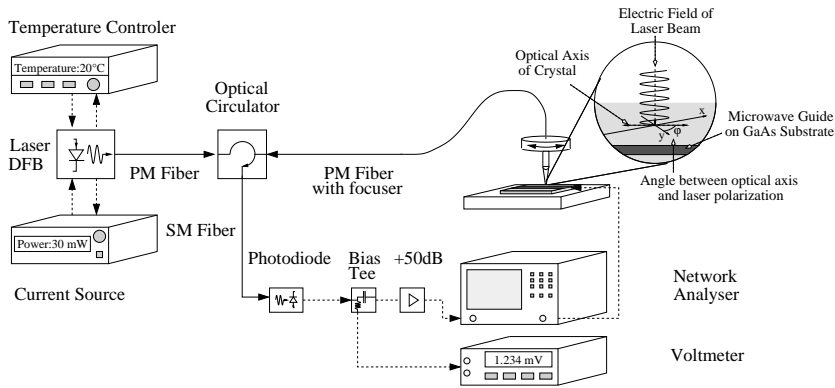


**Figure 77** Setup for the verification of the influence of the polarization of the laser beam.

### 12.2.2 Results

In Figure 78 we display the modulation for different orientation of the incident polarization. We can observe that the magnitude of the modulation is maximal if the polarization is aligned parallel with the optical axis of the GaAs crystal ( $\varphi=0^\circ$ ). The modulation becomes minimal around  $\varphi=45^\circ$ . Thus the magnitude of the modulation is roughly proportional to  $\cos(2\varphi)$ . We have to add that these measurements are rather difficult to execute as we have to adjust the position for each measurement and as the polarization of the incident laser beam is turning slightly.

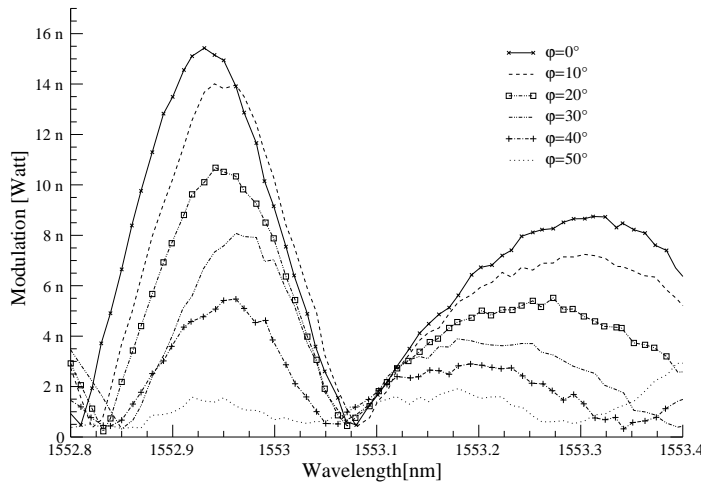


**Figure 78** Optical modulation for different values of  $\varphi$ .

In Figure 79 and Figure 80 we display the modulation for  $\varphi=0^\circ$  and for  $\varphi=90^\circ$  or with other words we aligned the polarization parallel with the first and the second optical axis of the crystal. In the first plot we can see that the magnitudes of the modulation are slightly different as the position are not identical. As the thickness of the substrate also changes slightly with the position, the periodicity of the Fabry Perot cavity is slightly different. Hence the “shape” of the electro-optic signal is not identical. In the second plot we display the phase shift of the modulation. In the previous para-

graph, we saw that the derivative  $\partial I_{\text{Reflected}}/\partial \lambda_o$  for the “higher peak” is always positive. By looking at Figure 79 and Figure 80 we can see that there is a phase shift of  $180^\circ$  between the “high peak” for  $\varphi=0^\circ$  and for  $\varphi=90^\circ$ . The reason for this phase shift is the different sign in Equation (129).

$$n_{\varphi=0^\circ} = n_o + \frac{1}{2}n_o^3 r_{41} E \tag{129}$$

$$n_{\varphi=90^\circ} = n_o - \frac{1}{2}n_o^3 r_{41} E$$

So we can observe that  $\Delta n_{\varphi=0^\circ} = -\Delta n_{\varphi=90^\circ}$ .

**Figure 79** Magnitude of the modulation for  $\varphi=0^\circ$  and  $\varphi=90^\circ$ .

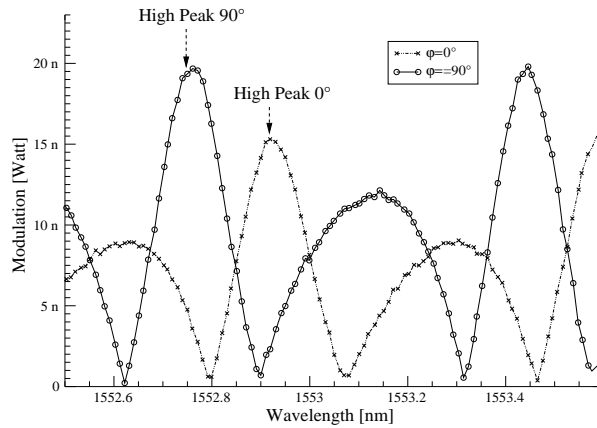
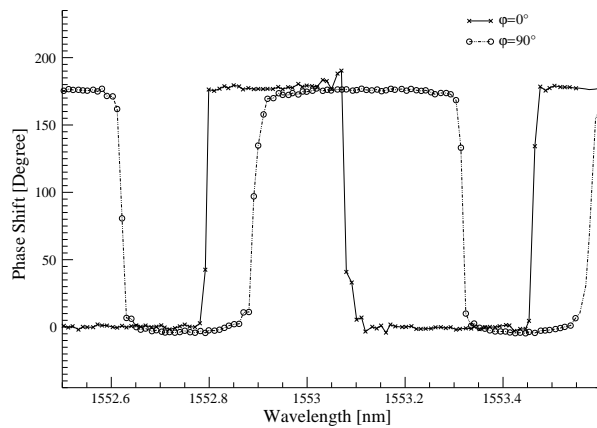


**Figure 80** Phase shift of the modulation for  $\varphi=0^\circ$  and  $\varphi=90^\circ$ .



## 12.3 Linearity and the Signal to Noise Ratio

### 12.3.1 Measurement Setup

In this paragraph we want to verify two other important probing parameters. First we will have a look at the linearity of the probing and hence the reliability of the measuring technique. Afterwards we determine the Signal to Noise Ration (SNR) and so we try to estimate the smallest detectable signal.

For these measurements we do some modification in the measurement configuration. Instead of the network analyzer, we use a spectrum analyzer with an integrated photodiode as shown in Figure 81. As the spectrum analyzer has an integrated photo detector including an option to measure the laser

beam intensity, we can discard of the external photodiode, the RF-amplifier and the voltmeter. On the other hand we insert a function generator for the microwave signal generation. The function generator allows us to have a microwave signal with a well-defined magnitude and frequency at the input of the microwave chip.

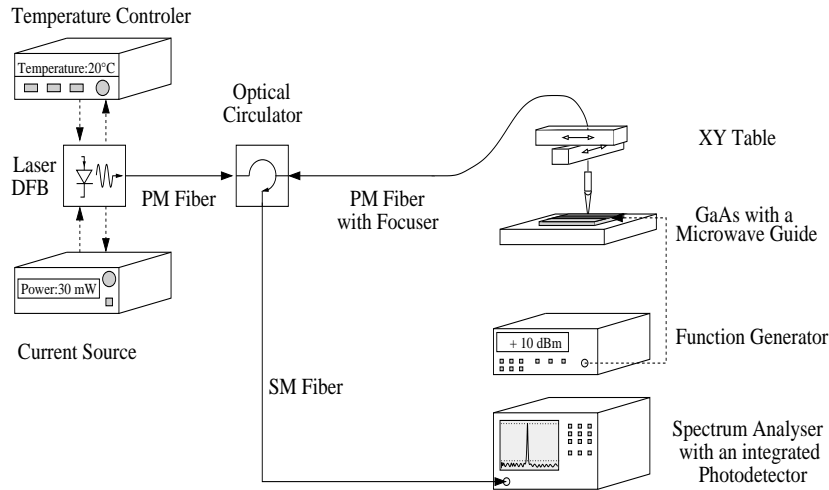


**Figure 81** Setup to determine the linearity and the signal to noise ratio. The network analyzer is replaced by a spectrum analyzer signal with an integrated photo detector (for the signal analysis) and a function generator (for the signal generation).

For the verification of the linearity, we apply different signal levels at the input of the DUT. We assume that the electric field due to the microwave signal inside the substrate is proportional to the magnitude of the input signal. So we will acquire the Fabry Perot response and the magnitude of the modulation with the spectrum analyzer. Afterwards we will calculate the electric field and the applied voltage.

For the measurement of the SNR we adjust the wavelength of the laser beam so that the electro-optic modulation becomes maximal. We adjusted the parameters of the spectrum analyzer and we store the display of the spectrum analyzer. Afterwards we use these plots to calculate the ratio between the peak amplitude or signal and the noise as well as the smallest detectable signal  $V_{Sensibility}$ .

### 12.3.2 Results

In Figure 82 we display the measured magnitude of the electric field for different applied signals. The intensity of the applied microwave signal is changing in the range between +23 [dBm<sub>Electric</sub>] and -40 [dBm<sub>Electric</sub>] at a carrier frequency of 1.5 [GHz]. This signal generates an applied voltage between 3.1585 [V] and 22 [mV] over the 50 [ $\Omega$ ] impedance at the end of the microwave guide. On the y-axis we plot the probed voltage. We can observe the linear relationship between the applied voltage and the sensed magnitude.

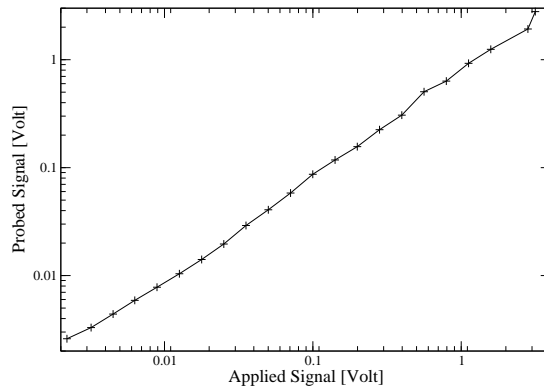
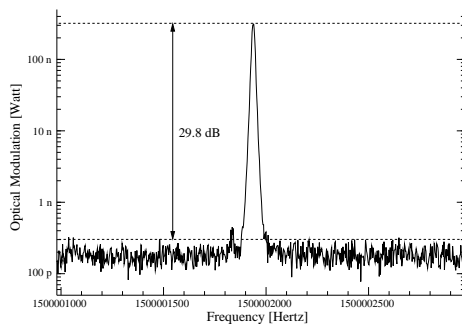


**Figure 82** The x-axis corresponds with the voltage of the applied microwave signal and the y-axis is the probed tension.

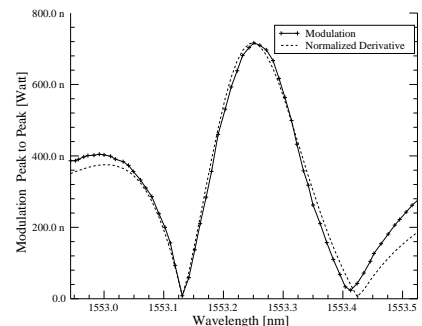
In the following figures we illustrate the SNR as well as the acquired electro-optic signal in function of the wavelength. In Figure 83 we can see that the SNR increases with the increasing applied microwave signal. A stronger microwave signal will cause an electro-optic probing signal with a higher SNR. For a typical microwave signal with a power of 8 [dBm<sub>Electric</sub>] we get a SNR around 22.4 [dB<sub>Optic</sub>].

For the determination of the smallest detectable signal called  $V_{\text{Sensitivity}}$ , we use a special approach. We always measure the response of the cavity to calculate its derivative. According to Equation (83) the derivative is proportional to the magnitude of the modulation. By calculating the cross correlation  $r^2$  between the measured modulation and the normalized derivative, we can quantify the quality of the data acquisition. By requiring that for a valid acquisition  $r^2 \geq 0.9$  and by considering the filter bandwidth (10 [Hz]) of the spectrum analyzer, we can estimate  $V_{\text{Sensitivity}}$  as given in Equation (130).

$$V_{\text{Sensitivity}} = \frac{5.94[mV]}{\sqrt{10[Hz]}} = 1.878 \left[ \frac{mV}{\sqrt{Hz}} \right] \quad (130)$$



Applied Signal:  
23 [dBm<sub>Electric</sub>]=3.1585 [V]  
  
Probed Voltage: 2.7874 [V]  
 $r^2=0.9711$



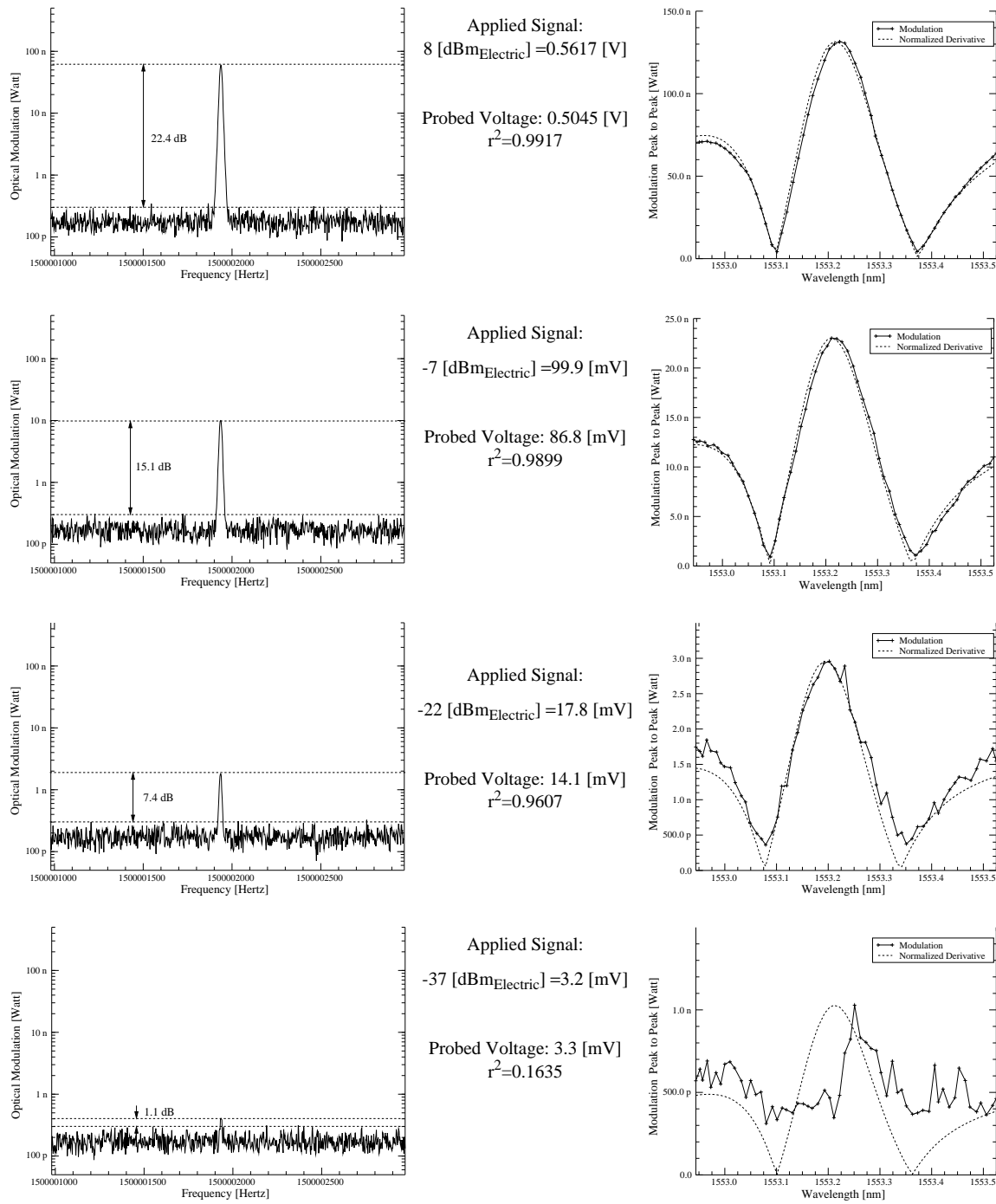


**Figure 83** Signal to noise ratio for different signal levels (left) and the according acquired electro-optic signal (right). The reference level of the spectrum analyzer is set to  $-35$  [dB<sub>Optic</sub>] or  $316$  [nW] and the resolution bandwidth to  $10$  [Hz]. For the signal to noise ratio the frequency span is  $2$  [kHz] and for the acquisition of the electro-optic signal to  $15$  [Hz]. The sweep time is automatically chosen in function of the other parameters.

We have to add that the SNR and especially the  $V_{Sensitivity}$  depend strongly on the parameters of the probing setup like the sweep time, resolution bandwidth and reference level of the spectrum analyzer, output power and SNR of laser as well on the amplifier of the photo detector.  $V_{Sensitivity}$  depends also on  $r$  and  $R$  as the reflected intensity changes with these parameters. Hence the presented values indicate only the order of magnitude.

## 12.4 Comment

In this paragraph we analyzed the behavior of the amplitude modulation for the realized setups. In our setup, we used polarization maintaining fibers and pigtailed focusers for the first time. Hence we could align properly the polarization of the incident laser beam. In general the probing tool worked well and the results matched the theory.

The interesting points of the probing setup are its linearity over a wide range of applied voltages (0.01[Volt] upto 1[Volt]) and its good sensibility 1.878[mV/Hz]. Another important point is the repeatability of the probing tools. There was no problem to reproduce similar results another day under the condition that we did not change the positioning or orientation of the laser beam.

It was valuable that for the calculation of the electric field you have to divide the magnitude of the optical modulation  $I_{\text{Modulation}}$  by the derivative  $\partial I_{\text{Reflected}}/\partial \lambda_o$  of the Fabry Perot response. Hence all attenuations in the optical path are irrelevant as both terms are affected in the same way. Another interesting point of the relation between the derivative and the electro-optic signal was the detection of crosstalk between the function generator and the laser current. As the probing beam has to be constant even a small unintentional modulation of the laser beam can decay the probing result. We were able to overcome the problem by placing RF-absorbing material around the laser and other sensitive devices. We could easily detect this cross talk by looking at the cross correlation between the modulation and the normalized derivative. The better the correlation is the lower is the cross talk. If both plots looks totally different, the modulation is caused by cross talk.

On the other hand we discovered several inconveniences. As the output power and polarization of the laser beam are not stable in the entire wavelength range, the resulting modulation could change in function of the wavelength. For probing near the microwave guide additional (harmful) reflections appeared and decayed the probing quality.

## 13 Mapping of the electric field in a MMIC

In the previous chapters, we probed the electric field only for one point. In this chapter we will measure the magnitude of the electric field for several different positions. Hence we can show the electric field distribution in a device.

### 13.1 Measurement of the electric field beside a microwave guide

For the following measurements, we use the GaAs circuits with a microwave guide described in Figure 67. We will probe the voltage and phase shift for different positions beside the microwave guide. As the setup of the GaAs is rather simple, we could simulate the electric field distribution with a professional computer program. So we are able to compare both results.

#### 13.1.1 Measurement Setup

The probing setup displayed in Figure 84 is identical with the setup used in chapter 12.1. We just changed the acquisition software in a way that it could change the position of the probing beam. It uses the acquired data to calculate automatically the wanted voltage.

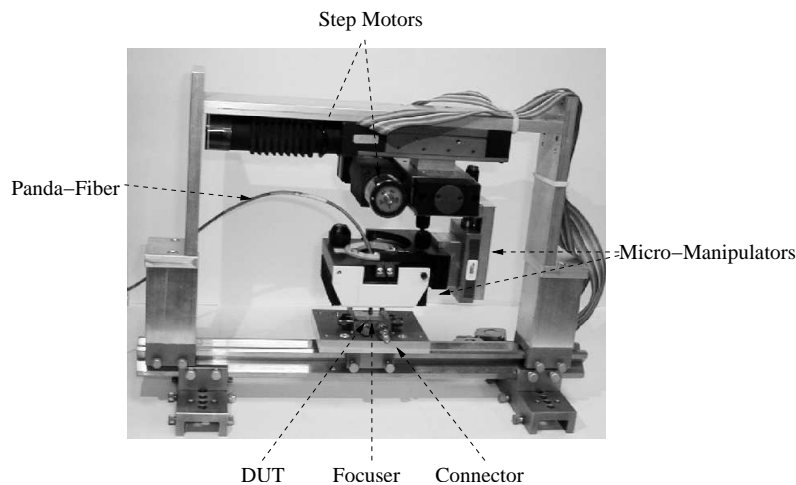


**Figure 84** Equipment used for the probing. At the bottom of the schema is the DUT with several SMA connectors for the input signal. Just above the DUT is the focuser at the end of the PM-Fiber. Two step-motors are used to change the position of the incident laser beam and several micro-manipulators are used to adjust the focus and the orientation of the polarization.

#### 13.1.2 Results

In Figure 85 and Figure 86 we display the voltage respectively the phase shift for different positions beside the microwave guide. The distance between the different probing points is 10 [ $\mu\text{m}$ ] and hence about a third of the diameter of the probing beam given in Table 3 on page 50. By taking into account the aberration of the focuser, the distance between the microwave guide and the first probing point is about 30 [ $\mu\text{m}$ ]. Again we apply a microwave signal of  $-11.2$  [ $\text{dBm}_{\text{Electric}}$ ] over the 50 [ $\Omega$ ] terminated DUT. Thus the measured voltage is lower than the applied microwave signal of 58 [ $\text{mV}_{\text{rms}}$ ] or 82 [ $\text{mV}_{\text{Amplitude}}$ ]. The frequency of the microwave signal is 1.5 [GHz].

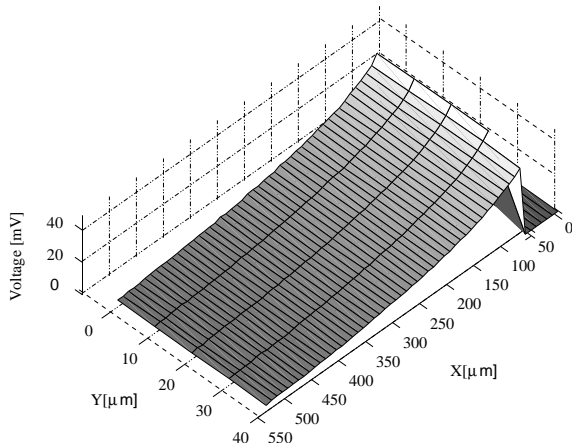


**Figure 85** Voltage between the air / GaAs interface and the golden back face for different position beside the microwave guide. If the probing failed, we set the voltage to zero. This was the case when the laser beam was partially or entirely focused onto the golden microwave guide.

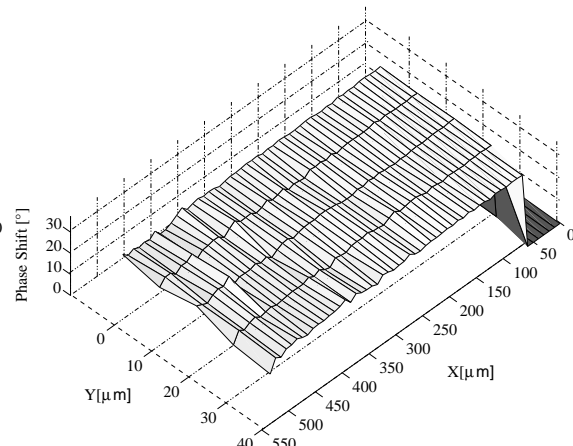


**Figure 86** Phase shift of the electro-optic signal for different position beside the microwave guide. If the probing failed, we set the according phase shift to zero.

### 13.1.3 Simulation

As the structure of the microwave guide is rather simple, there is no problem to create a computer model (Figure 87) and to calculate the electric field distribution with a commercial simulation tool for microwave applications (CST Microwave Studio).

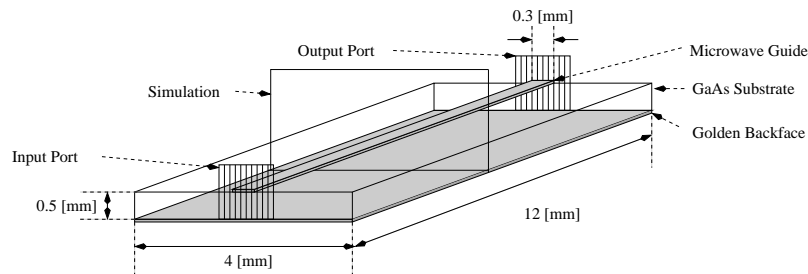


**Figure 87** Model of the microwave guide used for the computer simulation. We set up the simulation in a way that we compute the electric field distribution in the middle of the sample.

The software calculates the complex electric field vector as displayed in Figure 14 on page 12. With this database we can calculate the voltage between the air / GaAs interface and the golden back face and its phase shift. We calculate the voltage and phase shift by doing the integration for the real and the imaginary part of the z-component of the electric field vector over the entire distance between the air / GaAs interface and the golden back face. Afterwards we can deduce the absolute value (Figure 88) and the phase shift (Figure 89). In both figures we put also the results of the experimental measurements.

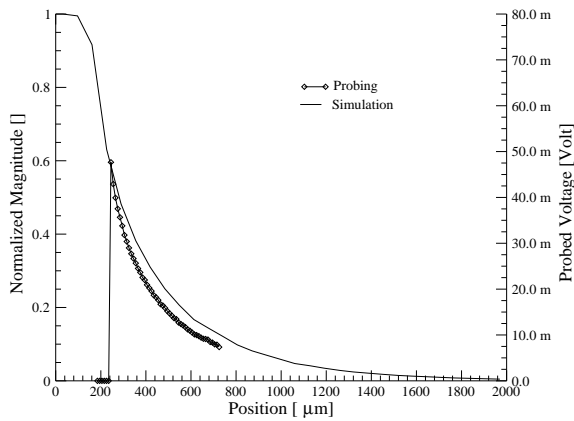


**Figure 88** Normalized voltage between the air / GaAs interface and the golden back face as well as the probed voltage.

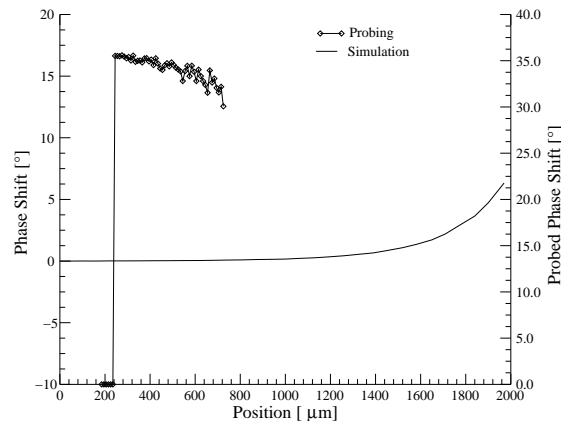


**Figure 89** Calculated and probed phase shift. Even if we take into account that the probed phase shift is only relative to arbitrary reference, it does not match the simulation. The origins for this mismatch might be the problem explained in Figure 92.

## 13.2 Mapping of the electric field on a chip

### 13.2.1 Measurement Setup

In the previous paragraphs, we used a “test device” with a single very wide microwave structure and 500 [μm] thick substrate. In this paragraph we will use a “real MMIC”. The microwave structures are much smaller and more complicated as displayed in Figure 94. Also the substrate is only 100 [μm] thick.

For the mapping of the microwave signal, we use the setup of Figure 81. We apply a microwave signal with a magnitude of 6 [dBm<sub>Electric</sub>] at carrier frequency of 1 [GHz]. We terminated all outputs with 50 [Ω] impedances. We probe the field at the intersection described in Figure 90.

### 13.2.2 Results

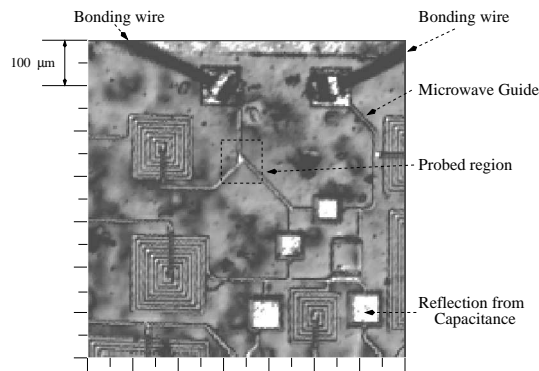


**Figure 90** Reflection from the surface of the DUT. Such plots are used to get to a wanted position on the device.

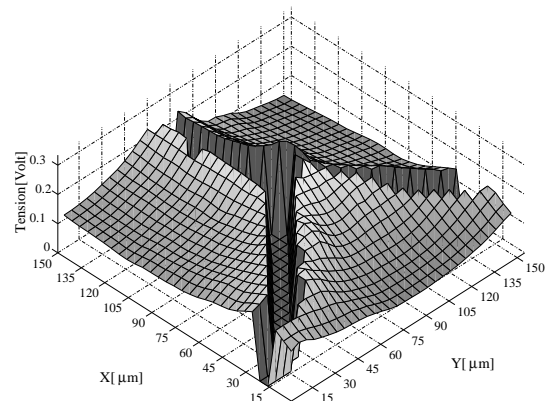


**Figure 91** Magnitude of the voltage probed in the MMIC.

One of the biggest problems of the probing is finding the desired positions on the ICs under test. The difficulty of finding the position is managed by scanning the reflection from the surface and by plotting them. In Figure 90 we can see the result of such a scan. Hence there is no problem to direct the laser beam to a specific position. In Figure 91 we probe the voltage around an intersection of two microwave guides. The acquisition of each point take between 30 [sec] and 1 [min] depending on the probing parameters and the position of the point. So it takes a long time to probe the electric field distribution for a large map.

### 13.3 Comment

In this chapter we saw that we can use our equipment to map the electric field distribution in a MMIC. The results are coherent and reproducible. On the other hand there are several theoretical and technical inconvenience. As we discussed in chapter 5.3, the optical axes move in function of the vector of the microwave signal. So the measurements are only correct under the condition  $E_z \gg E_x$  and  $E_z \gg E_y$ . Near the microwave structure the electric field is roughly parallel to the z-axis and hence the condition is satisfied. Further away from the microwave guide this assumption is not valid anymore and hence the polarization of the laser beam and the optical axes are misaligned. Hence we will have a systematic error for these measurements. Also the definition of the probed voltage and its phase shift becomes doubtful as the distribution of the electric field inside the substrate varies strongly in function of z as displayed in Figure 92.

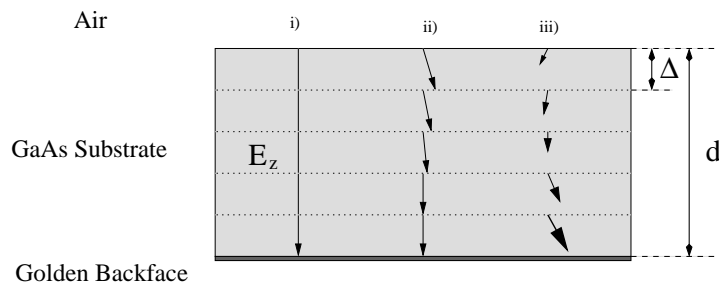


**Figure 92** For our measurements we define the voltage as  $\text{Voltage}_z = |E_z| \cdot d$ . We will probe the same voltage even if the electric field distribution is not identical as displayed in i), ii) and iii).

The major technical inconvenience is that it takes a long time to probe an entire device.

## 14 Measurement of the S-parameters

In the previous measurements, we always used a sinusoidal input signal with a constant carrier frequency. During the entire probing process, we did not change this carrier frequency. In our probing configuration, the two basic elements are the continuous probing beam and the fast photo detector which analyzes the modulation. The continuous probing beam does not depend on the microwave signal and the characteristics of the photo detector should only change slightly in function of frequency. Hence we can change the carrier frequency of the input signal. So we can determine the microwave signal in function of the carrier frequency. This kind of measurements are difficult to perform with probing techniques using pulsed probing beams as the probing beam as well as the detection unit depend on the carrier frequency.

By placing the probing beam just beside a wave guide, we can calculate the voltage of the microwave signal for an entire frequency range. If we perform the same acquisition for two different locations inside the integrated device, we can calculate the attenuation between these points in function of the carrier frequency. Hence we can determine parts of the s-parameter by using the electro-optic probing tool. Thus we can measure the transfer function of parts of the MMIC which are not connected with the inputs or outputs of the device.

### 14.1 Measurement Setup

For the probing of the s-parameters, we make only some minor changes in the setup described in Figure 73. There are no “hardware-modifications” apart an additional electric amplifier. But there are several changes in the acquisition procedure and hence in the acquisition software.

For the acquisition we execute first a data acquisition like in paragraph 12.1.2. Hence we know the function  $\partial I_{\text{Reflected}}/\partial \lambda_o$  and the wavelength  $\lambda_{\text{ModulationMax}}$  where the electro-optic signal becomes maximal. We perform this measurement for a single (constant) carrier frequency. Now we fix the wavelength of the incident laser beam to  $\lambda_{\text{ModulationMax}}$  and we sweep the frequency of the microwave signal over the requested frequency range and we calculate the voltage and the phase shift of the microwave signal.

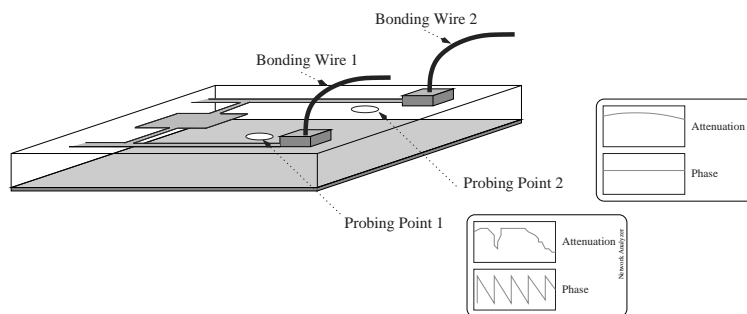


**Figure 93** Setup for the probing of the S-Parameter.

By doing the same procedure at the input and the output of structure under test, we can deduce the  $s_{21}$  parameter (Figure 93) under the condition that the input and output impedance are well defined. By switching the input and the output we can also find the  $s_{12}$  parameter. On the other hand our probing technique can only probe the  $s_{11}$  parameter respectively the  $s_{22}$  parameter under special

conditions (microwave signal with wavelength about the same length as the wave guide).

## 14.2 Results

As an example we analyze the GaAs MMIC displayed in Figure 94. We used the port “DP3” as input and “DP4” as output. The device is not supposed to operate this way but this setup allows use to verify the propagation of the microwave signal along the signal path and to apply our probing technique.

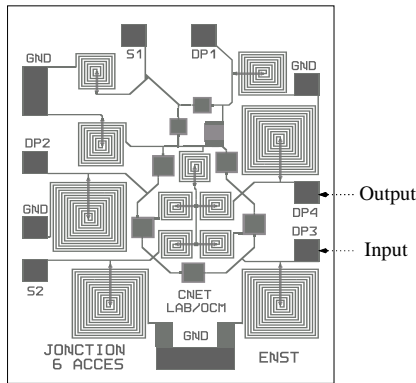


**Figure 94** Layout of the GaAs MMIC used for the probing of the s-parameter.

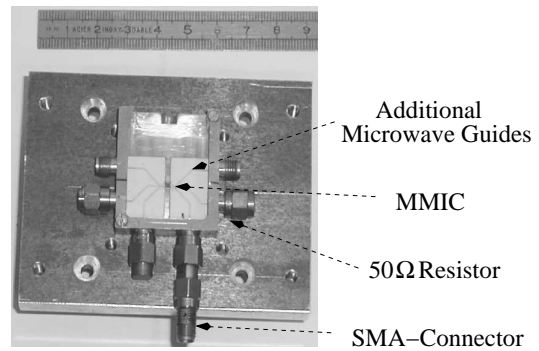


**Figure 95** Wiring of the MMIC with the corresponding SMA connectors.

We begin by measuring the  $s_{21}$  parameter ‘classically’ by connecting a calibrated network analyzer. Thus we measured the attenuation between the SMA connector of the input port and the SMA connector of the output port as displayed in Figure 95. In Figure 96 we have the attenuation in function of the frequency and in Figure 97 we have the corresponding phase shift. The measured parameters are different from the parameters between the bonding pads as the additional wave guides between the SMA connector and the bonding pad will influence the results. The measurement of the attenuation is only slightly affected but the probed phase shift will be wrong. Hence the s-parameter probed with the electro-optic probing tool will not match exactly these measurements.

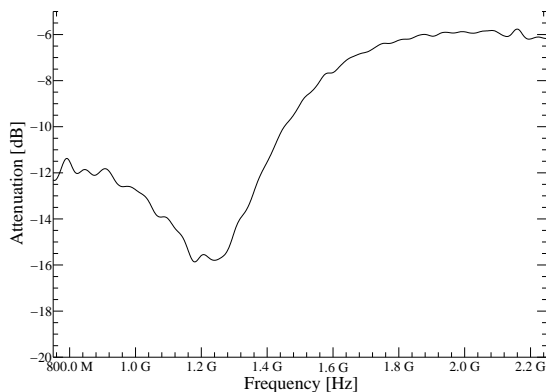


**Figure 96**  $S_{21}$  Attenuation.

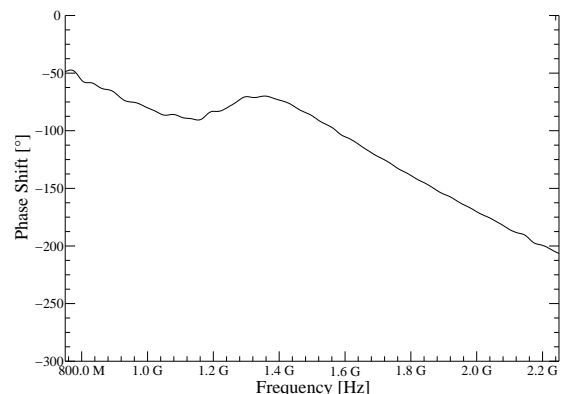


**Figure 97**  $S_{21}$  Phase Shift.

For this measurement we use a frequency range starting at 800 [Mhz] and stopping at 2250 [MHz]. There are two reasons for this choice: First the MMIC under test is designed for signals around

1500 [MHz]. The other reason is that we use several bandwidth critical instruments (amplifiers and photodiode) for the electro-optic probing.

For the electro-optic probing of the  $s_{21}$  parameter, we measured the electric field just beside the input and the output gate respectively. For identical settings we calculated the voltage and phase shift in the range between 800 [Mhz] and 2250 [MHz]. In Figure 98 is plotted the voltage and the phase shift probed beside the input port. This measurement is strongly affected by the frequency dependent gain of the photo detector and the transmission parameters of the microwave cables. This error is not critical as the probing at the output port (Figure 99) is affected in the same way. When we calculate the attenuation and the phase shift between Figure 98 and Figure 99, this error will fall out of the calculation. The calculated attenuation of Figure 100 is similar with the results of Figure 96. On the other hand the results of the phase shift does not match with the parameter of Figure 97 as we could not take into account the phase shift caused the additional wave guides and the bonding wires.

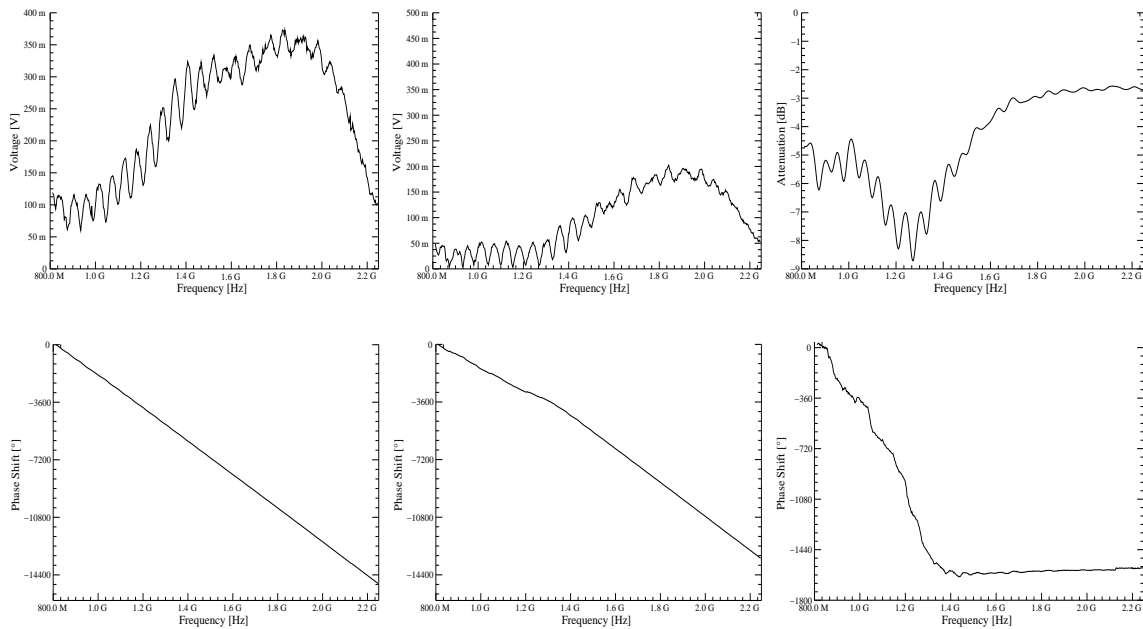


**Figure 98** Voltage and Phase shift probed beside the input port. **Figure 99** Voltage and phase shift probed beside the output port. **Figure 100**<sup>a</sup> Attenuation and difference in phase shift between the input and output signal.

- a. In this figure, we display the attenuation of the signal voltage. In Figure 96 we have the attenuation of the signal power. As  $dB_{Power} = 2dB_{Amplitude}$ , both plots match.

### 14.3 Comment

In this chapter we displayed that we can probe parts of the s-parameter under the condition that the input and output impedances are well defined. Hence we are able to analyze the functioning of parts of the design layout. The difference between the electro-optic probed attenuation and the electric acquired attenuation is caused by different configuration for the electro-optic probing at the input and output port. As the distance between the microwave guide and the probing point is not identical for both probing, there is a slight difference in amplitude. The two measurements of the phase shift do not match as the “lengths” of the microwave guides are different.

## 15 Signal processing with Stimulated Brillouin Scattering

As we could observe in the previous paragraphs, the magnitude of the electro-optic modulation is extremely weak. On the other hand the average power is several orders of magnitudes stronger. We illustrate a typical optical spectrum in Figure 101. The carrier represents the optical average power and the modulation corresponds with the electro-optic signal. This situation is disadvantageous for the further signal processing. Common commercial fast photo detectors have a “Maximum Operating Input Optical Power” (specifies the limits of its linearity) between 1 [mW] and 2 [mW]. Even without an optical amplifier, we risk to saturate or even damage the photo detector.

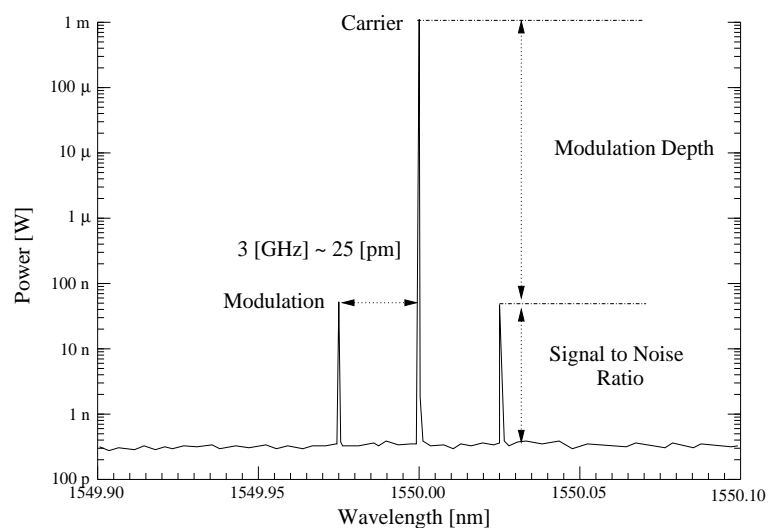


**Figure 101** Optical spectrum of the probing signal. The average power of the carrier is 1 [mW] and the amplitude of the modulation 100 [nW]. The noise level is supposed to be around 300 [pW].

So we are looking for an optical device that attenuates the power of the carrier and amplifies the modulation. Ideally such a device would not decay the signal to noise ratio or with other words would not generate additional noise. The attenuation of the carrier should be independent of the input power as well as the gain of the modulation.

The work presented in the following paragraph is the result of the thesis (Diplôme d’Études Approfondis) of Petra Schmitt. We realized the corresponding experimental setups together in the laboratory in winter 2001. The aim of this thesis was to investigate if we could use the proposition of [ 45 ] using Stimulated Brillouin Scattering (SBS) to enhance the modulation depth.

As nonlinear fiber optics is not the topic of this thesis, we will only indicate the basic ideas of Brillouin scattering. More detailed description of SBS can be found in [ 2 ], [ 9 ] or [ 10 ]. After an introduction of Brillouin scattering we will present the experimental results.

## 15.1 Principles of Stimulated Brillouin Scattering

In a “real” transparent material e.g. an optical fiber not the entire laser beam is passing through. A part of the injected laser beam is scattered backwards. One possible origin for the back-scattering is the local variations of the refractive index.

### 15.1.1 Spontaneous Brillouin Scattering

Acoustic waves are a possible source for inhomogeneities in optical fibers. According to [ 9 ] acoustical vibrations are already excited at normal temperatures due to thermal movement of the lattice. These waves propagate either in the forward or in the backward direction of the fiber. The acoustic wave induces region with different stress and hence generates an index grating inside the material. A laser beam can be reflected from this grating depending on the periodicity of the grating. As the acoustic wave propagates inside the optical fiber, the according grating is moving as well. An incident lightwave will be scatter backwards from this grating. As the grating is moving, the frequency of the reflected laser beam will be shifted due to the Doppler effect. If the acoustic wave co-propagates with the lightwave, the frequency of the back-scattered wave (called Stokes) will be downshifted. The frequency of the back-scattered laser beam will be shifted upwards (Anti-Stokes) if the acoustic wave moves in the opposite direction.

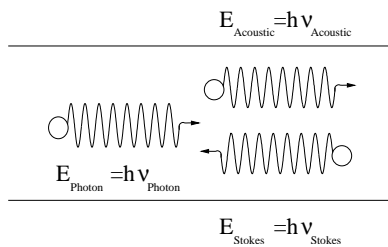


**Figure 102** Generation of the Stokes wave: A photon with an energy  $E_{\text{Photon}}$  and a Frequency of  $\nu_{\text{Photon}}$  is scattered backwards by an acoustic phonon.

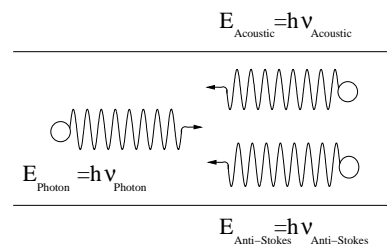


**Figure 103** Generation of the Anti-Stokes wave: A photon with an energy  $E_{\text{Photon}}$  and a Frequency of  $\nu_{\text{Photon}}$  is scattered backwards by an acoustic phonon.

The quantum theoretical explanation of this process is illustrated in Figure 102. On the left side is the incident photon with energy  $E_{\text{Photon}}$ . On the right hand we have an acoustic phonon with energy of  $E_{\text{Acoustic}}$ . The back-scattered Stokes photon has an energy of  $E_{\text{Stokes}}$ . The generation of the Anti-Stokes wave with an upwards shifted frequency is displayed in Figure 103.

### 15.1.2 Stimulated Brillouin Scattering

Now we will investigate the case of SBS. The difference between SBS and Spontaneous Brillouin Scattering is the generation of the acoustic wave. For SBS the acoustic wave is generated by the involved lightwaves themselves. Hence the SBS is not based on the acoustic phonons generated by thermal movements.

The main physical process behind the “optical” generation of acoustic phonons is the electrostriction in optical fibers. Dielectric materials like the silicon of optical fibers have the tendency to compress in the presence of an electric field. As the electric field of a laser beam inside a fiber can reach very high values, the electrostriction can trigger the generation of acoustic waves.

In Figure 104 we can see two contra propagating laser beams inside a glass fiber. The frequency and hence the wavelength of the two laser beams are slightly different. The electric field of the for-

ward and backward respectively traveling lightwave can be described by the wave equations given in Equation (131).

$$\begin{aligned} E_{\text{Forward}}(x, t) &= E_{\text{Amplitude}} \cdot \sin(2\pi v_{\text{Forward}}t - k_{\text{Forward}}x - \phi) \\ E_{\text{Backward}}(x, t) &= E_{\text{Amplitude}} \cdot \sin(2\pi v_{\text{Backward}}t + k_{\text{Backward}}x) \end{aligned} \quad (131)$$

$E_{\text{Amplitude}}$  is the magnitude of the electric field at the input. As we neglect for the moment all losses this parameter remains constant for the entire fiber.  $v_{\text{Forward}}$  and  $v_{\text{Backward}}$  respectively are the frequencies of the laser beams and  $k_{\text{Forward}}$  and  $k_{\text{Backward}}$  the corresponding wavevectors. The propagation direction is given by the signs of the wavevector  $k_{\text{Forward}}$  and  $k_{\text{Backward}}$ .  $x$  represents the position in the fiber,  $t$  the time and  $\phi$  is a phase shift between the two waves. Thus the sum of both electric fields is given by Equation (132).

$$\begin{aligned} E_{\text{Sum}}(x, t) &= E_{\text{Forward}}(x, t) + E_{\text{Backward}}(x, t) \\ &= 2 \cdot E_{\text{Amplitude}} \cdot \sin\left(2\pi t\left(\frac{v_{\text{Forward}} + v_{\text{Backward}}}{2}\right) - x\left(\frac{k_{\text{Forward}} - k_{\text{Backward}}}{2}\right) - \frac{\phi}{2}\right) \cdot \cos\left(2\pi t\left(\frac{v_{\text{Forward}} - v_{\text{Backward}}}{2}\right) - x\left(\frac{k_{\text{Forward}} + k_{\text{Backward}}}{2}\right)\right) \end{aligned} \quad (132)$$

The resulting distribution is illustrated in Figure 104. As we could expected the superposition of the two waves leads to interferences and hence to regions with very high electric field magnitudes and regions with weaker ones. Due to electrostriction, periodical compression patterns are induced in the material. The propagation velocity and periodicity of this pattern are given by the difference of the optical frequencies  $v_{\text{Forward}}$  and  $v_{\text{Backward}}$ . If this propagation velocity matches the speed of sound in silicon (typically around 5960 [m/s] [ 2 ]) a new acoustic wave is created.

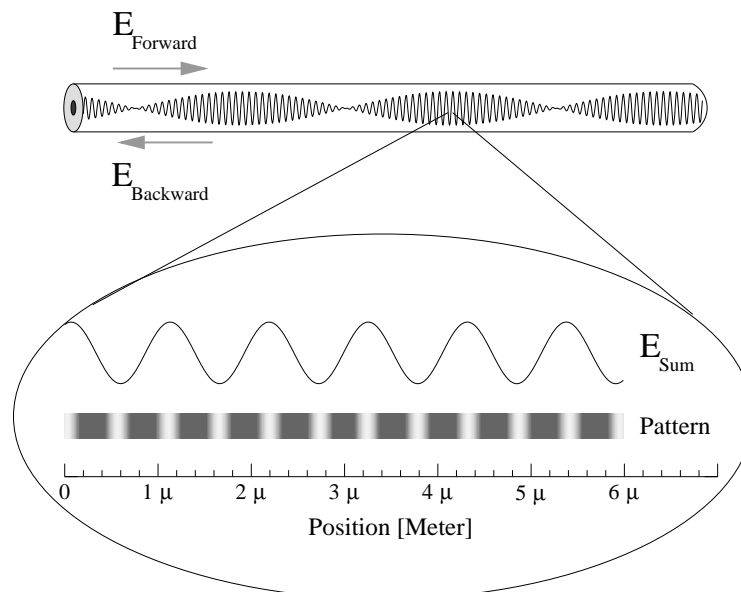


**Figure 104** Pattern generated by the interferences of the two lightwaves in function of the position (time is constant). The condition for the generation of a Stokes wave is that the periodicity of the pattern satisfies  $\lambda_{\text{Stokes}} = 2 \cdot n_{\text{Fiber}} \cdot \Lambda$ . The parameter  $\lambda_{\text{Stokes}}$  is the wavelength of the Stokes wave,  $n_{\text{Fiber}}$  the refractive index of the fiber and  $\Lambda$  is the periodicity of the pattern.

When we inject only one laser beam (often called the pump) into an optical fiber, there will be no generation of an acoustic wave at the beginning. As there is always some Spontaneous Brillouin Scattering, there will be a weak Stokes and Anti-Stokes wave traveling backwards. Hence we have

two (with the Anti-Stokes three) contra-propagating lightwaves in the glass fiber. These contra-propagating waves will cause the generation of new acoustic phonons and hence amplify the acoustic wave as well as the back-scattered laser beam. Thus we ignite a process that amplifies itself. This process is called the SBS.<sup>1</sup>

We have to add some comments about the Anti-Stokes wave. According to [ 9 ] the Stokes and the Anti-Stokes wave have similar intensities for the case of Spontaneous Brillouin Scattering. For SBS the Anti-Stokes wave becomes negligible. We can explain this by using the quantum theoretical explanation. The energy and the moment of the photons and the phonons have to be preserved during the “optical” generation of an acoustic phonon. Thus we can establish the relation of Equation (133) between the wavevectors and frequencies of the implied photons and phonons. By following [ 2 ] we can demonstrate that these conditions are not satisfied for the Anti-Stokes wave.

$$\begin{aligned} v_{\text{Photon}} &= v_{(\text{Anti-})\text{Stokes}} + v_{\text{Phonon - Acoustic}} \\ k_{\text{Photon}} &= k_{(\text{Anti-})\text{Stokes}} + k_{\text{Phonon - Acoustic}} \end{aligned} \quad (133)$$

Now there remains one important point to investigate. How will the SBS behave in function of the pump power? We are especially interested in the intensity of the Stokes wave in function of the pump power. We know that the SBS amplifies the scattered Stokes wave. This gain depends on the power of the pump wave as well as on the fiber properties and the linewidth of the injected pump. As long as this gain is smaller than the losses or attenuation in the optical fiber, the Stokes wave due to the SBS will not appear and we will find only Spontaneous Brillouin Scattering. If the gain becomes much stronger than the losses, the SBS will increase with the pump power. The mathematical description of this behavior can be found in [ 2 ] or [ 9 ]. The interesting point for our experiment is that we find a kind of threshold or nonlinearity. Below the threshold there is practically no back-scattering. The lightwave propagation in the forward direction is only affected by the absorption of the optical fiber. Above the threshold a big part of the incident laser beam is scattered backwards and hence the attenuation of the forward propagation wave becomes much higher.

So the basic idea behind the following experiment is to deplete the carrier with SBS as its magnitude is well above the threshold. The modulation should not be attenuated in the same manner, as it is below the threshold.

## 15.2 Verification of the threshold and spectrum of the lightwave

### 15.2.1 Measurement Setup

In this chapter we realize an experimental setup for the modulation depth enhancement following the proposition of [ 45 ]. In this proposition the optical signal to process is injected in a 10 [Km] long fiber. The Stokes wave generated in this fiber is recovered by an optical circulator and is re-injected at the other end of the fiber as illustrated in Figure 105. The reinjection of the Stokes wave enhances the Brillouin process as there is always a “significant” Stokes wave in the fiber even at its end. Hence the threshold is significantly lower and the depletion of the carrier is stronger.

In this paragraph we try to reproduce the results of [ 45 ] with the equipment of our laboratory. The goal of this measurement is to determine the Brillouin threshold and the optical spectra of the scattered and transmitted laser beams. For the moment we neglect the behavior of the modulation.

---

1. Another possibility is to inject a weak optic signal with a carrier frequency of  $v_{\text{Stokes}}$  into the fiber. This signal propagating in the opposite direction as the pump will be amplified by the Brillouin Scattering. This effect can be used to make amplifiers with narrow bandwidth.

As a signal source we use a DFB laser (Alcatel 1905LMP). We control its current and temperature so that the output power is about 43 [mW]. With an optical attenuator we adjust the power of the laser beam injected into the circulator between 0 [mW] and 28.8 [mW]. This laser beam is injected into the loop as displayed in Figure 105. In our setup we use an 11 [Km] long dispersion shifted fiber<sup>1</sup> for the generation of the Stokes wave. The end of this fiber is connected to port 1 of a 90:10 coupler. Port 2 of this coupler is connected to the output of a tunable attenuator linked to port 3 of the circulator. Port 3 and port 4 of the 90:10 coupler are used to monitor the transmitted signal and the back-scattered Stokes wave. The tunable attenuator has a special function. As the intensity of the Stokes waves increases with the injected power, there will be a point where the re-injected Stokes at the other end of the fiber will create a new Stokes wave itself. This would be very harmful, as this additional Stokes wave would scatter directly on the detection system. Hence we have an interest that the intensity of the re-injected Stokes remains below its Brillouin threshold. With the tunable attenuator and by observing the optical spectrum, we adjust the intensity of the re-injected Stokes wave so that it is just below this threshold.

With a power meter we trace the intensity of the back-scattered Stokes wave and the transmitted signal in function of the injected power. In this way we can determine the threshold for the Brillouin scattering. By opening the loop we can demonstrate that the SBS is much stronger and more stable with the reinjection of the Stokes wave. We open the loop by undoing the connection on port 1 of the coupler and on port 2 respectively.

After determining the Brillouin threshold, we will measure the optical spectrum. With an optical spectrum analyzer we measure the spectrum of the transmitted signal as well as the characteristics of the back-scattered beam. We execute this acquisition twice: Once for the injected laser beam power well above the threshold and another one for the power below it.

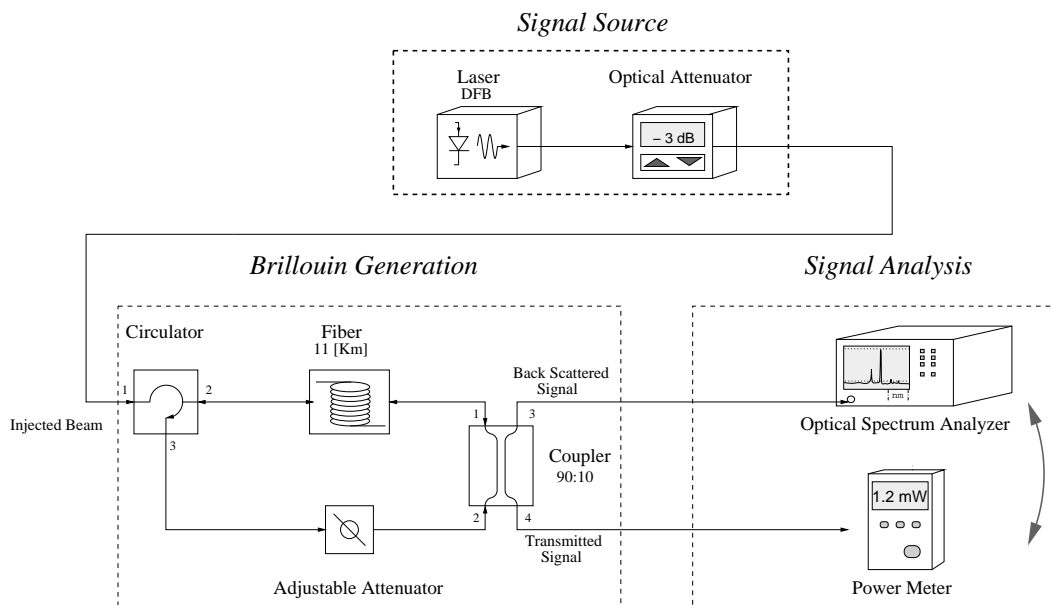


**Figure 105** Configuration used to verify the Brillouin threshold in function of the incident laser beam.

1. Dispersion null point=1560 [nm] and  $A_{\text{Effective}}=50 [\mu\text{m}^2]$ .

### 15.2.2 Results

In Figure 106 we display the intensity of the back-scattered Stokes wave in function of the injected power. As we can see there is hardly any power scattered backwards for low injected intensities. If the injected laser beam exceeds the threshold, the intensity of the back scattered Stokes waves increases linearly with the injected power. In Figure 107 we can see that transmitted power increases linearly up-to the threshold as no nonlinear effect affects its propagation. Above the threshold the transmitted power decreases even that injected power keeps increasing. For the maximal injected power, the transmitted signal is attenuated by about 20 [dB]. The dashed data indicates the same measurements without a re-injection of the Stokes wave. For this case the threshold is about four times higher.

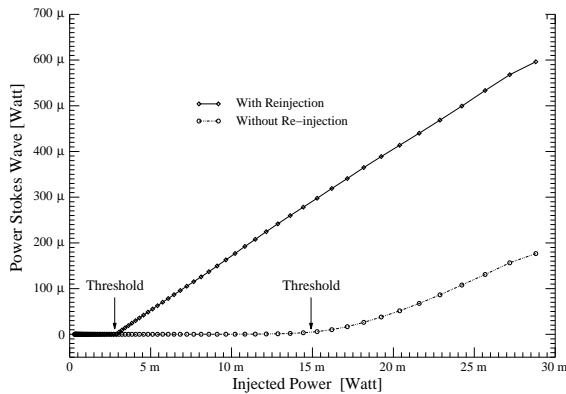


**Figure 106** Power of the back scattered Stokes wave in function of the injected power.

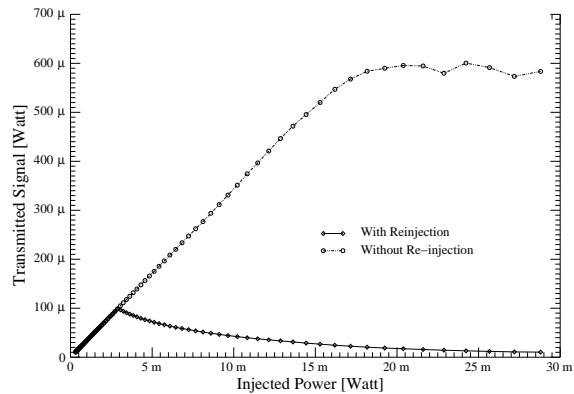


**Figure 107** Power of the transmitted wave in function of the injected power.

Now we investigate the spectra of the different signals. For all measurement we used the same spectrum analyzer with the same configuration (resolution of 10 [pm] etc.). We begin with the measurements below the threshold. Thus we set the attenuator in Figure 105 to -12 [dB]. In Figure 108 we can see the optical spectrum of the transmitted laser beam. The spectral characteristics of the lightwave are hardly affected. The lightwave is only attenuated by -15.2 [dB] due to the losses in the circulator (-1.8 [dB]), the dispersion shifted fiber (-3.2 [dB]) and the 10:90 coupler (-10.2 [dB]).

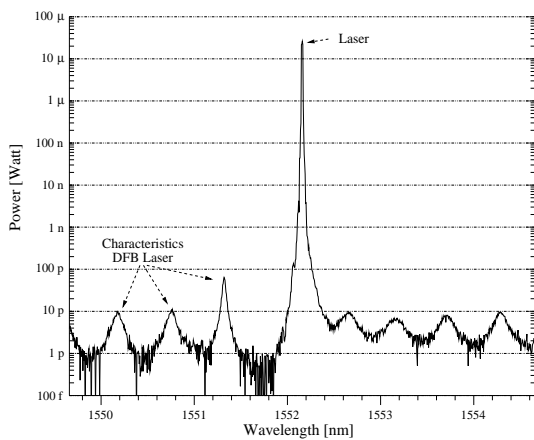


**Figure 108** Spectrum of the transmitted laser beam for an injected power below the threshold.

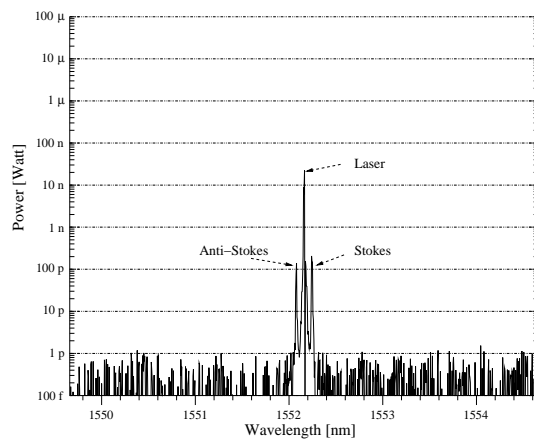


**Figure 109** Spectrum of the back-scattered waves. In this plot we can observe that the Stokes and the Anti-Stokes have about the same intensity.

In Figure 109 the back-scattered Stokes as well as the Anti-Stokes wave are very weak. Both have similar intensities. The reflected peak at the laser beam frequency is due to an unintentional reflection from a fiber connector.

Now we repeat the same measurement for the maximal injected power. These results are displayed in Figure 110 (transmission) and Figure 111 (reflections). We can observe that the transmitted beam is strongly attenuated by the depletion of the carrier. If we compare Figure 110 and Figure 111, we can see that the Stokes wave is now stronger than the transmitted signal.

In Equation (134) we determine the frequency shift  $\Delta\nu$  between the injected beam and the back scattered Stokes wave.  $\nu_{\text{InjectedBeam}}$  and  $\lambda_{\text{InjectedBeam}}$  is the frequency and the wavelength respectively of the injected laser beam.  $\nu_{\text{Stokes}}$  and  $\lambda_{\text{Stokes}}$  represent the same parameters for the Stokes wave.  $c_0$  is the speed of light in vacuum.

$$\begin{aligned} \Delta\nu &= \nu_{\text{InjectedBeam}} - \nu_{\text{Stokes}} = c_0 \left( \frac{1}{\lambda_{\text{InjectedBeam}}} - \frac{1}{\lambda_{\text{Stokes}}} \right) \\ &= 2.99792458 \cdot 10^8 \left[ \frac{m}{s} \right] \left( \frac{1}{1552.16 \cdot 10^8 [m]} - \frac{1}{1552.24 \cdot 10^8 [m]} \right) = 9.9544 \cdot 10^9 [Hz] \end{aligned} \quad (134)$$

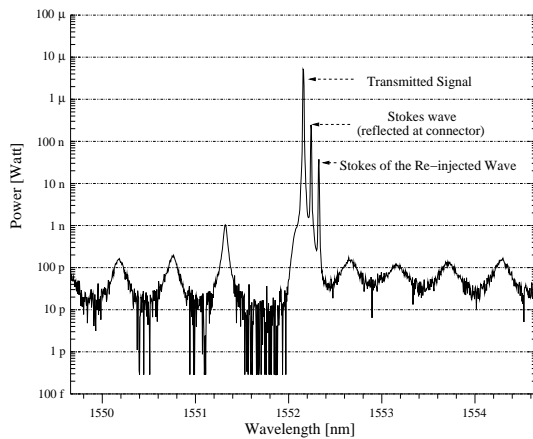


**Figure 110** Spectrum of the transmitted laser beam for the maximal injected power. The laser peak is attenuated. There is also a small Stokes wave due to an unintentional reflection from a connector. We can also observe an additional Stokes wave generated by the re-injected beam.

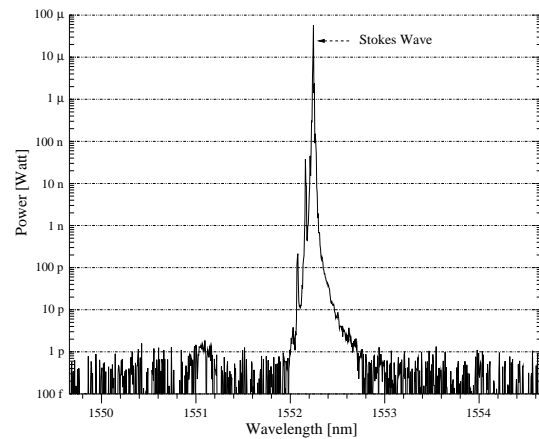


**Figure 111** Spectrum of the back scattered lightwaves for the maximal injected power (means attenuator set to  $-0[\text{dB}]$ ). We can see the spectrum of the back-scattered Stokes wave.

## 15.3 Modulation depth enhancement and the Signal to Noise Ratio

### 15.3.1 Measurement Setup

In the last chapter we analyzed the behavior of an unmodulated laser beam. In this chapter we will use a very weak modulation as described in Figure 101. The goal of this chapter is to verify if we can improve the modulation depth similar to [44] or [45]. Afterwards we will do some further investigation missing in these references. We will have a look at the signal to noise ratio at the input and the output. So we can verify if the Brillouin scattering induces additional noise.

As a signal source we use the same DFB laser. We modulate the laser current slightly by connecting

a signal generator to the RF-input of the laser. We adjust the magnitude of the microwave signal in a way that the carrier is 40 [dB] stronger than the modulation. The modulation frequency is 1 [GHz]. The rest of the experimental setup is similar to the configuration of the previous paragraph. The only difference is that we use an electrical spectrum analyzer with an integrated photo detector to measure the modulation, the noise level as well as the average power of the transmitted signal. With these data we can calculate the modulation depth and the signal to noise ratio. For the further deductions we define the modulation depth as the relation between the carrier power and the magnitude of the modulation according to Equation (135).

$$\text{ModulationDepth[dB]} = \text{Modulation[dBm]} - \text{AveragePower[dBm]} \tag{135}$$

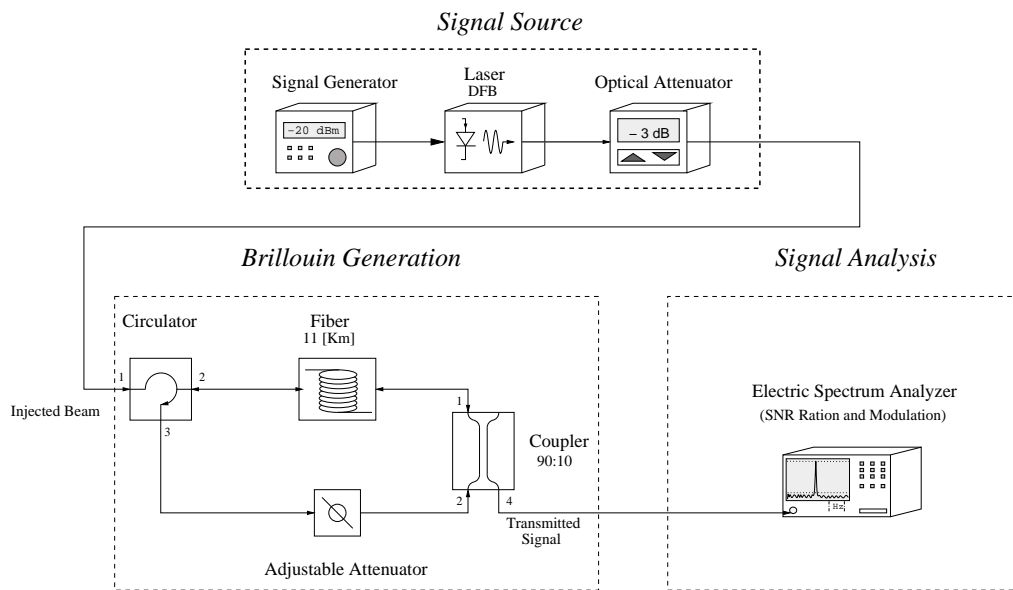
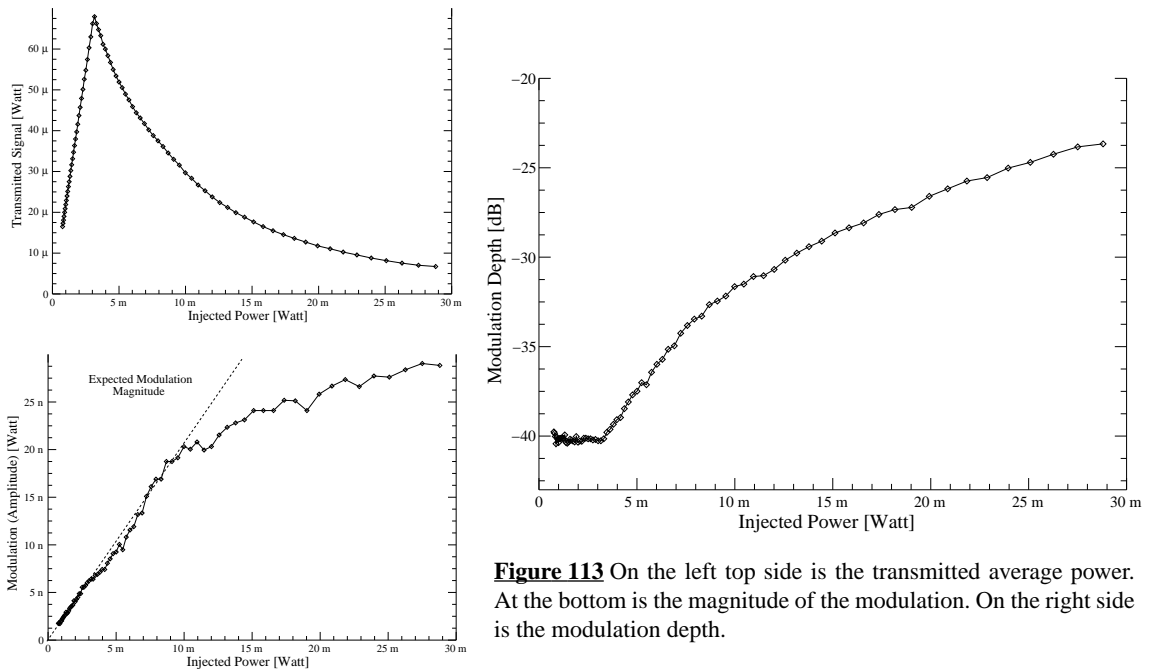


**Figure 112** Configuration used to measure the processing of the modulation.

### 15.3.2 Results

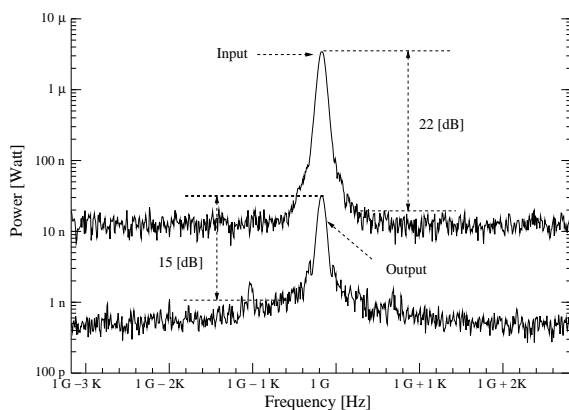
In Figure 113 we measure the power of the carrier as well as the magnitude of the modulation. The intensity differs slightly from the results in Figure 107 as another FC/PC connector induces some additional loss. In the discussion of theory we supposed that the weak modulation is not affected by the nonlinear effect. Following the setup of Figure 112, the modulation should only change in function of the attenuation induced by the attenuator. Hence it should decrease linearly with the injected power as the modulation is affected in the same way as this parameter.

Figure 113 shows the magnitude of the modulation. It increases linearly only for injected intensities below the threshold. Above the Brillouin threshold, it does not follow this relation anymore. Hence we have to assume that the modulation is affected by the scattering as well. On possible reason might be the “low” modulation frequency of 1 [GHz] as the modulation is only separated by 8 [pm] from the carrier. On the right hand of Figure 113, we see the modulation depth enhancement calculated following Equation (135). Below the Brillouin threshold, the modulation depth remains constant. Above the threshold it starts to increase with the injected intensity.



**Figure 113** On the left top side is the transmitted average power. At the bottom is the magnitude of the modulation. On the right side is the modulation depth.

Now we have a look at the noise level. We do this by looking at the spectrum of the modulation around 1 [GHz]. In Figure 114 we display the spectrum of the modulation of the injected signal (input) and of the transmitted signal (output). At the input we have a signal to noise ratio of about 22 [dB<sub>Optic</sub>]. The output signal is attenuated and hence the signal and noise level are lower. But also the signal to noise ratio decreased to 14 [dB<sub>Optic</sub>]. Thus the Brillouin scattering generates some additional noise. We can observe this effect in Figure 115. Here we plot the noise level in function of the injected power. We can see that the noise level remains constant as long as the input power does not exceed the Brillouin threshold. As the SBS becomes stronger, the noise level is significantly higher.



**Figure 114** Spectrum of modulation at the input and the output. The spectrum analyzer is set to a frequency span of 6 [KHz] and the resolution and video bandwidth are 61.9 [Hz] and 10 [Hz] respectively.

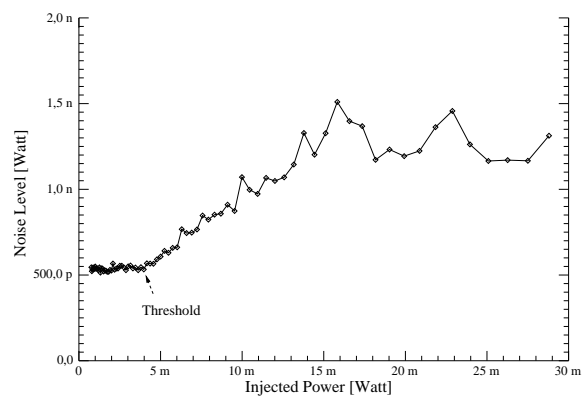


**Figure 115** Noise level in function of the injected power. The configuration of the spectrum analyzer is identical as in Figure 114.

## 15.4 Application of the Brillouin scattering in the probing setup

### 15.4.1 Measurement Setup

In the previous paragraphs, we used the signal of a modulated DFB laser. This had the advantage that we had a stable (relating to its intensity, modulation depth and wavelength) and simple signal source. In this experiment we will use the signal from the electro-optic probing tool.

The corresponding setup is displayed in Figure 116. We make an acquisition like in paragraph 12.1 and we investigate if we can still use the proposed calibration method. The output signal of the probing tool is rather weak (typically below 1 [mW]) and hence inferior to the threshold of Brillouin scattering. Hence we have to amplify the input signal. We do this by inserting an additional Erbium Doped Fiber Amplifier (EDFA) after the output of the electro-optic probing tool. As we have to tune the wavelength of the probing beam, we cannot use an optical filter to remove the spontaneous emission of the amplifier.

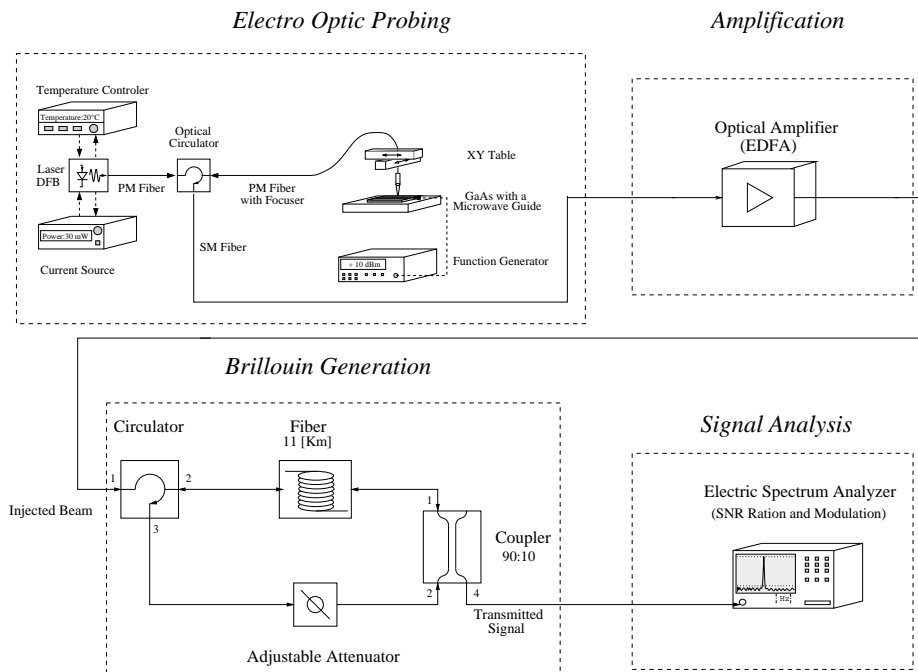


**Figure 116** Configuration used for the signal processing of the electro-optic probing signal.

### 15.4.2 Results

We begin by measuring the response of the Fabry Perot cavity similar to the acquisition of Figure 74. This signal is used as an input for the signal processing. In Figure 117 we can see the reflected intensity as the input as well as the processed signal at the output of the fiber loop. Ideally the Brillouin scattering would attenuate the input signal by a constant factor. This attenuation factor should be independent of the injected intensity. In this case the processed signal would show a sinusoidal behavior in function of the wavelength similar to the input signal. As we can observe, the attenuation factor is not constant at all. The origin of the problem is the spontaneous emission of the EDFA for very weak input signals. The Brillouin scattering does not attenuate this broadband spontaneous emission. Hence the average power at the output is very high for this case.

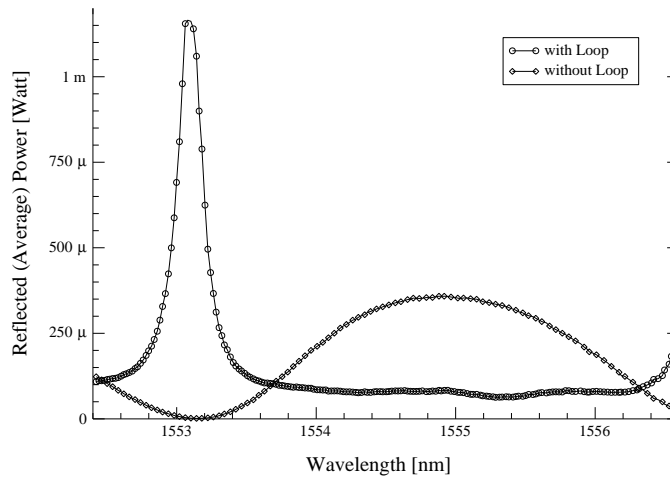


**Figure 117** Response of the Fabry-Perot response with and without signal processing by Brillouin scattering.

The variable attenuation of the average power makes it impossible to calculate the derivative  $\partial I_{\text{Reflected}} / \partial \lambda_o$  necessary for our probing technique. We could overcome this problem by adding an additional coupler before the input of the EDFA and measuring  $I_{\text{Reflected}}(\lambda_o)$  at this point.

In Figure 118 we can see the magnitude of the unprocessed electro-optic probing signal. This signal is equivalent to the signal of Figure 75. In Figure 119 we have the same modulation after signal processing with the Brillouin scattering. The modulation is also affected by the spontaneous emission of the EDFA. Hence the modulation depth enhancement is not linear in function of the injected power nor in function of the input modulation.

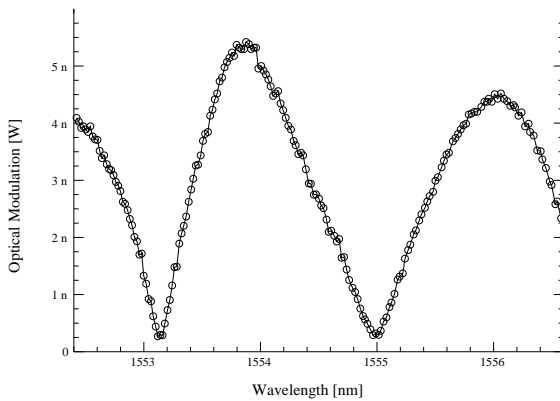


**Figure 118** Magnitude of the modulation before processing by Brillouin scattering.

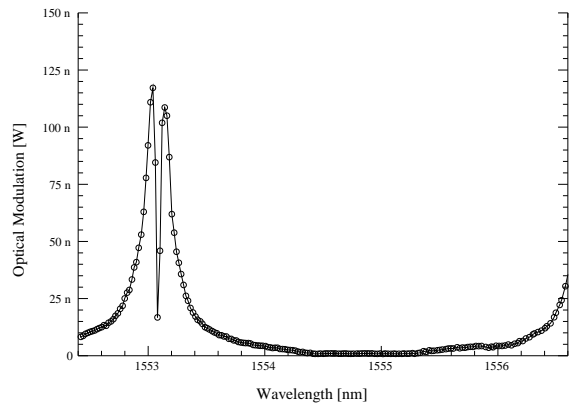


**Figure 119** Magnitude of the modulation after processing by Brillouin scattering.

## **15.5 Comments**

With the experiments presented in this paragraph, we could deplete the carrier with SBS. It was interesting to see that the increase in optical input power can cause a decrease of the output intensity. With this effect we could enhance the modulation depth of about 16 [dB] or about 40 times. This result is a little bit better than the results obtained in [ 45 ] (about 20 times). In our setup we attenuated intentionally the carrier but unfortunately also the modulation. For a decent signal processing the signal to noise ration should remain constant. As we could observe during our investigation, the Brillouin scattering generates some additional noise.

The noise generated by the Brillouin scattering is not the only problem. For the signal processing of the electro-optic probing tool, we have to amplify the signal. This additional amplifier adds even more noise and spontaneous emission.

The combination of problems makes the use of the signal processing very difficult. It would take all lot of work to analyze and solve these inconveniences (origin of the noise, relation between modulation depth enhancement and injected power and modulation at the input). We stopped the research on this topic at the end of the trainee-ship.

## 16 Conclusions of the Measurements

We realized a probing tool using only standard optical fiber and standard microwave equipment. By using polarization maintaining fibers, a pigtailed focuser and a powerful DFB laser we could improve the probing tool and simplify its configuration. The obtained results match well the theoretical calculations and thus we were able to calculate the electrical field caused by the microwave signal. With our probing setup we could measure the magnitude and phase shift with a sensitivity of about 2 [mV/Hz]. There was no problem to reproduce the measurements. By using this setup we could even determine parts of the s-parameter of a given structure. The bandwidth of the probing tool was limited only by the bandwidth of the photodiode and its amplifiers as well as by the bandwidth of the network analyzer.

On the other hand we had to handle a number of major principal and technical problems:

- The magnitude as well as the polarization of the probing beam changes in function of the wavelength. The origin of this problem is the DFB laser, as it is not designed for such an application.
- The divergence at the output of the glass fibers decays the spatial resolution and it causes additional loss. Ideally we should have a “perfectly” parallel laser beam (very small numerical aperture) with a beam diameter between 5 [μm] and 10 [μm]. We might improve the performance by using a laser with a shorter wavelength than 1550 [nm].
- We changed the wavelength of the laser by changing its operating temperature. As it takes some time to heat up or cool down the laser with the thermo-electric element, the probing of the voltage for one position can take between 30 [sec] and 1 [min]. So it is very time consuming to map the electric field distribution of an entire chip. The solution might be a tunable external cavity laser (ECL) with a high output power. As there was no adequate ECL available at the beginning of the thesis we could not check this option.

As “post scriptum” we want to mention that the entire measurement setup is computer controlled. The network analyzer, the voltmeter, the controller of the step motors as well as the temperature controller of the laser are linked to the computer through General Purpose Interface Bus (GPIB) cables. So we could launch all the data acquisition automatically which saved a lot of time (Figure 120). But on the other hand, I spent most of my Ph.D. thesis writing and correcting LabVIEW routines for our equipment (Until the end of my work I could not explain the origins of some crashes in the acquisition programs).

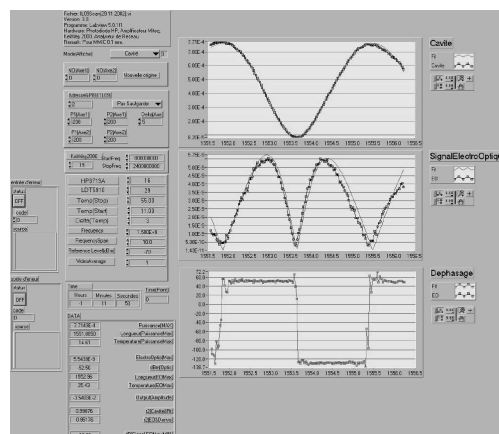


**Figure 120** Screen shot of a LabVIEW program acquiring the response of a cavity and the according modulation.



# Conclusion

In this thesis, we developed an electro-optic probing system for GaAs MMIC and we examined the technical and theoretical limits of a setup using standard optical fiber and microwave equipment. We used recent equipment like PM fibers, pigtailed focuser and a powerful DFB laser to improve previous measurement done in our laboratory.

As the GaAs crystal is electro-optic, we exploited this material property to probe the electric field caused by the microwave signal. We focused a laser beam into the DUT and we analyzed the modulated reflection. Hence we could probe the electric microwave signal inside the device and not outside as other probing techniques do. Different types of modulations are possible for the probing. We used an “amplitude modulation setup”, as this configuration is the simplest one for a continuous wave probing beam. This probing technique has also the advantage that for the calculation of the electric field and thus the applied voltage we have to divide the magnitude of the modulation  $I_{\text{Modulation}}$  by the derivative  $\partial I_{\text{Reflected}}/\partial \lambda_o$  of the Fabry Perot response. Hence all attenuations in the optical path are irrelevant as both terms are affected in the same way. Thus the only important point is to measure correctly the laser beam power and the magnitude of modulation of the reflected beam. An inconvenience is that this configuration allows us to measure only one component of the electric field vector. This is not a problem as long as the electric field is approximately parallel to the z-axis. Our assumption is satisfied as long as we probe the electric field near a microwave guide. For other probing positions the electric field vector could have other orientations. This effect causes a drawback as the optical axis of GaAs crystal depends on the electric field vector. Thus the measurements are systematically wrong for this condition.

During the realization of the probing setup, we faced several technical problems. One main problem is the shape of the laser beam. As the GaAs substrate is 100 [μm]-500 [μm] thick and as the microwave guides are typically 10 [μm] wide we should have a “perfectly” parallel laser beam (very small numerical aperture) with a beam diameter between 5 [μm] and 10 [μm]. Technically and also theoretically the output of standard fiber at 1550 [nm] cannot provide such a beam. We might enhance the system by using a laser with a shorter wavelength than 1550 [nm]. Another inconvenience is caused by the DFB laser source. For the probing of the electric field we have to sweep the wavelength over a certain range. We expected that the incident laser beam would have a well-defined polarization and a constant magnitude at the output of the PM fiber. In reality the output power as well as the polarization change in function of the wavelength. Though these problems decayed seriously the probing quality, we could sense the microwave signal inside the DUT. We are able to probe the amplitude and phase shift of a microwave signal with a sensitivity of  $2[\text{mV}/\sqrt{\text{Hz}}]$  and we can reproduce the measurements without any problem.

As a perspective we want to add that we might overcome most technical problems described in this thesis. But the necessary modifications and investments would harm the main goal of the presented work: The design of a simple and inexpensive tool for probing the electric field inside a GaAs MMIC. For the moment the market and hence the interest for such tools is rather small and so such an effort would not make any sense.



# *References*

## **17 Books and Thesis**

- [ 1 ] Sadao Adachi: "GaAs and related Materials", World Scientific Publishing Co., Page(s) 429, 1994.
- [ 2 ] Govind P. Agrawal: "Nonlinear Fiber Optics, Second Edition", Accademic Press, Page(s) 370-399, 1995.
- [ 3 ] Sadao Adachi: "Optical Constants of Crystalline and Amorphous Semiconductors", Boston : Kluwer, Page(s) 1-4 and 213-226, 1999.
- [ 4 ] F.T. Arecchi, E.O. Schulz-Dubois: "Laser Handbook", North-Holland Publishing Company, Page(s) 904-905, 1973.
- [ 5 ] B.E.A. Saleh, M.C. Teich: "Fundamentals of Photonics", John Willey & Sons, Inc, Page(s) 80-107, 193-235, 310-340, 696-735,1994.
- [ 6 ] DMK/DPK: "Formel und Tafeln", Orell Füssli Verlag Zürich, Page(s) 165, 1988.
- [ 7 ] Quang-Dai Le: "Sondage Electro-Optique de Circuits Intégrés avec des Lasers à Semiconducteurs en Fonctionnement Continu", Thesis ENST, 1995.
- [ 8 ] Philipp Olivier Müller: "Sondage Electro-Optique de Circuits Intégrés Hyperfréquences", Thesis ENST, 1997.
- [ 9 ] E.G. Sauter: "Nonlinear Optics", Wiley New York, Page(s) 77-91, 1996.
- [ 10 ] Petra Schmitt: "An electro-optical system for calibrated measurement of microwave monolithic integrated circuits", Diplomarbeit, TU-München (Lehrstuhl für Höchsthfrequenztechnik), Mai 2001.
- [ 11 ] John Wilson, John Hawkes: "Optoelectronics: An Introduction", Prentice Hall Europe, Page(s) 546, 1998.
- [ 12 ] Amon Yariv, Pochi Yeh: "Optical Waves in Crystals: Propagation and Control of Laser Radiation", John Wiley and Sons, Page(s) 54-154 and 220-316, 1983.

## **18 Publications, Journals and Proceedings**

### **18.1 Optical probing of Silicon CMOS chips**

- [ 13 ] William Lo, Steven Kasapi and Kenneth Wilsher: "Next-Generation optical probing tools for design debug of microprocessor integreted circuits" in *IEEE LEOS NEWSLETTERS*, Page(s) 3-7, December 2001.
- [ 14 ] J.A. Kash and J.C. Tsang:" Dynamic Internal Testing of CMOS Circuits Using Hot

- Luminescence” in *IEEE ELECTRON DEVICE LETTERS*, Volume 18, Number 7, Page(s) 320-332, July 1997.
- [ 15 ] James C. Tsang, Jefferey Alan Kash and David P. Vallett: “ Time-Resolved Optical Characterization of Electrical Activity in Integrated Circuits”, in *PROCEEDINGS OF THE IEEE*, Volume 88, Number 9, September 2000, Page(s) 1440-1459, September 2000.
- [ 16 ] Wai Mun Yee, Mario Paniccia, Travis Eiles and Valluri Rao: ” Laser Voltage Probe(LVP): A Novel Optical Probing Technology for Flip-Chip Packaged Microprocessors” in *PROCEEDINGS OF 7TH IPFA'99*, IEEE, Page(s) 15-20, 1999.

## 18.2 Electron Beam Probing

- [ 17 ] M. Batinic, B. Weisbrodt, W. Mertin and E. Kubalek: “ Comparison of measurement results obtained by electron beam testing and indirect electro optic sampling” in *MICRO-ELECTRONIC ENGINEERING*, Volume 31, Page(s) 33-40, 1996.
- [ 18 ] J. Frosien, C. Salvesen, R. Schmitt, K. Ueda and Y. Tokunaga: “High performance field emission column for next generation E-Beam Tester” in *NUCLEAR INSTRUMENTS AND METHODS IN PHYSICS RESEARCH (SECTION A)*, Volume 363, Page(s) 59-63, 1995.
- [ 19 ] Paul G. May, Jean-Marc Halbout, George L.-T. Chiu: “Noncontact High-Speed Waveform Measurements with the Picosecond Photoelectron Scanning Electron Microscope” in *IEEE JOURNAL OF QUANTUM ELECTRONICS*, Volume 24, Number 2, Page(s) 234-239, 1988.
- [ 20 ] William T. Lee: “ Engineering a device for Electron beam probing” in *IEEE DESIGN & TEST OF COMPUTERS*, June 1989, Page(s) 36-49.

## 18.3 Scanning Force Probing

- [ 21 ] G.E. Bridges: ”Vector-voltage scanning force probe for non-contact MMIC measurement” in *ELECTRONIC LETTERS*, Volume 35 Number 20, Page(s) 1724-1725, 1999.
- [ 22 ] C.J. Falkingham, I.H. Edwards and G.E. Bridges: “Non-contact internal-MMIC measurement using scanning force probing” in *MICROWAVE SYMPOSIUM DIGEST. 2000 IEEE MTT-S INTERNATIONAL*, Volume: 3, Page(s) 1619-1622, 2000.
- [ 23 ] R.A. Said: “Picoseconds measurement of internal waveforms in integrated circuits using sampling force probing. I. Principle and demonstration and II Applications, capabilities, and limitations” in *CIRCUITS AND SYSTEMS PROCEEDINGS ISCAS 2000 GENEVA*, Volume: 2, Page(s) 681-684 and 657-660, 2000.

## 18.4 Electro-Optic Probing

- [ 24 ] Lionel Duvillaret, Stephane Riolland and Jean-Louis Coutaz: “Electro-optic sensors for electric field measurements. I. Theoretical comparison among different modulation techniques” in *JOURNAL OF THE OPTICAL SOCIETY OF AMERICA B: OPTICAL PHYSICS*, Volume: 19, Issue 11, Page(s) 2692-2703, November 2002.
- [ 25 ] Lionel Duvillaret, Stephane Riolland and Jean-Louis Coutaz: ”Electro-optic sensors for electric field measurements. II. Choice of the crystals and complete optimization of their orientation” in *JOURNAL OF THE OPTICAL SOCIETY OF AMERICA B: OPTICAL PHYSICS*, Volume: 19, Issue 11, Page(s) 2704-2715, November 2002.

- [ 26 ] J. A. Valdmanis and G. Mourou: "Sub-picosecond electro-optic sampling: Principles and applications" in *IEEE JOURNAL OF QUANTUM ELECTRONICS*, Volume QE 22, Page(s) 69-78, 1986.

## 18.5 External Electro-Optic Probing

- [ 27 ] W. H. Chen, Wen-Kai Kuo, Sheng-Lung Huang and Yang-Tung Huang: "On-Wafer Electrooptic Probing Using Rotational Deformation Modulation" in *IEEE PHOTONICS TECHNOLOGY LETTERS*, Volume 12, Number 9, Page(s) 1228-1230, 2000.
- [ 28 ] Wen-Kai Kuo, Yang-Tung Huang and Sheng-Lung Huang: "Three Dimensional electric-field Vector measurement with an electro-optic sensing technique" in *OPTICS LETTERS*, Volume 24, Number 22, Page(s) 1546-1548, 1999.
- [ 29 ] Wen-Kai Kuo: "An electro-optic probing system for near electric field measurement using heterodyne method" in *LASERS AND ELECTRO-OPTICS CLEO/PACIFIC*, Volume 1, Page(s): I474-I475, 2001.
- [ 30 ] Mitsuru Shinagawa, Tadao Nagatsuma and Shintaro Miyazawa: "Sensitivity improvement of an electro-optic high-impedance probe" in *IEEE TRANSACTIONS ON INSTRUMENTATION AND MEASUREMENT*, Volume 47, Number 1, Page(s) 235 -239, 1998.
- [ 31 ] Kyoung Yang, Gerhard David, Jong-Gwan Yook, Ioannis Papapolymerou, Linda P.B. Katehi and John F. Whitaker: "Electrooptic Mapping and Finite-Element Modeling of the Near-Field Pattern of a Microstrip Patch Antenna" in *IEEE TRANSACTIONS ON INSTRUMENTATION AND MEASUREMENT*, Volume 48, Number 2, Page(s) 288-293, 2000.
- [ 32 ] Kyoung Yang, Todd Marshall, Michael Forman, John Hubert, Lee Mirth, Zoya Popovic, Linda P.B. Katehi and John F. Whiteaker: "Active-Amplifier-Array Diagnostics Using High-Resolution Electrooptic Field Mapping" in *IEEE TRANSACTIONS ON MICROWAVE THEORY AND TECHNIQUES*, Volume 49, Number 5, Page(s) 849-857, 2001.
- [ 33 ] Kyoung Yang, Linda P.B. Katehi and John F. Whiteaker: "Microwave-field imaging with a fiber-based electro-optic probe" in *LASER AND ELECTRO-OPTICS SOCIETY 2000 ANNUAL MEETING*, Volume 1, Page(s) 388 -389, 2000.

## 18.6 Internal Electro-Optic Probing

- [ 34 ] Didier Erasme, Stefan Lauffenburger, Bernard Huyart and Philipp Oliver Müller: "A all fibered measurement design for cw calibrated MMICs electro optic probing" in *Terahertz and Gigahertz Electronics and Photonics II, SPIE INTERNATIONAL SYMPOSIUM*, 2000.
- [ 35 ] Philipp Oliver Müller, Didier Erasme and Bernard Huyart: "New Calibration Method in Electrooptic Probing Due to Wavelength Control and Fabry-Perot Resonance" in *IEEE TRANSACTIONS ON MICROWAVE THEORY AND TECHNIQUES*, Volume 47, Number 3, Page(s) 308-309, 1999.
- [ 36 ] Philipp Oliver Müller, Stefan Lauffenburger, Didier Erasme and Bernard Huyart: "Système fibré de sondage électro-optique de circuits intégrés hyperfréquence" in *JOURNÉES NATIONALES D'OPTIQUE GUIDE*, Page(s) 327-329, 1999.
- [ 37 ] Quang-Dai Le, Didier Erasme and Bernard Huyart: "MMIC-Calibrated Probing by CW Electrooptic Modulation" in *IEEE TRANSACTIONS ON MICROWAVE THEORY AND*

*TECHNIQUES*, Volume 43, Number 5, Page(s) 1031-1035, 1995.

## 18.7 MMIC and GaAs

- [ 38 ] Alexander Hellemans: "Bonding Gallium Arsenide to Silicon Substrate" in *IEEE SPECTRUM*, Page(s) 33-34, Oktober 2001.
- [ 39 ] Philips Microwave GaAs MMIC Design Manual for Process D05ML, Ver. 1.0, July 1989.
- [ 40 ] Gail Purvis: "GaAs powers mobile phones" in *WIRELESS EUROPE*, Page(s) 35-37, April 2001.
- [ 41 ] Wolfgang Stieler: "Motorolas großer Sprung" in *C'T, MAGAZIN FÜR COMPUTER TECHNIK*, Number 20, Page(s) 62, 2001.

## 18.8 Other References

- [ 42 ] Andreas Kohlhaas, Carsten Frömchen and Ernst Brinkmeyer: "High-Resolution OCDR for Testing Integrated-Optical Waveguides: Dispersion-Corrupted Experimental Data Corrected by a Numerical Algorithm" in *JOURNAL OF LIGHTWAVE TECHNOLOGY*, Volume 9, Number 11, Page(s) 1493-1502, 1991.
- [ 43 ] Gabriel Campuzano, Carlos Palavicini, Philippe Gallion, Claude Chabran and Yves Jaouën: "Determination of Optically-induced complex index change using a phase-sensitive OLCR technique" in *PROCEEDINGS OF ECOC 2002*, 2002.
- [ 44 ] Alayn Loayssa, David Benito and Maria J. Garde: "Optical Carrier Brillouin Processing of micro wave photonic signals" in *OPTICS LETTERS*, Volume 25, Number 17, Pages(s) 1234-1236, 2000.
- [ 45 ] S. Tonda-Goldstein, D. Dolfi, J.-P. Huignard, G. Charlet and J. Chazelas: "Stimulated Brillouin scattering for micro wave signal modulation depth increase in optical links" in *ELECTRONICS LETTERS*, Volume 36, Number 11, Pages(s) 944-945, 2000.
- [ 46 ] Daomu Zhao: "Propagation of relative phase shift of apertured Gaussian beams through axis symmetric optical systems" in *OPTICAL AND QUANTUM ELECTRONICS*, Number 32, Page(s) 1239-1244, 2000.
- [ 47 ] Yingjie Gao and Ingo Wolff: "Miniature Electric Near-Field Probes for Measuring 3-D Fields in Planar Microwave Circuits" in *IEEE TRANSACTIONS ON MICROWAVE THEORY AND TECHNIQUES*, Volume 46, Number 7, Page(s) 907-913, 1998.

## 19 Internet/Electronic Data

- [ 48 ] <http://www.corning.com/opticalfiber/products> (12.3.2003).
- [ 49 ] <http://www.alcatel.com/opticalfiber> (12.3.2003).
- [ 50 ] <http://www.fujikura.co.uk> (12.3.2003).

# Appendix

## A. Constants

### A.1. General Constants in Vacuum

Speed of light in vacuum	$c_o = 2.99792458 \cdot 10^8 \left[ \frac{m}{s} \right]$
Permeability in vacuum	$\mu_o = 4 \cdot \pi \cdot 10^{-7} \cdot \frac{Vs}{Am} = 1.25663 \cdot 10^{-6} \left[ \frac{Vs}{Am} \right]$
Permittivity in vacuum	$\epsilon_o = 8.85418782 \cdot 10^{-12} \left[ \frac{As}{Vm} \right]$
Charge of electron	$e = 1.6021773 \cdot 10^{-19} [As]$
Planck constant	$h = 6.626075560 \cdot 10^{-34} [J] \quad [ 6 ]$

### A.2. Material Constants

#### A.2.1. Electro-Optic constants

Material	Group	$r_{xx}$ ([ 8 ])	Electro-optic coefficients in contracted notation ([ 5 ])	refraction indices n	$\epsilon/\epsilon_o$
GaAs (isotropic)	Cubic $\bar{4}3m$	$r_{41} = 1.4 \cdot 10^{-12} \left[ \frac{m}{V} \right]$ [ 1 ]	$\begin{bmatrix} 0 & 0 & 0 \\ 0 & 0 & 0 \\ 0 & 0 & 0 \\ r_{41} & 0 & 0 \\ 0 & r_{41} & 0 \\ 0 & 0 & r_{41} \end{bmatrix}$	$n_o = 3.374$ [ 3 ]	11.38 [ 3 ]
KDP (KH <sub>2</sub> PO <sub>4</sub> ) (anisotropic)	Tetragonal $\bar{4}2m$	$r_{41} = 1.4 \cdot 10^{-12} \left[ \frac{m}{V} \right]$ $r_{63} = 35 \cdot 10^{-12} \left[ \frac{m}{V} \right]$	$\begin{bmatrix} 0 & 0 & 0 \\ 0 & 0 & 0 \\ 0 & 0 & 0 \\ r_{41} & 0 & 0 \\ 0 & r_{41} & 0 \\ 0 & 0 & r_{63} \end{bmatrix}$	$n = 1.86$	

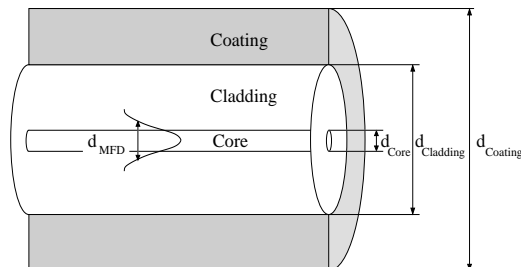
LiNbO <sub>3</sub> (anisotropic)	Trigonal 3m	$r_{33} = 30.8 \cdot 10^{-12} \left[ \frac{m}{V} \right]$ $r_{13} = 8.6 \cdot 10^{-12} \left[ \frac{m}{V} \right]$ $r_{22} = 3.4 \cdot 10^{-12} \left[ \frac{m}{V} \right]$ $r_{51} = 28 \cdot 10^{-12} \left[ \frac{m}{V} \right]$	$\begin{bmatrix} 0 & -r_{22} & r_{13} \\ 0 & r_{22} & r_{13} \\ 0 & 0 & r_{33} \\ 0 & r_{51} & 0 \\ r_{51} & 0 & 0 \\ -r_{22} & 0 & 0 \end{bmatrix}$	$n_o = 2.29$ $n_e = 2.20$	
-------------------------------------	----------------	--	--	------------------------------	--

### A.2.2. Semiconductor Constants at room temperature (300K)

Property	Si [ 11 ]	Ge [ 11 ]	GaAs [ 11 ]
Atomic (molecular) weight	28.09	72.60	144.6
Energy gap E <sub>g</sub>	1.12 [eV]	0.67 [eV]	1.43 [eV]
Intrinsic carrier concentration n <sub>i</sub>	$1.5 \cdot 10^{16} \left[ \frac{1}{m^3} \right]$	$2.4 \cdot 10^{19} \left[ \frac{1}{m^3} \right]$	$1 \cdot 10^{13} \left[ \frac{1}{m^3} \right]$
Electron mobility μ <sub>e</sub>	$0.135 \left[ \frac{m^2}{Vs} \right]$	$0.39 \left[ \frac{m^2}{Vs} \right]$	$0.85 \left[ \frac{m^2}{Vs} \right]$
Hole mobility μ <sub>h</sub>	$0.048 \left[ \frac{m^2}{Vs} \right]$	$0.19 \left[ \frac{m^2}{Vs} \right]$	$0.045 \left[ \frac{m^2}{Vs} \right]$
Relative permittivity ε <sub>r</sub>	11.8	16.0	10.9 <sup>a</sup>
Recombination constant B	$1.79 \cdot 10^{-21} \left[ \frac{m^3}{s} \right]$	$5.25 \cdot 10^{-20} \left[ \frac{m^3}{s} \right]$	$7.21 \cdot 10^{-16} \left[ \frac{m^3}{s} \right]$

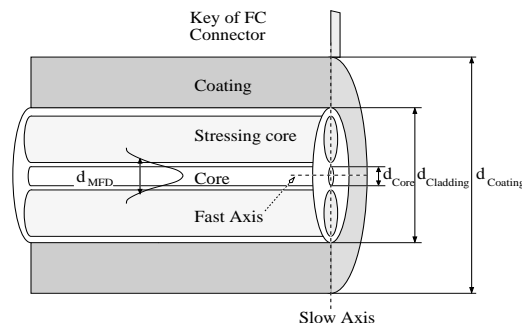
a. The range of values of relative permittivity of GaAs quoted in the literature is from about 10.7 to 13.6 [ 11 ].

### A.2.3. Typical dimensions and properties of Single Mode Silica Fiber



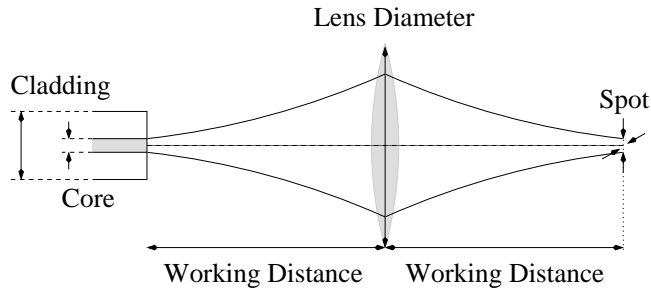
Properties	Corning SMF-28 at 1550 nm Alcatel [ 48 ]	Alcatel Cable Fiber 6900 Single Mode at 1550 nm [ 49 ]
Attenuation	$\leq 0.4 \left[ \frac{dB}{km} \right]$	$\leq 0.25 \left[ \frac{dB}{km} \right]$
Core Diameter	$8.2 [\mu m]$	$8.8 [\mu m]$
Cladding Diameter	$125 \pm 1 [\mu m]$	$125 \pm 1 [\mu m]$
Coating Diameter	$245 \pm 5 [\mu m]$	$242 \pm 7 [\mu m]$
Mode Field Diameter	$10.4 \pm 0.8 [\mu m]$	$10.2 \pm 1.0 [\mu m]$
Numerical Aperture	0.14	/
Zero Dispersion Wavelength	1313[nm]	$1310 \pm 10 [nm]$
Effective Group Index of Refraction	1.4682	1.47
Refractive Index Profile	0.36 %	/

#### A.2.4. Typical dimensions and properties of Panda Silica Fiber



Properties	Fujikura Panda at 1550 nm [ 50 ]
Attenuation	$0.5 \left[ \frac{dB}{km} \right]$
Core Diameter	$7 [\mu m]$
Cladding Diameter	$125 [\mu m]$
Coating Diameter	$900 [\mu m]$
Mode Field Diameter	$10.5 [\mu m]$
Numerical Aperture	0.12 – 0.13
Beat Length (Maximum)	$5 [mm]$

### A.2.5. Characteristics of pig tailed injectors



Focuser <sup>a</sup>	“A”	“B”	“C”
Working distance	3 [mm]	4.5 [mm]	10.1 [mm]
Fiber Core / Cladding Diameter	8 [μm] / 125 [μm]	8 [μm] / 125 [μm]	8 [μm] / 125 [μm]
Fiber Numerical Aperture	0.11	0.11	0.11
1/e <sup>2</sup> Spot Width (x-axis/y-axis)	12.8 [μm] / 13.3 [μm]	16.2 [μm] / 17.2 [μm]	21.5 [μm] / 22.3 [μm]
Lens Diameter	2 [mm]	3 [mm]	5 [mm]

a. Specifications according manufacturer.

## B. Acronyms

<b>AM</b>	Amplitude Modulation
<b>APC</b>	Angled Physical Contact
<b>BNC</b>	Bayonet Nut Connector
<b>CW</b>	Continuous Wave
<b>CMOS</b>	Complementary Metal-Oxide Semiconductor
<b>CNR</b>	Carrier to Noise Ratio
<b>dB</b>	Decibel
<b>dBm</b>	Decibels above/below one milliwatt
<b>DC</b>	Direct Current
<b>DFB</b>	Distributed FeedBack
<b>DUT</b>	Device Under Test
<b>ECL</b>	External Cavity Laser
<b>EDFA</b>	Erbium Doped Fiber Amplifier
<b>EO</b>	Electro-Optic
<b>FWHM</b>	Full Width Half Maximum
<b>FC</b>	Fibre Channel
<b>FP</b>	Fabry Perot
<b>GaAs</b>	Gallium Arsenide
<b>GPIB</b>	General Purpose Interface Bus
<b>IC</b>	Integrated Circuit
<b>LASER</b>	Light Amplification by the Stimulated Emission of Radiation
<b>LabVIEW</b>	LABoratory Virtual Instrument Engineering Workbench
<b>MFD</b>	Mode Field Diameter
<b>MMIC</b>	Microwave Monolithic Integrated Circuits
<b>NA</b>	Numerical Aperture
<b>PANDA</b>	Polarization maintaining AND Absorption reducing
<b>PM</b>	Polarization Maintaining
<b>PC</b>	Physical Contact
<b>QED</b>	Quod Erat Demonstrandum
<b>SMF</b>	Single Mode Fiber
<b>RF</b>	Radio Frequency
<b>SM</b>	Single Mode
<b>SiGe</b>	Silicon Germanium
<b>Si</b>	Silicon
<b>SNR</b>	Signal to Noise Ratio
<b>SOA</b>	Semiconductor Optical Amplifier
<b>SMA/B/C</b>	SMall connector type A/B/C

## C. Symbols

$c$	Speed of light in material	[Meter/Second]
$c_o$	Speed of light in vacuum	[Meter/Second]
$d$	Thickness of the substrate	[Meter]
$D$	Electric Displacement	[Ampère Second/Meter <sup>2</sup> ]
$E$	Electric Field	[Volt/Meter]
$f$	Frequency of a microwave signal	[Hertz]
$I$	Intensity	[Watt/Meter <sup>2</sup> ]
$n$	Refractive Index	[ ]
$n_o$	Refractive Index in the absence of an electric field	[ ]
$P$	Dielectric Polarization	[ ]
$r, R$	Reflection coefficient	[ ]
$r_{41}$	Electro-Optic coefficient	[Meter/Volt]
$r^2$	Cross correlation	[ ]
$t$	Time	[Second]
$V$	Voltage	[Volt]
$Z_{\text{Material}}$	Wave Impedance of a given Material	[Ohm]
$\epsilon$	Permittivity	[Ampère Second/ Volt Meter]
$\epsilon_o$	Permittivity of free space	[Ampère Second/ Volt Meter]
$\epsilon_r$	Relative Permittivity	[ ]
$\eta$	Impermeability Tensor	[ ]
$\xi$	Eigenvectors of a matrix	[ ]
$\lambda$	Wavelength	[Meter]
$\lambda_o$	Wavelength in vacuum	[Meter]
$\mu$	Permeability	[Volt Second/Ampère Meter]
$\mu_o$	Permeability of vacuum	[Volt Second/Ampère Meter]
$\mu_r$	Relative Permeability	[ ]
$\phi$	Phase Shift	[Radiant]
$\nu$	Frequency of a laser beam	[Hertz]
$\omega_o$	Beam waist of Gaussian Beam	[Meter]

## D. Units

There are several possibilities to characterize the power of laser beam or the amplitude of a microwave signal. This is a list of the most common units and the corresponding conversions.

### D.1. Optical Units

Units:	Watt or W	Power of the laser beam in Watt.
	Milliwatt or mW	Power of the laser beam in Milliwatt.
	dBm <sub>optic</sub>	Logarithmic unit based on Milliwatt.
	dB <sub>optic</sub>	Difference between the input and output optical power in dBm <sub>optic</sub> of a device to characterize its gain or loss.

Conversions and relations:

- Conversion Watt into Milliwatt (D.1):

$$y[mW] = 1000[W] \quad (D.1)$$

- Milliwatt into dBm<sub>optic</sub> (D.2):

$$y[dBm_{optic}] = 10 \cdot \log_{10} \left( \frac{x[mW]}{1[mW]} \right) \quad (D.2)$$

- dBm<sub>optic</sub> into Milliwatt (D.3):

$$y[mW] = 1[mW] \cdot 10^{\frac{x[dBm_{optic}]}{10}} \quad (D.3)$$

- Relation between input and output (D.4)

$$y[dB] = \text{Input}[dBm_{optic}] - \text{Output}[dBm_{optic}] \quad (D.4)$$

- Relation between input and output in per cent (D.5)

$$y[\%] = 100[\%] \cdot 10^{\frac{x[dB_{optic}]}{10[dB_{optic}]}} \quad (D.5)$$

### D.2. Electrical Units

Units:	Volt <sub>PeaktoPeak</sub> or V <sub>pp</sub>	Peak to peak value of the voltage.
	Volt or V <sub>amp</sub>	Amplitude of the voltage.
	Volt RMS or V <sub>rms</sub>	Root mean square value of the voltage.
	Milliwatt	Power of the electric signal in Milliwatt absorbed in a resistor (for micro wave signal typically 50 Ω).
	dBV	Logarithmic unit based on the rms voltage of the signal.
	dBm <sub>electric</sub>	Logarithmic unit based on the power of a microwave signal.
	dB <sub>electric</sub>	Difference between the input and output electric power in dB <sub>electric</sub> of a device to characterize its gain or loss.

Conversions and relations:

- $V_{pp}$  into  $V_{amp}$  and  $V_{amp}$  into  $V_{pp}$  (Figure D.1):

$$\begin{aligned} y[V_{amp}] &= \frac{1}{2}[V_{pp}] \\ y[V_{pp}] &= 2[V_{amp}] \end{aligned} \quad (D.6)$$

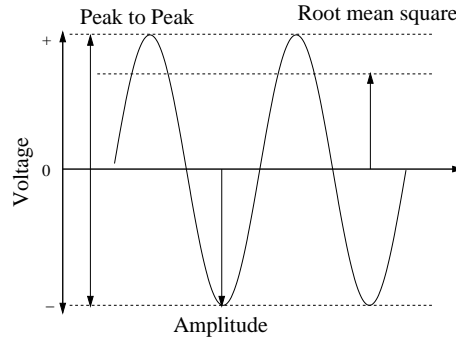


**Figure D.1** Different expressions for the voltage.

- $V_{rms}$  into  $V_{amp}$  and  $V_{rms}$  into  $V_{amp}$  (Figure D.1):

$$\begin{aligned} y[V_{amp}] &= \sqrt{2}[V_{rms}] \\ y[V_{rms}] &= \frac{1}{\sqrt{2}}[V_{amp}] \end{aligned} \quad (D.7)$$

- $V_{rms}$  into  $dB_{Volt}$  (D.8)<sup>1</sup>:

$$y[dB_{Volt}] = 20 \cdot \log_{10} \left( \frac{x[V_{rms}]}{1[V_{rms}]} \right) \quad (D.8)$$

- $dB_{Volt}$  into  $V_{rms}$  (D.9):

$$y[V_{rms}] = 1[V_{rms}] \cdot 10^{\frac{x[dB_{Volt}]}{20}} \quad (D.9)$$

- $V_{rms}$  into  $dBm_{electric}$  (in the case of a 50 [Ω] terminated connection) (D.10):

$$y[dBm_{electric}] = 10 \cdot \log_{10} \left( \frac{Power[W]}{1[mW]} \right) = 10 \cdot \log_{10} \left( \frac{x^2[V_{rms}^2]/50[\Omega]}{1[mW]} \right) \quad (D.10)$$

- $dBm_{electric}$  into  $V_{rms}$  (in the case of a 50 [Ω] terminated connection) (D.11):

$$y[V_{rms}] = \sqrt{50[\Omega] \cdot 0.001[W] \cdot 10^{\frac{x[dBm_{electric}]}{10}}} \quad (D.11)$$

---

1. For the conversion from linear into logarithmic units you have to multiply the normalize logarithms by a factor 20 if the unit is an amplitude (e.g. electric field, voltage, current etc.) and by 10 if the unit represents power or energy (e.g. electric power, laser beam intensity etc.). So you take into account that the power or energy is in general proportional to the square of its amplitude.

### D.3. Relation of Electrical and Optical Units

If a modulated laser beam is converted into an electric microwave signal by a 50 [Ω] terminated connection, we have to take into account that the current of the photodiode is proportional to the power of the incident laser beam  $I_{\text{Laserbeam}}$  (Figure D.1). Considering that the electric power  $P_{\text{Electrical}}$  of the signal is proportional to the square of the current, we have to convert the optical units of the modulation ( $\text{mW}_{\text{optic}}$  or  $\text{dBm}_{\text{optic}}$ ) into electrical units (Volt,  $\text{mW}_{\text{electric}}$  or  $\text{dBm}_{\text{electric}}$ ).

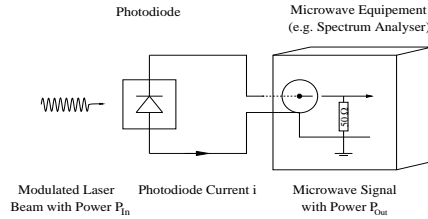


**Figure D.1** Conversion of a laser beam into a microwave signal with  $i_{\text{Photodiode}} = \alpha I_{\text{Laserbeam}}$ .

$$P_{\text{Electrical}} = i_{\text{PhotoDiode}}^2 \cdot R_{50\Omega} = \alpha^2 \cdot R_{50\Omega} \cdot I_{\text{Laserbeam}}^2 \quad (\text{D.12})$$

$$P_{\text{Electrical}} = \text{Constant}_{\text{Linear}} \cdot I_{\text{Laserbeam}}^2$$

For linear units (like watt) there is a quadratic relation between the electrical and the optical units (Equation (D.12)). For logarithmic units (like dBm) the relation between electrical and optical units are expressed by Equation (D.13).

$$y[\text{dBm}_{\text{electric}}] = 10 \cdot \log_{10} \left( \frac{\text{Constant}_{\text{Linear}} \cdot I_{\text{Laserbeam}}^2 [\text{Watt}^2]}{1[\text{mW}]} \right) = \quad (\text{D.13})$$

$$10 \cdot \log_{10} \left( \frac{\text{Constant}_{\text{Linear}}}{1[\text{mW}]} \right) + 20 \cdot \log_{10} \left( \frac{I_{\text{Laserbeam}} [\text{Watt}]}{1[\text{mW}]} \right) =$$

$$2 \cdot [\text{dBm}_{\text{optic}}] + \text{Constant}_{\text{Logarithmic}}$$

For consideration of gain or loss in a device, the constants of Equation (D.13) will strike out and so we find Equation (D.14).

$$y[\text{dB}_{\text{electric}}] = 2 \cdot [\text{dB}_{\text{optic}}] \quad (\text{D.14})$$



## E. Calculations

### E.1. Calculation of the eigenvalues

We want an analytic solution for the eigenvalues of Equation E.1.

$$\underline{\eta}(\vec{E}) = \begin{bmatrix} 1/n_o^2 & r_{41}E_z & r_{41}E_y \\ r_{41}E_z & 1/n_o^2 & r_{41}E_x \\ r_{41}E_y & r_{41}E_x & 1/n_o^2 \end{bmatrix} \quad \text{E.1}$$

So we have to calculate the roots of the determinant of Equation E.2 where  $\xi$  represents the eigenvalue.

$$\underline{\eta}(\vec{E}) = \begin{bmatrix} 1/n_o^2 - \xi & r_{41}E_z & r_{41}E_y \\ r_{41}E_z & 1/n_o^2 - \xi & r_{41}E_x \\ r_{41}E_y & r_{41}E_x & 1/n_o^2 - \xi \end{bmatrix} \quad \text{E.2}$$

By changing the variables we can rewrite Equation E.2 to simplify the calculations with  $\eta = 1/n_o^2$ ,

$$\underline{\eta}(\vec{E}) = \begin{bmatrix} \eta - \xi & \alpha z & \alpha y \\ \alpha z & \eta - \xi & \alpha x \\ \alpha y & \alpha x & \eta - \xi \end{bmatrix} \quad \text{E.3}$$

For simplification we define  $\alpha = r_{41}|E|$ ,  $x = E_x/|E|$ ,  $y = E_y/|E|$ ,  $z = E_z/|E|$  and,  $|E| = \sqrt{E_x^2 + E_y^2 + E_z^2}$  and hence we get for the determinant Equation E.4.

$$\text{Determinant} = (\eta - \xi)^3 + 2\alpha^3xyz - (\eta - \xi)\alpha^2(x^2 + y^2 + z^2) \quad \text{E.4}$$

By using the fact that  $x^2 + y^2 + z^2 = 1$  and by putting  $s = \eta - \xi$ , we get the cubic of Equation E.5.

$$s^3 - s \cdot \alpha^2 + 2\alpha^3xyz = 0 \quad \text{E.5}$$

By putting  $p = -\alpha^2/3$  and  $q = \alpha^3xyz$  we can calculate the discriminant of Equation E.5.

$$\text{Discriminant} = q^2 + p^3 = \alpha^6 \left( x^2 y^2 z^2 - \frac{1}{27} \right) \quad \text{E.6}$$

If the discriminant is smaller than 0 there will be three real solutions. Considering that the eigenvalues of a symmetric matrix are real, and that the product  $x \cdot y \cdot z$  becomes maximal if  $x = y = z = 1/\sqrt{3}$  we can show that we have three different real solutions. If  $x=y=z$ , the discriminant becomes 0 and hence we have only two solutions.

So by putting  $r = -1/(\sqrt{3})\alpha$  and  $\cos(\varphi) = q/r^3$  we get the following solution for the eigenvalues as given in Equation E.7, E.8 and E.9.

$$s_1 = -\frac{2}{\sqrt{3}}\alpha \cdot \cos\left(\frac{\arccos(-3\sqrt{3}xyz)}{3}\right) \quad \text{E.7}$$

$$s_2 = \frac{2}{\sqrt{3}}\alpha \cdot \cos\left(\frac{\pi}{3} - \frac{\arccos(-3\sqrt{3}xyz)}{3}\right) \quad \text{E.8}$$

$$s_3 = \frac{2}{\sqrt{3}}\alpha \cdot \cos\left(\frac{\pi}{3} + \frac{\arccos(-3\sqrt{3}xyz)}{3}\right) \quad \text{E.9}$$

Considering that  $|xyz|_{\text{Max}} = 1/3\sqrt{3}$ , we get for all values of  $x$ ,  $y$  and  $z$  a valid solution. So by resetting the previous definitions, we get Equation E.10, E.11 and E.12 for the seeked eigenvalues.

$$\xi_1 = \frac{1}{n_o^2} + \frac{2}{\sqrt{3}}|E| \cdot \cos\left(\frac{\arccos\left(-3\sqrt{3}\frac{E_x E_y E_z}{|E|^3}\right)}{3}\right) \cdot r_{41} \quad \text{E.10}$$

$$\xi_2 = \frac{1}{n_o^2} - \frac{2}{\sqrt{3}}|E| \cdot \cos\left(\frac{\pi}{3} - \frac{\arccos\left(-3\sqrt{3}\frac{E_x E_y E_z}{|E|^3}\right)}{3}\right) \cdot r_{41} \quad \text{E.11}$$

$$\xi_3 = \frac{1}{n_o^2} - \frac{2}{\sqrt{3}}|E| \cdot \cos\left(\frac{\pi}{3} + \frac{\arccos\left(-3\sqrt{3}\frac{E_x E_y E_z}{|E|^3}\right)}{3}\right) \cdot r_{41} \quad \text{E.12}$$

## E.2. Calculation of the eigenvectors

In this paragraph we are calculating the corresponding eigenvectors. So we are looking for the non-trivial solution of Equation E.13.

$$\begin{bmatrix} 1/n_o^2 - \xi_{1,2,3} & r_{41}E_z & r_{41}E_y \\ r_{41}E_z & 1/n_o^2 - \xi_{1,2,3} & r_{41}E_x \\ r_{41}E_y & r_{41}E_x & 1/n_o^2 - \xi_{1,2,3} \end{bmatrix} \cdot \begin{bmatrix} x \\ y \\ z \end{bmatrix} = \begin{bmatrix} 0 \\ 0 \\ 0 \end{bmatrix} \quad \text{E.13}$$

If there is a non trivial solution  $\vec{X}$  for Equation E.13, we can find another valid solution just by multiplying the solution with a constant factor (Constant  $\cdot \vec{X}$ ). In some case it is advantageous to normalize the result so that  $|\vec{X}| \equiv 1$ .

By multiplying the first row by  $r_{41}E_z/(1/n_o^2 - \xi_{1,2,3})$  respectively  $r_{41}E_y/(1/n_o^2 - \xi_{1,2,3})$  and by subtracting the first row from the second and from the third row respectively, we can simplify Equation E.13 into Equation E.14.

$$\begin{bmatrix} 1/n_o^2 - \xi_{1,2,3} & r_{41}E_z & r_{41}E_y \\ 0 & \frac{(1/n_o^2 - \xi_{1,2,3})^2 - (r_{41}E_z)^2}{1/n_o^2 - \xi_{1,2,3}} & \frac{r_{41}E_x(1/n_o^2 - \xi_{1,2,3}) - r_{41}^2E_yE_z}{1/n_o^2 - \xi_{1,2,3}} \\ 0 & \frac{r_{41}E_x(1/n_o^2 - \xi_{1,2,3}) - r_{41}^2E_yE_z}{1/n_o^2 - \xi_{1,2,3}} & \frac{(1/n_o^2 - \xi_{1,2,3})^2 - (r_{41}E_y)^2}{1/n_o^2 - \xi_{1,2,3}} \end{bmatrix} \cdot \begin{bmatrix} x \\ y \\ z \end{bmatrix} = \begin{bmatrix} 0 \\ 0 \\ 0 \end{bmatrix} \quad \text{E.14}$$

So by using the second row of Equation E.14 we find Equation E.15.

$$y \cdot \frac{(1/n_o^2 - \xi_{1,2,3})^2 - (r_{41}E_z)^2}{1/n_o^2 - \xi_{1,2,3}} + z \cdot \frac{r_{41}E_x(1/n_o^2 - \xi_{1,2,3}) - r_{41}^2E_yE_z}{1/n_o^2 - \xi_{1,2,3}} = 0 \quad \text{E.15}$$

$$y = z \cdot \left( \frac{r_{41}^2E_yE_z - r_{41}E_x(1/n_o^2 - \xi_{1,2,3})}{(1/n_o^2 - \xi_{1,2,3})^2 - (r_{41}E_z)^2} \right)$$

By putting the result of Equation E.15 into the first row Equation E.14, we get the Equation E.16 for x.

$$x \cdot (1/n_o^2 - \xi_{1,2,3}) + y \cdot r_{41}E_z + z \cdot r_{41}E_y = 0 \quad \text{E.16}$$

$$x \cdot (1/n_o^2 - \xi_{1,2,3}) + z \cdot \frac{r_{41}^2E_yE_z - r_{41}E_x(1/n_o^2 - \xi_{1,2,3})}{(1/n_o^2 - \xi_{1,2,3})^2 - (r_{41}E_z)^2} \cdot r_{41}E_z + z \cdot r_{41}E_y = 0$$

$$x \cdot (1/n_o^2 - \xi_{1,2,3}) = z \cdot \left( \frac{r_{41}E_x(1/n_o^2 - \xi_{1,2,3}) - r_{41}^2E_yE_z}{(1/n_o^2 - \xi_{1,2,3})^2 - (r_{41}E_z)^2} \cdot r_{41}E_z - r_{41}E_y \right)$$

$$x = z \cdot \frac{r_{41}^2E_xE_z(1/n_o^2 - \xi_{1,2,3}) - r_{41}^3E_yE_z^2 - r_{41}E_y((1/n_o^2 - \xi_{1,2,3})^2 - (r_{41}E_z)^2)}{((1/n_o^2 - \xi_{1,2,3})^2 - (r_{41}E_z)^2) \cdot (1/n_o^2 - \xi_{1,2,3})}$$

So now we can use the results of Equation E.15 and Equation E.16 to assemble the eigenvector in function of the eigenvalues  $\xi_{1,2,3}$ . The vector of Equation E.17 is not normalized.

$$\text{Eigenvector} = \begin{bmatrix} \frac{r_{41}^2E_xE_z(1/n_o^2 - \xi_{1,2,3}) - r_{41}^3E_yE_z^2 - r_{41}E_y((1/n_o^2 - \xi_{1,2,3})^2 - (r_{41}E_z)^2)}{((1/n_o^2 - \xi_{1,2,3})^2 - (r_{41}E_z)^2) \cdot (1/n_o^2 - \xi_{1,2,3})} \\ \frac{r_{41}^2E_yE_z - r_{41}E_x(1/n_o^2 - \xi_{1,2,3})}{(1/n_o^2 - \xi_{1,2,3})^2 - (r_{41}E_z)^2} \\ 1 \end{bmatrix} \quad \text{E.17}$$

We replace  $\xi_{1,2,3}$  by the first eigenvalue  $\xi_1$  to find the according eigenvector ‘‘Eigenvector<sub>1</sub>’’. According to Equation E.10 the first eigenvalue is  $\xi_1 = 1/n_o^2 + 2/\sqrt{3}|E| \cdot \cos(\dots) \cdot r_{41}$ . So for the first eigenvector we get Equation E.18.

$$\text{Eigenvector}_1 = \left[ \frac{r_{41}^2 E_x E_z \left( \frac{1}{n_o^2} - \frac{1}{n_o^2} - \frac{2|E|}{\sqrt{3}} \cos(\dots) r_{41} \right) - r_{41}^3 E_y E_z^2 - r_{41} E_y \left( \left( \frac{1}{n_o^2} - \frac{1}{n_o^2} - \frac{2|E|}{\sqrt{3}} \cos(\dots) r_{41} \right)^2 - (r_{41} E_z)^2 \right)}{\left( \left( \frac{1}{n_o^2} - \frac{1}{n_o^2} - \frac{2|E|}{\sqrt{3}} \cos(\dots) r_{41} \right)^2 - (r_{41} E_z)^2 \right) \cdot \left( \frac{1}{n_o^2} - \frac{1}{n_o^2} - \frac{2|E|}{\sqrt{3}} \cos(\dots) r_{41} \right)} \right] \quad \text{E.18}$$

$$\frac{r_{41}^2 E_y E_z - r_{41} E_x \left( \frac{1}{n_o^2} - \frac{1}{n_o^2} - \frac{2|E|}{\sqrt{3}} \cos(\dots) r_{41} \right)}{\left( \frac{1}{n_o^2} - \frac{1}{n_o^2} - \frac{2|E|}{\sqrt{3}} \cos(\dots) r_{41} \right)^2 - (r_{41} E_z)^2}$$

$$1$$

$$\text{Eigenvector}_1 = \left[ \frac{\left( E_x E_z \left( -\frac{2|E|}{\sqrt{3}} \cos(\dots) \right) - E_y E_z^2 - E_y \left( \left( \frac{2|E|}{\sqrt{3}} \cos(\dots) \right)^2 - E_z^2 \right) \right) \cdot r_{41}^3}{\left( \left( \frac{2|E|}{\sqrt{3}} \cos(\dots) \right)^2 - E_z^2 \right) \cdot \left( -\frac{2|E|}{\sqrt{3}} \cos(\dots) \right) \cdot r_{41}^3} \right]$$

$$\frac{\left( E_y E_z + E_x \frac{2|E|}{\sqrt{3}} \cos(\dots) \right) \cdot r_{41}^2}{\left( \left( \frac{2|E|}{\sqrt{3}} \cos(\dots) \right)^2 - E_z^2 \right) \cdot r_{41}^2}$$

$$1$$

After further simplifications we get Equation E.19 for the “Eigenvector<sub>1</sub>”.

$$\text{Eigenvector}_1 = \left[ \frac{-E_x E_z \frac{2|E|}{\sqrt{3}} \cos(\dots) - E_y E_z^2 - E_y \left( \left( \frac{2|E|}{\sqrt{3}} \cos(\dots) \right)^2 - E_z^2 \right)}{\left( \left( \frac{2|E|}{\sqrt{3}} \cos(\dots) \right)^2 - E_z^2 \right) \cdot \left( -\frac{2|E|}{\sqrt{3}} \cos(\dots) \right)} \right] \quad \text{where}$$

$$\frac{E_y E_z + E_x \frac{2|E|}{\sqrt{3}} \cos(\dots)}{\left( \frac{2|E|}{\sqrt{3}} \cos(\dots) \right)^2 - E_z^2}$$

$$1$$

$$\cos(\dots) = \cos \left( \frac{\arccos \left( -3\sqrt{3} \frac{E_x E_y E_z}{|E|^3} \right)}{3} \right) \quad \text{E.19}$$

With similar deductions, we get for the other eigenvectors the following vectors (Equation E.20 and E.21).

$$\text{Eigenvector}_2 = \left[ \frac{E_x E_z \frac{2|E|}{\sqrt{3}} \cos(\dots) - E_y E_z^2 - E_y \left( \left( \frac{2|E|}{\sqrt{3}} \cos(\dots) \right)^2 - E_z^2 \right)}{\left( \left( \frac{2|E|}{\sqrt{3}} \cos(\dots) \right)^2 - E_z^2 \right) \cdot \left( \frac{2|E|}{\sqrt{3}} \cos(\dots) \right)} \right] \quad \text{where}$$

$$\frac{E_y E_z - E_x \frac{2|E|}{\sqrt{3}} \cos(\dots)}{\left( \frac{2|E|}{\sqrt{3}} \cos(\dots) \right)^2 - E_z^2}$$

$$1$$

$$\cos(\dots) = \cos\left(\frac{\pi}{3} - \frac{\arccos\left(-3\sqrt{3}\frac{E_x E_y E_z}{|E|^3}\right)}{3}\right) \quad \text{E.20}$$

$$\text{Eigenvector}_3 = \begin{bmatrix} \frac{E_x E_z \frac{2|E|}{\sqrt{3}} \cos(\dots) - E_y E_z^2 - E_y \left(\left(\frac{2|E|}{\sqrt{3}} \cos(\dots)\right)^2 - E_z^2\right)}{\left(\left(\frac{2|E|}{\sqrt{3}} \cos(\dots)\right)^2 - E_z^2\right) \cdot \left(\frac{2|E|}{\sqrt{3}} \cos(\dots)\right)} \\ \frac{E_y E_z - E_x \frac{2|E|}{\sqrt{3}} \cos(\dots)}{\left(\frac{2|E|}{\sqrt{3}} \cos(\dots)\right)^2 - E_z^2} \\ 1 \end{bmatrix} \quad \text{where}$$

$$\cos(\dots) = \cos\left(\frac{\pi}{3} + \frac{\arccos\left(-3\sqrt{3}\frac{E_x E_y E_z}{|E|^3}\right)}{3}\right) \quad \text{E.21}$$

### E.3. Calculation of reflection and transmission coefficients

The air / GaAs interface will reflect a part of the laser beam and the rest will enter the GaAs crystal. The reflection and transmission coefficient for the intensity (Uppercase letters  $R_{\text{Intensity}}$ ,  $T_{\text{Intensity}}$ ) as well as for the magnitude of the electric field (Lowercase letter r, t) can be calculated with the Maxwell equations under the condition of power conservation (Figure E.1).

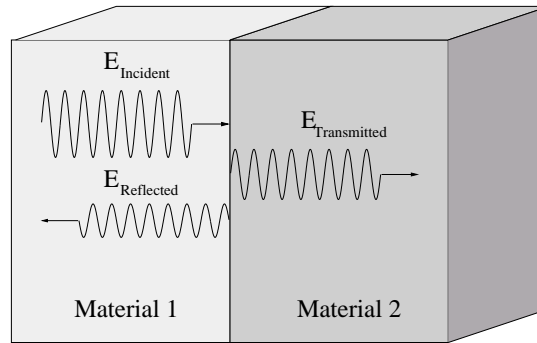


**Figure E.1** Electric field of the incident, the reflected and the transmitted laser beam.

The boundary condition for a plane wave impose that the summation of the addition of the electric fields on both sides has to be equal to avoid discontinuity (Equation E.22).

$$E_{\text{Incident}} + E_{\text{Reflected}} = E_{\text{Transmitted}} \quad \text{E.22}$$

We assume that there is no loss of power at/in the interface and that the materials show no magnetic properties ( $\mu_r=1$ ). So the energy conservation has to be satisfied as imposed by Equation E.23

$$\frac{E_{\text{Incident}} \cdot E_{\text{Incident}}^*}{2Z_{\text{Material1}}} = \frac{E_{\text{Transmitted}} \cdot E_{\text{Transmitted}}^*}{2Z_{\text{Material2}}} + \frac{E_{\text{Reflected}} \cdot E_{\text{Reflected}}^*}{2Z_{\text{Material2}}} \quad \text{with} \quad \text{E.23}$$

$$Z_{\text{Material1}} = \frac{Z_0}{n_{\text{Material1}}} \quad \text{and} \quad Z_{\text{Material2}} = \frac{Z_0}{n_{\text{Material2}}}$$

where  $Z_{\text{Material1}}$  and  $Z_{\text{Material2}}$  are the wave impedances of the different materials. By using Equation E.22 and Equation E.23, we get a quadratic equation for  $E_{\text{Reflected}}$  in function of  $E_{\text{Incident}}$ .

$$\frac{E_{\text{Incident}}^2 - E_{\text{Reflected}}^2}{2Z_{\text{Material1}}} = \frac{E_{\text{Transmitted}}^2}{2Z_{\text{Material2}}} \quad \text{E.24}$$

$$\frac{E_{\text{Incident}}^2 - E_{\text{Reflected}}^2}{2Z_{\text{Material1}}} = \frac{(E_{\text{Incident}} + E_{\text{Reflected}})^2}{2Z_{\text{Material2}}}$$

$$n_{\text{Material1}} \cdot (E_{\text{Incident}}^2 - E_{\text{Reflected}}^2) = n_{\text{Material2}} \cdot (E_{\text{Incident}} + E_{\text{Reflected}})^2$$

$$0 = E_{\text{Reflected}}^2 \cdot (n_{\text{Material2}} + n_{\text{Material1}}) + E_{\text{Reflected}} \cdot 2E_{\text{Incident}}n_{\text{Material2}} + E_{\text{Incident}}^2(n_{\text{Material2}} - n_{\text{Material1}})$$

We can solve Equation E.24 and thus we get the reflection coefficient of the air GaAs interface as defined in Equation E.25.

$$E_{\text{Reflected}} = \frac{-2E_{\text{Incident}}n_{\text{Material2}} \pm 2E_{\text{Incident}}n_{\text{Material1}}}{2 \cdot (n_{\text{Material1}} + n_{\text{Material2}})} = E_{\text{Incident}} \cdot \frac{\pm n_{\text{Material1}} - n_{\text{Material2}}}{n_{\text{Material1}} + n_{\text{Material2}}} \quad \text{or}$$

$$\Gamma_{\text{Material1-Material2}} = \frac{n_{\text{Material1}} - n_{\text{Material2}}}{n_{\text{Material1}} + n_{\text{Material2}}} \quad \text{E.25}$$

For the transmission we can proceed in the same way (Equation E.26).

$$\frac{E_{\text{Incident}}^2 - (E_{\text{Transmitted}} - E_{\text{Incident}})^2}{2Z_{\text{Material1}}} = \frac{E_{\text{Transmitted}}^2}{2Z_{\text{Material2}}} \quad \text{E.26}$$

$$n_{\text{Material1}} \cdot (-E_{\text{Transmitted}}^2 + 2E_{\text{Transmitted}}E_{\text{Incident}}) = n_{\text{Material2}} \cdot E_{\text{Transmitted}}^2$$

$$0 = E_{\text{Transmitted}} \cdot (E_{\text{Transmitted}}(n_{\text{Material2}} + n_{\text{Material1}}) - 2E_{\text{Incident}}n_{\text{Material1}})$$

So for the transmission coefficient we get Equation E.27.

$$t_{\text{Material1-Material2}} = \frac{2n_{\text{Material1}}}{n_{\text{Material1}} + n_{\text{Material2}}} \quad \text{E.27}$$

So for the air GaAs interface we get the transmission and reflection coefficients of Equation E.28 and Equation E.29. The coefficients are defined by Figure E.1.

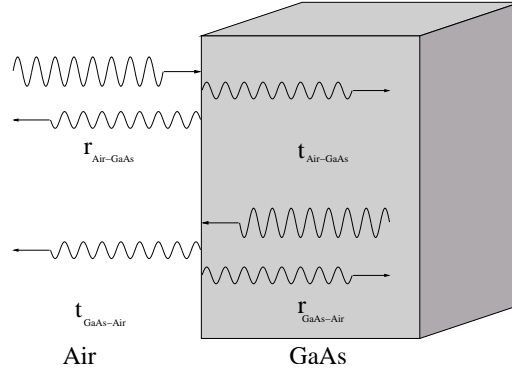


**Figure E.2** Definition of the transmission and reflection coefficient at the Air GaAs interface.

$$r_{\text{Air-GaAs}} = \frac{n_{\text{Air}} - n_{\text{GaAs}}}{n_{\text{Air}} + n_{\text{GaAs}}} \quad \text{and} \quad t_{\text{Air-GaAs}} = \frac{2n_{\text{Air}}}{n_{\text{Air}} + n_{\text{GaAs}}} \quad \text{E.28}$$

$$r_{\text{GaAs-Air}} = \frac{n_{\text{GaAs}} - n_{\text{Air}}}{n_{\text{Air}} + n_{\text{GaAs}}} \quad \text{and} \quad t_{\text{GaAs-Air}} = \frac{2n_{\text{GaAs}}}{n_{\text{Air}} + n_{\text{GaAs}}} \quad \text{E.29}$$

The reflection and transmission coefficient for the intensity can be calculated using Equation E.30.

$$R_{\text{Intensity}} = r_{\text{MaterialX-MaterialY}}^2 \quad \text{and} \quad T_{\text{Intensity}} = \frac{Z_{\text{Material1}}}{Z_{\text{Material2}}} \cdot t_{\text{Material1-Material2}}^2 = \frac{n_{\text{Material2}}}{n_{\text{Material1}}} \cdot t_{\text{Material1-Material2}}^2 \quad \text{E.30}$$

## E.4. Calculation of the Cavity response

According to Figure 27 on page 28, the sum of the reflections is Equation E.31.

$$E_{\text{Reflected}} = E_{\text{Incident}} (r_{\text{Air-GaAs}} + t_{\text{Air-GaAs}} t_{\text{GaAs-Air}} \text{Re}^{-i\pi} e^{-i\phi} + t_{\text{Air-GaAs}} t_{\text{GaAs-Air}} (\text{Re}^{-i\pi})^2 r_{\text{GaAs-Air}} e^{-i2\phi} + \dots) \quad \text{E.31}$$

By defining  $t^2 = t_{\text{Air-GaAs}} t_{\text{GaAs-Air}}$  and  $r = r_{\text{GaAs-Air}} = -r_{\text{Air-GaAs}}$  we can rewrite Equation E.31 as Equation E.32.

$$E_{\text{Reflected}} = E_{\text{Incident}} (-r + t^2 \text{Re}^{-i\pi} e^{-i\phi} + t^2 (\text{Re}^{-i\pi})^2 r e^{-i2\phi} + t^2 (\text{Re}^{-i\pi})^3 r^2 e^{-i2\phi} + \dots) \quad \text{E.32}$$

By putting  $e^{-i2\pi} = 1$  as well as  $e^{-i\pi} = -1$  we can describe the sum of  $E_{\text{Reflected}}$  by Equation E.33.

$$E_{\text{Reflected}} = E_{\text{Incident}} (-r - t^2 \text{Re}^{-i\phi} (1 - \text{Rre}^{-i\phi} + (\text{Rre}^{-i\phi})^2 - (\text{Rre}^{-i\phi})^3 + \dots)) \quad \text{E.33}$$

Under the condition that  $|\text{Rre}^{-i\phi}| < 1$  (always satisfied as  $r$  as well as  $R$  are smaller than one) and by considering Equation E.34, we get for  $E_{\text{Reflected}}$  Equation E.35 also called the Airy Equation.

$$r^2 + t^2 = \left( \frac{n_{\text{GaAs}} - n_{\text{Air}}}{n_{\text{Air}} + n_{\text{GaAs}}} \right)^2 + \frac{2n_{\text{Air}}}{n_{\text{Air}} + n_{\text{GaAs}}} \cdot \frac{2n_{\text{GaAs}}}{n_{\text{Air}} + n_{\text{GaAs}}} = 1 \quad \text{E.34}$$

$$\begin{aligned} E_{\text{Reflected}} &= E_{\text{Incident}} \left( \frac{-r - t^2 R e^{-i\phi}}{1 + R r e^{-i\phi}} \right) = E_{\text{Incident}} \left( \frac{-r - R r^2 e^{-i\phi} - R t^2 e^{-i\phi}}{1 + R r e^{-i\phi}} \right) \\ &= E_{\text{Incident}} \left( \frac{-r - R e^{-i\phi} (r^2 + t^2)}{1 + R r e^{-i\phi}} \right) = -E_{\text{Incident}} \left( \frac{r + R e^{-i\phi}}{1 + R r e^{-i\phi}} \right) \end{aligned} \quad \text{E.35}$$

The problem is, that in our setup we are not measuring the electric field but the intensity of the Laser beam or with other words the power of the reflected beam. So we have to calculate the intensity by using Equation E.36 which describes the intensity of a electromagnetic wave in a given material. In our case this material is the surrounding air. Hence we get the intensity of the reflected laser beam Equation E.37.

$$I_{\text{Laserbeam}} = \frac{1}{2Z_{\text{Material}}} |E_{\text{Laserbeam}} \cdot E_{\text{Laserbeam}}^*| \quad \text{E.36}$$

$$\begin{aligned} I_{\text{Reflected}} &= \frac{1}{2Z_{\text{Material}}} |E_{\text{Reflected}} \cdot E_{\text{Reflected}}^*| = \frac{E_{\text{Incident}}^2}{2Z_{\text{Material}}} \left| \left( \frac{r + R e^{-i\phi}}{1 + R r e^{-i\phi}} \right) \cdot \left( \frac{r + R e^{-i\phi}}{1 + R r e^{-i\phi}} \right)^* \right| = \\ &= \frac{E_{\text{Incident}}^2}{2Z_{\text{Material}}} \cdot \left| \left( \frac{r + R \cos \phi - i R \sin \phi}{1 + R r \cos \phi - i R r \sin \phi} \right) \cdot \left( \frac{r + R \cos \phi + i R \sin \phi}{1 + R r \cos \phi + i R r \sin \phi} \right) \right| = \\ &= \frac{E_{\text{Incident}}^2}{2Z_{\text{Material}}} \cdot \left| \frac{r^2 + 2R r \cos \phi + R^2 (\cos \phi)^2 + R^2 (\sin \phi)^2}{1 + 2R r \cos \phi + R^2 r^2 (\cos \phi)^2 + R^2 r^2 (\sin \phi)^2} \right| = \frac{E_{\text{Incident}}^2}{2Z_{\text{Material}}} \cdot \frac{r^2 + R^2 + 2R r \cos \phi}{1 + r^2 R^2 + 2R r \cos \phi} \end{aligned} \quad \text{E.37}$$

By replacing  $E_{\text{Incident}}^2 / 2Z_{\text{Material}} = I_{\text{Incident}}$  we get for the reflected beam Equation E.38.

$$I_{\text{Reflected}} = I_{\text{Incident}} \frac{r^2 + R^2 + 2R r \cos \phi}{1 + r^2 R^2 + 2R r \cos \phi} \quad \text{E.38}$$

## E.5. Calculation of the partial derivative

When we apply an electric field across the cavity, the refractive index of the material and hence the response will change as indicated by Equation E.39.

$$I_{\text{Reflected}} = I_{\text{Incident}} \frac{r^2 + R^2 + 2R r \cos \left( \frac{4\pi d}{\lambda_o} \left( n_o + \frac{1}{2} n_o^3 r_{41} E_z \right) \right)}{1 + R^2 r^2 + 2R r \cos \left( \frac{4\pi d}{\lambda_o} \left( n_o + \frac{1}{2} n_o^3 r_{41} E_z \right) \right)} \quad \text{E.39}$$

If we linearize Equation E.39 in function of the  $E_z$ , we get Equation E.40.

$$I_{\text{Reflected}}(\lambda_o, E_z) \approx I_{\text{Reflected}}|_{E_z=0} + \left. \frac{\partial I_{\text{Reflected}}}{\partial E_z} \right|_{E_z=0} \cdot E_z \quad \text{E.40}$$

We have an interest to replace the unknown derivative  $\partial I_{\text{Reflected}} / \partial E_z|_{E_z=0}$  by an “known” function. By using Equation E.41 and E.42 we find the relation of Equation E.43.

$$\frac{\partial I_{\text{Reflected}}}{\partial E_z} = \frac{\partial I_{\text{Reflected}}}{\partial \phi} \cdot \frac{\partial \phi}{\partial E_z} \quad \text{and} \quad \frac{\partial I_{\text{Reflected}}}{\partial \phi} = \frac{\partial I_{\text{Reflected}}}{\partial \lambda_o} \cdot \frac{\partial \lambda_o}{\partial \phi} \quad \text{E.41}$$

$$\frac{\partial \phi}{\partial E_z} \approx \frac{2\pi d n_o^3 r_{41}}{\lambda_o} \quad \text{and} \quad \frac{\partial \phi}{\partial \lambda} \approx \frac{-4\pi d}{\lambda_o^2} \cdot \left( n_o + \frac{1}{2} n_o^3 r_{41} E_z \right) \quad \text{E.42}$$

$$\frac{\partial I_{\text{Reflected}}}{\partial E_z} \cdot \frac{\partial E_z}{\partial \phi} = \frac{\partial I_{\text{Reflected}}}{\partial \lambda_o} \cdot \frac{\partial \lambda_o}{\partial \phi} \quad \text{E.43}$$

$$\begin{aligned} \frac{\partial I_{\text{Reflected}}}{\partial E_z} \cdot \frac{\lambda_o}{2\pi d n_o^3 r_{41}} &\approx \frac{\partial I_{\text{Reflected}}}{\partial \lambda_o} \cdot \frac{\lambda_o^2}{-4\pi d \cdot \left( n_o + \frac{1}{2} n_o^3 r_{41} E_z \right)} \\ \frac{\partial I_{\text{Reflected}}}{\partial E_z} \Big|_{E_z=0} &\approx \frac{\partial I_{\text{Reflected}}}{\partial \lambda_o} \cdot \frac{-n_o^2 r_{41} \lambda_o}{2} \end{aligned}$$

## E.6. Calculation of the Minimum and Maximum of the Fabry-Perot Cavity response

We can find the maximum and minimum by setting the derivation of Equation E.44 equal to zero.

$$I_{\text{Reflected}} = I_{\text{Incident}} \frac{r^2 + R^2 + 2Rr \cos(\phi)}{1 + R^2 r^2 + 2Rr \cos(\phi)} \quad \text{E.44}$$

$$\begin{aligned} \frac{dI_{\text{Reflected}}}{d\phi} &= I_{\text{Incident}} \frac{d}{d\phi} \frac{r^2 + R^2 + 2Rr \cos \phi}{1 + r^2 R^2 + 2Rr \cos \phi} = 0 \\ \frac{((r^2 + R^2 + 2Rr \cos \phi)(-2Rr \sin \phi) - (r^2 + R^2 + 2Rr \cos \phi)(-2Rr \sin \phi))}{(1 + r^2 R^2 + 2Rr \cos \phi)^2} &= 0 \end{aligned}$$

By looking only at the denominator of Equation E.44 we find the product of two terms as displayed in Equation E.45.

$$\begin{aligned} ((r^2 + R^2 + 2Rr \cos \phi) - (1 + r^2 R^2 + 2Rr \cos \phi))(-2Rr \sin \phi) &= 0 \\ (r^2 + R^2 - 1 - r^2 R^2)(-2Rr \sin \phi) &= 0 \end{aligned} \quad \text{E.45}$$

The first one does not indicate any solution because it is independent of  $\phi$ . So with the second term we find the solution indicated in Equation E.46.

$$(-2Rr \sin \phi) = 0 \rightarrow \phi_A = 0, \phi_B = \pi \quad \text{E.46}$$

So now we have to verify which one is the maximum and minimum. We do this by putting both result into Equation E.44 and by comparing them.

$$I_A(0) = I_{\text{Incident}} \frac{r^2 + R^2 + 2Rr}{1 + r^2 R^2 + 2Rr} = I_{\text{Incident}} \frac{(r+R)^2}{(1+rR)^2} \quad \text{E.47}$$

$$I_B(\pi) = I_{\text{Incident}} \frac{r^2 + R^2 - 2Rr}{1 + r^2 R^2 - 2Rr} = I_{\text{Incident}} \frac{(r-R)^2}{(1-rR)^2} \quad \text{E.48}$$

When we compare Equation E.47 and Equation E.48, we have to take into account that  $0 < r, R < 1$  and that  $I_A$  and  $I_B$  are positive per definition.

$$\begin{aligned}
 I_{\text{Incident}} \frac{(r+R)^2}{(1+rR)^2} &> I_{\text{Incident}} \frac{(r-R)^2}{(1-rR)^2} && \text{E.49} \\
 \frac{(r+R)}{(1+rR)} &> \frac{(r-R)}{(1-rR)} \\
 (r+R)(1-rR) &> (r-R)(1+rR) \\
 r - r^2R + R - rR^2 &> r + r^2R - R - rR^2 \\
 2R &> 2r^2R \\
 1 &> r^2
 \end{aligned}$$

So our assumption was right and we get the maximum for  $\phi=0$  (Equation E.50) and for  $\phi=\pi$  the minima (Equation E.51).

$$I_{\text{Maximum}} = I_{\text{Incident}} \frac{(r+R)^2}{(1+rR)^2} \quad \text{E.50}$$

$$I_{\text{Minimum}} = I_{\text{Incident}} \frac{(r-R)^2}{(1-rR)^2} \quad \text{E.51}$$

## E.7. Calculation of the relation between the reflection and R and r

With equation E.50 and E.51 we can calculate r and R in function of  $I_{\text{Maximum}}$ ,  $I_{\text{Minimum}}$  and  $I_{\text{Incident}}$ . It is interesting to know this coefficient even if we do not need them for the calculation of the electric field.

$$A = \sqrt{\frac{I_{\text{Maximum}}}{I_{\text{Incident}}}} = \frac{r+R}{1+rR} \quad \text{E.52}$$

$$B = \sqrt{\frac{I_{\text{Minimum}}}{I_{\text{Incident}}}} = \frac{r-R}{1-rR} \quad \text{E.53}$$

By defining the parameter A (Equation E.52) and B (Equation E.53) we get the equation system given in the Equation E.54.

$$\begin{aligned}
 A(1+rR) &= r+R \\
 B(1-rR) &= r-R
 \end{aligned} \quad \text{E.54}$$

By putting  $r = \frac{R-A}{AR-1}$  into the second part of Equation E.54 we find a quadratic Equation E.55 for R.

$$\begin{aligned}
 B\left(1 - \frac{R-A}{AR-1}R\right) &= \frac{R-A}{AR-1} - R && \text{E.55} \\
 B\left(\frac{(AR-1) - (R-A)R}{AR-1}\right) &= \frac{(R-A) - R(AR-1)}{AR-1} \\
 ABR - B - BR^2 + ABR &= R - A - AR^2 + R \\
 R^2(A-B) + R2(AB-1) + (A-B) &= 0
 \end{aligned}$$

So we calculate the discriminant to determine the number of solutions (Equation E.56).

$$D = 4(AB - 1)^2 - 4(A - B)^2 = 4(A^2B^2 - 2AB + 1 - A^2 + 2AB - B^2) = 4(A^2B^2 + 1 - A^2 - B^2) = 4(1 - A^2)(1 - B^2) > 0 \quad \text{E.56}$$

With the conditions  $0 < A < 1$  and  $0 < B < 1$  we find that  $D$  is positive and hence we have two possible solutions for  $R$ .

$$R_{1,2} = \frac{1-AB \pm \sqrt{(1-A^2)(1-B^2)}}{A-B} \quad \text{E.57}$$

So we have to verify if both solutions satisfy the condition  $0 < R_{1,2} < 1$  to make sure that we do not get negative values for  $R$  (would introduce another phase shift) or values bigger than 1 (generation of energy during reflection).

$$R_1 > 0$$

With  $1-AB > 0$ ,  $D > 0$ , and  $A-B > 0$  all terms of Equation E.58 are positive, and so  $R_1$  is positive as well.

$$\frac{1-AB + \sqrt{(1-A^2)(1-B^2)}}{A-B} > 0 \quad \text{E.58}$$

$$R_1 < 1$$

With  $\sqrt{(1-A^2)(1-B^2)} > 0$ , and  $(1-A)(1+B) > 0$ , we can show that  $R_1$  is bigger than 1.

$$\begin{aligned} (1-A)(1+B) + \sqrt{(1-A^2)(1-B^2)} &> 0 \quad \text{E.59} \\ 1-AB + \sqrt{(1-A^2)(1-B^2)} &> A-B \\ \frac{1-AB + \sqrt{(1-A^2)(1-B^2)}}{A-B} &> 1 \end{aligned}$$

Considering that Equation E.59 is wrong  $R_1$  is not a valid solution. So we have to check the second possibility.

$$R_2 > 0$$

With  $A-B > 0$ ,  $1+A^2B^2=1+A^2B^2$ ,  $(A-B)^2 > 0$  and  $A-B > 0$  we can show that the denominator (Equation E.60) as well as the nominator of  $R_2$  are positive.

$$\begin{aligned} A^2 - 2AB + B^2 + 1 + A^2B^2 &> 1 + A^2B^2 \quad \text{E.60} \\ 1 - 2AB + A^2B^2 &> 1 + A^2B^2 - A^2 - B^2 \\ (1-AB)^2 &> (1-A^2)(1-B^2) \\ 1-AB &> \sqrt{(1-A^2)(1-B^2)} \\ 1-AB - \sqrt{(1-A^2)(1-B^2)} &> 0 \end{aligned}$$

$$R_2 < 1$$

With  $1+A^2B^2=1+A^2B^2$ ,  $A-B > 0$  or  $B-A < 0$  and  $1-A+AB+B > 0$  we can demonstrate

(Equation E.61) that  $R_2$  is a valid solution.

$$\begin{aligned}
 & \text{with } 1+A^2B^2 = 1+A^2B^2, A-B>0 \text{ or } (B-A)<0 \text{ and } (1-A+AB+B)>0 & \text{E.61} \\
 & 2(B-A)(1-A+AB+B) < 0 \\
 & 2B-2AB+2AB^2+2B^2-2A+2A^2-2AB^2-2AB < 0 \\
 & 1+A^2B^2-2B-4AB+2AB^2+2B^2-2A+2A^2-2AB^2 < 1+A^2B^2 \\
 & 1+A^2B^2-2B-4AB+2AB^2+B^2-2A+A^2-2AB^2 < 1+A^2B^2-A^2-B^2 \\
 & (A-B-1+AB)(A-B-1+AB) < (1-A^2)(1-B^2) \\
 & (A-B-1+AB) < \sqrt{(1-A^2)(1-B^2)} \\
 & A-B < 1-AB-\sqrt{(1-A^2)(1-B^2)} \\
 & 1 < (1-AB-\sqrt{(1-A^2)(1-B^2)})/(A-B)
 \end{aligned}$$

So we get for r and R equation E.62 and E.63.

$$R = \frac{1-AB-\sqrt{(1-A^2)(1-B^2)}}{A-B} \quad \text{E.62}$$

$$r = \frac{1-\sqrt{(1-B^2)/(1-A^2)}}{B-A\sqrt{(1-B^2)/(1-A^2)}} \quad \text{E.63}$$

## E.8. Calculation of the modulation for a polarization between the optical axis

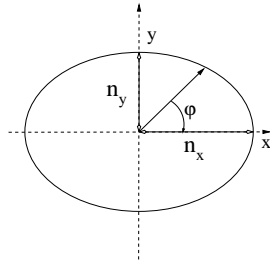


**Figure E.3** The axis of an ellipsoid.

If the applied electric field  $E_z$  is parallel to the z-axis and the optical axis are parallel to the x respective y axis, the ellipsoid of the refraction index is given by Equation E.64.

$$\begin{aligned}
 n_x(E_z) & \approx n_o + \frac{1}{2}n_o^3 r_{41} E_z & \text{E.64} \\
 n_y(E_z) & \approx n_o - \frac{1}{2}n_o^3 r_{41} E_z \\
 n_z(E_z) & = n_o
 \end{aligned}$$

In Figure E.3  $\phi$  is the angle between the x axis and the polarization given by the direction of the electric field of the laser beam. For the further analysis, we will project the electric field of the laser beam

onto the x and the y axis and execute the calculation for both axis separately (Equation E.65).

$$\begin{aligned} E_{x, \text{Laser}} &= \cos(\varphi) \cdot E_{\text{Amplitude, Laser}} \\ E_{y, \text{Laser}} &= \sin(\varphi) \cdot E_{\text{Amplitude, Laser}} \end{aligned} \quad \text{E.65}$$

So for the response of the cavity we get Equation E.66.

$$\begin{aligned} E_{x, \text{Reflected}} &= \cos(\varphi) \cdot E_{\text{Amplitude, Laser}} \cdot \left( \frac{r + \text{Re} \cdot \frac{-i \frac{4\pi d}{\lambda_0} \left( n_0 + \frac{1}{2} n_0^3 r_{41} E_z \right)}{-i \frac{4\pi d}{\lambda_0} \left( n_0 + \frac{1}{2} n_0^3 r_{41} E_z \right)}}{1 - r \text{Re}} \right) \\ E_{y, \text{Reflected}} &= \sin(\varphi) \cdot E_{\text{Amplitude, Laser}} \cdot \left( \frac{r + \text{Re} \cdot \frac{-i \frac{4\pi d}{\lambda_0} \left( n_0 - \frac{1}{2} n_0^3 r_{41} E_z \right)}{-i \frac{4\pi d}{\lambda_0} \left( n_0 - \frac{1}{2} n_0^3 r_{41} E_z \right)}}{1 - r \text{Re}} \right) \end{aligned} \quad \text{E.66}$$

For the output intensity we get Equation E.67.

$$\begin{aligned} I_{\text{Output}} &= \frac{1}{2 \cdot Z_{\text{Material}}} \cdot (E_{x, \text{Reflected}} \cdot E_{x, \text{Reflected}}^* + E_{y, \text{Reflected}} \cdot E_{y, \text{Reflected}}^*) = \\ &= I_{\text{Incident}} \cdot \left( \cos(\varphi)^2 \cdot \frac{r + \text{Re} \cdot \frac{-i \frac{4\pi d}{\lambda_0} \left( n_0 + \frac{1}{2} n_0^3 r_{41} E_z \right)}{-i \frac{4\pi d}{\lambda_0} \left( n_0 + \frac{1}{2} n_0^3 r_{41} E_z \right)}}{1 - r \text{Re}} \cdot \left( \frac{\dots}{\dots} \right)^* + \sin(\varphi)^2 \cdot \frac{r + \text{Re} \cdot \frac{-i \frac{4\pi d}{\lambda_0} \left( n_0 - \frac{1}{2} n_0^3 r_{41} E_z \right)}{-i \frac{4\pi d}{\lambda_0} \left( n_0 - \frac{1}{2} n_0^3 r_{41} E_z \right)}}{1 - r \text{Re}} \cdot \left( \frac{\dots}{\dots} \right)^* \right) \\ &= I_{\text{Incident}} \cdot \left( \cos(\varphi)^2 \cdot \frac{r^2 + R^2 + 2Rr \cos\left(\frac{4\pi d}{\lambda_0} \left( n_0 + \frac{n_0^3}{2} r_{41} E_z \right)\right)}{1 + R^2 r^2 + 2Rr \cos\left(\frac{4\pi d}{\lambda_0} \left( n_0 + \frac{n_0^3}{2} r_{41} E_z \right)\right)} + \sin(\varphi)^2 \cdot \frac{r^2 + R^2 + 2Rr \cos\left(\frac{4\pi d}{\lambda_0} \left( n_0 - \frac{n_0^3}{2} r_{41} E_z \right)\right)}{1 + R^2 r^2 + 2Rr \cos\left(\frac{4\pi d}{\lambda_0} \left( n_0 - \frac{n_0^3}{2} r_{41} E_z \right)\right)} \right) \end{aligned} \quad \text{E.67}$$

For the estimation of the modulation, we can linearize both terms separately. So by using Equation E.42. and by adapting the signs of the partial derivative we get find Equation E.68.

$$\begin{aligned} I_{\text{ElectroOptic}} &\approx \frac{\lambda_0 n_0^2 r_{41}}{2} \left( \cos(\varphi)^2 \frac{\delta I_{\text{Reflected}}}{\delta \lambda_0} \cdot E_z - \sin(\varphi)^2 \frac{\delta I_{\text{Reflected}}}{\delta \lambda_0} \cdot E_z \right) \\ &= \frac{\lambda_0 n_0^2 r_{41}}{2} \cdot \frac{\delta I_{\text{Reflected}}}{\delta \lambda_0} \cdot (\cos(\varphi)^2 - \sin(\varphi)^2) E_z \\ &= \frac{\lambda_0 n_0^2 r_{41}}{2} \cdot \frac{\delta I_{\text{Reflected}}}{\delta \lambda_0} \cdot \cos(2\varphi) \cdot E_z \end{aligned} \quad \text{E.68}$$

By doing the same consideration as in paragraph 5.1 and by taking the absolute value of  $\cos(\varphi)$  we find Equation E.69.

$$I_{\text{Modulation}} \approx \lambda n_0^2 r_{41} \cdot |\cos(2\varphi)| \cdot \left| \frac{\delta I_{\text{Ref}}}{\delta \lambda} \right| \cdot E_z \quad \text{E.69}$$

## E.9. Calculation of the modulation for $\mathbf{E}=\mathbf{E}_x+\mathbf{E}_z$

In this section we will try to estimate the systematic error introduced by an electric field not parallel to the z-axis. The electric field is given by Equation E.70 where  $\theta$  is the angle between the electric

field and the x-axis as defined in Figure E.4.

$$\vec{E}_{\text{Microwave}} = E_{\text{Amplitude}} \cdot \begin{bmatrix} \cos(\theta) \\ 0 \\ \sin(\theta) \end{bmatrix} \quad \text{E.70}$$

By using the Equation (57) to (59) we get for the (normalized) optical axes the vectors given in Equation E.71:

$$\text{Vector}_1 = \begin{bmatrix} -\cos(\theta) \\ 0 \\ \sin(\theta) \end{bmatrix}, \text{Vector}_2 = \begin{bmatrix} \frac{\sin(\theta)}{\sqrt{2}} \\ -\frac{1}{\sqrt{2}} \\ \frac{\cos(\theta)}{\sqrt{2}} \end{bmatrix}, \text{Vector}_3 = \begin{bmatrix} \frac{\sin(\theta)}{\sqrt{2}} \\ \frac{1}{\sqrt{2}} \\ \frac{\cos(\theta)}{\sqrt{2}} \end{bmatrix} \quad \text{E.71}$$

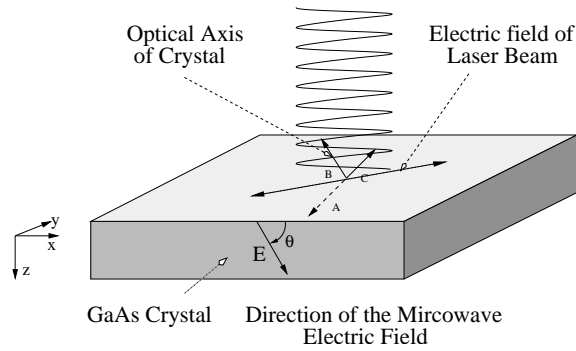


**Figure E.4** Configuration using the polarization shift to measure the signal.

The according eigenvalues respectively the refractive indices are given by Equation E.72.

$$\begin{aligned} n_1 &= n_o & \text{E.72} \\ n_2 &\approx n_o + \frac{1}{2}n_o^3r_{41}E_{\text{Amplitude}} \\ n_3 &\approx n_o - \frac{1}{2}n_o^3r_{41}E_{\text{Amplitude}} \end{aligned}$$

The incident laser beam is aligned parallel to the vector  $\text{Polarization}_{\text{Laser}}$  as given in Equation E.73.

$$\text{Polarization}_{\text{Laser}} = \begin{bmatrix} -1 \\ 1 \\ 0 \end{bmatrix} \parallel \begin{bmatrix} \frac{1}{\sqrt{2}} \\ \frac{1}{\sqrt{2}} \\ 0 \end{bmatrix} \quad \text{E.73}$$

So for the projection of the laser beam on the different optical axis we get Equation E.74

$$\begin{aligned}
 \alpha &= \begin{bmatrix} -\frac{1}{\sqrt{2}} \\ \frac{1}{\sqrt{2}} \\ 0 \end{bmatrix} \times \begin{bmatrix} -\cos(\theta) \\ 0 \\ \sin(\theta) \end{bmatrix} = \frac{\cos(\theta)}{\sqrt{2}}, \quad \beta = \begin{bmatrix} -\frac{1}{\sqrt{2}} \\ \frac{1}{\sqrt{2}} \\ 0 \end{bmatrix} \times \begin{bmatrix} \frac{\sin(\theta)}{\sqrt{2}} \\ -\frac{1}{\sqrt{2}} \\ \frac{\cos(\theta)}{\sqrt{2}} \end{bmatrix} = \frac{-(1 + \sin(\theta))}{2} \quad \text{and} \\
 \gamma &= \begin{bmatrix} -\frac{1}{\sqrt{2}} \\ \frac{1}{\sqrt{2}} \\ 0 \end{bmatrix} \times \begin{bmatrix} \frac{\sin(\theta)}{\sqrt{2}} \\ \frac{1}{\sqrt{2}} \\ \frac{\cos(\theta)}{\sqrt{2}} \end{bmatrix} = \frac{1 - \sin(\theta)}{2}
 \end{aligned} \tag{E.74}$$

By defining the three phase shifts  $\phi_1 = \frac{4\pi d n_o}{\lambda_o}$ ,  $\phi_2 = \frac{4\pi d}{\lambda_o} \cdot \left( n_o + \frac{1}{2} n_o^3 r_{41} E_{\text{Amplitude}} \right)$  and  $\phi_3 = \frac{4\pi d}{\lambda_o} \cdot \left( n_o - \frac{1}{2} n_o^3 r_{41} E_{\text{Amplitude}} \right)$  and by using Equation E.35, we get for the response of the cavity Equation E.75.

$$E_{\text{Reflected}} = \begin{bmatrix} \frac{\cos(\theta)}{\sqrt{2}} \cdot \frac{r + \text{Re}^{-i\phi_1}}{1 + \text{Re}^{-i\phi_1}} \\ \frac{-(1 + \sin(\theta))}{2} \cdot \frac{r + \text{Re}^{-i\phi_2}}{1 + \text{Re}^{-i\phi_2}} \\ \frac{1 - \sin(\theta)}{2} \cdot \frac{r + \text{Re}^{-i\phi_3}}{1 + \text{Re}^{-i\phi_3}} \end{bmatrix} \tag{E.75}$$

By using the norm  $|\text{Vector} \times \text{Vector}^*|$  as definition for the intensity, we get for the reflected intensity Equation E.76.

$$I_{\text{Reflected}} = \frac{\cos(\theta)^2}{2} \cdot \frac{r^2 + R^2 + 2Rr \cos(\phi_1)}{1 + R^2 r^2 + 2Rr \cos(\phi_1)} + \frac{(1 + \sin(\theta))^2}{4} \cdot \frac{r^2 + R^2 + 2Rr \cos(\phi_2)}{1 + R^2 r^2 + 2Rr \cos(\phi_2)} + \frac{(1 - \sin(\theta))^2}{4} \cdot \frac{r^2 + R^2 + 2Rr \cos(\phi_3)}{1 + R^2 r^2 + 2Rr \cos(\phi_3)} \tag{E.76}$$

If  $\phi_1 = \phi_2 = \phi_3$  or with other words if  $E_{\text{Amplitude, Microwave}} = 0$  we find again Equation E.36. For the analysis of the modulation, we will use the same approach as in chapter 5.1 but we will linearize each term of Equation E.76 separately. So we get for the electro-optic signal Equation E.77.

$$I_{\text{ElectroOptic}} = \frac{\cos(\theta)^2}{2} \cdot \left. \frac{\partial}{\partial E_{\text{Amplitude}}} \left( \frac{r^2 + R^2 + 2Rr \cos(\phi_1)}{1 + R^2 r^2 + 2Rr \cos(\phi_1)} \right) \right|_{E_{\text{Amplitude}} = 0} \cdot E_{\text{Amplitude}} + \frac{(1 + \sin(\theta))^2}{4} \cdot \dots + \frac{(1 - \sin(\theta))^2}{4} \cdot \dots \tag{E.77}$$

By using Equation E.43 we get the electro-optic signal for this setup Equation E.78.

$$I_{\text{ElectroOptic}} = \frac{(1 + \sin(\theta))^2}{4} \cdot \frac{\partial I_{\text{Reflected}}}{\partial \lambda_o} \cdot \frac{-n_o^2 r_{41} \lambda_o}{2} \cdot E_{\text{Amplitude}} + \frac{(1 - \sin(\theta))^2}{4} \cdot \frac{\partial I_{\text{Reflected}}}{\partial \lambda_o} \cdot \frac{n_o^2 r_{41} \lambda_o}{2} \cdot E_{\text{Amplitude}} = \frac{\partial I_{\text{Reflected}}}{\partial \lambda_o} \cdot \frac{n_o^2 r_{41} \lambda_o}{2} \left( \frac{1 + \sin(\theta)^2}{2} \right) \cdot E_{\text{Amplitude}} \quad \text{E.78}$$

Finally we get for the resulting modulation Equation E.79.

$$I_{\text{Modulation}} = \left| \frac{\partial I_{\text{Reflected}}}{\partial \lambda_o} \right| \cdot n_o^2 r_{41} \lambda_o \frac{1 + \sin(\theta)^2}{2} \cdot E_{\text{Amplitude}} \quad \text{E.79}$$

## E.10. Calculation of the Polarization Modulation

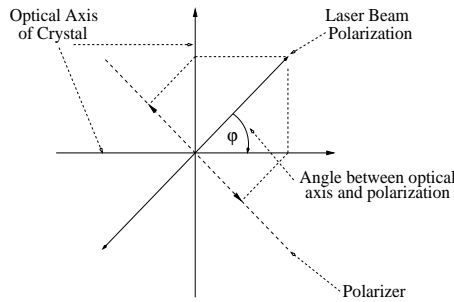


**Figure E.5.** Configuration using the polarization shift to measure the signal.

By projecting the vector of the electric field onto the optical axis of the crystal (Figure E.5), we get Equation E.80,

$$\begin{aligned} E_{x, \text{Incident}} &= E_{\text{Amplitude, Laser}} \cdot \cos(\varphi) \\ E_{y, \text{Incident}} &= E_{\text{Amplitude, Laser}} \cdot \sin(\varphi) \end{aligned} \quad \text{E.80}$$

where  $\varphi$  is the angle between the optical axis 'x'. So now will study the propagation of laser beam for both optical axis separately. We assume that the direction of the applied microwave signal is parallel to the z-axis. By using the result of Equation E.35, we get for the reflected laser beam Equation E.81.

$$\begin{aligned} E_{x, \text{Reflected}} &= -E_{\text{Amplitude, Laser}} \cdot \frac{r + \text{Re}^{-i\phi_1}}{1 + \text{Re}^{-i\phi_1}} \cdot \cos(\varphi) & \text{with } \phi_1 &\approx \frac{4\pi d}{\lambda_o} \left( n_o + \frac{1}{2} n_o^3 r_{41} E_z \right) \\ E_{y, \text{Reflected}} &= -E_{\text{Amplitude, Laser}} \cdot \frac{r + \text{Re}^{-i\phi_2}}{1 + \text{Re}^{-i\phi_2}} \cdot \sin(\varphi) & \phi_2 &\approx \frac{4\pi d}{\lambda_o} \left( n_o - \frac{1}{2} n_o^3 r_{41} E_z \right) \end{aligned} \quad \text{E.81}$$

The reflected laser beam will pass a analyzer which is aligned perpendicular to the polarization of the incident laser beam. So after projecting  $E_{x, \text{Reflected}}$  and  $E_{y, \text{Reflected}}$  onto the axe of the analyzer the laser beam is given by Equation E.82.

$$\begin{aligned}
 E_{x, \text{Polarizer}} &= -E_{\text{Amplitude, Laser}} \cdot \frac{r + \text{Re}^{-i\phi_1}}{1 + \text{Rre}^{-i\phi_1}} \cdot \sin(\varphi) \cdot \cos(\varphi) \\
 E_{y, \text{Polarizer}} &= -E_{\text{Amplitude, Laser}} \cdot \frac{r + \text{Re}^{-i\phi_2}}{1 + \text{Rre}^{-i\phi_2}} \cdot \cos(\varphi) \cdot \sin(\varphi)
 \end{aligned} \tag{E.82}$$

According to Figure E.5 we have to subtract  $E_{y, \text{Reflected}}$  from  $E_{x, \text{Reflected}}$  to get the resulting electric field.

$$E_{\text{Polarizer}} = -E_{\text{Amplitude, Laser}} \cdot \left( \frac{r + \text{Re}^{-i\phi_1}}{1 + \text{Rre}^{-i\phi_1}} - \frac{r + \text{Re}^{-i\phi_2}}{1 + \text{Rre}^{-i\phi_2}} \right) \cdot \cos(\varphi) \cdot \sin(\varphi) \tag{E.83}$$

For the calculation of the laser beam intensity we use again Equation E.36 on page 122.

$$\begin{aligned}
 I_{\text{Polarizer}} &= \frac{-E_{\text{Amplitude, Laser}}^2}{2Z_{\text{Material}}} \cdot (\cos(\varphi) \cdot \sin(\varphi))^2 \cdot \left| \left( \frac{r + \text{Re}^{-i\phi_1}}{1 + \text{Rre}^{-i\phi_1}} - \frac{r + \text{Re}^{-i\phi_2}}{1 + \text{Rre}^{-i\phi_2}} \right) \cdot \left( \frac{r + \text{Re}^{-i\phi_1}}{1 + \text{Rre}^{-i\phi_1}} - \frac{r + \text{Re}^{-i\phi_2}}{1 + \text{Rre}^{-i\phi_2}} \right)^* \right|^2 \\
 &= I_{\text{Incident}} \cdot \left( \frac{\sin(2\varphi)}{2} \right)^2 \cdot \left| \left( \frac{r + \text{Re}^{-i\phi_1}}{1 + \text{Rre}^{-i\phi_1}} - \frac{r + \text{Re}^{-i\phi_2}}{1 + \text{Rre}^{-i\phi_2}} \right) \cdot \left( \frac{r + \text{Re}^{-i\phi_1}}{1 + \text{Rre}^{-i\phi_1}} - \frac{r + \text{Re}^{-i\phi_2}}{1 + \text{Rre}^{-i\phi_2}} \right)^* \right|^2 \\
 &= I_{\text{Incident}} \cdot \left( \frac{\sin(2\varphi)}{2} \right)^2 \cdot \left| \frac{((r + \text{Re}^{-i\phi_1}) \cdot (1 + \text{Rre}^{-i\phi_2}) - (r + \text{Re}^{-i\phi_2}) \cdot (1 + \text{Rre}^{-i\phi_1}))}{(1 + \text{Rre}^{-i\phi_1}) \cdot (1 + \text{Rre}^{-i\phi_2})} \right|^2 \\
 &= \frac{((r + \text{Re}^{-i\phi_1}) \cdot (1 + \text{Rre}^{-i\phi_2}) - (r + \text{Re}^{-i\phi_2}) \cdot (1 + \text{Rre}^{-i\phi_1}))^*}{(1 + \text{Rre}^{-i\phi_1})^* \cdot (1 + \text{Rre}^{-i\phi_2})^*} \Big| = \\
 &= I_{\text{Incident}} \cdot \left( \frac{\sin(2\varphi)}{2} \right)^2 \cdot \left| \frac{(R(1-r^2) \cdot (e^{-i\phi_1} - e^{-i\phi_2})) \cdot (R(1-r^2) \cdot (e^{-i\phi_1} - e^{-i\phi_2}))^*}{(1 + \text{Rre}^{-i\phi_1}) \cdot (1 + \text{Rre}^{-i\phi_1})^* \cdot (1 + \text{Rre}^{-i\phi_2}) \cdot (1 + \text{Rre}^{-i\phi_2})^*} \right|^2 \\
 &= I_{\text{Incident}} \cdot \left( \frac{\sin(2\varphi)}{2} \right)^2 \cdot R^2(1-r^2)^2 \cdot \left| \frac{(e^{-i\phi_1} - e^{-i\phi_2}) \cdot (e^{-i\phi_1} - e^{-i\phi_2})^*}{(1 + \text{Rre}^{-i\phi_1}) \cdot (1 + \text{Rre}^{-i\phi_1})^* \cdot (1 + \text{Rre}^{-i\phi_2}) \cdot (1 + \text{Rre}^{-i\phi_2})^*} \right|^2
 \end{aligned} \tag{E.84}$$

By using Equation E.85 and Equation E.86 we can simplify Equation E.84.

$$\begin{aligned}
 &(e^{-i\phi_1} - e^{-i\phi_2}) \cdot (e^{-i\phi_1} - e^{-i\phi_2})^* = \\
 &(\cos(\phi_1) - i \sin(\phi_1) - \cos(\phi_2) + i \sin(\phi_2)) \cdot (\cos(\phi_1) + i \sin(\phi_1) - \cos(\phi_2) - i \sin(\phi_2)) = \\
 &(\cos(\phi_1) - \cos(\phi_2))^2 + (-\sin(\phi_1) + \sin(\phi_2))^2 = \\
 &\cos(\phi_1)^2 - 2\cos(\phi_1)\cos(\phi_2) + \cos(\phi_2)^2 + \sin(\phi_1)^2 - 2\sin(\phi_1)\sin(\phi_2) + \sin(\phi_2)^2 = \\
 &2 \cdot (1 - \cos(\phi_1 - \phi_2)) = \\
 &4 \cdot \sin\left(\frac{\phi_1 - \phi_2}{2}\right) \\
 &(1 + \text{Rre}^{-i\phi}) \cdot (1 + \text{Rre}^{-i\phi})^* = \\
 &(1 + rR(\cos(\phi) - i \sin(\phi))) \cdot (1 + rR(\cos(\phi) + i \sin(\phi))) \\
 &= (1 + rR \cos(\phi))^2 + (rR \sin(\phi))^2 = \\
 &1 + 2rR \cos(\phi) + r^2 R^2 \cos(\phi)^2 + r^2 R^2 \sin(\phi)^2 = \\
 &1 + r^2 R^2 + 2rR \cos(\phi)
 \end{aligned} \tag{E.86}$$

By putting together the previous results, we get for the output intensity given in Equation E.87.

$$I_{\text{Polarizer}}(E_z, \lambda_o, \varphi) = I_{\text{Incident}} \cdot \sin(2\varphi)^2 \cdot \frac{\sin\left(\frac{2\pi d n_o^3 r_{41} E_z}{\lambda_o}\right)^2 \cdot R^2 (1-r^2)^2}{\left(1 + r^2 R^2 + 2rR \cos\left(\frac{4\pi d}{\lambda_o} \left(n_o + \frac{1}{2} n_o^3 r_{41} E_z\right)\right)\right) \cdot \left(1 + r^2 R^2 + 2rR \cos\left(\frac{4\pi d}{\lambda_o} \left(n_o - \frac{1}{2} n_o^3 r_{41} E_z\right)\right)\right)} \quad \text{E.87}$$

Considering that the electro-optic coefficient is very small (for GaAs  $r_{41}=1.41 \cdot 10^{-12}$  m/V), we can neglect its influence in the denominator (Equation E.88).

$$I_{\text{Polarizer}}(E_z, \lambda_o, \varphi) \approx I_{\text{Incident}} \cdot \sin(2\varphi)^2 \cdot \frac{\sin\left(\frac{2\pi d n_o^3 r_{41} E_z}{\lambda}\right)^2 \cdot R^2 (1-r^2)^2}{\left(1 + r^2 R^2 + 2rR \cos\left(\frac{4\pi d}{\lambda} n_o\right)\right)^2} \quad \text{E.88}$$

### E.11. Calculation of the Polarization Modulation with two $\lambda/8$ wave plate

The modulation is not effective for the setup discussed in the previous paragraph. It is very weak because of a bad choice of the working point. We can see that by considering that Equation E.89 becomes zero.

$$\frac{\partial}{\partial \varphi} \cdot \text{Sin}(\varphi)^2 \Big|_{\varphi=0} = 0 \quad \text{E.89}$$

In the most configurations, the working point is changed by introducing a quarter wave plate. In our case we introduce a  $\lambda/8$  wave plate, because the laser beam will pass it twice. The optical axis of the  $\lambda/8$  wave plate have the same directions as the optical axis of the GaAs crystal as displayed in Figure E.5.

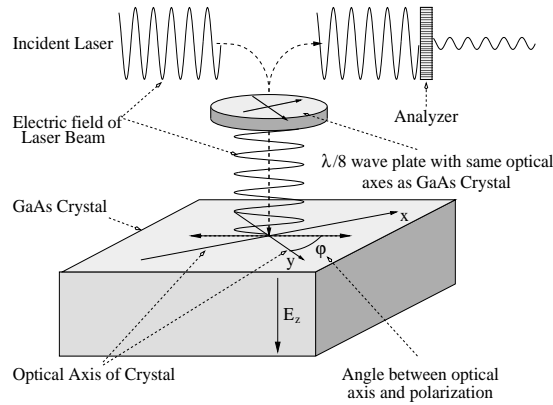


**Figure E.6** Configuration using the polarization shift to measure the signal and  $\lambda/8$  wave plat.

So Equation E.81 becomes Equation E.90 where  $e^{+i\pi/4}$  and  $e^{-i\pi/4}$  respectively  $e^{+i0}$  and  $e^{-i\pi/2}$  are the phase shifts caused by the wave plate.

$$\begin{aligned}
 E_{x, \text{Reflected}} &= -E_{\text{Amplitude, Laser}} \cdot e^{i0} \cdot \frac{r + \text{Re}^{-i\phi_1}}{1 + \text{Rre}^{-i\phi_1}} \cdot \cos(\varphi) & \text{with } \phi_1 &\approx \frac{4\pi d}{\lambda_o} \left( n_o + \frac{1}{2} n_o^3 r_{41} E_z \right) \\
 E_{y, \text{Reflected}} &= -E_{\text{Amplitude, Laser}} \cdot e^{-\frac{i\pi}{2}} \cdot \frac{r + \text{Re}^{-i\phi_2}}{1 + \text{Rre}^{-i\phi_2}} \cdot \sin(\varphi) & \phi_2 &\approx \frac{4\pi d}{\lambda_o} \left( n_o - \frac{1}{2} n_o^3 r_{41} E_z \right)
 \end{aligned} \tag{E.90}$$

So for the electric field at the output of the analyzer becomes Equation E.91.

$$\begin{aligned}
 E_{\text{Polarizer}} &= -E_{\text{Amplitude, Laser}} \cdot \left( e^{i0} \cdot \frac{r + \text{Re}^{-i\phi_1}}{1 + \text{Rre}^{-i\phi_1}} - e^{-\frac{i\pi}{2}} \cdot \frac{r + \text{Re}^{-i\phi_2}}{1 + \text{Rre}^{-i\phi_2}} \right) \cdot \cos(\varphi) \cdot \sin(\varphi) \\
 &= -E_{\text{Amplitude, Laser}} \frac{\sin(2\varphi)}{2} \cdot \left( 1 \cdot \frac{r + \text{Re}^{-i\phi_1}}{1 + \text{Rre}^{-i\phi_1}} + i \cdot \frac{r + \text{Re}^{-i\phi_2}}{1 + \text{Rre}^{-i\phi_2}} \right)
 \end{aligned} \tag{E.91}$$

So for the reflected intensity at the output of the analyzer we get Equation E.92.

$$\begin{aligned}
 I_{\text{Polarizer}} &= \frac{1}{2 \cdot Z_{\text{Material}}} \cdot |E_{\text{Polarizer}} \cdot E_{\text{Polarizer}}^*| = \\
 &= \frac{E_{\text{Amplitude}}^2}{2 \cdot Z_{\text{Material}}} \cdot \frac{\sin(2\varphi)^2}{4} \cdot \left( \frac{r + \text{Re}^{-i\phi_1}}{1 + \text{Rre}^{-i\phi_1}} + i \cdot \frac{r + \text{Re}^{-i\phi_2}}{1 + \text{Rre}^{-i\phi_2}} \right) \cdot \left( \frac{r + \text{Re}^{-i\phi_1}}{1 + \text{Rre}^{-i\phi_1}} + i \cdot \frac{r + \text{Re}^{-i\phi_2}}{1 + \text{Rre}^{-i\phi_2}} \right) = \\
 I_{\text{Incident}} &\cdot \frac{\sin(2\varphi)^2}{4} \cdot \frac{\left( (r + \text{Re}^{-i\phi_1})(1 + \text{Rre}^{-i\phi_2}) + i(r + \text{Re}^{-i\phi_2})(1 + \text{Rre}^{-i\phi_1}) \right)}{\left( (1 + \text{Rre}^{-i\phi_1}) \cdot (1 + \text{Rre}^{-i\phi_2}) \right)} \cdot (\dots)^* = \\
 I_{\text{Incident}} &\cdot \frac{\sin(2\varphi)^2}{4} \cdot \frac{\left( (r + \text{Re}^{-i\phi_1})(1 + \text{Rre}^{-i\phi_2}) + i(r + \text{Re}^{-i\phi_2})(1 + \text{Rre}^{-i\phi_1}) \right) \cdot \left( (r + \text{Re}^{-i\phi_1})^* (1 + \text{Rre}^{-i\phi_2})^* - i(r + \text{Re}^{-i\phi_2})^* (1 + \text{Rre}^{-i\phi_1})^* \right)}{\left( (1 + \text{Rre}^{-i\phi_1}) \cdot (1 + \text{Rre}^{-i\phi_1})^* \cdot (1 + \text{Rre}^{-i\phi_2}) \cdot (1 + \text{Rre}^{-i\phi_2})^* \right)} = \\
 &= I_{\text{Incident}} \cdot \frac{\sin(2\varphi)^2}{4} \cdot \frac{\left( (r + \text{Re}^{-i\phi_1}) \cdot (\dots)^* \cdot (1 + \text{Rre}^{-i\phi_2}) \cdot (\dots)^* + i \left( (r + \text{Re}^{-i\phi_2})(1 + \text{Rre}^{-i\phi_1}) (r + \text{Re}^{-i\phi_1})^* (1 + \text{Rre}^{-i\phi_2})^* - (\dots)^* \right) + (r + \text{Re}^{-i\phi_2}) \cdot (\dots)^* (1 + \text{Rre}^{-i\phi_1}) \cdot (\dots)^* \right)}{\left( (1 + \text{Rre}^{-i\phi_1}) \cdot (\dots)^* \cdot (1 + \text{Rre}^{-i\phi_2}) \cdot (\dots)^* \right)}
 \end{aligned} \tag{E.92}$$

By using Equation E.93 we can simplify the expression for the intensity at the output.

$$(r + \text{Re}^{-i\phi}) \cdot (\dots)^* = r^2 + R^2 + 2rR \cos(\phi) \quad , \quad (1 + \text{Rre}^{-i\phi}) \cdot (\dots)^* = 1 + r^2 R^2 + 2rR \cos(\phi) \quad \text{and} \tag{E.93}$$

$$\begin{aligned}
 &i \cdot \left( (r + \text{Re}^{-i\phi_2})(1 + \text{Rre}^{-i\phi_1})(r + \text{Re}^{-i\phi_1})^* (1 + \text{Rre}^{-i\phi_2})^* - (\dots)^* \right) = \\
 &-2 \cdot \Im m \left( (r + \text{Re}^{-i\phi_2})(1 + \text{Rre}^{-i\phi_1})(r + \text{Re}^{-i\phi_1})^* (1 + \text{Rre}^{-i\phi_2})^* \right) = \\
 &-2 \cdot \Im m \left( (r + R(\cos(\phi_1) + i \sin(\phi_1))) \cdot (r + R(\cos(\phi_2) - i \sin(\phi_2))) \cdot \right. \\
 &\quad \left. (1 + rR(\cos(\phi_1) - i \sin(\phi_1))) \cdot (1 + rR(\cos(\phi_2) + i \sin(\phi_2))) \right) = \\
 &2 \cdot (1 + rR(\cos(\phi_1) - \sin(\phi_1))) \cdot (r \sin(\phi_1) + R \sin((\phi_1 - \phi_2) - r \sin(\phi_2))) \cdot (1 + rR(\cos(\phi_2) - \sin(\phi_2)))
 \end{aligned}$$

So finally we get for the intensity at the output Equation E.94.

$$I_{\text{Output}}(\lambda_o, E_z, \varphi) = I_{\text{Incident}} \cdot \frac{\sin(2\varphi)^2}{4} \quad \text{E.94}$$

$$\frac{(r^2 + R^2 + 2rR \cos(\phi_1))(1 + r^2 R^2 + 2rR \cos(\phi_2)) + \Pi + (r^2 + R^2 + 2rR \cos(\phi_2))(1 + r^2 R^2 + 2rR \cos(\phi_1))}{(1 + r^2 R^2 + 2rR \cos(\phi_1)) \cdot (1 + r^2 R^2 + 2rR \cos(\phi_2))}$$

$$\text{with } \Pi = -4 \cdot \left( r \cdot (1 - r^2) \cdot R \cdot \left( R(1 + r^2) \cos\left(\frac{\phi_1 - \phi_2}{2}\right) + r(1 + R^2) \cos\left(\frac{\phi_1 + \phi_2}{2}\right) \right) \cdot \sin\left(\frac{\phi_1 - \phi_2}{2}\right) \right) ,$$

$$\phi_1 \approx \frac{4\pi d}{\lambda_o} \left( n_o + \frac{1}{2} n_o^3 r_{41} E_z \right) \quad \text{and} \quad \phi_2 \approx \frac{4\pi d}{\lambda_o} \left( n_o - \frac{1}{2} n_o^3 r_{41} E_z \right)$$

So the expressions is more complicated than the response (  $2 \cdot (1 + \sin(2\Delta))$  ) of a ‘standard’ polarization modulation cell (the beam just passes through the crystal without any reflections) with a  $\lambda/4$  wave plate.

## E.12. Calculation of the phase shift modulation

In the setup for the phase modulation, we split the incident laser beam ( $E_{\text{Input,Laser}}$ ) into two equal parts, one part for probing and one part as a reference. At the output we recombine the sensed ( $A_{\text{Probe}} \cdot e^{-i\vartheta_{\text{Probe}}}$ ) and the reference beam ( $A_{\text{Reference}} \cdot e^{-i\vartheta_{\text{Reference}}}$ ).  $A_x$  indicates an attenuation and  $\vartheta$  indicates a phase shift cause by the propagation of a laser beam or caused by the ‘modulation’.

$$E_{\text{Output,Laser}} = \frac{E_{\text{Input,Laser}}}{2} (A_{\text{Probe}} \cdot e^{-i\vartheta_{\text{Probe}}} + A_{\text{Reference}} \cdot e^{-i\vartheta_{\text{Reference}}}) \quad \text{E.95}$$

In the following deductions we assume that there are no further loss or gain in the system, and hence  $A_{\text{Probe}} < 1$  and  $A_{\text{Reference}} < 1$ . For the intensity of the laser beam we get Equation E.96.

$$I_{\text{Response}} = \frac{1}{2Z_{\text{Material}}} |E_{\text{Output,Laser}} \cdot E_{\text{Output,Laser}}^*| = \quad \text{E.96}$$

$$\frac{I_{\text{Incident}}}{4} | (A_{\text{Probe}} (\cos(\vartheta_{\text{Probe}}) - i \sin(\vartheta_{\text{Probe}})) + A_{\text{Reference}} (\cos(\vartheta_{\text{Reference}}) - i \sin(\vartheta_{\text{Reference}}))) \cdot (\dots)^* | =$$

$$\frac{I_{\text{Incident}}}{4} | (A_{\text{Probe}} \cos(\vartheta_{\text{Probe}}) + A_{\text{Reference}} \cos(\vartheta_{\text{Reference}}))^2 + (A_{\text{Probe}} \sin(\vartheta_{\text{Probe}}) + A_{\text{Reference}} \sin(\vartheta_{\text{Reference}}))^2 |$$

$$= \frac{I_{\text{Incident}}}{4} (A_{\text{Probe}}^2 + A_{\text{Reference}}^2 + 2A_{\text{Reference}} \cdot A_{\text{Probe}} \cdot \cos(\vartheta_{\text{Probe}} - \vartheta_{\text{Reference}}))$$

By calculation the real and imaginary part of Equation E.35 on page 122 in Equation E.97 and by exploiting Equation E.37, we can calculate the attenuation  $A_{\text{probe}}$  (Equation E.98) and the phase shift  $\vartheta_{\text{Probe}}$  (Equation E.99) caused by the cavity.

$$E_{\text{Reflected,Laser}} = -E_{\text{Incident,Laser}} \left( \frac{r + R e^{-i\phi}}{1 + R r e^{-i\phi}} \right) = -E_{\text{Incident,Laser}} \left( \frac{r + R e^{-i\phi}}{1 + R r e^{-i\phi}} \right) \cdot \left( \frac{1 + R r e^{-i\phi}}{1 + R r e^{-i\phi}} \right)^* \quad \text{E.97}$$

$$= -E_{\text{Incident,Laser}} \left( \frac{r + R e^{-i\phi}}{1 + R r e^{-i\phi}} \right) \cdot \left( \frac{1 + R r e^{-i\phi}}{1 + R r e^{-i\phi}} \right)^* =$$

$$-E_{\text{Incident,Laser}} \left( \frac{(r + R \cos(\phi) - i R \sin(\phi)) \cdot (1 + R r \cos(\phi) + i R r \sin(\phi))}{1 + R^2 r^2 + 2R r \cos(\phi)} \right)$$

$$= -E_{\text{Incident,Laser}} \left( \frac{r + R(1 + r^2) \cos(\phi) + R^2 r + i(R(r^2 - 1) \sin(\phi))}{1 + R^2 r^2 + 2R r \cos(\phi)} \right)$$

$$A_{\text{Probe}} = \sqrt{\frac{r^2 + R^2 + 2Rr \cos(\phi)}{1 + R^2 r^2 + 2Rr \cos(\phi)}} \quad \text{with } \phi \approx \frac{4\pi d}{\lambda_o} \left( n_o + \frac{1}{2} n_o^3 r_{41} E_z \right) \quad \text{E.98}$$

$$\vartheta_{\text{Probe}} = \text{ArcTan} \left( \frac{R(r^2 - 1) \sin(\phi)}{r(1 + R^2) + \cos(\phi)R(1 + r^2)} \right) \quad \text{with } \phi \approx \frac{4\pi d}{\lambda_o} \left( n_o + \frac{1}{2} n_o^3 r_{41} E_z \right) \quad \text{E.99}$$

So now we have to choose  $A_{\text{Reference}}$  and  $\vartheta_{\text{Reference}}$  in a way that we get a “good” modulation. Considering that we are interested in “strong” variations, we are looking for the working point where Equation E.100 gets maximal or minimal.

$$\frac{\partial}{\partial \vartheta_{\text{Probe}}} \cos(\vartheta_{\text{Probe}} - \vartheta_{\text{Reference}}) \Big|_{E_z=0} = -\sin(\vartheta_{\text{Probe}} - \vartheta_{\text{Reference}}) \Big|_{E_z=0} \quad \text{E.100}$$

So the optimal choice for  $\vartheta_{\text{Reference}}$  will be equation Equation E.101.

$$\vartheta_{\text{Reference}} = \vartheta_{\text{Probe}} \Big|_{E_z=0} \pm \frac{\pi}{2} \quad \text{E.101}$$

Finally we choose  $A_{\text{Reference}}=1$  to simplify the calculations and hence get Equation E.102 for the response of the phase modulation.

$$I_{\text{Response}} = \frac{I_{\text{Incident}}}{4} \cdot \left( (1 + A_{\text{Probe}}^2) + 2A_{\text{Probe}} \cdot \cos \left( \vartheta_{\text{Probe}} - \vartheta_{\text{Probe}} \Big|_{E_z=0} + \frac{\pi}{2} \right) \right) \quad \text{E.102}$$

### E.13. Calculation of the Gaussian beam in free space

We start with the calculation of the spot size in free space. The laser beam leaves the optical fiber, passes through a lens and is focuses to a spot (Figure E.7). The distance output fiber / lens is called A. For the first example this distance should match the distance B between lens and spot or with other words the magnification factor B/A should be one.

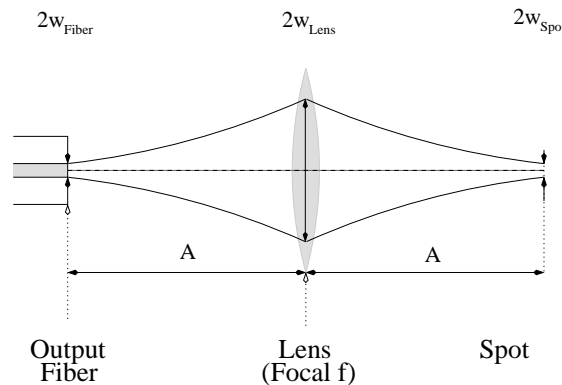


**Figure E.7** Calculation of the spot size and the focal distance with a lens at the fiber output.

For this calculation the given parameters are the wavelength of the laser beam  $\lambda_o$ , the refraction indices of the air  $n_{\text{Air}}$ , the beam waist at the output of the fiber  $w_{\text{Fiber}}$  as well as the focal distance  $f$  of

the lens. We assume that at the output of the fiber the laser beam is a plane wave. Also we do the assumption that the beam waist has the same size as the Mode Field Diameter and so according to Appendix A.2.3. on page 106 we do our calculations with a value of  $w_{\text{Fiber}}=w_{\text{AirOutputFiber}}=5 \text{ [\mu m]}$ . The seeked parameters are the focal distance  $A$  and the spot size in free space  $w_{\text{spot}}$ .

As the output of the fiber is a plane wave, the complex Gaussian beam parameter can be describe by Equation E.103.

$$\frac{1}{q_{\text{Air}}} = -\frac{i \cdot \lambda_o}{\pi w_{\text{Fiber}}^2 n_{\text{Air}}} \quad \text{E.103}$$

If we redefine  $z_o = \lambda_o / (\pi w_{\text{Fiber}}^2 n_{\text{Air}})$  we can rewrite  $q_{\text{Air}}$  as Equation E.104.

$$q_{\text{Air}} = \frac{i \cdot \pi w_{\text{Fiber}}^2 n_{\text{Air}}}{\lambda_o} = i \cdot z_o \quad \text{E.104}$$

By using Table 2 on page 45 we can determine the characteristics of the beam propagation by Equation E.105.

$$\frac{1}{f} \cdot \begin{bmatrix} f-A & A(2f-A) \\ -1 & f-A \end{bmatrix} = \begin{bmatrix} 1 & A \\ 0 & 1 \end{bmatrix} \cdot \begin{bmatrix} 1 & 0 \\ -1/f & 1 \end{bmatrix} \cdot \begin{bmatrix} 1 & A \\ 0 & 1 \end{bmatrix} \quad \text{E.105}$$

So the complex beam parameter after the fiber is given by Equation E.106.

$$q_{\text{Spot}} = \frac{A(2f-A) + iz_o(f-A)}{f-A-iz_o} \quad \text{E.106}$$

To determine the position of the focus, we have to find the point where the Gaussian beam is a plane wave. So the real part of  $q_{\text{Spot}}$  has to vanish and for this value we can calculate the beam radius (Equation E.107).

$$\Re\left(\frac{(A(2f-A) + iz_o(f-A)) \cdot (f-A + iz_o)}{(f-A-iz_o) \cdot (f-A + iz_o)}\right) = 0 \quad \text{E.107}$$

$$\Re\left(\frac{(A(2f-A))(f-A) - z_o^2(f-A) + iz_o f^2}{(f-A)^2 + z_o^2}\right) = 0$$

$$(f-A)(A^2 - 2Af + z_o^2) = 0$$

$$(f-A)(f + \sqrt{f^2 - z_o^2} - A)(f - \sqrt{f^2 - z_o^2} - A) = 0$$

In Equation E.107 we get three solution but only one is the wanted one. The first solution  $A=f$  indicates the case with the fiber output in the focus of the lens. So at the output of the lens the Gaussian beam becomes (exceptionally) a plane wave. The second solution ( $A = f - \sqrt{f^2 - z_o^2}$ ) indicates the trivial solution when the output of the fiber is about in the center of lens. So the searched solution is Equation E.108.

$$A = f + \sqrt{f^2 - z_o^2} \quad \text{E.108}$$

In most case  $z_0$  is much smaller than the focal distance  $f$  and in this case we get for  $A \approx 2f$ .

By putting the solution of Equation E.108 into Equation E.106 we get the complex Gaussian beam parameter for the focal point. It is not surprising that this parameter is identical with the parameter at the output of the fiber and hence the beam waist of the spot is identical with the beam waist at the output of the fiber.

$$q_{\text{Spot}} = \frac{i \cdot z_0 f^2}{(f - A)^2 + z_0^2} = \frac{i \cdot z_0 f^2}{(f - f - \sqrt{f^2 - z_0^2})^2 + z_0^2} = i \cdot z_0 = q_{\text{Airy}} \quad \text{E.109}$$

and hence

$$\frac{i \cdot \pi w_{\text{Fiber}}^2 n_{\text{Airy}}}{\lambda_0} = \frac{i \cdot \pi w_{\text{Spot}}^2 n_{\text{Airy}}}{\lambda_0} \quad \text{E.110}$$

$$w_{\text{Fiber}} = w_{\text{Spot}}$$

### E.13.1. Magnification factor $\neq 1$

In the previous section, we assumed that the lens is exactly in the middle between the fiber output and the focal spot. We will modify the calculation so that we can analyze the common case where  $A \neq B$  (Figure E.8).  $A$  as well as  $B$  have to be bigger than the focal distance  $f$  to guarantee the generation of an image. In this setup  $A$  is given and  $B$  is the searched variable.

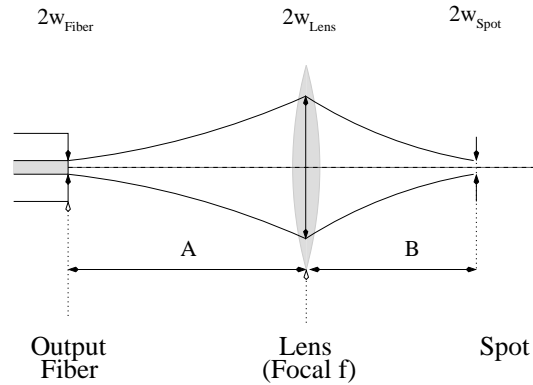


**Figure E.8** Calculation of the spot size and the focal distance with a lens at the fiber output.

So for the ray matrix of our setup we get Equation E.111.

$$\frac{1}{f} \cdot \begin{bmatrix} f - B & f(A + B) - AB \\ -1 & f - A \end{bmatrix} = \begin{bmatrix} 1 & B \\ 0 & 1 \end{bmatrix} \cdot \begin{bmatrix} 1 & 0 \\ -1/f & 1 \end{bmatrix} \cdot \begin{bmatrix} 1 & A \\ 0 & 1 \end{bmatrix} \quad \text{E.111}$$

So for the complex Gaussian beam parameter we get Equation E.112.

$$q_{\text{Spot}} = \frac{(f(A + B) - AB)(f - A) - z_0^2(f - B) + iz_0 f^2}{(f - A)^2 + z_0^2} \quad \text{E.112}$$

So by requiring that the real part of Equation E.112 is zero, we get for B Equation E.113.

$$(f(A + B) - AB)(f - A) - z_o^2(f - B) = 0 \quad \text{E.113}$$

$$B = \frac{f(A(A - f) + z_o^2)}{(A - f)^2 + z_o^2}$$

So for  $q_{\text{Spot}}$  we get Equation E.114.

$$q_{\text{Spot}} = \frac{f^2}{(f - A)^2 + z_o^2} \cdot iz_o \quad \text{E.114}$$

$$q_{\text{Spot}} = \frac{f^2}{(f - A)^2 + z_o^2} \cdot q_{\text{Fiber}}$$

So we can calculate the beam waist in the spot Equation E.115.

$$\frac{i \cdot \pi w_{\text{Spot}}^2 n_{\text{Air}}}{\lambda_o} = \frac{f^2}{(f - A)^2 + z_o^2} \cdot \frac{i \cdot \pi w_{\text{Fiber}}^2 n_{\text{Air}}}{\lambda_o} \quad \text{E.115}$$

$$w_{\text{Spot}}^2 = w_{\text{Fiber}}^2 \frac{f^2}{(f - A)^2 + z_o^2}$$

$$w_{\text{Spot}} = w_{\text{Fiber}} \cdot \sqrt{\frac{f^2}{(f - A)^2 + z_o^2}}$$

So the beam waist depends on the parameter A or on the magnification factor A/B. It becomes maximal if A=f.

## E.14. Spot Size of our probing device

In this paragraph we will have a look at a Gaussian beam focused on the back side of a GaAs substrate (Figure E.9). The laser beam propagates a distance A (with  $A > f$ ) and is focused by a lens with a focal distance f. Afterwards the beam propagates again distance C where it hits the Air / GaAs interface. After the interface the beam goes through the substrate of a given thickness d and the focal point should be at the end of it.

The given parameters are the beam waist at the output of the fiber  $w_{\text{Air}}$ , the distance A, the focal distance of the lens f, the thickness of the substrate, the refraction indices of Air  $n_{\text{Air}}$  and GaAs  $n_{\text{GaAs}}$  as well as the laser beam wavelength  $\lambda_o$  in free space. The unknown values are the beam waists  $w_{\text{Lens}}$ ,  $w_{\text{Surface}}$  and  $w_{\text{Gold}}$  and the distances C and x. All parameters are defined according to Figure E.9. As in the previous sections we assume that the Gaussian beam is a plan wave at the output of the fiber as well as in the spot.

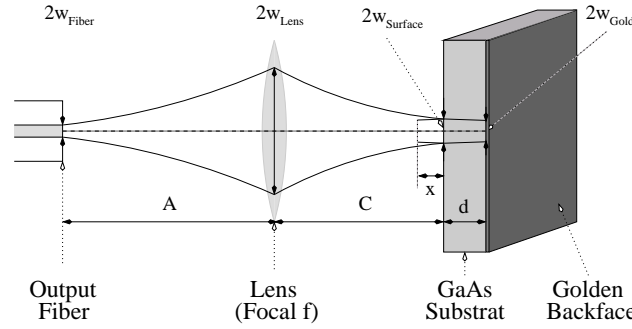


**Figure E.9** Calculation of the spot sizes and the focal distances with a lens at the fiber output.

So for the ray matrix of our setup we get Equation E.116.

$$\begin{aligned} \frac{n_{\text{Air}}}{n_{\text{GaAs}} \cdot f} \begin{bmatrix} \frac{n_{\text{GaAs}}}{n_{\text{Air}}} (f - C) - d \cdot A \frac{n_{\text{GaAs}}}{n_{\text{Air}}} (f - C) + d(f - A) + C f \frac{n_{\text{GaAs}}}{n_{\text{Air}}} \\ -1 \\ f - A \end{bmatrix} & \quad \text{E.116} \\ = \begin{bmatrix} 1 & d \\ 0 & 1 \end{bmatrix} \cdot \begin{bmatrix} 1 & 0 \\ 0 & n_{\text{Air}}/n_{\text{GaAs}} \end{bmatrix} \cdot \begin{bmatrix} 1 & C \\ 0 & 1 \end{bmatrix} \cdot \begin{bmatrix} 1 & 0 \\ -1/f & 1 \end{bmatrix} \cdot \begin{bmatrix} 1 & A \\ 0 & 1 \end{bmatrix} \end{aligned}$$

So for the complex Gaussian beam parameter we get Equation E.117

$$q_{\text{Spot}} = \frac{A \frac{n_{\text{GaAs}}}{n_{\text{Air}}} (f - C) + d(f - F) + C f \frac{n_{\text{GaAs}}}{n_{\text{Air}}} + iz_0 \left( \frac{n_{\text{GaAs}}}{n_{\text{Air}}} (f - C) - d \right)}{f - A - iz_0} \quad \text{E.117}$$

By using some software to simplify Equation E.117 we get the following term:

$$q_{\text{Spot}} = \frac{1}{n_{\text{Air}}} \left( d \cdot n_{\text{Air}} + n_{\text{GaAs}} \left( C + \frac{fA + fz_0}{f - A - iz_0} \right) \right) \quad \text{E.118}$$

By requiring that the real part of  $q_{\text{Spot}}$  is zero we get the following value for the parameter C as given in Equation E.119. If we assume that  $A=2f$  and that the beam waist at the fiber output becomes very small ( $z_0 \rightarrow 0$ ), the solution becomes  $C=2f \cdot d \cdot n_{\text{Air}}/n_{\text{GaAs}}$ .

$$C = \frac{f(A(A-f) + z_0^2)}{(f-A)^2 + z_0^2} - \frac{n_{\text{Air}}}{n_{\text{GaAs}}} d \quad \text{E.119}$$

So for the complex beam parameter in the focal point, we get Equation E.120 as well as the corresponding beam waist. If the magnification factor is one,  $A = f + \sqrt{f^2 - z_0^2}$  and so we find that  $w_{\text{Gold}}$  is equal to  $w_{\text{Air}}$ .

$$q_{\text{Spot}} = \frac{n_{\text{GaAs}}}{n_{\text{Air}}} \cdot \frac{f^2 \cdot iz_0}{(f-A)^2 + z_0^2} \quad \text{and so } w_{\text{Gold}} = w_{\text{Air}} \cdot \sqrt{\frac{f^2}{(f-A)^2 + z_0^2}} \quad \text{E.120}$$

With the previous result it is easy to deduce to other unknown parameters.

$$w_{\text{Surface}} = w_{\text{Gold}} \cdot \sqrt{1 + \left( \frac{d\lambda_o}{\pi w_{\text{Gold}}^2 n_{\text{GaAs}}} \right)^2} \quad \text{E.121}$$

$$w_{\text{Lens}} = w_{\text{Air}} \cdot \sqrt{1 + \left( \frac{A\lambda_o}{\pi w_{\text{Air}}^2 n_{\text{Air}}} \right)^2} \quad \text{E.122}$$

By subtracting the result of Equation E.119 to the value of Equation E.113, we find the according value for x.

$$x = B - C = \frac{f(A(A-f) + z_o^2)}{(A-f)^2 + z_o^2} - \left( \frac{f(A(A-f) + z_o^2)}{(A-f)^2 + z_o^2} - \frac{n_{\text{Air}}}{n_{\text{GaAs}}} d \right) = \frac{n_{\text{Air}}}{n_{\text{GaAs}}} d \quad \text{E.123}$$

## E.15. Recalculation of the cavity response

In the previous calculation we neglected the fact, that the incident beam is an Gaussian beam with finite dimensions. So we did not take into account that the beam waist spreads considerably while the beam is propagating in the GaAs substrate and that the reflection of the Air / GaAs interface will not be re-injected properly into the fiber because the focus will be slightly off. Considering that the beam has to be re-injected into the fiber output, this will cause supplementary losses for the second, third and further reflections.

### E.15.1. The first reflection

Another neglected problem is the location of the focus of the Air / GaAs interface. The reflection will not be focused properly into the output of the fiber (Figure E.10). We will calculate the beam waist of the reflected beam at the output of fiber. Afterwards we use Equation E.125 to determine the supplementary attenuation.

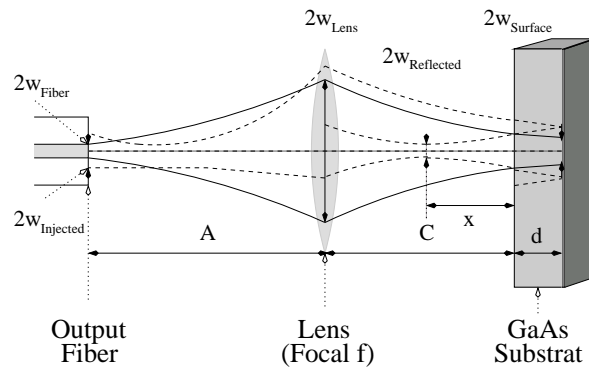


**Figure E.10** The reflection from the interface Air / GaAs are not re-injected properly into the fiber.

For the calculation of this attenuation coefficient  $R_{\text{Attenuation}}$ , we assume that both Gaussian beam are approximately plane waves. In this case we can use the equation which describes the losses due to MFD mismatch between two single mode fibers. For this calculation we use the scalar product between the two Gaussian modes and we normalize it as indicated in Equation E.124.

$$\text{Loss}_{\text{MisMatch}} = \frac{4 \cdot \text{MFD}_1^2 \cdot \text{MFD}_2^2}{(\text{MFD}_1^2 + \text{MFD}_2^2)} \quad \text{E.124}$$

For the calculations of the Fabry Perot Cavity, we use the electric field and not the intensity of the beam. Hence by replacing  $\text{MFD} = 2 \cdot w_x$  and by using the root of  $\text{Loss}_{\text{MisMatch}}$  we find Equation E.125.

$$R_{\text{Attenuation}} = \frac{2 \cdot w_{\text{Injected}} \cdot w_{\text{Fiber}}}{w_{\text{Injected}}^2 + w_{\text{Fiber}}^2} \quad \text{E.125}$$

For  $w_{\text{Fiber}}=w_{\text{Input}}$  we find Equation E.126.

$$R_{\text{Loss}}(w_{\text{Injected}}=w_{\text{Fiber}}) = \frac{2 \cdot w_{\text{Fiber}}^2}{2w_{\text{Fiber}}^2} = 1 \quad \text{E.126}$$

According to Figure E.10 we can calculate the complex beam parameter  $q_{\text{Input}}$ .

$$\frac{1}{f} \cdot \begin{bmatrix} f-A & f(C-x+A) + A(x-C) \\ -1 & f-C+x \end{bmatrix} = \begin{bmatrix} 1 & A \\ 0 & 1 \end{bmatrix} \cdot \begin{bmatrix} 1 & 0 \\ -1/f & 1 \end{bmatrix} \cdot \begin{bmatrix} 1 & C-x \\ 0 & 1 \end{bmatrix} \quad \text{E.127}$$

$$\text{with } x = \frac{n_{\text{Air}}}{n_{\text{GaAs}}} d, C = \frac{f(A(A-f) + z_o^2)}{(f-A)^2 + z_o^2} - x \text{ and } z_o = \frac{\pi w_{\text{Fiber}}^2 n_{\text{Air}}}{\lambda_o}$$

A and f are the given distance between the fiber output and the lens respectively the focal distance of the lens. By using Equation E.115 as the beam waist in the reflected spot we get for the complex beam parameter of the reflected beam at the position of the fiber output Equation E.128.

$$\frac{1}{q_{\text{Injected}}} = \frac{(f-C+x) - q_{\text{Reflection}}}{(f(C-x+A) + A(x-C)) + (f-A) \cdot q_{\text{Reflection}}} \quad \text{E.128}$$

$$\text{with } q_{\text{ReflectionFront}} = \frac{i \cdot \pi w_{\text{Reflection}}^2 n_{\text{Air}}}{\lambda_o} = \frac{i \cdot \pi \cdot w_{\text{Fiber}}^2 \cdot f^2 \cdot n_{\text{Air}}}{\lambda_o \cdot ((f-A)^2 + z_o^2)} = i \cdot z_{\text{ReflectedFront}}$$

As the reflected beam is not focused on this point  $\Re(q_{\text{Reflection}}) \neq 0$ . By using the definition of the complex beam parameter we can calculate the beam waist by using equation Equation E.129.

$$w_{\text{Injected}} = \sqrt{\frac{\lambda_o}{\pi \cdot -\Im(q_{\text{Injected}})} \cdot n_{\text{Air}}} \quad \text{E.129}$$

So we calculate  $\Im(q_{\text{Reflection}})$ .

$$\begin{aligned}
 \Im m\left(\frac{1}{q_{\text{Injected}}}\right) &= \tag{E.130} \\
 \Im m\left(\frac{((f-C+x)-i \cdot z_{\text{ReflectedFront}}) \cdot ((f(C-x+A)+A(x-C))+(f-A) \cdot i \cdot z_{\text{ReflectedFront}})^*}{((f(C-x+A)+A(x-C))+(f-A) \cdot i \cdot z_{\text{ReflectedFront}}) \cdot ((f(C-x+A)+A(x-C))+(f-A) \cdot i \cdot z_{\text{ReflectedFront}})^*}\right) &= \\
 \Im m\left(\frac{(\dots)+i \cdot z_{\text{ReflectedFront}} \cdot (-(f-A)(f-C+x)-(f(C-x+A)+A(x-C)))}{(f(C-x+A)+A(x-C))^2+((f-A) \cdot z_{\text{ReflectedFront}})^2}\right) &= \\
 \frac{z_{\text{ReflectedFront}} \cdot (-(f-A)(f-C+x)-(f(C-x+A)+A(x-C)))}{(f(C-x+A)+A(x-C))^2+((f-A) \cdot z_{\text{ReflectedFront}})^2} &= \\
 \frac{-z_{\text{ReflectedFront}} \cdot f^2}{(f(C-x+A)+A(x-C))^2+((f-A) \cdot z_{\text{ReflectedFront}})^2} &
 \end{aligned}$$

Hence we can calculate the beam waist of the re-injected laser beam (Equation E.131) and the according attenuation.

$$w_{\text{Injected}} = \sqrt{\frac{\lambda_o \cdot ((f(C-x+A)+A(x-C))^2+((f-A) \cdot z_{\text{Reflected}})^2)}{\pi \cdot z_{\text{ReflectedFront}} \cdot n_{\text{Air}} \cdot f^2}} \tag{E.131}$$

$$\begin{aligned}
 R_{\text{Front}} &= \frac{2 \cdot w_{\text{Fiber}} \cdot \sqrt{\frac{\lambda_o \cdot ((f(C-x+A)+A(x-C))^2+((f-A) \cdot z_{\text{Reflected}})^2)}{\pi \cdot z_{\text{ReflectedFront}} \cdot n_{\text{Air}} \cdot f^2}}}{\left(w_{\text{Fiber}}^2 + \frac{\lambda_o \cdot ((f(C-x+A)+A(x-C))^2+((f-A) \cdot z_{\text{Reflected}})^2)}{\pi \cdot z_{\text{ReflectedFront}} \cdot n_{\text{Air}} \cdot f^2}\right)} \tag{E.132}
 \end{aligned}$$

### E.15.2. Calculation for the loss in the substrate

Also the higher order reflections from the golden back face will not be reinjected properly. For the calculations of this attenuation coefficient, we proceed as in the previous paragraph.

$$\begin{aligned}
 \frac{1}{\tilde{f}} \cdot \begin{bmatrix} f-A & \frac{n_{\text{Air}} d N (f-A) + n_{\text{GaAs}} (f(A+C) - AC)}{n_{\text{Air}}} \\ -1 & \frac{n_{\text{GaAs}} (f-C) - n_{\text{Air}} d N}{n_{\text{Air}}} \end{bmatrix} &= \tag{E.133} \\
 \begin{bmatrix} 1 & A \\ 0 & 1 \end{bmatrix} \cdot \begin{bmatrix} 1 & 0 \\ -1/f & 1 \end{bmatrix} \cdot \begin{bmatrix} 1 & C \\ 0 & 1 \end{bmatrix} \cdot \begin{bmatrix} 1 & 0 \\ 0 & n_{\text{GaAs}}/n_{\text{Air}} \end{bmatrix} \cdot \begin{bmatrix} 1 & d \cdot (2N+1) \\ 0 & 1 \end{bmatrix}
 \end{aligned}$$

With  $q_{\text{Spot}} = \frac{n_{\text{GaAs}}}{n_{\text{Air}}} \cdot \frac{f^2 i z_o}{(f-A)^2 + z_o^2} = i z_{\text{Spot}}$ ,  $x = \frac{n_{\text{Air}}}{n_{\text{GaAs}}} d$ ,  $C = \frac{f(A(A-f) + z_o^2)}{(f-A)^2 + z_o^2} - x$ ,  $z_o = \frac{\pi w_{\text{Fiber}}^2 n_{\text{Air}}}{\lambda_o}$  and  $N$  (0,1,2,..) indicating the order of reflection, we get for the imaginary part of the complex beam parameter of the reinjected beam Equation E.134.

$$\begin{aligned}
& \Im\left(\frac{1}{q_{\text{Spot}}}\right) \tag{E.134} \\
&= \Im\left(\frac{n_{\text{GaAs}}(f-C) - n_{\text{Air}}d(2N+1) - iz_{\text{Spot}} \cdot n_{\text{Air}}}{n_{\text{Air}}d(2N+1)(f-A) + n_{\text{GaAs}}(f(A+C) - AC) + iz_{\text{Spot}} \cdot n_{\text{Air}}(f-A)}\right) \\
&\Im\left(\frac{(n_{\text{GaAs}}(f-C) - n_{\text{Air}}d(2N+1) - iz_{\text{Spot}} \cdot n_{\text{Air}}) \cdot (n_{\text{Air}}d(2N+1)(f-A) + n_{\text{GaAs}}(f(A+C) - AC) + iz_{\text{Spot}} \cdot n_{\text{Air}}(f-A))^*}{(n_{\text{Air}}d(2N+1)(f-A) + n_{\text{GaAs}}(f(A+C) - AC) + iz_{\text{Spot}} \cdot n_{\text{Air}}(f-A))(n_{\text{Air}}d(2N+1)(f-A) + n_{\text{GaAs}}(f(A+C) - AC) + iz_{\text{Spot}} \cdot n_{\text{Air}}(f-A))^*}\right) \\
&= \frac{z_{\text{Spot}} \cdot n_{\text{Air}} \cdot (n_{\text{Air}}d(2N+1)(f-A) + n_{\text{GaAs}}(f(A+C) - AC) + (f-A) \cdot (n_{\text{GaAs}}(f-C) - n_{\text{Air}}d(2N+1)))}{(n_{\text{Air}}d(2N+1)(f-A) + n_{\text{GaAs}}(f(A+C) - AC))^2 + (z_{\text{Spot}} \cdot n_{\text{Air}}(f-A))^2} \\
&= \frac{z_{\text{Spot}} \cdot n_{\text{Air}} \cdot n_{\text{GaAs}} \cdot f^2}{(n_{\text{Air}}d(2N+1)(f-A) + n_{\text{GaAs}}(f(A+C) - AC))^2 + (z_{\text{Spot}} \cdot n_{\text{Air}}(f-A))^2}
\end{aligned}$$

Hence we can calculate the beam waist of the re-injected laser beam (Equation E.131) and the according attenuation.

$$w_{\text{Injected}} = \sqrt{\frac{\lambda_o \cdot (n_{\text{Air}}d(2N+1)(f-A) + n_{\text{GaAs}}(f(A+C) - AC))^2 + (z_{\text{Spot}} \cdot n_{\text{Air}}(f-A))^2}{\pi \cdot z_{\text{Spot}} \cdot n_{\text{Air}}^2 \cdot n_{\text{GaAs}} \cdot f^2}} \tag{E.135}$$

$$\begin{aligned}
R_{\text{Back}} &= \frac{w_{\text{Fiber}}^2 \cdot \sqrt{\frac{\lambda_o \cdot (n_{\text{Air}}d(2N+1)(f-A) + n_{\text{GaAs}}(f(A+C) - AC))^2 + (z_{\text{Spot}} \cdot n_{\text{Air}}(f-A))^2}{\pi \cdot z_{\text{Spot}} \cdot n_{\text{Air}}^2 \cdot n_{\text{GaAs}} \cdot f^2}}}{w_{\text{Fiber}}^2 + \frac{\lambda_o \cdot (n_{\text{Air}}d(2N+1)(f-A) + n_{\text{GaAs}}(f(A+C) - AC))^2 + (z_{\text{Spot}} \cdot n_{\text{Air}}(f-A))^2}{\pi \cdot z_{\text{Spot}} \cdot n_{\text{Air}}^2 \cdot n_{\text{GaAs}} \cdot f^2}} \tag{E.136}
\end{aligned}$$

### E.15.3. Re-calculation of the Fabry Perot cavity response

As we could see in the previous paragraphs, there are additional losses due to the divergence of the laser beam. Hence we have to modify our calculation a little bit.

$$r^+ = r \cdot R_{\text{Front}} \cdot e^{-i\Lambda} \tag{E.137}$$

$$R^+ = R \cdot R_{\text{Back}} \tag{E.138}$$

According to Equation E.137 and Equation E.138 we modify the reflection coefficient. For the reflection coefficient  $r$  we introduce a supplementary phase shift.

$$\begin{aligned}
I_{\text{Reflected}} &= \frac{1}{2Z_{\text{Material}}} |E_{\text{Reflected}} \cdot E_{\text{Reflected}}^*| = \frac{E_{\text{Incident}}^2}{2Z_{\text{Material}}} \left| \frac{r^+ + R^+ e^{-i\phi}}{1 + R^+ r^+ e^{-i\phi}} \cdot \frac{(r^+ + R^+ e^{-i\phi})^*}{(1 + R^+ r^+ e^{-i\phi})^*} \right| \tag{E.139} \\
&= \frac{E_{\text{Incident}}^2}{2Z_{\text{Material}}} \left| \frac{(r \cdot R_{\text{Front}} \cdot e^{-i\Lambda}) + (R \cdot R_{\text{Back}}) e^{-i\phi}}{1 + (r \cdot R_{\text{Front}} \cdot e^{-i\Lambda})(R \cdot R_{\text{Back}}) e^{-i\phi}} \cdot \frac{(r \cdot R_{\text{Front}} \cdot e^{-i\Lambda}) + (R \cdot R_{\text{Back}}) e^{-i\phi}}{(1 + (r \cdot R_{\text{Front}} \cdot e^{-i\Lambda})(R \cdot R_{\text{Back}}) e^{-i\phi})} \right|^* \\
&= I_{\text{Incident}} \left| \frac{(r \cdot R_{\text{Front}} \cdot e^{-i\Lambda} + R \cdot R_{\text{Back}} e^{-i\phi}) \cdot (r \cdot R_{\text{Front}} \cdot e^{-i\Lambda} + R \cdot R_{\text{Back}} e^{-i\phi})^*}{(1 + r \cdot R_{\text{Front}} R \cdot R_{\text{Back}} e^{-i(\phi+\Lambda)}) \cdot (1 + r \cdot R_{\text{Front}} R \cdot R_{\text{Back}} e^{-i(\phi+\Lambda)})^*} \right| = \\
&I_{\text{Incident}} \left| \frac{(r \cdot R_{\text{Front}} \cdot (\cos(\Lambda) - i \sin(\Lambda)) + R \cdot R_{\text{Back}} (\cos(\phi) - i \sin(\phi))) \cdot (\dots)^*}{(1 + r \cdot R_{\text{Front}} R \cdot R_{\text{Back}} (\cos(\phi + \Lambda) - i \sin(\phi + \Lambda))) \cdot (\dots)^*} \right| \\
&= I_{\text{Incident}} \frac{(r \cdot R_{\text{Front}})^2 + (R \cdot R_{\text{Back}})^2 + 2(r \cdot R_{\text{Front}} \cdot R \cdot R_{\text{Back}}) \cos(\phi - \Lambda)}{1 + (r \cdot R_{\text{Front}} \cdot R \cdot R_{\text{Back}})^2 + 2(r \cdot R_{\text{Front}} \cdot R \cdot R_{\text{Back}}) \cos(\phi + \Lambda)}
\end{aligned}$$

